UNIVERSITY OF LIVERPOOL

Role of p38 and p62 in age-related bone loss

Thesis submitted in accordance with the requirements of the University of Liverpool for the degree of Doctor in Philosophy

By

Jacqueline Siew Yeen Lim

April 2021

Abstract

The most common age-related metabolic bone diseases, osteoporosis, and Paget's disease of bone (PDB) are characterised by osteoclast-mediated increased bone resorption, which is generalised in the former and focal, coupled to increased bone formation, in the latter. For reasons incompletely understood, in ageing, osteoclast differentiation increases, which is associated with hyperactivity and hypersensitivity to RANKL. In studies performed on animal models demonstrated an age-dependent increased stromal/osteoblastic-induced osteoclastogenesis, increased expression of *RANKL* and *M-CSF*, as well as decreased expression of *OPG* in stromal/osteoblastic cells. The latter was also observed in studies performed on human BMSCs. Both p38 and p62 are important in OC differentiation and play a role in autophagy, which typically decreases with ageing, but their role in age-related increased bone resorption is unclear.

The aim of this work was to delineate the role of p38 (and other MAPKs) and autophagy during osteoclastogenesis in ageing *in vitro,* (if there is age-related changes in MAPKs' activity and in the expression of the molecular players that are involved in autophagy pathway during osteoclast differentiation) and determine the effect of p62 on age-related bone loss using transgenic mice: $p62^{-/-}$, or p62 knock-in P394L ($p62^{P394L}$, mouse model of PDB).

I found that the p38 MAPK and (marginally) ERK phosphorylation was enhanced in a RANKL-specific manner in BMMs but not in pre-osteoclasts from aged vs young mice indicating increased p38 (and ERK) phosphorylation at the early stage of OC differentiation. Moreover, I found upregulated expression of genes encoding dual-specificity phosphatases (DUSPs): *Dusp 1, 3, 4* and *9* in POCs with ageing using a next generation RNA sequencing data set. Expression of genes associated with OC differentiation: *Nfkb1/2, Plekhm1, Mmp9, Atp6v0d2,* and *Acp5* was also significantly higher in POCs from aged vs young mice. Increased *Atp6v0d2* expression in BMMs, POCs and OCs with ageing was verified by qPCR. As *Atp6v0d2* is induced by NFATc1, master regulator of osteoclastogenesis, it is possible that enhanced p38 MAPK phosphorylation leads to increased NFTAc1 activation, followed by the *Atp6v0d2* upregulation.

I found increased expression of autophagy-related genes: *LC3b, p38IP, Atg9a, Sqstm1, Atg5, Atg12, Atg4B* and *Atg7* in POCs from aged mice on NGS. Indeed, the level of LC3-II was higher in POCs derived from aged vs young mice before and after treatment with Bafilomycin, suggesting increased autophagic flux. In keeping with increased p38 phosphorylation and LC3, immunostaining of resorbing aged vs young OCs showed similar results. These data taken together suggest that age-related activation of the autophagy pathway may play a non-canonical role contributing to increased osteoclastogenesis.

p62 deletion showed a protective effect against age-related bone loss in mice. The relatively high bone volume phenotype in $p62^{-/-}$ mice was associated with lower bone resorption and

higher bone formation. No significant difference was observed between the bone phenotype of *p62*^{P394L} and WT mice at any age. Whilst performing bone morphometry extensive PDB-like lesions were observed on μCT in many 18-month-old *p62*$^{-/-}$ animals, which seem to be more severely affected than the *p62*^{P394L} mice.

Taken together, my results demonstrate that increased phosphorylation of p38 along with the induction of the autophagy pathway explain (at least in part) increased age-related osteoclastogenesis. p62 contributes to age-related bone loss as p62 deletion is protective, however the latter induces PDB-like lesions, which require further investigation.

List of presentations

Poster communications

Lim, J., Cremasco, F., Resnati, M., Orfanelli, U., Merlotti, D., Charlesworth, G., van 't Hof, R., Cenci, S. & Daroszewska, A. Deletion of p62 has a protective effect on age-related bone loss in mice. *Calcified Tissue International* **100,** S44, doi:10.1007/s00223-017-0267-2 (2017). Presented at the European Calcified Tissue Society annual general meeting in Salzburg, Austria.

Lim, J., Brito, F., McConachie, E., Charlesworth, G., Prior, M., van 't Hof, R. & Daroszewska, A. Age-related increased osteoclastogenesis is due to increased phosphorylation of p38 and enhanced expression of V-ATPase. *Calcified Tissue International* **102**, S89, doi:10.1007/s00223-018-0418-0 (2018). Presented at the European Calcified Tissue Society annual general meeting in Valencia, Spain.

Lim, J., Brito, F., McConachie, E., Charlesworth, G., Prior, M., van 't Hof, R. & Daroszewska, A. RANKL-specific increase in p38 phosphorylation enhances NFATc1 and *Atp6v0d2* causing increased osteoclastogenesis in ageing. *Calcified Tissue International* **104,** S96, doi:10.1007/s00223-019-00541-0 (2019). Presented at the European Calcified Tissue Society annual general meeting in Budapest, Hungary.

Acknowledgements

Foremost, I would like to thank my primary supervisor, Dr. Anna Daroszewska for her support, patience, encouragement, and guidance throughout these 4 years, especially through my thesis writing. Without which, the completion of this PhD journey would not have been possible. You always gave me a push when I needed it. I am truly grateful to have you as my supervisor.

Next, I would like to thank my secondary supervisor, Professor Rob van 't Hof for his infectious passion for research that helped motivate me and for all he has taught me from how to dissect mouse legs to culturing macrophages, pre-osteoclasts and resorbing osteoclasts, and to mastering western blot analysis etc., that allowed me to grow and develop as a scientist.

I would also like to thank my tertiary supervisor, Professor George Bou-Gharios. His challenging questions made me work even harder to be the best I can be.

They are who I will call my inspirational role models.

I have been fortunate to have an amazing lab group which I could not have asked for more. To Gemma, Mandie and Cath, I am greatly thankful for always lending a helping hand, especially in histology, without which my work would not have been completed in time, and for always making sure I had whatever I needed to get my research done. To Francesca, my conference buddy, thank you for showing me how to do PCR, for the incredible Portuguese egg tarts and extra virgin olive oil you brought back from Portugal, and for the unforgettable experience in Salzburg. To Andy, my second conference buddy, thank you for all your help during the difficult times, and for the hilarious moments during the conference trips. To Mikele, thank you for the warmest hugs and for all his support and encouragement.

To Dr. James Henstock and Dr. Blandine Poulet, thank you for being my advisors and for giving suggestions on workshops or talks that I could attend to be a well-rounded researcher.

I have also worked with excellent collaborators from Italy. I have collaborated with Dr. Daniela Merlotti, Prof. Luigi Gennari and Dr. Simone Cenci to study the role of p62 on age-related bone loss. To Dr. Maria Materozzi (at the time PhD student), thank you for arranging all the shipping of samples. I am immensely grateful to be involved in this productive and fruitful collaboration.

To Joshua, whom I never expected to meet, thank you for your patience, support and encouragement, I am truly grateful. You always find your way to cheer me up and to motivate me during the difficult times.

To Helen, my neighbour, thank you for lending me a shoulder to cry on, for feeding me when I was too tired and can't be bothered to cook, and many fun late nights. To Melody, who was in the same boat, although in Malaysia has always been a text away, thank you.

Finally, to my parents, you have loved me unconditionally and encouraged me to pursue my dreams, to you I dedicate this thesis.

List of Figures

List of Tables

Abbreviations

3-MA	3-methyladenine
β-catenin	beta-catenin
β-TrCP	β-transducing repeat-containing protein
AF	Alexa Fluor
AHPrBP	bisphosphonate 3-amino-1-hydroxypropylidene-1-bisphosphonate
ALK1	activin-like kinase receptor 1
ALK2	activin-like kinase receptor 2
ALK5	activin-like kinase receptor 5
ALP	alkaline phosphatase
ALR	autophagic lysosome reformation
Ambra1	autophagy/becin-1 regulator 1
α-MEM	alpha-minimum essential medium
ANOVA	analysis of variance
AP-1	activator protein 1
APC	adenomatous polyposis coli
aPKC	atypical protein kinase C
ARE	antioxidant-responsive element
ATF2	activating transcription factor 2
Atg	autophagy-related
Atp6v0d2	ATPase H+ transporting V0 subunit D2
AUC	Area under the curve
BCA	bicinchoninic acid
BECN1	Beclin 1
BFR/BS	bone formation rate per bone surface
BMC	bone mineral content
BMD	bone mineral density

BMI	body mass index
BMMs	bone marrow-derived MCSF-dependent macrophages
BMSCs	bone marrow-derived mesenchymal stem cells
BMPs	bone morphogenetic proteins
BMPRIA	BMP receptor type IA
BMU	basic multicellular unit
BTK	Bruton's tyrosine kinase
BV/TV	bone volume per tissue volume
C1P	ceramide-1-phosphate
CaMK	Ca^{2+}/calmodulin-dependent protein kinase
CCR2	C-C chemokine receptor type 2
Cdc42	cell division cycle protein 42
CK2	casein kinase 2
ClC-7	chloride channel 7
Conn.Dn	connectivity density
CpG-ODN	CpG-oligodeoxynucleotides
CSF1	colony stimulating factor 1
CTR	calcitonin receptor
CtsK	cathepsin K
CTX-1	C-telopeptide of type I collagen
CYLD	CYLD lysine 63 deubiquitinase
DC-STAMP	dendritic cell-specific transmembrane protein
DKK1	Dickkopf 1
DMSO	dimethyl sulfoxide
DUSPs	dual-specificity phosphatases
Dvl	Dishevelled
E_2	17β-estradiol

EBF2	early B-cell factor 2
EEA1	early endosome antigen 1
EoPDB	early onset familial Paget's disease
ER	estrogen receptor
ERK	extracellular signal-regulated kinase
ESH	expansile skeletal hyperphosphatasia
FEO	familial expansile osteolysis
FIP200	focal adhesion kinase family interacting protein of 200kD
FOXO	forkhead box O
FRET	fluorescence resonance energy transfer
GDI	guanosine nucleotide dissociation inhibitor
GFAP	glial fibrillary acidic protein
GH	growth hormone
GM-CSF	granulocyte-macrophage colony-stimulating factor
Grb2	growth factor receptor-binding protein 2
GSK-3β	glycogen synthase kinase-3β
GWAS	genome-wide association studies
H&E	haematoxylin and eosin
HA	hydroxyapatite
HECT	homologous to E6-AP carboxyl terminus
HOPS	homotypic fusion and vacuole protein sorting
HRT	hormone replacement therapy
HSCs	hematopoietic stem cells
Hsp70	heat shock protein 70
IBMPFD	inclusion body myopathy with early onset Paget's disease of bone and fronto-temporal dementia
IGF-1	insulin-like growth factor 1

IGF-1R insulin-like growth factor 1 receptor

IGFBP insulin-like growth factor binding protein

IκB inhibitor of nuclear factor-kappa B

IκBα inhibitor of nuclear factor-kappa B alpha

IKK inhibitor of nuclear factor-kappa B kinase

IKKβ inhibitor of nuclear factor-kappa B kinase beta

IL-1 interleukin-1

IL-1β interleukin-1 beta

IL-1RI interleukin-1 receptor type I

IL-6 interleukin-6

JNK c-Jun N-terminal kinase

LAMP1 lysosomal-associated membrane protein 1

LAMP-2 lysosomal-associated membrane protein-2

LAP latency-associated protein

LC3 microtubule-associated protein 1A/1B-light chain 3

LEF lymphoid-enhancer factor

LIR LC3-interacting region

LPS lipopolysaccharide

LRP low-density lipoprotein receptor-related protein

Mac-1 macrophage-1 antigen

MAPK mitogen-activated protein kinase

MKK mitogen-activated protein kinase kinase

MEKK mitogen-activated protein kinase kinase kinase

MAR mineralising apposition rate

mAtg9 mammalian Atg9

M-CSF macrophage colony-stimulating factor

MCP-1 monocyte chemotactic protein-1

MCPIP	monocyte chemotactic protein-induced protein
MEA	monoethanolamine
MEFs	mouse embryonic fibroblasts
MHC	major histocompatibility complex
μCT	micro-computed tomography
MIG	monokine induced by interferon-γ
MITF	microphthalmia-associated transcription factor
MK2	MAPK-activated protein kinase-2
MMP9	matrix metalloproteinase 9
MS/BS	mineralising surface per bone surface
mTOR	mammalian target of rapamycin
mTORC1	mammalian target of rapamycin complex 1
MVNP	measles virus nucleocapsid gene
Nbr1	neighbour of Brca1 gene 1
NFATC1	nuclear factor of activated T cells, cytoplasmic 1
NF-κB	nuclear factor kappa-light-chain-enhancer of activated B cells
NES	nuclear export signal
NGS	Next Generation Sequencing
NLS	nuclear localisation signal
N.Oc/BS	number of osteoclasts per bone surface
N.Oc/BV	number of osteoclasts per bone volume
N.Oc/TV	number of osteoclasts per tissue volume
NRF2	nuclear factor erythroid 2-related factor 2
NSAIDs	nonsteroidal anti-inflammatory drugs
NUP205	nucleoporin 205 KDA
OC(s)	osteoclast(s)
OCLs	osteoclast-like cells

Oc.S/BS	osteoclast surface per bone surface
OPG	osteoprotegerin
OPTN	optineurin
ORIF	open reduction and internal fixation
OSCAR	osteoclast associated receptor
P38BS	p38 binding sequence
P38IP	p38 interacting protein
PAS	phagophore assembly site
PB1	Phox and Bem1p
PBMC	peripheral blood mononuclear cell
PCL	polygonatum cyrtonema lectin
PCR	polymerase chain reaction
PDB	Paget's disease of bone
PDGF	platelet-derived growth factor
P-ERK	phosphorylated-ERK
PE	phosphatidylethanolamine
PFA	paraformaldehyde
PI3K	phosphatidylinositol 3-kinase
P-I*κ*B	phosphorylated-I*κ*B
PINP	procollagen type I N propeptide
P-JNK	phosphorylated-JNK
PKA	protein kinase A
PLEKHM1	pleckstrin homology and RUN domain containing M1
P-MKK3/6	phosphorylated-MKK3/6
PML	promyelocytic leukemia gene
PP2A	protein phosphatase 2
P-p38	phosphorylated-p38

PPARγ2 peroxisome proliferator-activated receptor gamma isoform-2

POCs pre-osteoclasts

PtdIns(3,4,5)P_3. phosphatidylinositol-(3,4,5)-phosphate

PTH parathyroid hormone

PTHrP parathyroid hormone-related protein

RA rheumatoid arthritis

RANK receptor activator of nuclear factor kappa B

RANKL receptor activator of nuclear factor kappa B ligand

RB ruffled border

rGM-CSF recombinant granulocyte-macrophage-colony stimulating factor

RIN3 ras and rab interactor 3

RING really interesting new gene

RIP receptor-interacting protein

RIPA radioimmunoprecipitation assay

ROD renal osteodystrophy

ROS reactive oxygen species

RPPA reverse phase protein arrays

RT-PCR reverse transcription polymerase chain reaction

RT-qPCR real time-quantitative polymerase chain reaction

Runx2 Runt-related transcription factor 2

S403 serine 403

S405 serine 405

S409 serine 409

SBE Smad binding element

SBF Simulated Body Fluid

SERMs selective estrogen receptor modulators

SF-36 36-item Short-Form General Health Survey

sFRPs	secreted Frizzled-related proteins
SHH	Sonic Hedgehog
SMI	structural model index
SOST	sclerostin
SQSTM1	sequestosome 1
SRXN1	sulfiredoxin
STAT1	signal transducer and activator of transcription 1
STAT5	signal transducer and activator of transcription 5
TAB1	transforming growth factor *β*-activated kinase 1-binding protein 1
TAB2	transforming growth factor *β*-activated kinase 1-binding protein 2
TAB3	transforming growth factor *β*-activated kinase 1-binding protein 3
TAK1	transforming growth factor *β*-activated kinase 1
TBK1	TANK-binding kinase 1
Tb.N	trabecular number
Tb.Pf	trabecular pattern factor
TBS	TRAF6 binding sequence
TCF	T-cell factor
TGF-β	transforming growth factor-beta
TGN	trans-Golgi network
TLR4	toll-like receptor 4
TLR9	toll-like receptor 9
TNF-α	tumour necrosis factor alpha
TNFR1	tumour necrosis factor receptor 1
TRAF6	tumour necrosis factor receptor-associated factor 6
TRAP	tartrate-resistant acid phosphatase
TREM-2	triggering receptor expressed on myeloid cells
TXN	thioredoxin

TXNRD1	thioredoxin reductase 1
UBA	ubiquitin-associated
ULK1	Unc-51 like autophagy activating kinase 1
UPS	ubiquitin-proteasome system
UVRAG	ultraviolet irradiation resistance-associated gene
V-ATPase	vacuolar-type adenosine triphosphatases
Vps15	vacuolar protein sorting-15 subunit
Vps34	vacuolar protein sorting-34 subunit
WHO	World Health Organisation
WIF	Wnt-inhibitor factor
WT	wildtype
ZA	zoledronic acid

Table of Contents

Chapter 1: Introduction

1.1 Skeletal system

The skeletal system is composed of bones and cartilage. Bone is a specialised connective tissue serving the following functions: it supports the body, protects organs, serves as levers and muscle attachments for movement, stores and provides mineral, stores fat, produces certain hormones and stores the bone marrow[1].

Long bones consist of the outer layer which is made of dense compact (cortical) bone that forms the shaft, and the inner layer which is made of honeycomb-like spongy (trabecular) bone, with the open spaces filled with bone marrow[2]. Anatomically, long bones are divided into three sections: diaphysis, metaphysis, and epiphysis (**Figure 1.1**). Diaphysis is the tubular shaft that is composed of a thick collar of compact bone surrounding the medullary cavity, or marrow cavity where the bone marrow is stored[3]. Epiphysis is the proximal or distal end of a long bone and contains trabecular bone within the compact bone filled with red bone marrow which produces blood cells[4]. The exterior of the bone and interior of the trabecular bone layer are covered with periosteum and endosteum respectively[5]. Osteons are the cylindrical units that can be found in the cortical bone and are made up of a series of lamellae which contain collagen fibres running in a specific direction[6]. Lacuna connected by canaliculi is where the lamellae meet and house an osteocyte[7]. Moreover, interstitial lamellae and circumferential lamellae fill the gaps between osteons, and encircle the diaphysis and osteons, respectively[8]. The open canal at the centre of osteons which is known as Haversian canal contains blood vessels and nerve fibres which fulfil the needs of cells surrounding the osteons (e.g. provide oxygen and nutrients, remove waste products, transmits signals)[1]. Volkmann's canals are the canals that connect the Haversian canals of osteons.

In terms of the chemical composition, bones are made up of 30% organic protein and 70% inorganic mineral. Organic components include the bone cells and osteoid which is made up of 5-10% osteopontin, osteocalcin, thrombospondin and fibronectin, and 90-95% type I collagen that are secreted by osteoblasts. Inorganic components include hydroxyapatite (HA) which are crystals of calcium phosphate that surround the collagen fibres and cement them in the bone tissue[9,10].

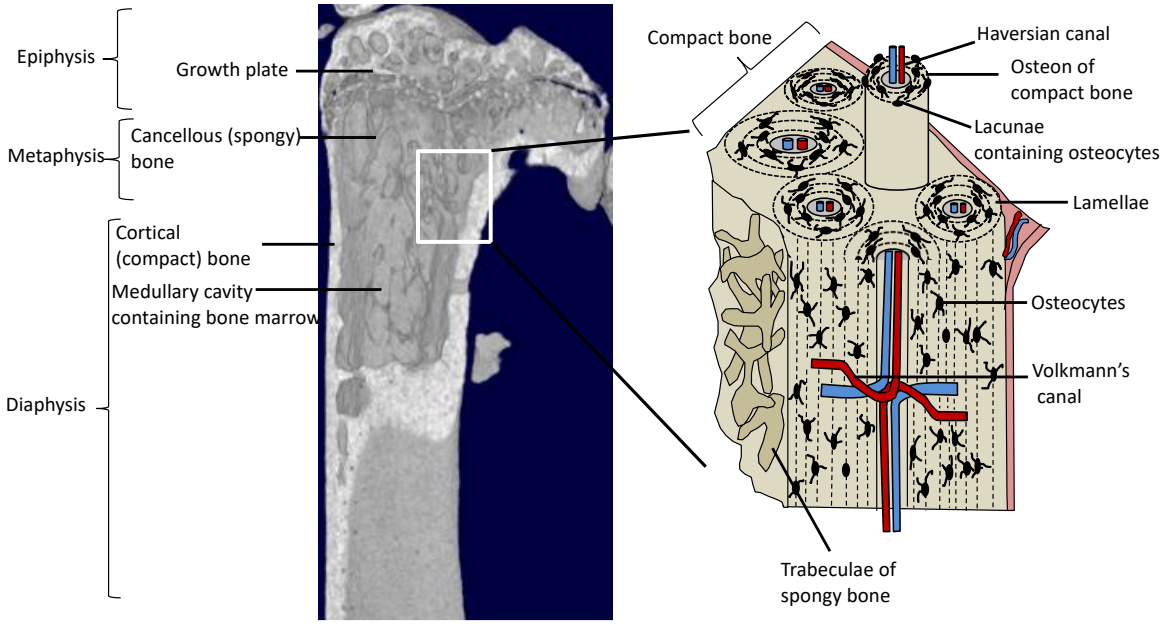

Figure 1.1: Representation of the internal structure of a tibia from an aged mouse scanned by μCT (on the left) with a magnified representation of the interior structure of the cortical bone (on the right). The tubular shaft, called diaphysis, extends towards the proximal end to form metaphysis, where cancellous (spongy) bone can be found. Growth plate is located between the metaphysis and epiphysis. Periosteum covers the outer surface of the bone. Osteon (also known as Haversian system) is the cylinder-shaped structure unit in compact bone which is made up of concentric lamellae and contains a central Haversian canal that is responsible for nutrient supply. Lacunae are the intersection points of lamellae and are tiny cavities containing osteocytes. Volkmann's canal that houses nerves and blood vessels connects Haversian canals[2]. The schematic on the right is adapted from doblaré *et al.*[11]. Similar to humans, mice exhibit cancellous bone loss, increased porosity and cortical thinning with ageing[12]. Yet, the murine skeletal growth does not cease after puberty as it does in humans[12].

1.2 Bone remodelling

Bone remodelling is a process that is carried out by a tightly regulated group of cells organised within the basic multicellular unit (BMU) which replaces old and damaged bone throughout the lifetime in order to preserve bone integrity and maintain mineral homeostasis[13]. BMU consists of bone-resorbing osteoclasts (OCs), bone-forming osteoblasts, osteocytes within the bone matrix and a capillary blood supply[14]. The bone remodelling cycle involves the following sequential phases: activation and resorption, reversal, formation, and quiescence (**Figure 1.2**). The remodelling process begins with the contraction of the lining cells and the recruitment of OC precursors from the circulation in response to mechanical strains or microdamage, followed by the fusion of multiple mononuclear cells to form multinucleated OCs[15]. Upon the differentiation and activation of multinucleated OCs, they adhere to the bone surface and initiate the resorption process, primarily through the action of hydrochloric acid, which dissolves mineral and cathepsin K, which breaks down collagen[16]. Bone resorption products such as calcium and phosphate are released into the bloodstream[17,18]. Bone resorption takes approximately two weeks to complete[16]. Once the bone resorption has finished, the reversal phase is initiated with the OCs detached from the resorption pit and undergoing apoptosis, while the osteoblast precursors are recruited and attach to the resorption pit[15]. The osteoblast precursors proliferate and differentiate into pre-osteoblasts. The reversal phase is a transition from bone resorption to formation, indicating the two processes are coupled[19]. This phase lasts about four to five weeks[20]. At the formation phase, pre-osteoblasts mature into osteoblasts and begin to re-build the bone by synthesising collagenous organic matrix known as osteoid[9]. Subsequently, osteoid undergoes mineralisation through the deposition of inorganic HA which crystallises on organic collagen[9]. This phase lasts for approximately four months[21]. During this phase, some osteoblasts become trapped within the bone matrix and undergo terminal differentiation into osteocytes. Once mineralisation is complete, osteoblasts either undergo apoptosis or become inactive quiescent bone lining cells which remain dormant until the next cycle begins[16]. The next phase is known as the quiescence phase. The rate of bone remodelling for the entire human skeleton is about 10% per year[22].

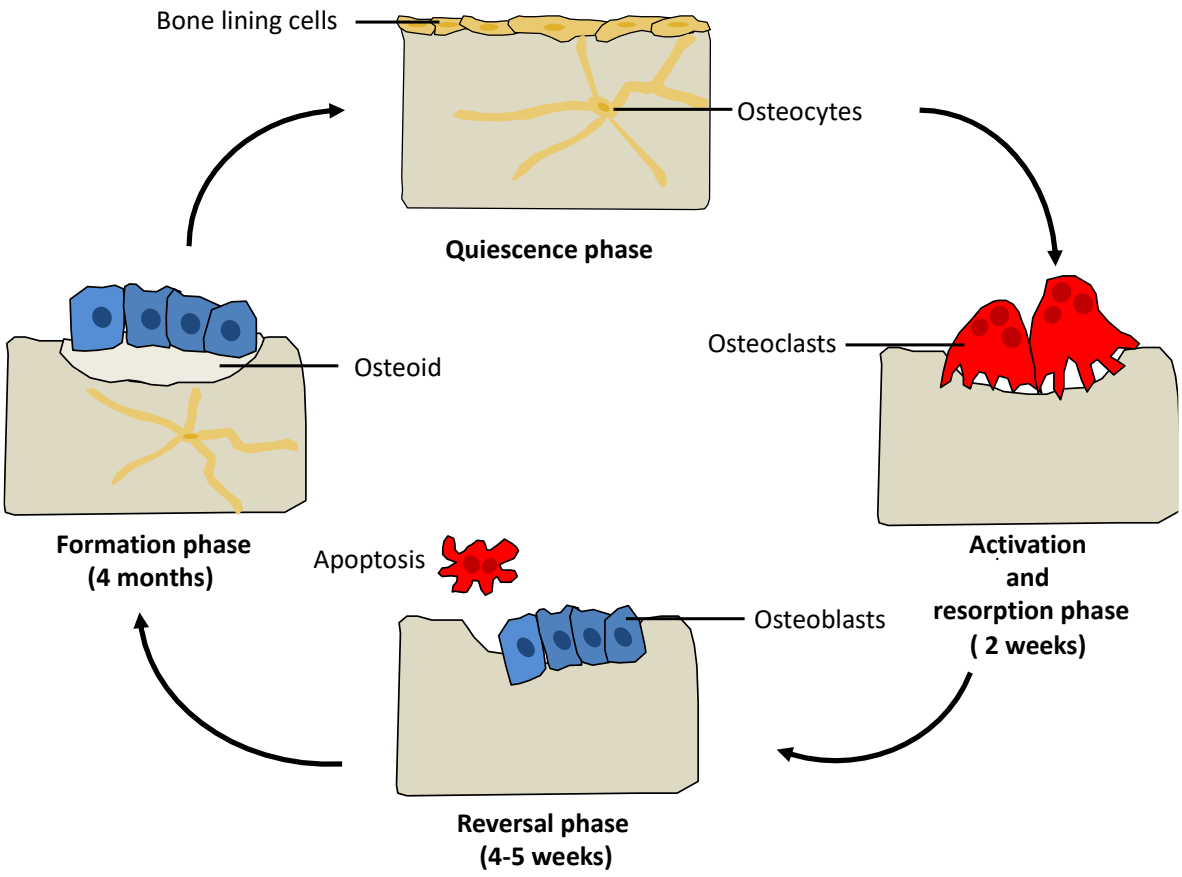

Figure 1.2: Bone remodelling cycle. The remodelling cycle begins with the activation and resorption phase in which the pre-OCs are recruited and activated to become mature OCs and resorb bone. The OCs then undergo apoptosis and osteoblasts are recruited in the reversal phase. During the formation phase, mature osteoblasts begin to form new bone osteoid. During new bone formation, some osteoblasts become trapped in the bone matrix and become osteocytes. When the bone formation is completed, the osteoblasts either undergo apoptosis or become bone lining cells, and the remodelling cycle enters the quiescence phase until the new remodelling cycle begins. The osteoid undergoes mineralisation, which takes about 4 months.

1.3 Bone cells

As mentioned, several types of cells can be found within the bones including osteogenic cells, osteoblasts, osteocytes, bone lining cells and OCs. Osteogenic cells, also known as osteoprogenitor cells, are stem cells located in the periosteum and endosteum that can differentiate into osteoblasts[23]. Osteoblasts produce collagen and express alkaline phosphatase (ALP), which facilitates mineralisation. Once osteoblasts are surrounded and trapped by bone matrix, they undergo terminal differentiation into osteocytes which are the most abundant bone cells that maintain bone matrix, allow for communication among bone cells and sense mechanical loading[24]. Bone lining cells which are found on the surface of bones also help in maintaining bone matrix. OCs are specialised giant cells with multiple nuclei that break down the bone matrix and release minerals into the bloodstream[25]. The following sections describe OCs, osteoblasts and osteocytes in detail.

1.3.1 OCs

OCs derived from the monocyte/macrophage haematopoietic lineage are formed by the fusion of mononuclear progenitors in the process of osteoclastogenesis[26]. OCs are found on endosteal surfaces within the Harversian system of compact bone and on the periosteal surface beneath the periosteum[15,27].

OCs alternate between two functional states, the motile and the resorptive phases[28], which can be distinguished morphologically: OCs in the former phase are “spread” and flattened, while OCs in the latter phase appear to be rounded and are dome-shaped[29]. The presence of membrane protrusions termed lamellipodia permits flattened and non-polarised OCs to exist in the motile phase and migrate from the bone marrow to the resorption site[15]. Upon adhesion to the resorption site, they undergo polarisation by reorganising the cytoskeleton, resulting in the formation of four functionally and structurally distinct membrane domains: ruffled border (RB), podosome-containing sealing zone which contains the actin ring, functional secretory domain and basolateral membrane[15].

The sealing zone formed by the “sealing membrane” at the “clear zone” and RB are OC specific structures, which separate the acidic resorptive environment from the rest of the cell, creating an organelle free area, and segregate the outer “fusion zone” and the inner “uptake

zone", respectively[30,31]. The actin rings are made up of podosomes in which the core components include actin microfilaments, actin-binding proteins, adhesion proteins, adaptor proteins, tyrosine kinases, signalling proteins and integrin receptors[32,33]. The integrin receptor, $\alpha_v\beta_3$ is highly expressed in OCs and serves as an anchor protein, allowing OCs to attach to the bone matrix proteins such as osteopontin[34]. For more details, please refer to **Figure 1.4**.

Vesicles from the endo/lysosomal compartment fuse at the outer "fusion zone" for inserting ion transporters or specialised proton-pump ATPase into the RB and secrete lysosomal enzymes and acid to solubilise the mineral phase[35]. In fact, the autophagy proteins such as p62, autophagy-related (Atg)5, Atg7, Atg4B and microtubule-associated protein 1A/1B-light chain 3 (LC3) play a non-canonical role in regulating the lysosomal secretion, which will be further discussed in **Sub-section 1.5.5[36]**. The protons needed for creating the acidic environment are generated and transported by carbonic anhydrase (type II isoenzyme) within the OCs, and vacuolar H (+) ATPases (V-ATPases), respectively. Together with the Cl^- flux provided by the chloride channels into the resorption site, hydrochloric acid (HCl) is generated[37]. The bone matrix adjacent to the RB is resorbed in the acidic environment by proteases such as cathepsin K (CtsK) that act at low pH. The degradation products derived from the bone resorption are removed by transcytosis at the inner "uptake zone" and released into the vascular stream through the functional secretory domain of the basolateral membrane[30,38,39]. This process is explained in more detail in **Sub-section 1.3.1.2** and shown in **Figure 1.4**.

1.3.1.1 OC differentiation

1.3.1.1.1 M-CSF-c-Fms signalling

Macrophage-colony stimulating factor (M-CSF) is one of the cytokines that is essential for OC differentiation and is produced by osteoblasts and stromal cells. M-CSF is also a potent chemotactic stimulus and actin regulator for OCs. Stimulation of quiescent macrophages and OCs with M-CSF results in podosome dissolution, rapid cytoskeletal reorganisation and lamellipodia formation[40,41]. There is evidence to suggest that M-CSF attracts OCs to resorptive sites, maintains OC survival, and continues to mediate the activity of OCs even when they are on resorptive sites by regulating the balance between osteoclastic bone resorption and OC migration[41].

Mice with non-functional M-CSF due to a point mutation in the *csf1* gene develop severe osteopetrosis because of an absence of OCs[42]. The binding of M-CSF to its cell-surface receptor c-Fms on OCs auto- and trans-phosphorylates eight specific tyrosine residues in the cytoplasmic tail of the receptor, and recruits the adaptor molecule c-Src and growth factor receptor bound protein 2 (Grb2)[43] (**Figure 1.3**). The interaction of phosphorylated Y559 residue of c-Fms and c-Src activates phosphatidylinositol 3-kinase (PI3K) and c-Cbl complex, which in turn stimulates the activity of Akt (protein kinase B) and c-Fms ubiquitination[44,45]. Phosphorylated Y721 residue of c-Fms also involves the activation of Akt pathway by directly interacting with PI3K[44,46]. On the other hand, phosphorylated Y697 and Y974 of c-Fms interact with Grb2, thereby activating the extracellular signal-regulated kinase (ERK) pathway[47].

Furthermore, c-Fos and PU.1 which are the transcription factors critical in the early stage of osteoclastogenesis, are activated by M-CSF-c-Fms interaction. OCs and macrophages are absent in mice deficient in M-CSF and PU.1 while the inactivation of c-Fos gives rise to osteopetrotic phenotype due to an arrest in osteoclastogenesis[48,49]. Therefore, M-CSF signal transduction is crucial for the survival and proliferation of OC precursors and OCs.

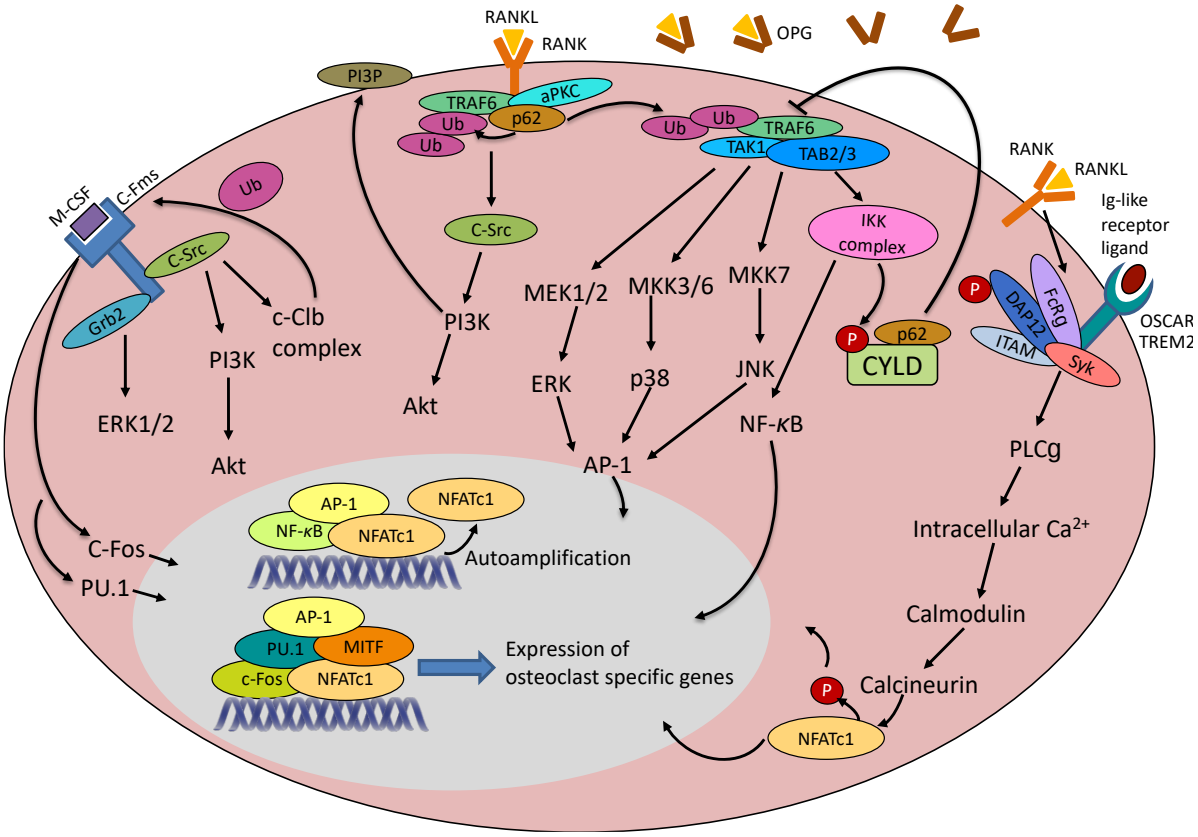

Figure 1.3: Signalling pathways in OC differentiation. M-CSF/c-Fms interaction is important for the proliferation and survival of OC precursors. RANKL/RANK interaction promotes the expression of OC key marker genes such as *CtsK* (cathepsin K), *Acp5* (TRAP), *DC-STAMP* and *NFATc1*, thereby stimulating OC differentiation. P62 acts as a scaffold, interacts and forms a complex with CYLD, which in turn facilitates tumour necrosis factor receptor-associated factor 6 (TRAF6) deubiquitination, thus forming a negative feedback mechanism after sustained RANKL-induced NF-κB activation. OPG secreted by osteoblasts binds to RANKL and intercepts RANKL-RANK interaction, hence it inhibits osteoclastogenesis and bone resorption. Costimulatory signals via the calcium/calcineurin pathway are required for NFATc1 autoamplification. In contrast to the calcineurin-mediated nuclear translocation of dephosphorylated NFATc1 reported by Kim *et al.*[50], Matsumoto *et al.* showed NFTAc1 translocates to the nucleus after being phosphorylated by the activated p38 MAPK[51].

1.3.1.1.2 RANKL-RANK signalling

Receptor activator of nuclear factor kappa B ligand (RANKL) is a cytokine that plays an important role in OC differentiation. M-CSF alone is unable to induce OC precursors to complete the differentiation process and become mature OCs. RANKL is required for OC differentiation and activation, as well as the survival of mature OCs[52-55]. The binding of RANKL (expressed by osteocytes, osteoblasts, T-cells and endothelial cells) to receptor activator of nuclear factor kappa B (RANK) which is expressed on the surface of OCs and their precursors, activates osteoclastogenic signalling cascades (**Figure 1.3**).

RANKL-RANK interaction recruits the adaptor protein, TRAF6 to the C-terminal cytoplasmic tail of RANK[56,57]. In association with p62 and atypical protein kinase (aPKC), a ternary complex is formed[58]. TRAF6 polyubiquitination mediated by p62 and the interaction of transforming growth factor *β*-activated kinase 1 (TAK1) with TAK1-binding protein 2 (TAB2) and TAK1-binding protein 3 (TAB3) allow TAK1 to activate the inhibitor of nuclear factor-kappaB (I*κ*B) kinase beta (IKK*β*)-subunit of the I*κ*B kinase (IKK) complex[59,60]. It is then followed by the phosphorylation of I*κ*B alpha (I*κ*B*α*) by IKK*β*, targeting I*κ*B*α* for proteasomal degradation, ultimately releasing nuclear factor kappa-light-chain-enhancer of activated B cells (NF-*κ*B) to translocate into the nucleus and activate NF-*κ*B-dependent gene transcription[61].

Apart from activating NF-*κ*B, the TRAF6-TABs-TAK1 complex also acts as a critical upstream mediator of mitogen-activated protein kinase (MAPK) pathway including ERK, p38 and c-Jun N-terminal kinase (JNK)[62]. Together with activator protein 1 (AP-1) the downstream target of MAPKs, NF-*κ*B orchestrate the expression of genes that encode proteins essential for osteoclastogenesis such as c-Fos, microphthalmia-associated transcription factor (MITF) and nuclear factor of activated T cells, cytoplasmic 1 (NFATc1) at the initial stage of RANK signalling[49,63,64]. On the other hand, RANKL also activates PI3K which in turn generates phosphatidylinositol-(3,4,5)-phosphate [PtdIns(3,4,5)P_3] for Akt recruitment at the plasma membrane which induces OC differentiation by regulating the glycogen synthase kinase-3β (GSK3β)/NFATc1 signalling axis[65,66]. Furthermore, Akt has also been reported to be mediating the OC activity and the formation of the sealing zone together with GSK3β by stabilising microtubules through regulation of the binding of microtubule associated proteins[66,67].

1.3.1.1.3 The role of p62 in RANKL-induced osteoclastogenesis

As mentioned in the previous subsection, p62 regulates the polyubiquitination of TRAF6 which is important for RANKL-induced OC differentiation[68,69]. P62 interacts with TRAF6 via C-terminal ubiquitin-associated (UBA) domain and N-terminal Phox and Bem1p (PB1) domain, thereby stimulating TRAF6 K63-linked autoubiquitination and E3 ligase activity, as well as regulating the synthesis of K63-polyubiquitin chains on target substrates[58,70]. Apart from promoting TRAF6 polyubiquitination, p62 is also found to be involved in the negative feedback loop to ensure transient NF-κB activation by associating with CYLD lysine 63 deubiquitinase (CYLD). P62 links CYLD deubiquitinating enzyme with polyubiquitinated TRAF6 through C-terminal UBA domain, thereby facilitating the deubiquitination of TRAF6, resulting in decreased NF-κB activity and inhibition of osteoclastogenesis[71,72](**Figure 1.3**). This negative feedback regulation requires the UBA domain of p62 as the loss of this domain causes the inability of p62 to form a complex with CYLD and TRAF6[71]. Furthermore, CYLD which is phosphorylated by IKKβ, IKKε and/or IKKγ (NEMO) also inhibits NF-κB activity by disrupting TRAF6-mediated signalling[73-76]. Since CYLD-mediated inhibition of NF-κB requires the presence of functional UBA domain of p62, and the Paget's disease of bone (PDB)-associated $p62^{P392L}$ mutation affecting the UBA domain abolishes the interaction with CYLD, this leads to increased levels of polyubiquitinated TRAF6 and eventually higher NF-κB activity in Pagetic OCs[77]. Moreover, CYLD deletion in mice results in hyperactivation of NF-κB and enhanced osteoclastogenesis that leads to osteoporosis[71].

1.3.1.1.4 RANKL-OPG system

Apart from secreting RANKL, osteoblasts also produce osteoprotegerin (OPG) which is a soluble tumor necrosis factor (TNF) receptor family member that acts as a decoy receptor for RANKL and inhibits OC formation, preventing excessive bone resorption[78] (**Figure 1.3**). Hence, RANKL/OPG ratio is important in maintaining the balance between bone resorption and formation, and determining bone mass and skeletal integrity[78]. The expression of OPG is regulated by β-catenin via Wnt signalling, in which β–catenin interacts with T-cell factor (TCF) or lymphoid enhancer factor (LEF), and activates the OPG gene promoter and transcription of *TNFRSF11B*, which encodes OPG[79,80]. Previous studies have shown that the overexpression of β-catenin in differentiated mouse osteoblasts leads to osteopetrosis, while its deletion in osteoblasts causes increased OC activity, leading to low bone mass[80,81]. In addition, OPG promoter is also synergistically activated by another transcription factor, early B-cell factor 2 (EBF2)[82]. *Ebf2*$^{-/-}$ mice develop osteoporosis due to reduced expression of OPG[82]. Moreover, OPG deletion in mice results in severe, early-onset osteoporosis which is characterized by increased trabecular and cortical bone porosity, marked thinning of the parietal bones of the skull, and a high incidence of fractures[83].

1.3.1.1.5 Calcium-calcineurin signalling

RANKL-RANK interaction only partially activates NFATc1 in OC precursors, the cooperation of costimulatory pathways is required to fully activate NFATc1 such as calcium-calmodulin-calcineurin pathway.

RANKL-induced intracellular calcium-calmodulin-calcineurin signalling regulates NFATc1 nuclear translocation and robust amplification[84]. RANKL stimulates calcium oscillation indirectly via the co-stimulation of immunoglobulin like receptors such as osteoclast associated receptor (OSCAR) and triggering receptor expressed on myeloid cells (TREM-2)[85] (**Figure 1.3**). Immunoreceptor tyrosine-based activation motif (ITAM)-bearing molecules such as DNAX-activating protein 12 (DAP12) and Fc receptor common γ chain (FcRγ) which are associated with TREM2 and OSCAR also take part in the activation of NFATc1 via calcium signalling pathways[86]. Moreover, phosphorylation of ITAM by RANKL activates phospholipase C γ (PLCγ) and subsequent intracellular calcium signalling in a Syk-dependent manner[15].

Furthermore, RANKL activates Tec family tyrosine kinases such as Bruton's tyrosine kinase (BTK) and Tec, resulting in the phosphorylation of PLCγ[87]. The activation of PLCγ leads to the release of intracellular Ca^{2+} which in turn activates the calmodulin-dependent phosphatase calcineurin[87]. Dephosphorylation of serine residues in NFATc1 by calcineurin permits NFATc1 to translocate into the nucleus[50]. Dephosphorylated-NFATc1 then binds to the *NFATc1* promoter, inducing transcription and autoamplification within the nucleus[50]. In contrast, it has also been reported that NFATc1 is phosphorylated by the activated p38 MAPK and is in turn translocated into the nuclei of OCs (please refer to **Sub-section 1.4.1**)[51].

In the late stage of RANK signalling, NFATc1, the master regulator of osteoclastogenesis after being amplified, combines with other transcription factors such as c-Fos, MITF and PU.1 to mediate OC cell-cell fusion by upregulating dendritic cell-specific transmembrane protein (DC-STAMP) and ATPase H+ transporting V0 subunit D2 (Atp6v0d2)[88]. Also, NFATc1 governs the osteoclastic bone resorption by inducing CtsK, tartrate-resistant acid phosphatase (TRAP) and chloride channel 7 (CLC-7)[51,84,88-90].

1.3.1.2 OC polarisation

OCs undergo cellular and membrane polarisation to become mature and be able to resorb bone (**Figure 1.4**). Podosomes assemble into dynamic short-lived filamentous-actin (F-actin) rings, resulting in the formation of the sealing zone which defines the "resorption lacuna", also known as 'Howship lacuna"[91,92]. An intracellular mechanism is required to deliver the proteins involved in osteoclastic bone resorption into the resorption lacuna which is maintained at a low pH and a high calcium concentration[93]. The acidic extracellular microenvironment is generated by the activity of carbonic anhydrase type II (CAII) which catalyses the hydration of carbon dioxide (CO_2) into carbonic acid (H_2CO_3)[94]. The carbonic acid dissociates into protons (H^+) and bicarbonate (HCO_3^-) equivalents. Subsequently, vacuolar H^+-adenosine triphosphate (V-ATPase) transports the protons into the resorption lacuna. In parallel to the V-ATPase activity, a 2:1 chloride/proton antiporter type 7 (ClC7) releases negatively charged chloride ions which have entered the OC through a chloride/bicarbonate exchanger localised in the basolateral membrane, to balance the electroneutrality[94-96]. Furthermore, the chloride/bicarbonate exchanger also serves as a shunt to allow HCO_3^- produced by the dissociation of the carbonic acid to exit, thereby balancing the alkaline equivalents[94,96]. The coupled action of V-ATPase and ClC7 at the RB allows the formation and secretion of hydrochloric acid (HCl) into the extracellular resorption lacuna. The extracellular acidification results in increased HA solubility, and permits the dissolution of HA crystals and solubilisation of calcium ions, hence exposing the organic matrix which is made up by 95% of type I collagen[97-99].

In addition, pleckstrin homology and RUN domain containing M1 (PLEKHM1) is involved in the vesicular trafficking to the RB[100,101]. After acidification of the resorption area and dissolution of HA, OCs release lysosomal enzymes such as cysteine protease CtsK and tartrate resistant acid phosphatase (TRAP) for the degradation of organic components of bone[99,102]. The bone resorption products are then actively transported via transcytotic vesicles and released at the functional secretory domain, which is localised on the opposite side of the OC to where the RB is located[17,18].

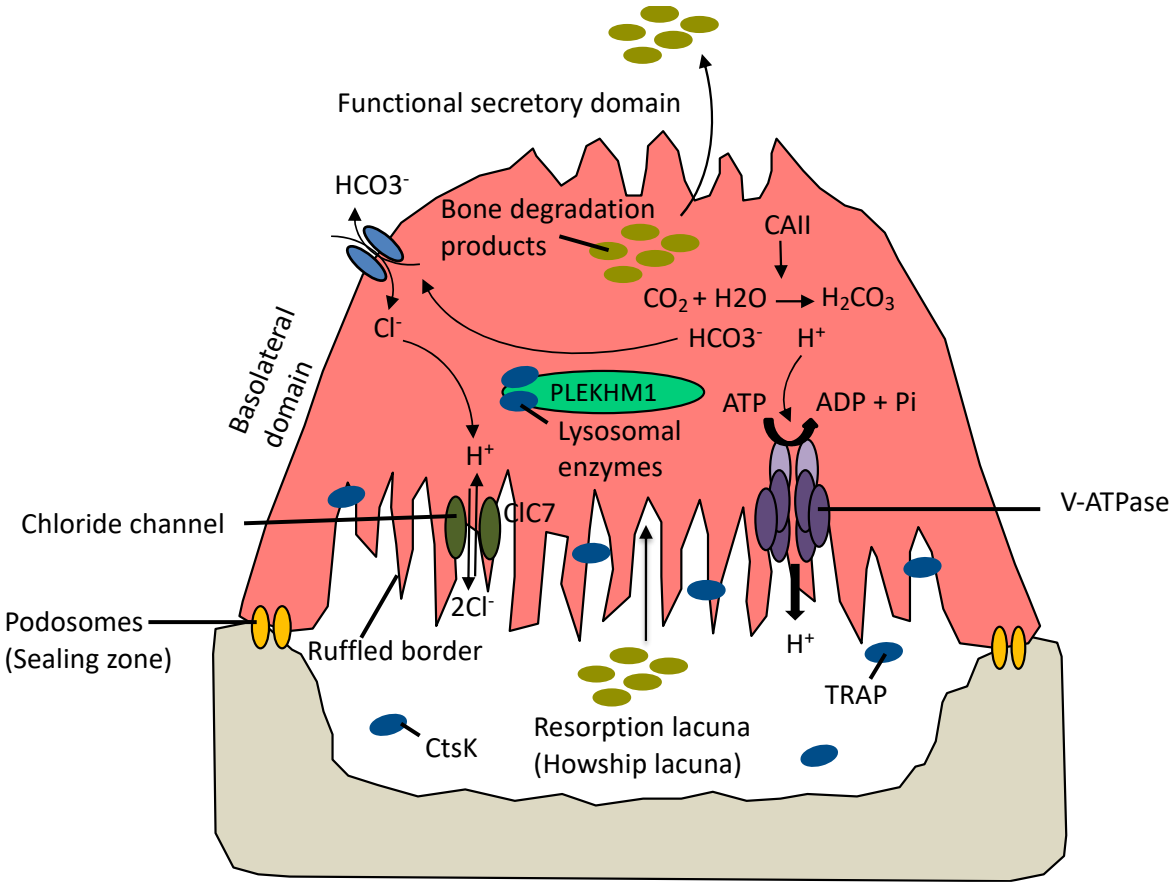

Figure 1.4: Mechanism of osteoclastic bone resorption. The specialised adhesion structures, called podosomes, reorganise to form the sealing zone. Hydrochloric acid and lysosomal enzymes such as CtsK and TRAP are released into the resorption lacuna. The acidification of the resorption lacuna causes a disruption of both the organic and inorganic bone matrix, in which the inorganic components are dissolved by HCl and the organic components are degraded by CtsK and TRAP. The transcytotic vesicles actively transport the bone degradation products from the resorption lacuna to the functional secretory domain.

1.3.2 Osteoblasts

Osteoblasts derived from mesenchymal stem cells are bone forming cells[103]. They display cuboidal morphology and produce collagen and non-collagenous proteins such as osteocalcin and membrane proteins including ALP which play a vital role in mineral deposition[1].

1.3.2.1 Intramembranous and endochondral ossification

During skeletal development, bone formation occurs by two distinct modes: intramembranous ossification and endochondral ossification, both of which involve the transformation of pre-existing mesenchymal tissue into bone tissue[104]. Intramembranous ossification forms the flat bones of the skull, clavicle, and most of the cranial bones by directly converting the mesenchymal tissue to bone. It begins with the proliferation of neural crest-derived mesenchymal progenitor cells, which differentiate into osteoblasts. The osteoblasts condense into compact nodules and form an ossification centre. This is followed by the secretion of osteoid which is an unmineralised collagen-proteoglycan matrix that can bind calcium salts. The deposition of calcium phosphate in the matrix results in the bone matrix calcification and the entrapment of osteoblasts that eventually transform into osteocytes.

In contrast, in endochondral ossification, the mesenchymal tissue first transform into hyaline cartilage, which is later replaced with mature lamellar bone and forms the remainder of the axial skeleton and the long bones[104]. It begins with the differentiation of mesoderm-derived mesenchymal cells into chondrocytes. The chondrocytes proliferate rapidly to form a temporary cartilage model that resembles the shape of the bone[15]. Subsequently, the chondrocytes undergo hypertrophy and alter the cartilage-specific extracellular matrix they secreted by adding collagen X and more fibronectin, allowing it to be calcified by calcium carbonate. Due to the lack of nutrients caused by the calcification of the extracellular matrix, the chondrocytes undergo apoptosis, creating spaces in the cartilage template that permits the invasion of blood vessels and houses the bone marrow. The osteoblasts then deposit collagenous organic matrix on the degraded cartilage which is eventually replaced by bone[105,106]. When bone formation is completed, the mature osteoblasts either undergo apoptosis or convert into inactive quiescent bone lining cells.

1.3.2.2 Osteoblast differentiation

1.3.2.2.1 Wnt/β-catenin signalling

Wnt proteins are secreted glycoproteins that bind to Frizzled (Fzd) family G-protein coupled receptors[107,108]. Fzd receptors contain a cysteine-rich N-terminus extracellular domain 7-(pass)-transmembrane domains and a C-terminus intracellular domain. The Wnt signalling pathway is important in embryogenesis, stem cell renewal and osteoblast differentiation[109-111].

Wnt signalling is complex and involves: the canonical Wnt signalling pathway (β-catenin-dependent) and the non-canonical Wnt signalling (β-catenin-independent) pathway. The canonical Wnt signalling (see **Figure 1.5**) involves the binding of Wnt proteins to a multi-protein receptor complex comprised of Fzd and low-density lipoprotein receptor-related protein (LRP) 5 or LRP6 coreceptor[107,112]. In the canonical signalling, Wnt proteins bind to the Fzd/LRP5/6 receptor complex at the cell surface and activate Dishevelled (Dvl), which in turn inhibits the activity of GSK-3β. In fact, GSK-3β is part of the β-catenin destruction complex, which also includes Axin, the tumour repressor protein adenomatous polyposis coli (APC), protein phosphatase 2A (PP2A) and casein kinase 1α (CSK1α). The activation of Dvl and the inhibition of GSK-3β disrupts the protein complex and hypophosphorylates β-catenin[113], thereby increasing the post-translational stability of β-catenin and preventing β-catenin from degradation[114]. Subsequently, stabilised β-catenin accumulates in the cytoplasm and translocates to the nucleus to activate the transcription of target genes such as *Siamois, Twin, Myc* and *CyclinD1* during embryogenesis and oncogenesis[115,116]. Within the nucleus, β-catenin disrupts the association between Lef/Tcf transcription factor and its corepressor Groucho[117,118], and forms a heterodimer with Lef/Tcf proteins. This heterodimer then binds to the promoters of target genes such as *Runx2* and *Sp7* which are involved in osteoblast differentiation[119].

Without the Wnt ligand binding, β-catenin is phosphorylated within the β-catenin destruction complex in which the APC and axin serve as a scaffold, permitting CSK1α and GSK-3β to bind and perform the phosphorylation. This results in the targeting of β-catenin for ubiquitination and subsequent degradation by the β-transducing repeat-containing protein (β-TrCP)-

mediated ubiquitin/proteasome pathway[120,121]. A number of secreted antagonists in the extracellular matrix that bind to Wnt ligands and prevent the interaction with either Fzd receptors or LRP5/6 coreceptor have been identified. These include sclerostin (SOST)[122], Dickkopf 1 (DKK1)[123,124], secreted Frizzled-related proteins (sFRPs)[125] and Wnt-inhibitor factor (WIF)[126] which bind to LRP5/6 or Wnt, or act as a decoy receptor, and inhibit the Wnt signalling[127-129].

Previous reports have demonstrated the importance of β-catenin in mesenchymal stem cells in osteoblast differentiation[109]. Inactivation of β-catenin in mesenchymal progenitor cells interferes with the skeletal development by affecting osteoblast differentiation and causing abnormal chondrocytes differentiation[109]. Furthermore, the loss of β-catenin in osteoblasts leads to osteopenia which is characterised by reduced bone density due to high bone resorption[80]. Therefore, β-catenin is also found to be vital in the coupling mechanism between osteoblasts and OCs as β-catenin/Tcf complex regulates the *OPG* expression in osteoblasts and causes the inhibition of OC differentiation[80].

The non-canonical Wnt signalling is further categorised into two groups: The Planar Cell Polarity pathway and the Wnt/calcium pathway[130]. Moreover, in non-canonical Wnt signalling, Wnt proteins bind Fzd receptors and induce the integrated action of Rho kinase, JNK and actin-binding protein Profilin for cytoskeletal changes in actin[111,131]. The binding of Wnt protein to Fzd receptors also increases the release of intracellular calcium through protein kinase C-dependent mechanisms[111,131].

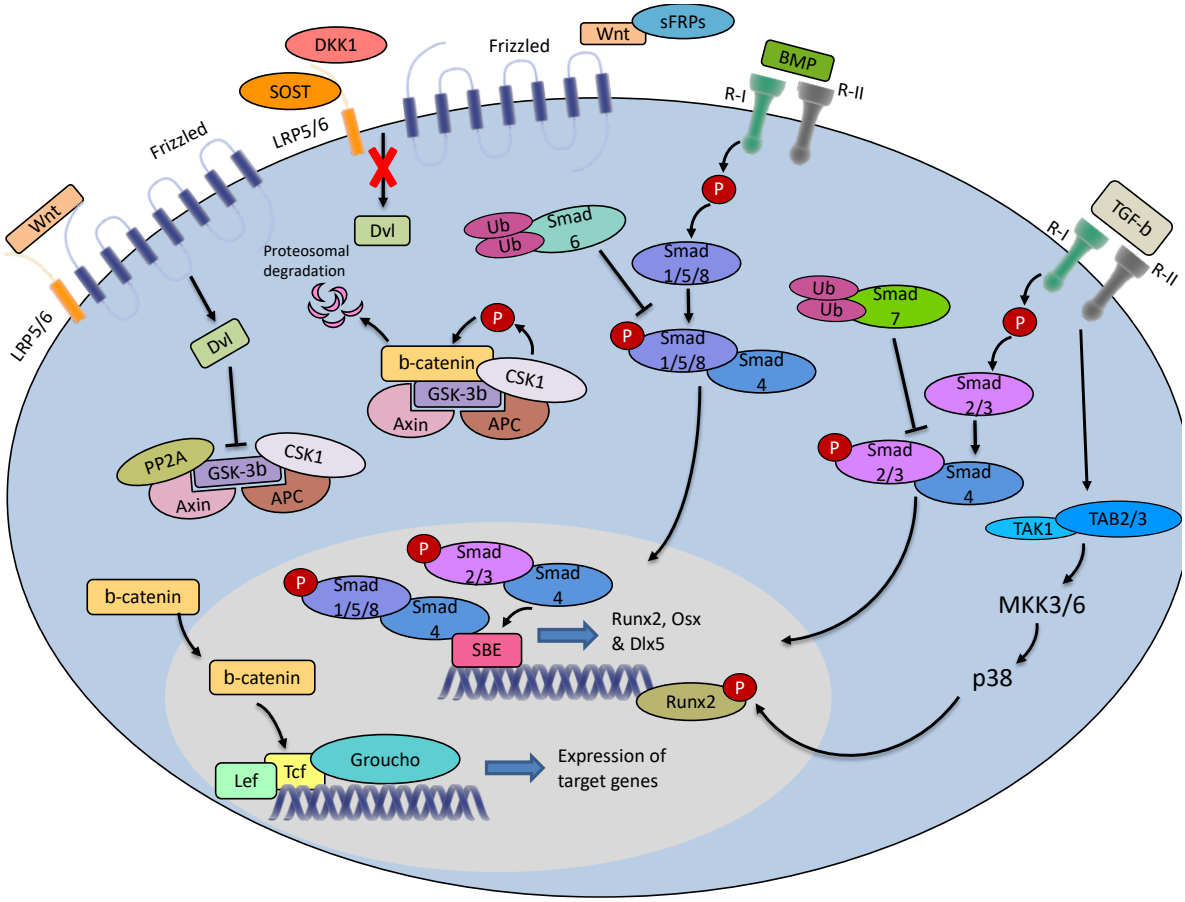

Figure 1.5: Signalling pathways in osteoblast differentiation. Wnt signalling is essential for the proliferation and survival of osteoblast precursors. BMP signalling is required for osteoblast differentiation and maturation. TGF-β signalling promotes early differentiation and the commitment to the osteoblastic lineage via p38 MAPK and Smad2/3 pathways.

1.3.2.2.2 BMP/Smad signalling

Bone morphogenetic proteins (BMPs) are members of the transforming growth factor-beta (TGF-β) family of proteins that have been determined as the inducers of ectopic bone formation and associated endochondral bone formation when implanted into muscle tissue[132-134]. BMP signalling is involved in the stimulation of osteoprogenitors during osteoblast differentiation and the induction of osteogenic cells for committing into the osteoblast lineage[135].

BMPs bind to two types of membrane-bound serine-threonine kinase receptors on the surface of mesenchymal stem cells, termed BMP type I (BMPR-I) and type II (BMPR-II) receptors[136,137]. BMPR-I receptors include activin-like kinase receptor 1 (ALK1), activin-like kinase receptor 2 (ALK2), BMPR-1A and BMPR-1B. BMPR-II receptors include activin receptor type II A (ActR-IIA) and activin receptor type II B (ActR-IIB). Both types of receptors are required to transduce the BMP signals. However, BMPR-I also binds BMPs directly when the BMPR-II is absent, unlike the TGF-β type I receptor that does not bind to TGF-β when the TGF-β type II receptor is absent[138-140]. Moreover, BMPR-I shows a higher ligand binding ability and specificity compared to that of BMPR-II[141].

The binding of BMPs to the N-terminal extracellular domain of BMPR-I phosphorylates the serines and threonines in the cytoplasmic juxtamembrane region that is rich in glycine and serine residues, termed GS domain[142]. This in turn leads to the activation of BMPR-II and the phosphorylation of Smad1/5/8 which allows Smad1/5/8 to form a heterodimeric complex with Smad 4[143-145]. This complex is then translocated into the nucleus and induces the target gene expression (**Figure 1.5**). Within the nucleus, the activated heterodimeric Smad proteins binds to the Smad binding element (SBE), thereby triggering the expression of Runt-related transcription factor 2 (Runx2), Osterix (Osx) and Dlx5, which play an indispensable role in osteoblast differentiation[146-149]. The inhibitor of BMP signalling, Smad6 acts as a selective Smad4 decoy and interacts with Smad1, preventing the formation of the Smad complex[150].

The BMP signalling can be modulated by extracellular BMP antagonists which inhibit the signalling pathway by binding competitively to the BMPs and preventing them from binding to the cell surface receptors[132,151-153]. These include chordin, noggin, ventroptin, follistatin,

follistatin-related gene, twisted gastrulation and differential screening-selected gene aberrative in neuroblastoma (DAN) family members[132,151-154]. Previous studies have demonstrated that noggin plays an essential role in normal skeletal development by negatively regulating the activity of BMPs during neural tube patterning and joint formation[155,156]. The *Noggin* null mutant mice have showed increased BMP activity that causes larger growth plates, and the failure of joint formation[155]. Apart from elevated BMP activity, the addition of deficiency of chordin, in *Chr* $^{-/-}$*; Nog* $^{+/-}$ mice led to defects in the craniofacial skeleton[157].

Furthermore, the presence of crosstalk between BMP and Wnt signalling plays a role in the regulation of bone mass. *Dkk1* and *Sost* which are Wnt inhibitors, are also the downstream targets of BMP signalling through the BMPR-1A in osteoblasts[158]. BMPs negatively regulate bone mass by inducing the expression of *Dkk1* and *Sost* via MAPK and Smad signalling, respectively[158,159]. Moreover, osteoblast-specific deletion of BMPR-1A increases bone mass, which is caused by the hyperactivation of Wnt signalling and decreased expression and activity of both of its inhibitors, Sost and Dkk1[159]. Furthermore, Smad4 binds to β-catenin in a competitive manner, preventing β-catenin from binding to the Lef/Tcf transcription factor[160]. As a result, the loss of Smad4 in osteoblasts promotes bone formation by upregulating the canonical Wnt signalling[160].

1.3.2.2.3 TGF-β signalling

TGF-β is a cytokine secreted by osteoblasts as a large precursor molecule which is composed of mature TGF-β and latency-associated protein (LAP), and is found abundantly in bone matrix[161-164]. The latent form of TGF-β within the bone matrix is cleaved and released during osteoclastic bone resorption[163,165,166]. TGF-β has been reported to be involved in the coupling of bone formation by osteoblasts and bone resorption by OCs[164,167,168]. During bone remodelling, TGF-β is activated through Atp6i-specific extracellular acidification of the resorption lacuna by OCs[165], which in turn stimulates the bone formation[169].

TGF-β isoforms are divided into two categories based on the degree of sequence similarity and the receptor-binding ability[170]. As mentioned previously in ***Subsection 1.3.2.1.2***, the presence of both TGF-β type I and II receptors are necessary for the ligand binding[138-140]. TGF-β sequentially binds to receptor type II (R-II) which is a constitutively active kinase that phosphorylates receptor type-I (R-I). This is then followed by the transduction of signals to Smad2/3 and the recruitment of Smad4 to form a complex for nuclear translocation[146](**Figure 1.5**). Similar to the BMP signalling, the activated heterodimeric Smad proteins bind to the SBE in the nucleus, which in turns regulates the expression of *Runx2*[171]. Smad7 acts as an inhibitor of TGF-β signalling by disrupting the interaction between phosphorylated-Smad2/3 and Smad4, and subsequently forms a complex with Smad4[172]. TGF-β at low concentrations stimulates secretion of RANKL and to a lesser degree OPG, however this effect is not observed at high TGF-β concentrations[173]. TGF-β released by OCs from the bone matrix during bone resorption limits the activity of OCs[164].

On the other hand, TAK1-TAK1-binding protein 1 (TAK1-TAB1) complex also participates in osteoblast differentiation and bone formation in a Smad-independent manner. TAK1/TAB1 complex activates mitogen-activated protein kinase kinase 3/6 (MKK3/6), which in turn phosphorylates p38 MAPK, resulting in the phosphorylation of Runx2 and the induction of type I collagen expression by TGF-β1[149,174]. Furthermore, crosstalk between TGF-β and Wnt signalling is shown through the activation of β-catenin signalling stimulated by TGF-β via activin-like kinase receptor 5 (ALK5), Smad3, protein kinase A (PKA), and PI3K pathways[175].

1.3.3 Osteocytes

Osteocytes are terminally differentiated osteoblasts that became embedded in newly formed bone matrix.[176]. While incorporating into the bone matrix, osteoblasts lose more than 70% of the cytoplasmic organelles and acquire stellar shape with dendritic processes rich in actin cytoskeleton, resulting in the formation of small osteocytes with thin extensions that enable them to communicate with one another and with osteoblasts on the bone surface[177]. Furthermore, the long extensions of osteocytes enable them to form filopodial actin networks and act as mechano-sensors to transduce mechanical input into biological output[178].

Microdamage causes the local osteocytes to undergo apoptosis, which is accompanied by an increased RANKL production and enhanced OC formation, resulting in the initiation of the bone remodelling cycle[179]. Moreover, osteocytes are a major source of RANKL, as it has been shown that osteocyte-specific RANKL deficiency leads to an osteopetrotic phenotype in mice[180]. It has also been suggested that osteocytes use their long processes to connect with OCs and supply RANKL, thus contributing to OC formation and bone remodelling[181]. However, it is also possible that osteocytes may have a negative effect on osteoclastic bone resorption as increased *RANKL/*OPG ratio was showed in targeted ablation of osteocytes in young mice that caused rapid induction of bone resorption[179].

Osteocytes also secrete the bone formation inhibitor, SOST (encoded by the *SOST* gene). It is hypothesised that SOST travels to the bone surface via the osteocytic network and binds to LRP5, and LRP6[182,183], hence preventing the Wnt ligands binding to these coreceptors. Moreover, it has also been reported that SOST antagonises *Wnt1, Wnt 3* and *Wnt 3a*-induced signalling activation in Wnt reporter assays[182]. By exerting the antagonistic effect, SOST inhibits the Wnt/β-catenin signalling pathway, therefore arresting osteoblast proliferation and enhancing apoptosis of osteoblasts, which eventually leads to decreased bone formation[182,183]. Furthermore, SOST supports osteoclastogenesis and osteoclastic bone resorption in a RANKL-dependent manner as well[184]. The formation of TRAP-positive cells was observed in the cocultures of murine osteocyte-like cell line MYLO-Y4 with splenocytes and peripheral blood mononuclear cell (PBMC) upon SOST treatment. Indeed, the cell formation and the increased OC activity in response to SOST were arrested when OPG was added[184].

In short, with the role as an inhibitor of bone formation and a stimulator of RANKL secretion from osteocytes to induce osteoclastogenesis[184,185], osteocyte-derived SOST plays an essential role in the regulation of bone turnover. Interestingly, the expression of SOST was also found in the aged OCs from 24-month-old mice, suggesting that SOST may contribute to the age-related decoupling of bone resorption and formation[186], which eventually leads to remodelling imbalance, and results in bone disorders such as osteoporosis.

1.4 MAPK

As mentioned in **Subsection 1.3.1.1.2**, the binding of RANKL to RANK receptor induces MAPK phosphorylation through the activation of TRAF-TABs-TAK1 complex, and thus OC differentiation and activation[62]. In fact, M-CSF-c-Fms interaction activates MAPK phosphorylation as well which is monophasic and immediate (lasts from 5 to 20 minutes), resulting in the proliferation of OC precursors. Thus, RANKL-RANK interaction results in biphasic activation consisting of both immediate (5 to 20 minutes) and delayed phosphorylation (8 to 24 hours) of MAPKs, leading to OC differentiation[187]. Although the MAPKs share signal mediators, the activation differs in term of extent, duration and isoform specificity of MAPKs, therefore giving rise to distinct cell fates of OC precursor proliferation or differentiation[188]. Two ERK isoforms ERK1/2 and three JNK isoforms JNK1/2/3 play a key role in the proliferation of OC precursors and OC apoptosis, respectively[188-190]. There are four p38 isoforms p38α, β, γ and δ, of which p38α is highly expressed in OC precursors and mature OCs and is involved in OC differentiation and activity[191].

MAPKs transduce signals and act as a signalling hub in response to a variety of extracellular stimuli, thereby regulating cellular processes including growth, proliferation, differentiation, development, apoptosis, stress and inflammatory responses. MAPK pathways are formed by three-tiered cascades comprised of three components: MAPK, MKK and MAPK kinase kinase (MEKK). In response to stimuli, MEKKs, which are serine/threonine protein kinases, phosphorylate and activate MKKs, which in turn dually phosphorylate the tyrosine and serine/threonine residues of MAPKs[192]. The MAPK pathways are regulated through dephosphorylation of the threonine or tyrosine residue by phosphatases such as DUSPs[193].

1.4.1 P38 MAPK

P38 MAPK is involved in the regulation of OC formation, maturation and bone resorption. Following cytokine stimulation, p38 MAPK is phosphorylated by MKK3 and MKK6 and induces osteoclastogenesis[194-196]. Increased trabecular bone mass and number in association with decreased trabecular spacing were found in *Mkk3*$^{-/-}$ and *Mkk6*$^{-/-}$ mice, compared to control littermates at 4-months-of-age[194]. This was accompanied by reduced p38 MAPK activation and downregulation of *Nfatc1*, *CtsK*, *Oscar* and matrix metallopeptidase 9 (*Mmp9)*, hence impaired bone resorption[194-196].

It has been reported that p38 MAPK regulates the OC progenitor proliferation and differentiation in a cell-density- and an age-dependent manner[197]. The proliferation of p38α-deficient monocytes obtained from 2.5- and 6-month-old mice was enhanced compared to the control monocytes[197]. Moreover, p38α deficiency in monocytes at both ages induced OC differentiation when the cell density was low, but caused inhibition when the cell density was high[197]. Furthermore, increased bone mineral density (BMD) of 10% and bone volume in association with decreased bone erosion surfaces and OC number were observed in 2.5-month-old mice with monocyte-specific p38α-deletion compared to controls [197]. On the other hand, the bone density and volume, trabecular number (Tb.N) and thickness were reduced by approximately 30%, accompanied by increased trabecular separation and OC number in 6-month-old mice with monocyte-specific p38α-deletion compared to controls[197].

In support of the positive role of p38 in OC differentiation, Matsumoto *et al.* demonstrated inhibition of RANKL-induced osteoclastogenesis in RAW264.7 cells (which can be differentiated into osteoclast-like cells upon RANKL treatment) when the cells were transfected with a dominant negative mutant of p38α or were treated with p38 MAPK specific inhibitor SB203580[196]. P38 MAPK is also involved in coupling osteoclastogenesis and osteoblastogenesis. Cong *et al.* showed that the expression of coupling factors *BMP-2* and platelet-derived growth factor (*PDGF*)- *AA* were downregulated in p38α-deficient monocytes and OCs via p38 MAPK-Creb axis, thereby indirectly inhibiting osteoblast proliferation and differentiation[197].

P38 MAPK is activated by M-CSF-c-Fms signalling during macrophage development[188,198] and by RANKL-RANK signalling which involves the recruitment of TRAF6 during OC differentiation[194,196]. It has been proposed that p38 MAPK activation is required for OC differentiation, but not for OC function[199]. RANKL-induced osteoclastogenesis was inhibited when the bone marrow cultures were treated with p38 inhibitor SB203580, however, the dentine-resorbing activity of OCs was not affected[199]. Moreover, phosphorylated-p38 (P-p38) was detected in bone marrow-derived M-CSF-dependent macrophages (BMMs), but not in mature OCs when stimulated with RANKL[199].

Apart from acting as a decoy receptor for RANKL, OPG was found to induce the expression of MMP-9, which is a type IV collagenase that is highly expressed in OCs, via p38 MAPK phosphorylation[200]. Moreover, OPG induces podosome disruption and the retraction of OC adhesion structures lamellipodia and filopodia through p38 MAPK activation[201].

Furthermore, p38 MAPK can be directly activated by TNF-α, which is a pro-inflammatory cytokine that regulates inflammatory responses in rheumatoid arthritis (RA)[202,203]. TNF-α-induced OC differentiation was inhibited upon the treatment with SB203580, indicating the involvement of p38 MAPK signalling pathway in TNF-α-mediated differentiation of BMMs into OCs[202]. It has also been shown that the number of OCs differentiated from BMMs obtained from $p38^{+/-}$ mice due to TNF-α induction was decreased[202]. Nevertheless, interleukin-1 (IL-1) is required for the maturation and activation of OCs in which the differentiation is induced by TNF-α[204,205]. Therefore, the actions of TNF-α and IL-1 are coupled and may play an important role in the pathogenesis of inflammatory and metabolic bone diseases such as RA, periodontitis and postmenopausal osteoporosis[206-209]. Although IL-1 is able to enhance osteoclastogenesis and bone resorption through a mechanism independent of the RANKL-RANK interaction, and has a synergistic effect on RANKL-induced OC formation, IL-1 alone is insufficient to induce OC differentiation[210]. However, the inability of IL-1 to induce OC differentiation via p38 MAPK activation can be rescued by overexpressing its receptor IL-1 receptor type I (IL-1RI) in OC precursors[210].

RANKL-induced p38 MAPK activation leads to the phosphorylation of the p65 NF-κB subunit on Ser536, hence increased NF-κB transcriptional activity[195]. Moreover, the activated p38

MAPK also has been shown to phosphorylate NFATc1, which is the master transcription factor regulating osteoclastogenesis[51]. Interestingly, it has been reported that the phosphorylated NFATc1 is in turn translocated into the nuclei of OCs, in contrast to other NFAT members, which translocate into nuclei after undergoing calcineurin-mediated dephosphorylation. It has been further suggested that this phenomenon may not only be NFATc1-specific, but also cell-type dependent and more complex, requiring further investigations[51]. Nevertheless, NFATc1 has been shown to form a complex with PU.1, thereby upregulating the gene expression of *CtsK* and *Acp5* in OCs[51]. In addition, *CtsK* and *Atp5* expression was enhanced following the increased transactivation of MITF after being phosphorylated by p38 at Ser307 due to RANKL stimulation[211]. Furthermore, signal transducer and activator of transcription 1 (STAT1) phosphorylation at Ser727 induced by p38 MAPK promotes the secretion of monokine induced by interferon-γ (MIG), which stimulates the adhesion and migration of OCs[212]. In addition, p38 MAPK activates MAPK-activated protein kinase-2 (MK2) which regulates the expression of OC markers[213,214]. The loss of MK2 leads to the downregulation of *CtsK, Acp5, Mmp9, DC-STAMP, OC-STAMP* and *Oscar*, in association with impaired DNA-binding of c-Fos and NFATc1 to the promoter of *CtsK* and *Acp5*, thus failure in OC differentiation after the treatment of M-CSF and RANKL[215]. This is accompanied by increased trabecular bone mass and cortical thickness, lower number of OCs and bone resorption *in vivo*[215].

RANKL-induced p38 activation is negatively regulated by IL-3 via the activation of signal transducer and activator of transcription 5 (STAT5) and the upregulation of Id1 and Id2, which are negative regulators of OC differentiation, hence suppressing osteoclastogenesis[216]. Moreover, IL-4 and IL-27 inhibits OC differentiation by downregulating p38 MAPK and NF-κB activation, with IL-4 exerting the inhibition in a STAT6-dependent manner[217,218]. Furthermore, p38 MAPK is also inactivated by DUSP1 through dephosphorylation of threonine and tyrosine residues of activated p38 MAPK[219,220]. Sartori *et al.* showed increased OC formation and activity in *DUSP1*$^{-/-}$ mice upon receiving lipopolysaccharide (LPS) injection compared to the wild-type group[220].

1.4.2 ERK

The ERK signalling pathway has been implicated in the proliferation, formation, differentiation, survival, apoptosis, migration and polarity of OCs. It has been reported that ERK1 deletion leads to decreased number of OC progenitor cells and OCs, compromised OC activity, impaired M-CSF-induced pre-osteoclast adhesion and migration[221]. This was accompanied by increased BMD and bone volume in *Erk1*$^{-/-}$ mice compared to age- and gender-matched WT mice, hence proving an enhancing effect of ERK on OC differentiation and activity[221].

As mentioned above, ERK plays a significant role in OC survival and polarity. Following cytokine stimulation, isoforms of Raf (a family of kinases related to retroviral oncogenes; Raf stands for Rapidly accelerated fibrosarcoma) including A-Raf, B-Raf, C-Raf and Raf-1 are activated via Ras-Raf interactions (whereby Ras is a small GTP-binding protein, upstream in many signalling pathways). This Ras-Raf interactions stimulate MEK1 and MEK2, which in turn phosphorylate ERK1 and ERK2[222,223]. Upon the treatment with MEK1 inhibitor, PD98059, for 1 hour, the accumulation of vesicles and vacuoles in association with the loss of RB have been observed in OCs[224]. Prolonged treatment of PD98059 (3 to 6 hours) caused apoptosis with nuclear condensation, loss of OC polarity and detachment of OCs from the bone surface[224].

Similar to p38 MAPK, the binding of RANKL to its receptor RANK recruits TRAF6 to the intracellular cytoplasmic tail of RANK and subsequently activates the ERK signalling pathway for OC differentiation and activity. Interestingly, it has also been suggested that ERK phosphorylation may be involved in the inhibitory effects of OPG on OC differentiation and OPG-mediated podosome disassembly as ERK inhibition attenuated the inhibitory effect of OPG on osteoclastogenesis[201].

Moreover, pro-inflammatory cytokine IL-1β acts synergistically with RANKL to stimulate ERK activation in a Ca^{2+}-dependent manner, thereby increasing the lipidation of LC3 and the formation of secretory lysosomes which contain LC3-II in OC precursors and accelerating the release of cathepsin K[225]. ERK is also activated by IL-1α, which results in a decrease in caspase 3 activity and OC apoptosis, therefore promoting OC survival. In addition, ERK phosphorylation is induced by IL-34 via c-Fms activation during osteoclastogenesis[226]. Apart

from the pro-inflammatory cytokines, ERK can be stimulated by granulocyte-macrophage colony-stimulating factor (GM-CSF), which in turn induces the expression of c-Fos and subsequently NFATc1[227]. This leads to the induction of DC-STAMP expression, hence the promotion of pre-osteoclast fusion and OC formation[227].

M-CSF- or RANKL-induced ERK activation phosphorylates c-Fos, which is a transcription factor essential for OC differentiation[228]. In fact, the duration of ERK activation is controlled by toll-like receptor 9 (TLR9) ligand CpG-oligodeoxynucleotides (CpG-ODN), which induces the expression of PP2A which in turn dephosphorylates ERK[228]. Thus, sustained ERK activation is prevented and the rate of *c-Fos* degradation is increased, resulting in the inhibition of osteoclastogenesis[228].

Similar to p38 MAPK, the IL-3 and IL-4 exert inhibitory effect on ERK via STAT5 and STAT6 activation respectively, thereby inhibiting osteoclastogenesis[216,218]. IL-3-induced STAT5 decreases the level of phosphorylated-ERK (P-ERK) in the early stages of RANKL-induced OC differentiation by upregulating the expression of *Dusp1* and *Dusp2* in OCs which dephosphorylate ERK, therefore preventing sustained activity of ERK[229]. Mice with OC-specific conditional deletion of *Stat5* exhibited osteoporotic bone phenotype, which was accompanied by increased ERK activation[216,229].

1.4.3 JNK

JNK signalling is involved in the regulation of OC formation, differentiation and apoptosis. The binding of RANKL to RANK recruits TRAF6 and subsequently activates MEKK1 and TAK1[190,230,231]. This is then followed by the stimulation of MKK4 and MKK7, and consequently JNK, which in turn phosphorylates c-Jun, a component of AP-1 in OCs[190,231].

It has been shown that the overexpression of TRAF6 and MEKK1 led to the activation of JNK signalling and inhibited OC apoptosis, which was induced by withdrawing RANKL *in vitro*[190]. Indeed, acceleration of apoptosis in OCs was observed when JNK was inhibited by its specific inhibitor SP600125 or the dominant negative *JNK1*, *c-Jun* or *c-fos* were overexpressed[190]. By using the mice lacking JNK1 (*Jnk1*$^{-/-}$), *c-Jun* or expressing a mutated form of c-Jun (*JunAA/JunAA*) which cannot be phosphorylated by JNK, David *et al.* showed that the differentiation of OCs and the surface of resorbed bone was reduced by approximately 50%[232]. Moreover, a three-fold increase in apoptosis of RANKL-treated *Jnk1*$^{-/-}$ OC precursors was observed, which may explain the reduction of osteoclastogenesis and indicates that JNK1 exerts an anti-apoptotic effect on OC precursors[232].

Furthermore, JNK commits macrophages towards the OC lineage by modulating the expression of Ca^{2+}/calmodulin-dependent protein kinase (CaMK) and NFATc1[233]. The $TRAP^{+}$ mononuclear pre-osteoclasts (POCs) treated with SP600125 in which the JNK signalling was inhibited were provoked to reverse into $TRAP^{-}$ cells with the characteristics of macrophage lineage even in the presence of RANKL[233]. Increased cell population expressing the macrophage cell-surface markers CD11b, CD68, CD14 and F4/80, and decreased mRNA expression of TRAP, calcitonin receptor (CTR) and Mmp9 which are osteoclastogenesis-related genes were seen in the SP600125-treated POCs[233]. This was accompanied by the downregulation of CaMK and NFATc1 mRNA level, expression of which is required for the POCs to remain committed and complete the osteoclastogenesis successfully[233].

In addition, JNK is activated by pro-inflammatory cytokines such as TNF-α, IL-1 and IL-17A and takes part in cell-cell fusion, OC survival and autophagy of OC precursors. IL-1 plays a role in bone resorption under pathological conditions such as in RA and periodontal bone diseases by prolonging the survival of OCs and inducing the fusion of pre-OCs through the activation

of JNK[234]. Furthermore, the level of phosphorylated-JNK (P-JNK) has been shown to increase in association with enhanced LC3 lipidation and the upregulation of autophagy protein Beclin1 (BECN1), when the OC precursors were treated with a low concentration of IL-17A[235]. However, the stimulatory effect of IL-17A on JNK activation and autophagic activity in OC precursors was absent upon high concentration of IL-17A treatment[235]. This suggests that IL-17A at low concentration induces autophagy in OC precursors via JNK activation, which is coupled with enhanced osteoclastogenesis.

1.5 Protein degradation systems

The maintenance of cellular homeostasis is essential for cell development and function. The ubiquitin-proteasome system (UPS) and autophagy-lysosome pathway are two major intracellular protein degradation systems in the protein quality control pathway[236]. Both enzyme systems target proteins in a ubiquitin-dependent manner, marking the cargo protein for proteasomal or lysosomal degradation[236,237].

Ubiquitin is a small 8.5 kDa, globular regulatory protein containing 76 amino acid residues[238]. The covalent conjugation of ubiquitin to the target substrate occurs through a process known as ubiquitination. Ubiquitination begins with the activation of free ubiquitin in an energy-dependent manner. A high-energy thioester linkage is formed between a ubiquitin-activating enzyme E1 and the carboxyl terminus of ubiquitin[238]. The activated ubiquitin is then transferred to the active cysteine residue of ubiquitin-conjugating enzyme E2, which catalyses the shifting of ubiquitin to the target substrate with the assistance of ubiquitin-ligases E3s. Ubiquitin-ligases E3s are classified into two groups: homologous to E6-AP carboxyl terminus (HECT) domain E3s and really interesting new gene (RING)-finger domain E3s[238,239]. The activated ubiquitin is either first transferred to an active cysteine residue on the HECT domain of E3s before ultimately shifting to the target substrate or is directly transferred from the E2 enzyme to the target substrate via RING-finger domain of E3s[240]. The E3s catalyses the transfer of ubiquitin to the target substrate by forming a link between the α-carboxyl terminal glycine of ubiquitin and the ε-amino group of a lysine residue on the target substrate[241,242].

Seven different lysine (K) residues in ubiquitin: K6, K11, K27, K29, K33, K48, and K63 have been identified to be involved in the ubiquitin chain synthesis[238]. Whether the target substrates are degraded through proteolytic or non-proteolytic molecules, depends on which of the lysine residues take part in attaching the monomers in the polyubiquitin polymer[238]. The target proteins that are tagged by K48 ubiquitin chain are recognised by ubiquitin-binding shuttling proteins which then deliver the target proteins for proteasomal proteolysis[243-245]. In contrast, those that are tagged by K11 or K63 ubiquitin chains are ubiquitinated mainly for non-proteolytic functions[238,246].

Short-lived, misfolded, damaged, and abnormal soluble proteins are degraded through the UPS in which the unfolded polyubiquitinated proteins are recognised by the α subunits and catalytically cleaved into single amino acids by the β subunits of proteasomes[247-249]. The proteins that are degraded through the UPS are mainly endogenous proteins which are proteins synthesised in the cells. The UPS system is important in the regulation of several cellular events, including cell cycle progression, cell signalling, transcription, proliferation and apoptosis[243].

In contrast, long-lived, large and insoluble protein aggregates are eliminated via the autophagy-lysosome pathway which is also known as macroautophagy (hereafter referred as autophagy) [250-252]. It is primarily extracellular proteins and cell-surface membrane proteins that are delivered into the cell in vesicles via endocytosis for the lysosomal degradation. It acts as a coping mechanism for cellular stresses including nutrient or growth factor deprivation, serum starvation, hypoxia and oxidative stress[252], promoting cell survival. Defective autophagy gives rise to neurodegenerative disorders (e.g. Parkinson's disease), lysosomal storage disorders, cancer, Crohn's disease and has been implicated in Paget's disease[253].

1.5.1 UPS

Protein targeted for degradation is tagged with ubiquitin via ubiquitination as outlined above. The consecutive addition of ubiquitin moieties with variable length is termed as polyubiquitination. An isopeptide bond is formed between the ε-amino group of a lysine residue of one ubiquitin and the α-carboxyl terminal glycine of the next ubiquitin in the chain, resulting in the formation of a polyubiquitin chain[254,255]. The polyubiquitin chain with at least four ubiquitin molecules is recognised and rapidly degraded by the 26S proteasomes[256].

The 26S proteasome is a 2.5MDa protease complex which is made up of two subcomplexes: a barrel-shaped, catalytic core particle (20S proteasome) containing a stack of 4 seven-membered rings of proteins around the central core, and one or two terminal 19S regulatory particle(s) that serves as a proteasome activator[257-260]. The 19S regulatory particle recognises folded target proteins which have been covalently conjugated to K48-linked polyubiquitin chain, and unfolds the proteins for translocation into the interior of the 20S proteasome[241,256]. The 20S proteasome bears two outer α-rings and two inner β-rings, which are composed of seven structurally similar α and β subunits, respectively, forming an $\alpha_{1-7}\beta_{1-7}\beta_{1-7}\alpha_{1-7}$ structure[238,261]. The β-type subunits β1, β2 and β5 of each inner ring is catalytically active and has threonine residues at the N-terminus. Moreover, the three β-type subunits also show N-terminal nucleophile hydrolase activity, and are associated with caspase-like, trypsin-like and chymotrypsin-like activities, allowing them to cleave peptide bonds at the C-terminal side of acidic, basic, and hydrophobic amino acid residues, respectively[238,261].

After being recognised by the proteasomes, the polyubiquitinated proteins are cut into small peptides which are then further degraded into amino acids through enzymatic activity and eventually enter the amino acid pool to be recycled into new proteins. The ubiquitin molecules are recycled in the process as well[262,263]. Failure to adequately remove toxic misfolded proteins and oncoproteins, as well as having excess degradation of tumor suppressor proteins leads to the development of a variety of chronic disorders such as neurodegenerative diseases, liposarcoma and human papillomavirus-associated carcinomas[264]. With ageing, the proteasomal system has been shown to decline, resulting in the reduced capability to degrade misfolded proteins which in turn causes the formation of pathological protein aggregates[265-268]. Furthermore, the presence of aggregated proteins

which are resistant to ubiquitin-mediated proteolysis, aggregated β-sheet-rich prion proteins, for instance, blocks the entrance of the 20s proteasome, thereby inhibiting the proteasomal activity[269].

However, studies have shown that several proteins such as IκBα, heat shock protein 70 (Hsp70) and c-Fos also undergo ubiquitin-independent degradation by the 20S proteasome (apart from ubiquitin-dependent degradation by the 26S proteasome, which is the primary route for proteasomal degradation)[270-273]. To be degraded by this route, the proteins must possess unstructured regions caused by ageing, oxidation, or mutation, which allowed the proteins to interact with the proteasome[274,275]. Moreover, intrinsically disordered proteins that are partially or completely unfolded are degraded independent of ubiquitination through 20S proteasome as well[276].

1.5.2 Canonical autophagy

As mentioned above, the autophagy-lysosome pathway which involves lysosomal degradation is another enzyme system to degrade extracellular proteins and cell-surface membrane proteins[277]. Lysosomes are dense cellular membrane-enclosed vesicles that are formed from the Golgi complex and contain digestive and hydrolytic enzymes which are also known as acid hydrolases. Active transport pumps are located in the lysosomal membrane to import hydrogen ions (H^+) into the interior of lysosomes for maintaining the internal pH at pH 5, which is the pH that the acid hydrolases most active at[278]. The lysosomal membrane also bears transporters that deliver the degradation end-products such as glucose, fatty acids, and amino acids, into the cytosol. The autophagy-lysosome pathway is mainly triggered by nutrient starvation and is comprised of initiation and nucleation, elongation, closure and maturation, fusion and degradation.

Initiation and nucleation

Autophagy is initiated with the activation of Unc-51 like autophagy activating kinase 1 (ULK1) complex, which is composed of ULK1, ATG13, ATG101, and focal adhesion kinase family interacting protein of 200kD (FIP200). This leads to ULK1 complex dissociation from mammalian target of rapamycin complex 1 (mTORC1) after dephosphorylation[279] (**Figure 1.6**). It is followed by the recruitment of the class III PI3K complex, consisting of BECN1, vacuolar protein sorting-15 subunit (Vps15), vacuolar protein sorting-34 subunit (Vps34), autophagy/becin-1 regulator 1 (Ambra1), and ultraviolet irradiation resistance-associated gene (UVRAG), to the phagophore assembly site (PAS)[280,281]. No organelle that has similar structure to the yeast PAS was found in mammalian cells, therefore mammalian phagophore is considered to be equivalent to yeast PAS[280,282-284]. In mammalian cells, the endoplasmic reticulum, plasma membrane, outer membrane of mitochondria and recycling endosomes have been reported to contribute to the phagophore with the most comprehensive evidence related to the involvement of the endoplasmic reticulum[285-289].

Elongation

Subsequently, two ubiquitin-like conjugation systems Atg12-Atg5 & the LC3-phosphatidylethanolamine (PE) participate in the phagophore expansion. The Atg12-Atg5 is covalently conjugated by E1- & E2- like enzymes, Atg7 & Atg10, respectively, and associated with Atg16L, in which the forming oligomers serve as E3 ligases, facilitating the conjugation of LC3 to PE[290] (**Figure 1.6**). LC3-PE (also known as lipidated LC3, LC3-II) contributes to the expansion and closure of the autophagosomes. The scaffold protein p62 recognises the ubiquitinated proteins and interacts with the ubiquitin on the cargo noncovalently and LC3-II via the UBA and LC3-interacting region (LIR) domains, respectively, thus delivering the cargo to the autophagosomes[291,292]. The role of p62 in autophagy will be further discussed in **Section 1.5.3**.

Closure and maturation

During maturation, SNARE protein syntaxin 17 is recruited and interacts with homotypic fusion and vacuole protein sorting (HOPS) to promote the membrane expansion and the fusion of autophagosomes with lysosomes[293-295]. SNARE proteins catalyse the fusion of autophagosomes with lysosomes by increasing the permeability of membranes and create an opening for fusion[296,297]. An acidic environment is generated via the fusion with lysosomes which is aided by lysosomal integral membrane protein, lysosomal-associated membrane protein-2 (LAMP-2), SNARE proteins and Rab proteins, resulting in the formation of autolysosomes (**Figure 1.6**).

Fusion and degradation

The internal pH of lysosomes is maintained by the proton pump, vacuolar-type adenosine triphosphatases (V-ATPase) in the lysosomal membrane which actively transports H^+ ions into the lysosomes from the cytosol (**Figure 1.6**). After fusion of autophagosomes with lysosomes, the content of the autolysosomes is degraded into amino acids, fatty acids and nucleotides by lysosomal hydrolases. These degradation products are then released and recycled in the cytosol for reuse in the cell metabolism. The adaptor protein p62 is degraded during the process as well. The autolysosomes then undergo fission and a process known as autophagic lysosome reformation (ALR) to recycle the lysosomal compartment and reform the lysosomes from the autolysosomal membrane, respectively[298,299]. As a result, the lysosomes are prepared and ready for another new cycle of autophagosome initiation[298].

The inhibition of autophagy leads to the accumulation of p62- and ubiquitin-positive protein aggregates[300-302]. A reduction of the protein aggregates was observed in *p62*-deficient mice[303], while overexpression of *p62* enhanced protein aggregation and exerted protective effects on cell survival[292].

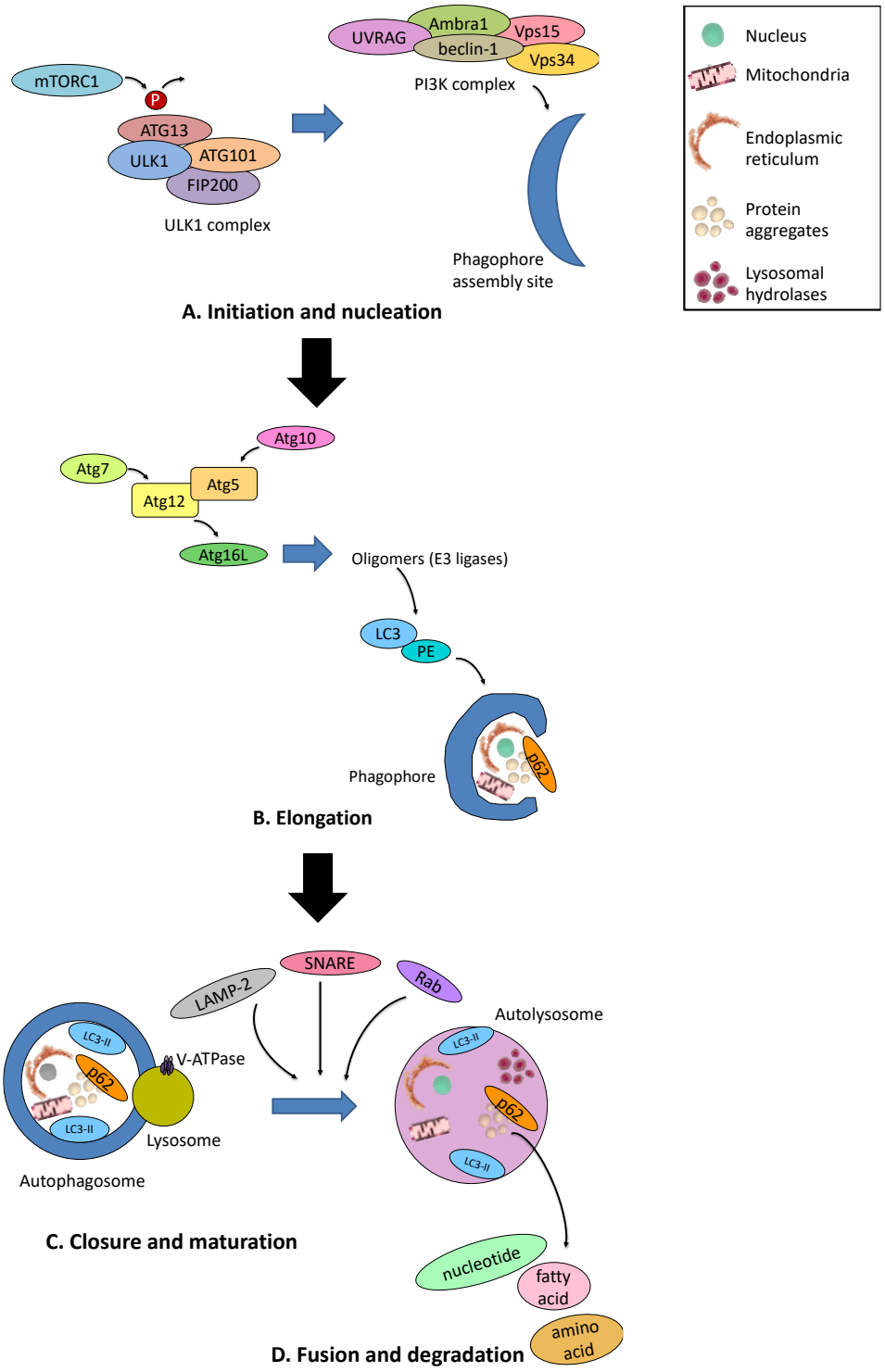

Figure 1.6: Autophagy protein degradation pathway. During early-phase autophagy, ULK1 complex is activated by mTORC1, and recruited to the phagophore assembly site along with PI3K. Atg12-Atg5-Atg16L complex promotes the conjugation of LC3 to PE which leads to the elongation and closure of the autophagosomes. The autophagosomes undergo maturation by fusing with lysosomes to form autolysosomes. Lysosomal hydrolases within the autolysosomes degrade the protein aggregates, followed by the degradation of p62. For more details on this process, please refer to the text.

1.5.3 The role of p62 in autophagy and other signalling pathways

As mentioned in the previous subsection, p62 is a signalling scaffold protein, which recognises the ubiquitinated proteins via the C-terminal UBA domain and delivers the cargo to the autophagosomes via the LIR for lysosomal degradation. In fact, p62 also facilitates proteasomal degradation by interacting with the 26S proteasome via the N-terminal PB1 domain[304-306].

As an adaptor protein, p62 possesses multiple domains including: an N-terminal PB1 domain, a ZZ-type zinc finger domain, a p38 binding sequence (p38BS), two nuclear localisation signals (NLS1/2), a nuclear export signal (NES), a TRAF6 binding sequence (TBS), an LIR, a Keap1-interacting region (KIR), and a C-terminal UBA domain[307,308] (**Figure 1.7**). These domains allow p62 to interact with a number of proteins and involve p62 in diverse array of signalling pathways.

P62 undergoes self-oligomerisation through the PB1 domain to localise to the autophagosome formation site[309-311]. p62 can also hetero-oligomerise with structurally similar adaptor proteins e.g. neighbour of breast cancer 1 gene (NBR1) or other proteins that contain PB1 domain such as atypical protein kinase C (aPKC), MEKK3, MKK5, and ERK via the PB1 domain[312]. Thus, hetero-oligomerisation enables p62 to get involved in osteoclastogenesis and adipogenesis[312]. Indeed, NF-κB signalling, which is essential in osteoclastogenesis, is activated when aPKC and MEKK3 bind to the PB1 domain of p62[313,314]. The binding of receptor-interacting protein (RIP) to the ZZ domain and tumor necrosis factor receptor-associated factor 6 (TRAF6) to TBS aids aPKC and MEKK3, respectively in NF-κB activation[313,314]. Furthermore, p62 mediates the polyubiquitination of TRAF6, which in turn activates the inhibitor of nuclear factor-kappa B kinase (IKK) complex[315]. P62 also inhibits ERK activity and adipocyte differentiation by interacting with ERK through the PB1 domain[316,317].

Interestingly, p62 does not only facilitate the proteasomal degradation of proteins in the cytosol through the PB1 domain, but also in the nucleus via the NLS and NES. The presence of NLS and NES permits p62 to shuttle rapidly between nuclear and cytosolic compartments[305,318]. It has been reported that the nucleo-cytoplasmic shuttling is mediated by p62 phosphorylation at serine 266, threonine 269 and serine 272[305]. Therefore, p62 is

found localised in nuclear aggregates and facilitates proteasome recruitment to the ubiquitinated inclusions in the nucleus[305,319]. To have a more efficient proteasomal degradation, p62 may also export the ubiquitinated cargoes from the nucleus to the cytosol[305].

The nuclear colocalisation of p62 with p38 upon anisomycin stimulation and the positive regulation of p62 in p38 activity via p38BS have been reported[320,321]. Furthermore, p62 was found to be phosphorylated by p38δ in a proteasomal stress-dependent manner which promotes the aggresome formation[322]. p38δ-mediated p62 phosphorylation is also required for mTORC1 activation in response to amino acid stimulation[323]. Although TAK1 (upstream of p38 MAPK) was showed to play a negative role in regulating p62 activity in autophagy, whether it is direct phosphorylation of p62 by TAK1 or indirect interaction via p38 MAPK is yet to be investigated[322,324].

Moreover, p62 acts as a bridge between proteasomal degradation and autophagy-lysosomal degradation. The inhibition of proteasomal degradation causes protein aggregates to accumulate, resulting in the upregulation and phosphorylation of p62 at serine 403 (S403), serine 405 (S405) and serine 409 (S409) in the UBA domain by ULK1[325]. P62 phosphorylation at S409 destabilises the dimer interface of the UBA domain and increases the binding affinity of p62 to ubiquitinated proteins, thereby promoting the autophagic degradation[325]. It has also been demonstrated that the S409 phosphorylation is required for facilitating S405 phosphorylation by ULK1, casein kinase 2 (CK2) or TANK-binding kinase 1 (TBK1), the assembly of autophagy proteins, and the clearance of ubiquitinated proteins[325-327].

Furthermore, proteasome inhibition increases nuclear factor erythroid 2-related factor 2 (NRF2) transcriptional activity due to increased oxidative stress caused by mitochondrial function impairment[328,329]. This in turn promotes p62 gene expression as NRF2 binds specifically to the antioxidant-responsive element (ARE) motif located in the p62 promoter[330]. Moreover, p62 is phosphorylated at serine 351 in the KIR motif, leading to an increase in the binding affinity of p62 to Kelch-like ECH-associated protein 1 (KEAP1), which is a E3 ubiquitin ligase[331]. As a result, NRF2 is activated after dissociating from KEAP1, followed by the translocation into nucleus for the regulation of antioxidant gene expression such as *TXN*, *TXNRD1* and *SRXN1*, which encode for thioredoxin, thioredoxin reductase 1 and sulfiredoxin,

respectively[332,333]. Subsequently, the p62-KEAP1 complex facilitates the protein aggregate clearance through autophagic degradation with the assistance of LC3 and induces a positive feedback loop for NRF2[330,334,335]. In the absence of oxidative stress, inactive NRF2 bound to KEAP1 is retained in the cytoplasm, therefore preventing the nuclear translocation of NRF2[336].

On the other hand, the inhibition of autophagy causes p62 and non-degraded proteins to accumulate in aggregates, which in turn delays the delivery of ubiquitinated proteins to proteasomes and inhibits the proteasomal degradation, compromising the UPS system[337]. No aggregate formation was observed when p62 was knocked out in autophagy-null mice, indicating that the enhanced aggregate formation is due to increased level of p62 during autophagy inhibition[303]. Furthermore, p62 knockdown rescues the effect of autophagy inhibition on the increased level of ubiquitinated proteins, which further demonstrates that p62 is responsible for the UPS substrate accumulation after autophagy inhibition[337]. Interestingly, the effect of alteration of p62 on aggregate formation is independent of autophagy as p62 overexpression has shown to enhance protein aggregation and exhibit a protective effect on cell survival but has no influence on the autophagosome formation[300,338-340]. Moreover, knockdown and knockout of p62 does not seem to impact the autophagic flux in terms of LC3 lipidation and the autophagosome formation after starvation[303,338].

The mutations of *p62/sequestosome 1* (*SQSTM1)* in the UBA domain (with the $p62^{P392L}$ being identified as the most common) are associated with PDB. PDB is characterised by focal and excessive bone turnover, primarily due to abnormal OCs[341]. It is caused by the hyperactivity of OCs followed by a compensatory increase in osteoblastic bone deposition. As a result, the newly formed bone is structurally disorganised and weak with increased risk for deformity and fracture. It has been reported that the OC precursors obtained from patients with PDB were hyper-responsive to receptor activator of nuclear kappa-B ligand (RANKL) and $1,25(OH)_2$ vitamin D_3[342-345]. Furthermore, autophagy has been found to be dysregulated in the $p62^{P394L}$ (the murine equivalent of human $p62^{P392L}$) OCs[253]. More details of PDB will be discussed in **Section 1.6.2**.

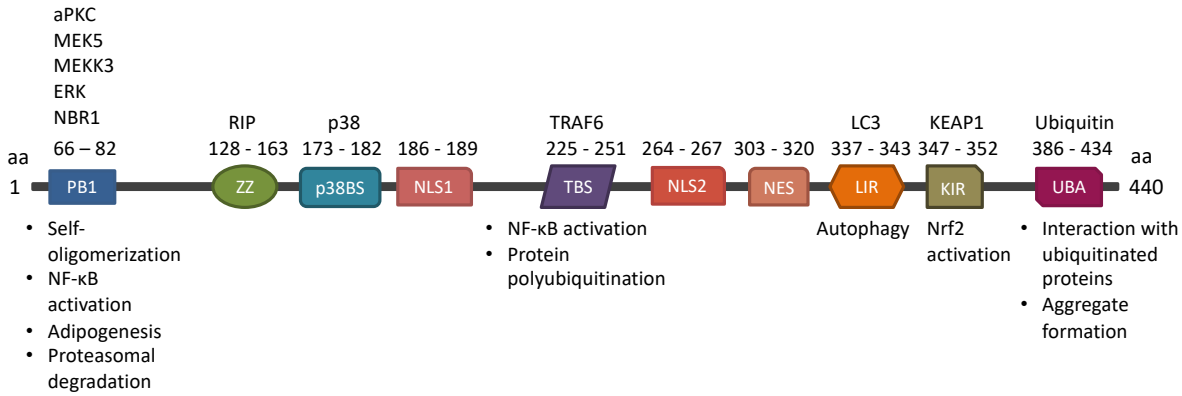

Figure 1.7: The schematic structure of p62 with functional and protein interaction motifs. Interacting partners are indicated above the respective domains and the signalling pathway(s) that the domains are involved in are indicated below. P62 has a number of domains including: an N-terminal Phox and Bemp1 (PB1) domain, a ZZ-type zinc finger domain, a p38 binding sequence (p38BS), two nuclear localisation signals (NLS1/2), a nuclear export signal (NES), a TRAF6 binding sequence (TBS), an LC3-interacting region (LIR), a Keap1-interacting region (KIR), and a C-terminal ubiquitin UBA domain. aa, amino acid; aPKC, atypical protein kinase C; MEK5, mitogen-activated protein kinase kinase 5; MEKK3, mitogen-activated protein kinase kinase kinase 3; ERK, extracellular signal-regulated kinase; NBR1, neighbour of Brca1 gene 1; RIP, receptor-interacting protein; TRAF6, tumor necrosis factor receptor-associated factor 6-binding; LC3, microtubule-associated protein 1A/1B-light chain 3; KEAP1, Kelch-like ECH-associated protein 1. The schematic is adapted from Rea *et al.*[77].

1.5.4 The role of p38 MAPK in autophagy

There have been conflicting reports regarding the role of p38 MAPK in autophagy. It seems that p38 MAPK activation can indirectly promote or suppress autophagy induced by anti-cancer agents such as oridonin, resveratrol and bromelain, in a cell-specific manner[346-349].

Cancer cells are generally found to have downregulation of autophagy in association with tumour progression[350-352]. The anti-cancer agents have been shown to induce autophagy through p38 MAPK phosphorylation. It has been demonstrated that the pre-treatment of resveratrol-challenged glioma cells with p38 MAPK inhibitor, SB203580 reduced the percentage of GFP-LC3-positive autophagosomes, indicating the positive regulation of resveratrol-induced autophagy by p38 MAPK activation[347]. On the other hand, in human hepatocellular carcinoma Huh-7 cells, resveratrol was showed to induce the autophagic cell death by downregulating the expression of P-p38, indicating the negative regulation of autophagy by p38 MAPK[349]. Furthermore, p38 MAPK as a positive regulator in autophagy induced by hepatic-protectant silibinin and bromelain, in human fibrosarcoma HT1080 cells and in mammary carcinoma cells, respectively, has been reported as well[348,353].

On the other hand, there are reports showing negative regulation of autophagy by p38 MAPK. In order to inhibit autophagy, p38 MAPK competes with the transmembrane protein mammalian Atg9 (mAtg9) for binding to p38 interacting protein (p38IP)[354] (**Figure 1.8**). In nutrient-rich medium, autophagy is inhibited due to the presence of P-p38 at the basal level, while mAtg9 is localized at and traffics between the trans-Golgi network (TGN) and peripheral endosomes. Under these conditions, p38IP binds equivalently to mAtg9 on peripheral endosomes, and to P-p38 in the cytosol in which it is required for p38 MAPK activation. Upon the activation of p38 MAPK, mAtg9 dispersion to the cell periphery is inhibited, and the interaction between p38IP and mAtg9 is decreased as p38IP binds to P-p38 with a higher affinity, therefore inhibiting autophagy.

During starvation, the reduction of amino acid levels leads to dephosphorylation of p38 MAPK which causes it to bind to p38IP with lower affinity and favours the interaction between p38IP and mAtg9. Moreover, the equilibrium between p38IP and mAtg9 is disrupted. As a result, mAtg9 traffics to the autophagosome formation sites, thereby facilitating autophagy.

Full medium

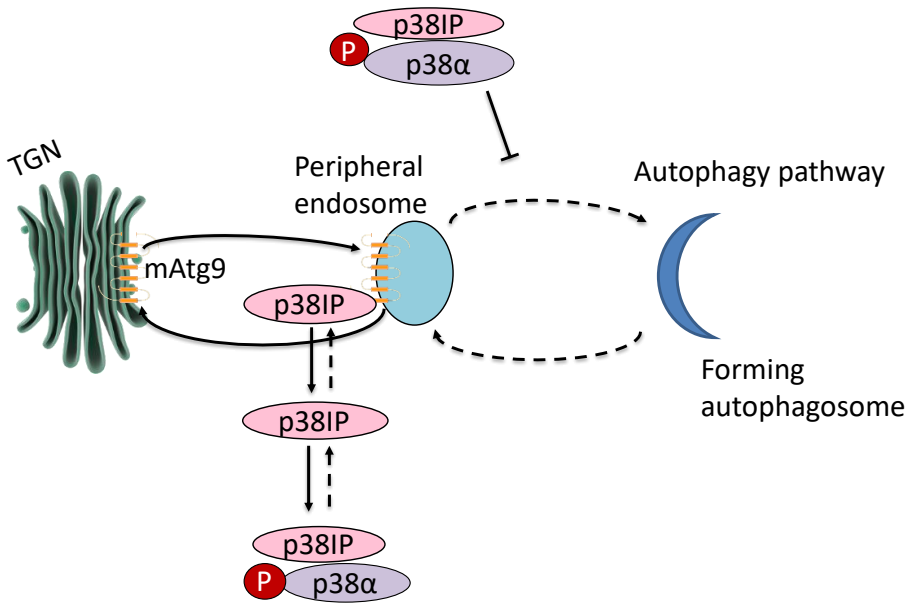

Starvation

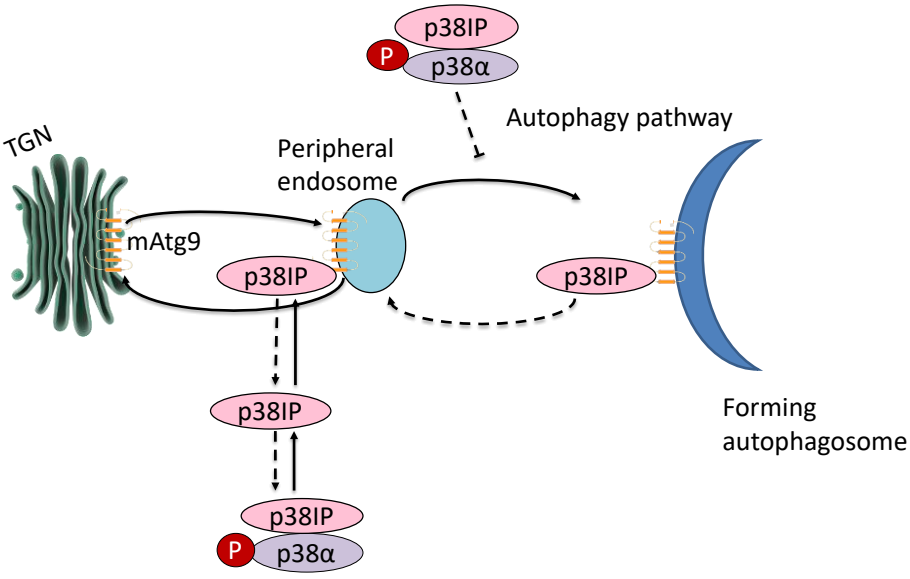

Figure 1.8: Regulation of autophagy by p38α through mAtg9 trafficking and p38IP. In full medium, p38IP interacts with both p38α and mAtg9, but with a higher affinity with p38α thereby decreasing the interaction with mAtg9 and inhibiting mAtg9 dispersion to the cell periphery, which inhibits autophagy. During starvation, p38IP binds with p38α with a lower affinity due to dephosphorylation of p38α caused by reduced level of amino acids. Decreased p38α–p38IP interaction and increased mAtg9–p38IP interaction permits mAtg9 to travel to forming autophagosomes to facilitate autophagy. TGN, trans-Golgi network; p38IP, p38 interacting protein. The schematic is adapted from Webber and Tooze[354].

1.5.5 Autophagy in OCs

As mentioned previously in **Subsection 1.5.3**, mutations of *p62/SQSTM1* in the UBA domain, are associated with PDB. The p62 P394L mutation in mice (equivalent to the p62 P392L mutation in human) causes a pagetic-like phenotype with ageing[253]. The primary cellular abnormality is seen in OCs, which are increase in size, number, nucleation and activity[341,355]. It has been reported that the PDB-associated *p62/SQSTM1* mutations in the UBA domain cause p62 to lose the ability to bind to ubiquitin[356]. As a result, p62 fails to link CYLD with polyubiquitinated TRAF6. The deubiquitination of TRAF6 and the deactivation of NF-κB are disrupted, which enhances OC differentiation and activation[357].

Activation of autophagy has also been reported during osteoclastogenesis. Upregulation of the mRNA expression levels of Atg5, BECN1, Atg7 and Atg12 in mature OCs has been shown, as compared to OC precursors[358]. Furthermore, LC3 lipidation and Atg5 protein expression were found to be increased in a time-dependent manner, in association with p62 degradation during OC differentiation[358]. When p62 was knocked down, the mRNA expression levels of Atg5, Atg7, LC3 and Atg12 were decreased, as well as the mRNA expression levels of TRAP, NFATc1 and Cathepsin K, indicating the inhibition of autophagy activation and osteoclastogenesis[358].

Another study has demonstrated the involvement of autophagic proteins Atg5, Atg7, Atg4B and LC3 in regulating the generation of OC RB, lysosomal secretion and osteoclastic bone resorption[36]. Atg5-deficient OCs showed defective autophagy, impaired RB formation, lysosomal fusion and secretion, resulting in reduced resorptive capacity of the OCs, and hence shallower resorption pits in vitro, increased bone volume in vivo and protection from ovariectomy-induced bone loss[36]. The targeting of LC3 to the RB was reduced as well due to the deficiency of Atg5 in OCs. Similarly, Atg7 was showed to be required for LC3-I to LC3-II conversion, the localisation of CtsK and lysosomal-associated membrane protein 1 (LAMP1) at the RB, and the efficient bone resorption. However, the loss of Atg5 or Atg7 did not affect OC differentiation and actin ring formation.

In contrast, Chung *et al.* showed downregulation of the cell division cycle protein 42 (Cdc42) activity and actin-ring disruption when LC3 lipidation was inhibited in Atg5 siRNA-treated RAW264.7 cells[359]. Moreover, LC3 knockdown inhibited actin ring formation, CtsK secretion and bone resorption activity, but had no influence on OC differentiation, indicating that LC3 mediates OC activity by regulating Cdc42 which is a key regulator of actin cytoskeleton[359].

The efficiency of autophagy declines with age, resulting in the accumulation of intracellular waste products, thereby reducing the ability of the organism to survive under stress conditions[360-363]. Reduced autophagy capability may lead to mitochondrial dysfunction, and thus increased reactive oxygen species (ROS). It has been shown that the deletion of *Atg7* in skeletal muscle and mouse embryonic fibroblasts (MEFs) impaired mitochondrial function and increased ROS levels, respectively[362]. Similar outcomes were reported in pancreatic B cells, T lymphocytes and erythroid cells when *Atg7* was ablated[364-368]. It may also be possible that ROS level is elevated during ageing in an autophagy-independent manner, which in turn causes mitochondrial dysfunction. The damaged mitochondria are unable to be removed effectively due to reduced autophagic activity with age, hence the accumulation of damaged mitochondria followed by enhanced ROS production[369].

Studies have shown that the reduction of autophagic activity and the increased oxidative stress contribute to age-related bone loss, which could eventually lead to the onset of osteoporosis[370-372]. Ma *et al.* showed reduced bone mass in 16-month-old (aged) mice when compared with 3-month-old (young) mice, and decreased autophagic activity in aged bone marrow derived mesenchymal stem cells (BMSCs)[373]. Aged BMSCs displayed reduced osteogenic differentiation and proliferation capacity, in association with increased adipogenic differentiation capacity. Upon treatment of young BMSCs with 3-methyladenine (3-MA), which is an autophagy inhibitor, stem cell senescence was induced due to increased level of ROS[373]. They further demonstrated that treatment with the autophagy inducer, rapamycin, rescued the degenerative fate of aged BMSCs with a decreased level of ROS[373]. Moreover, it has also been reported that the OC number, formation, and activity were reduced in young rats, experimental mouse models of arthritis, and renal transplant patients, respectively after treating with rapamycin[374-376]. In addition, *in vivo* studies showed that autophagy activation has a protective effect on senile osteoporosis[373]. These studies have illustrated the positive

effect of autophagy on OC formation and activity, therefore the reduction of autophagic activity with age may be the factor that contributes to overactivity of OCs which drives increased bone resorption.

Moreover, reduced autophagic activity during ageing also plays a role in the pathogenesis of RA. Monocyte chemotactic protein -1 (MCP-1) which is expressed by mature OCs and found in RA patients, is stimulated by RANK activation and binds to a G-protein-couple receptor, C-C chemokine receptor type 2 (CCR2)[377,378]. This in turn leads to the activation of a zinc-finger protein monocyte chemotactic protein-induced protein (MCPIP) in human monocytes, followed by the induction of ROS synthesis and endoplasmic reticulum stress[378,379]. Consequently, the protein expression of BECN1 which plays an essential role in autophagosome formation, TRAP and cathepsin K, as well as LC3 lipidation are upregulated[379]. MCPIP-induced OC differentiation was inhibited when the monocytes were treated with 3-MA or had *BECN1* or *Atg7* knocked down[379].

Taken together, these data indicate that autophagy plays a role in regulating OC differentiation, activation, and function, and could be a potential therapeutic target for age-related bone disorders. However, the precise mechanisms on how autophagy regulates the OCs in different stages and the effect of ageing are still yet to be studied thoroughly.

1.6 Ageing of bone

Ageing results in imbalanced bone remodelling, mainly due to decreased osteoblast differentiation and activity, in association with an increase in OC differentiation and activity, as well as enhanced adipogenesis, hence lower rate of new bone formation and increased bone resorption[16,380]. This causes net bone loss and eventually reduced bone mass and increased fracture risk[16]. The age-related imbalance in bone remodelling is multifactorial including enhanced oxidative stress and hormonal effects.

As mentioned previously in **Subsection 1.5.5**, reduced autophagic activity during ageing leading to high rate of ROS synthesis is one of the causal factors for age-related bone loss. Moreover, the elevated ROS level can also be caused by increased osteocyte apoptosis with age[381]. It has been shown in animal studies that the oxidative stress plays a pivotal role in bone loss and deterioration of bone strength with age, however, the decline of sex hormones oestrogen and testosterone, worsens the effect of ageing on bone by reducing the defense mechanisms of bone cells against oxidative stress[382]. With increasing age, elevated level of ROS causes the limited pool of beta-catenin (β-catenin) to divert from TCF- to forkhead box O (FOXO)-mediated transcription in osteoblasts precursors[383]. β-catenin mediated transcription overall increases osteoblastogenesis, decreases osteoblast apoptosis and decreases osteoclastogenesis with a net effect of increased bone mass. However, FOXO-mediated transcription has an opposite effect: decreased osteoblastogenesis, increased osteoblast apoptosis and increased osteoclastogenesis with consequent bone loss. Almeida *et al.* further showed that the expression of FOXO target genes was upregulated, while the expression of Wnt target genes was downregulated in C57BL/6 mice in ageing, resulting in decreased osteoblastogenesis and increased osteoclastogenesis, hence low bone mass[383]. The antagonistic effect of increased ROS with age on bone and the shift of balance in favour of FOXO-mediated transcription is thought to contribute to the development of osteoporosis[383].

Furthermore, a progressive decline in the level of circulating growth hormone (GH) and insulin-like growth factor 1 (IGF-1) with age plays a role in the reduction of bone formation[384,385]. It is accompanied by an elevation in the circulating IGF binding protein (IGFBP) level which binds to IGF-1, preventing IGF-1 to bind to its own receptor IGF-1 receptor (IGF-

1R), thereby inhibiting osteoblast differentiation and activity[386-388]. The response of osteoprogenitor cells towards GH and IGF-1 is decreased with ageing as well[384,385]. It has been demonstrated that the bone marrow-derived mesenchymal stem cells (BMSCs) obtained from patients aged 36-43 receiving total knee replacement surgery had a higher response to IGF-1 and the ability to differentiate into osteoblasts, compared to the samples derived from 69–79-year-old patients[384]. The reduction in proliferation and osteoblastic differentiation of BMSCs from aged donors was rescued by overexpressing IGF-1[384].

In addition, ageing causes the lineage commitment of BMSCs to shift from osteoblast lineage to adipogenic lineage[389,390]. Downregulation of osteoblast-specific transcription factors and markers such as Runx2, collagen and osteocalcin were observed in the BMSCs derived from 26-month-old mice, compared to that of 8-month-old mice[389]. In contrast, the expression of adipocyte-specific transcription factor peroxisome proliferator-activated receptor gamma isoform-2 (PPARγ2) was upregulated in the BMSCs from aged mice[389]. In fact, the activation of PPARγ2 (which promotes adipogenesis) suppresses osteoblast commitment, acting as a dominant-negative regulator of osteoblastogenesis and a positive regulator of adipocyte differentiation via the TGF-β/bone morphogenetic protein (BMP) signalling pathway[389,391,392].

Moreover, circulating pro-inflammatory cytokines such as interleukin-6 (IL-6), tumor necrosis factor alpha (TNF-α) and ROS were shown to have a two- to four-fold increase during ageing, even without the presence of chronic inflammatory disease[393]. Both IL-6 and TNF-α contribute to the pathogenesis of RA, which is an autoimmune disorder and is characterised by synovial inflammation, bone and cartilage destruction, swelling, and the involvement of more than one organ or system such as cardiovascular, pulmonary, and skeletal disorders[394]. These pro-inflammatory cytokines promote OC differentiation and activity, as well as inhibiting osteoblastogenesis and osteoblast function. It has been shown that TNF-α induces BMMs to undergo osteoclastogenesis with the assistance of macrophage colony-stimulating factor (MCSF) through the p55 TNF receptor which is expressed on the surface of macrophages[395,396]. On the other hand, the addition of TNF-α inhibited fetal calvaria precursor cells differentiation into osteoblasts in a dose-dependent manner[397]. Furthermore, the mRNA expression level of IGF-1 and Runx2 was also inhibited upon TNF-α treatment, hence arresting the osteoblast differentiation[397,398].

The two most common age-related metabolic bone disorders are osteoporosis and PDB. Each of the diseases will be further discussed in **Section 1.6.1 and 1.6.2**.

1.6.1 Osteoporosis

Bone remodelling is a lifelong process in which the osteoblastic bone formation is tightly coupled to the osteoclastic bone resorption. Peak bone mass is a key predictor of future osteoporosis. Women generally reach the peak bone mass and size at the age of 15 to 20 years and men somewhat later[380]. After the age of about 40-50, the delicate balance between bone formation and resorption is disrupted and shifts to favour bone resorption, resulting in net bone loss[380]. Men have a slow rate of decline in BMD, while the bone loss in women is accelerated when there is a decline in the ovarian function during the perimenopausal period. During and after the menopause, oestrogen deficiency leads to a reduction in the protective effect against oxidative stress, which contributes to the activation of the NF-κB signalling pathway leading to increased osteoclastogenesis. There is also cytokine production and enhanced phosphorylation of $p66^{Sch}$, which is a redox enzyme that augments mitochondrial ROS synthesis and stimulates osteoblast apoptosis[382].

Ageing impairs bone functions, leading to structural and geometric changes in bone, reduced bone mass, low rigidity, increased stiffness, and may eventually result in osteoporosis[399]. Osteoporosis is characterised by low bone mass and deterioration in skeletal microarchitecture with a consequent decrease in bone strength and increase in risk of fracture[400,401]. Osteoporotic bone has a lower Tb.N, a decrease in trabecular thickness and an increase in trabecular spacing. Moreover, cortical thinning and the expansion of medullary cavity due to decreased bone formation on the periosteal surface and increased bone resorption on the endocortical surface is also seen[402]. Osteoporosis is considered a silent disease as it has no clinical symptoms until fractures occur, which lead to significant pain, decrease of physical function, and can cause morbidity and mortality[403]. The most common fractures caused by osteoporosis are spine (vertebrae), hip (proximal femur) and wrist (distal radius)[404]. Osteoporosis severely reduces quality of life and imposes financial burden on the health services worldwide.

1.6.1.1 Epidemiology

As the ageing population is growing, especially those over the age of 65 years, the incidence and risk of having fractures and osteoporosis are predicted to increase. In the United States, 8 million women and 2 million men over the age of 50 years have osteoporosis (based on a T-score of ≤ -2.5), and an additional 34 million individuals have low bone mass with a T-score < -1.0 and are at high risk of developing osteoporosis[405]. According to the United Kingdom General Practice Research Database, the lifetime risk of osteoporotic fracture is estimated to be 1 in 2 for women at the age of 50 years and 1 in 5 for men at the same age[406]. Due to age-related bone loss, the incidence of osteoporotic fractures increases with age. Furthermore, women lose the ovarian function during menopause at about the age of 50, therefore osteoporotic fractures occur in women approximately twice as frequently as in men[404].

Moreover, the incidence of osteoporotic fractures is influenced by ethnicity and race. Scandinavia is reported to have the highest frequency of osteoporotic fractures, while Africa has the lowest[407,408]. The lifetime risk of sustaining a fracture is approximately 14% for white women at the age of 50 years and 5% for white men at the same age, whereas the risk for African Americans is about half these rates[409]. Moreover, geography is one of the factors causing variation as well. In Europe, the rate of hip fractures varies by a factor of approximately 11-fold, with the highest rates in northern Europe and the lowest rates in Mediterranean countries[410].

1.6.1.2 Pathophysiology and clinical manifestations

1.6.1.2.1 Bone remodelling

As mentioned previously in **Section 1.6**, bone mass decreases with age due to age-related changes in bone remodelling, frequently leading to the development of osteoporosis which affects both men and women, or postmenopausal osteoporosis which is caused by the deficiency of oestrogen[411]. As mentioned earlier, OCs typically undergo apoptosis after the bone resorption process which takes approximately 2 weeks to complete, while the osteoblastic bone formation takes 4 months. Low level of oestrogen results in decreased OC apoptosis, extends the resorption phase of the remodelling cycle and expands the erosion depth and space.

Postmenopausal women first experience a short phase of trabecular bone loss which lasts for 3-5 years, followed by a long phase of bone loss that lasts 10-20 years. The latter affects men and women, and involves both cortical and trabecular compartments[412,413]. As postmenopausal women suffer from menopause-related bone loss and age-related bone loss, they are more vulnerable and susceptible to osteoporotic fractures compared to age-matched men[414-416]. Interestingly, fat mass also plays a role in maintaining BMD through the conversion of adrenal androgens (such as androstenedione and dehydroepiandrosterone sulfate, catalysed by the enzyme aromatase found in gonadal tissue and highly expressed in white adipose tissue) to oestrogen, which protects the bones against osteoporosis[417,418]. However, bone loss is accelerated in patients with breast cancer who take aromatase inhibitors that block the conversion of peripheral androgen to oestrogen[417].

1.6.1.2.2 Oestrogen

Oestrogen binds to estrogen receptor (ER, which is a nuclear receptor and can be found in bone marrow stromal cells, OCs, osteoblasts and osteocytes), with high affinity and mediates the differentiation, activity and regulates apoptosis of the bone cells[412,419-421]. ER changes conformation and forms dimers after interacting with oestrogen, which is followed by the binding of the receptor to DNA sequences known as estrogen-response elements (EREs) and the subsequent interaction with transcriptional coactivator or corepressor at the promoter[422]. The expression of oestrogen-responsive genes encoding proteins such as IL-1, IL-6, and IGF-1 is stimulated or inhibited depending on whether the ligand binding to the receptor acts as an

agonist or an antagonist in bone. Moreover, ER can also bind to transcription factors, NF-κB for instance, preventing NF-κB from binding to DNA, thereby inhibiting IL-6 production[423].

Apart from the intracellular nuclear receptor, another class of ERs which are bound to plasma membrane can produce rapid nongenomic effects in response to oestrogen by promoting ERK phosphorylation and repressing JNK activity[424-426]. This results in the induction of OC apoptosis, but inhibition of apoptosis of osteoblasts and osteocytes[424,425]. It has been shown that the activation of ERK signalling pathway induced by oestrogen, was inhibited by specific ERK inhibitor PD98059, which abolished the anti-apoptotic effect of E_2 on osteoblasts and osteocytes[424]. This indicates that the ERK phosphorylation is indispensable for the anti-apoptotic action and bone-protective effect of oestrogen[424]. Furthermore, oestrogen was also demonstrated to exert the osteoprotective action by recruiting osteoblasts and enhancing osteoblastic activity[427]. The recruitment and productivity of osteoblasts were found to be increased in ovariectomised rats treated with E_2 and bisphosphonate 3-amino-1-hydroxypropylidene-1-bisphosphonate (AHPrBP) which supresses bone resorption, compared to just the administration of AHPrBP alone[427]. Thus, oestrogen plays an essential role in promoting the differentiation and activity of osteoblasts, as well as prolonging the lifespan of osteoblasts and osteocytes by inhibiting apoptosis via ERK signalling pathway[427].

As mentioned before in **Section 1.6.1**, the ovarian function in women approximately at the age of 51 starts to decline, resulting in the loss of oestrogen. This causes increased expression of pro-inflammatory cytokines on OCs such as IL-1 and tumour necrosis factor alpha (TNF-α). These cytokines drive OC differentiation by inducing the stromal cells and osteoblasts to produce RANKL, also, by increasing the responsiveness of OC precursors to TNF-α, thereby enhancing OC differentiation and activity, and inhibiting osteoblast differentiation[428-432]. Moreover, TNF-α and IL-1 have anti-apoptotic effects on OCs and contribute to the prolonged OC lifespan, thus accelerating bone resorption. Hence, the bone turnover is increased with resorption outpacing formation, and eventually leading to permanent decrement of bone mass. This is supported by the studies using rodents which showed that mice deficient in either TNF-α or TNF receptor type I (TNFR1) p55 or treated with TNF-binding protein which is a TNF inhibitor were protected from ovariectomy-induced bone loss[433-435].

Furthermore, oestrogen increases the production of OPG by osteoblasts and stromal cells, which acts as an antagonist of RANKL and therefore inhibits OC formation and activity by preventing RANKL from binding to RANK[436-438]. Therefore, oestrogen deficiency reduces OPG production and increases the ratio of RANKL to OPG, resulting in enhanced OC differentiation, excessive bone resorption, and induction of bone loss. It has been reported that the mRNA expression of OPG was reduced in osteoblasts and BMSCs derived from aged animal and human subjects[439-442]. This shows that the profile of pro-osteoclastogenic factors is increased in ageing bone, shifting the balance to favour OC differentiation and activity, thus promoting bone resorption and accelerating bone loss[443].

1.6.1.2.3 Calcium, vitamin D and parathyroid hormone (PTH)

Calcium depletion and vitamin D deficiency contribute to secondary hyperparathyroidism and are involved in the pathogenesis of osteoporosis as well. The calcium intake is decreased in ageing, but the amount of calcium required to maintain the calcium balance is increased with age due to the reduction in intestinal calcium absorption and in the efficiency of kidney reabsorption[444]. The dietary calcium requirement for adults is approximately 700 mg/day and is increased to about 1300 mg/day for the elderly to maintain the calcium balance[445,446]. As a result of decreased serum calcium, parathyroid glands are stimulated to secrete PTH which reduces urinary calcium excretion and induces OC activity and bone resorption, hence bone loss (predominantly in the cortical compartment)[447,448]. PTH has also been shown to stimulate intestinal calcium absorption[449].

Moreover, a decline in glomerular filtration rate with ageing results in impaired kidney function and decreased hydroxylation of 25-hydroxyvitamin D_3 by the 25(OH)D-1α-hydroxylase to the active hormonal form of vitamin D, 1,25-$(OH)_2D_3$[450]. This causes a decrease in gastrointestinal calcium absorption and a decrease in serum calcium which stimulates the secretion of PTH. The calcium storage in bones is mobilised when there is excessive PTH secretion, which together with reduced intestinal calcium absorption, leads to a negative calcium balance and contributes to bone loss[451,452]. 1,25-$(OH)_2D_3$ stimulates osteoblasts through the Vitamin D receptor (VDR) to express RANKL, which promotes osteoclastogenesis, however recent evidence suggests that vitamin D also promotes osteoblast differentiation

and bone formation, as well as increases the OPG mRNA expression in osteoblasts, therefore, the deficiency in vitamin D contributes to bone loss[453].

1.6.1.3 Diagnosis and management of osteoporosis

According to the World Health Organisation (WHO), a BMD at the lumbar spine, total hip or femoral neck which is measured by dual-energy X-ray adsorptiometry (DXA) and falls 2.5 standard deviations below the mean for young healthy adults of the same gender (*T-score* of 2.5 or less) is diagnosed as osteoporosis[454,455]. DXA is a highly precise X-ray-based technique that uses two X-ray sources of energies with low level of radiation to estimate the area of mineralised tissue and the bone mineral content (BMC) is divided by the area.

Management of osteoporosis aims to reduce fracture risk. Calcium and vitamin D supplementations are important in cases of low calcium intake and suboptimal vitamin D levels, respectively. Calcium can be found in dairy products such as milk, yogurt and cheese as well as in fortified food, cereals, juices and crackers for instance, while vitamin D is produced naturally in the skin through sunlight exposure. It has been shown that adequate calcium and vitamin D intake reduces bone loss and supresses bone turnover[456]. Calcium supplementation was demonstrated to decrease the bone remodelling unit (BMU) remodelling space which is the number of osteoclastic resorption cavities spread across the bone surface[457]. Moreover, the hip fractures and non-vertebral fractures were reduced by approximately 30% in 3270 women who had optimal calcium and vitamin D intake, indicating the reduction in the risk of hip fractures and non-vertebral fractures by both the supplementations[458,459].

When considering pharmacologic intervention, two main classes of agents that are available for the treatment of osteoporosis are most commonly used in clinical practice: antiresorptive drugs which suppress OC activity and anabolic drugs which target osteoblasts to enhance bone formation.

1.6.1.3.1 Antiresorptive agents

This class of agents includes bisphosphonates and the RANKL antibody, denosumab.

Bisphosphonates

The nitrogen-containing bisphosphonates such as alendronate, risedronate and zoledronic acid (ZA) are potent anti-osteolytic compounds that have been used widely for the prevention and treatment of osteoporosis. Bisphosphonates supresses protein prenylation by inhibiting activity of the enzyme farnesyl pyrophosphate synthase in the mevalonate pathway, thereby disrupting intracellular protein trafficking, which is necessary for OC function and survival, thus reduce the OC number and induce OC apoptosis[460-464]. Moreover, the agents also increase secondary mineralisation of preformed osteons[465].

Bisphosphonates can be administered orally or intravenously, but side effects are common. The oral bisphosphonates may give rise to upper gastrointestinal complications such as abdominal pain, nausea, gastritis, esophagitis and diarrhoea, while the intravenous bisphosphonates may lead to fever and flu-like symptoms[404]. Patients must remain upright for 30-60 minutes after taking the oral bisphosphonates to prevent complications[466]. On the other hand, acetaminophen and antihistamine when administered concurrently help in minimising the risk of complications arising from intravenous bisphosphonates[466].

Alendronate and risedronate are oral bisphosphonates effective in increasing BMD and reducing the risk of vertebral, non-vertebral and hip fractures in postmenopausal women with osteoporosis. It has been reported that the 3658 women with osteoporosis who received alendronate therapy for 3-4 years had a reduced risk of developing a fracture by 48%, compared to placebo[467]. Furthermore, combination therapy of etidronate and alfacalcidol also showed an additive effect on BMD[468]. According to a double-blind, multicenter clinical trial of 414 women who received the combined therapy, the BMD was effectively maintained, and the incidence of new fractures was reduced[468]. Some bisphosphonates have long retention in bones and may exert long-term effects, resulting in the oversuppression of bone turnover, hence increased risk of atypical femoral fractures[469,470]. Other rare, related side effects of long-term exposure to bisphosphonates include osteonecrosis of the jaw and osteonecrosis of the external ear canal.

Denosumab

Denosumab is a fully human monoclonal antibody against RANKL that inhibits the differentiation and activity of OCs and is administered subcutaneously every 6 months for osteoporosis treatment. The agent increases BMD, reduces bone turnover and reduces the risk of hip, vertebral and non-vertebral fractures. However, it has been shown that BMD of the lumbar spine and total hip decreases by 6.6% and 5.3% respectively, which is associated with an increased bone turnover within the first 12 months after stopping the treatment[471], and there is an increased vertebral fracture risk as well[472]. The withdrawal effects can be reversed with the resumption of treatment. It has been demonstrated that the BMD of lumbar spine increased by 9.0% when the therapy was resumed[471]. However, long term use related side effects due to oversuppression of bone turnover have been reported.

1.6.1.3.2 Anabolic agents

Teriparatide is a recombinant form of the human PTH consisting of N-terminal 34 amino acids that stimulates both bone resorption and formation and is very effective for osteoporosis treatment. It is administered daily by subcutaneous injection for 18-24 months to increase BMD and reduce the risk of new vertebral fractures[473-475]. It has been shown that the risk of vertebral and non-vertebral fractures was reduced by 70% and 50% respectively, in postmenopausal women with osteoporosis who received teriparatide treatment at a dose of 20 μg per day for 21 months[475]. In fact, early treatment with teriparatide displayed a more pronounced increase in lumbar spine and total hip BMD, compared to alendronate treatment[476]. Additive effects on BMD were seen when using a combination treatment of teriparatide with bisphosphonates or denosumab[477,478]. The main drawback of teriparatide use is the relatively short timeframe (up to 2 years) due to potential for overstimulation of osteoblasts with consequent transformation to osteosarcoma.

1.6.2 PDB

PDB is the second most common metabolic bone disease after osteoporosis. PDB is named after Sir James Paget, a prominent English surgeon and pathologist, who first believed this condition to be a rare inflammatory bone disorder and described it as osteitis deformans[479]. It is a late-onset, chronic, focal skeletal disorder that affects one (monostotic) or more areas (polyostotic) of the skeleton, which are characterised by a high rate of bone remodelling[480]. PDB begins with increased osteoclastic bone resorption followed by a compensatory increase in osteoblastic bone formation in association with inefficient mineralisation. This results in the production of woven bone, which is weak (eventually becomes sclerotic), has a disorganised pattern and is more susceptible to fractures and deformities[481]. The rate of bone turnover at the affected sites is approximately 20 times higher than the normal rate and the hematopoietic marrow is replaced by highly vascular fibrocellular marrow[480,482]. PDB mostly affects individuals over 50 years of age[483]. Although most patients are asymptomatic, others present with a variety of symptoms and complications such as bone pain, bone enlargement, deformity and fracture[484,485]. The most common affected bones are the pelvis (70% of cases), femur (55%), lumbar spine (53%), skull (42%) and tibia (32%)[486,487]. Very rarely PDB can undergo sarcomatous transformation[486].

1.6.2.1 Epidemiology

Prevalence of PDB varies by ethnicity and geographical regions, and is most common in the United Kingdom and Western Europe (especially Spain, Italy, France), but it is low in Scandinavia and Switzerland[488]. In the United Kingdom, it affects 1-2% of the population aged 55 and above, but the prevalence increases with age to affect 8% of the population aged over 80[485,489,490]. High prevalence is also found in North America, Australia and New Zealand, which has been attributed to the migration of British nationals in early 18th–20th centuries, whereas the disease is rare in the native populations [491]. Based on the analysis of hospital radiographs obtained over the period 1971-1975, the prevalence in the United States and France is estimated to be 1-2% and 1.1-1.8%, respectively[492-494]. PDB is rare in the Indian subcontinent, Africa, Southeast and East Asia[485,488-490]. Overall, PDB is more prevalent in men than in women and affects about 2.5% men aged 55 and above and 1.6% women at the same age[489]. The incidence and severity of PDB in most countries except Italy has declined in recent years, to

only approximately 10-20% of those seen 20-30 years ago[495]. The changes in migration patterns with increased immigration from countries of low incidence, the change in lifestyle, improved nutrition and a lower exposure to infections may all have contributed to the decrease in the prevalence of PDB[488].

1.6.2.2 Pathophysiology

PDB is characterised by focal and excessive bone resorption coupled with accelerated bone formation. The pathologic process is initiated by an osteolytic phase which involves focal increase in bone resorption by larger and more nucleated than normal, and higher number of OCs in association with marked hypervascularisation[495-498]. Pagetic OCs may contain up to 100 nuclei in a single cross-section compared to 3-20 nuclei found in normal OCs. Furthermore, total surfaces resorbed by the hyperactive OCs is increased by approximately seven-fold with an erosion rate of 9 μg/d, which is also increased by about nine-fold as compared to the normal rate of 1 μg/d[497,499]. It is followed by the mixed phase of osteolytic and osteoblastic activity which is characterised by enhanced bone formation by higher number of overactive but morphologically normal osteoblasts[496-498]. The newly formed bone is abnormal with collagen fibres being placed in a disorganised manner, resulting in the formation of mosaic pattern of woven bone which has reduced mechanical strength and load-bearing capacity, thus high risk for deformity and fracture. Although both the activity of OCs and osteoblasts are present, the osteoblastic bone formation is dominant in this phase. Subsequently, it enters the final sclerotic phase in which the osteoclastic bone resorption declines progressively, and the osteoblastic bone formation predominates. Despite the increased production of osteoid, the thickness of the osteoid seams is decreased, leading to the formation of thick, dense and less vascular bone with haphazardly arranged collagen fibres, which is weaker[497].

Pagetic OC precursors are hypersensitive to RANKL and 1,25-$(OH)_2D_3$, resulting in enhanced OC activity and bone resorption. Moreover, the expression of proto-oncogene *c-fos*, antiapoptotic oncogene *Bcl-2*, IL-6, IL-6 receptor and NF-κB in pagetic OCs is upregulated which could partly explain the increased recruitment of OC precursors, OC number, OC activity and resistance to apoptosis[500-502]. Furthermore, the expression of RANKL in marrow stromal cells from pagetic lesions mediated in part by IL-6 is elevated[503]. OCs of pagetic bone

frequently contain nuclear or cytoplasmic inclusions, indicating the involvement of autophagy dysregulation in the pathogenesis of PDB[253,355].

1.6.2.3 Environmental factors

Incidence and severity of PDB have reduced in many continents such as Europe, Oceania and North America over recent years, suggesting that environmental factors may play a role in causing PDB[504]. Viral infection is the most widely studied potential environmental trigger for PDB. Cytoplasmic and nuclear inclusion bodies resembling paramyxovirus (measles and canine distemper virus) which were thought to be viral nucleocapsids were observed in pagetic OCs[505]. This led researchers to propose that the slow paramyxovirus infection of OC precursors may contribute to the causation of PDB.

Nevertheless, no conclusive evidence has been found in subsequent studies on the role of viral infection in PDB as some studies (possibly conducted from a group of researchers presumably from the same laboratory) showed positive results[506-508], but others showed negative results[509-512]. It is possible that this disparity was due to polymerase chain reaction (PCR) contamination or the difference in the sensitivity of reverse transcription polymerase chain reaction (RT-PCR) approach in detecting the virus. However, the most comprehensive study performed by Ralston *et al.* investigating this issue on a blinded basis using the most sensitive assays evaluated failed to detect measles or canine distemper transcripts in pagetic samples[513]. Moreover, no evidence was found to suggest that the RT-PCR assays used in the laboratories that failed to detect the viral transcripts were less sensitive[513]. However, as the incidence of canine distemper or measles virus infection reduced after the introduction of vaccination in European countries, it has been proposed that the viral infection may be responsible for the decline in the frequency of PDB.

On the other hand, arsenic pesticide (calcium arsenate) which was used to combat boll weevils in Lancanshire cotton mills predominantly from the American cotton belt, has been speculated to play a role in the aetiology of PDB as well[514]. Lancashire has historically had a high incidence of PDB. A considerable amount of wastewater containing arsenic was discharged from the cotton mills. The incidence of PDB remained high during 1917-1945 when

the pesticide was intensively used, and gradually declined after 1974 when the pesticide use was reduced[514]. Yet, no direct evidence was found to support this notion.

In addition, childhood dietary calcium deficiency[515], vitamin D deficiency that leads to childhood rickets[516] and excessive mechanical loading of the skeleton[517] have all been suggested as environmental triggers for PDB.

1.6.2.4 Genetics of PDB

Genetic factors play a crucial role in the pathogenesis of PDB. It has been proposed that susceptibility to PDB may result from a combination of rare pathogenic large-effect mutations that cause autosomal dominant inheritance of the disease and more common small-effect variants that predispose to the disease[518,519]. Based on the linkage studies in families and genome-wide association studies (GWAS), several candidate genes that predispose to PDB have been identified. The genes implicated in rare PDB-like syndromes and PDB are *TNSRSF11A* which encodes RANK*, TNSRSF11B* which encodes OPG*, VCP* which encodes valosin-containing protein and *SQSTM1* which encodes p62. Most of these genes are involved in the differentiation and function of OCs. Mutations in some of these genes lead to a spectrum of rare bone disorders which exhibit clinical, radiological, or histological features similar to PDB. These include: familial expansile osteolysis (FEO)[520], expansile skeletal hyperphosphatasia (ESH), early onset familial Paget's disease (EoPDB), juvenile PDB (also known as idiopathic hyperphosphatasia), and the syndrome of hereditary inclusion body myopathy with early onset Paget's disease of bone and fronto-temporal dementia (IBMPFD).

Activating duplication in *TNFRSF11A* encoding RANK causes FEO, ESH and EoPDB which share several features in common including the presence of focal osteolytic lesions, premature deafness and premature tooth loss (**Figure 1.9**)[521-524]. Inactivating mutations in *TNFRSF11B* encoding OPG promote the binding of RANKL to RANK, thus enhanced OC differentiation and activity, leading to Juvenile PDB[521,525,526]. Loss of function mutations in *VCP* cause IBMPFD which may be due to impaired degradation of target proteins as VCP binds to ubiquitylated proteins and helps target them for proteasomal degradation[527,528].

SQSTM1 is the most important susceptibility gene for classical PDB and the mutations affecting this gene were identified as a common cause of PDB. Mutations in *SQSTM1* are

found in up to 40% of patients having a positive family history of PDB and approximately 10% of patients with sporadic PDB[521,529-531]. Relatives of an affected individual have a 7- to 10-fold higher risk of developing PDB compared to relatives of an unaffected individual[532,533]. In most families, PDB segregates in an autosomal dominant manner with incomplete penetrance that increases with age[533-537].

Following the identification of a susceptibility locus for PDB on chromosome 5q35 via genomewide search and studies on French Canadian families, subsequent positional cloning studies and mutation screening of genes within the region allowed Laurin *et al.* to identify a mutation in exon 8 of *SQSTM1* in affected patients, causing a proline to leucine amino acid substitution at codon 392 (P392L) of the protein[531]. In a parallel independent study Hocking *et al.* also identified the same mutation and truncating mutations at codons 390 and 396 of *SQSTM1* in other, predominantly British families affected by PDB[530]. The presence of truncating mutations tends to increase disease severity shown by the genotype-phenotype analysis[538]. Among the approximately 30 different missense or non-sense mutations which all affect the p62 UBA domain or are in its close proximity[539], P392L is the most common p62 mutation[531,538,540,541]. Since all PDB-associated mutations affect the p62 UBA domain (or are relatively close by), aberration in ubiquitin-mediated degradation of proteins that interact with p62 via the domain may be involved in the mechanism of how the mutations cause PDB. In fact, both missense and non-sense PDB-causing mutations in the UBA domain of a full-length p62 lead to a loss of function in the binding affinity for poly-ubiquitin chains[356]. This impairs p62 interaction with CYLD (which inhibits NF-κB activity and osteoclastogenesis), hence prolonged activation of NF-κB and increased OC differentiation[71,72] (Refer to **Sub-section 1.3.1.1.3** for more details).

Based on GWAS of PDB patients not carrying *SQSTM1* mutation, other susceptibility genes for PDB have been identified (**Table 1.1**). The genes implicated include colony stimulating factor 1 (*CSF1)*, nucleoporin 205 KDa (*NUP205)*, *TM7SF4*, optineurin (*OPTN)*, ras and rab interactor 3 (*RIN3)*, promyelocytic leukemia gene (*PML)*, *TNFRSF11A*.

Table 1.1: Candidate genes for PDB susceptibility.

Chromosome locus	Nearest susceptibility gene	Protein	Function	Reference
1p13	*CSF1*	MCSF	Involved in OC differentiation, activity and survival	[41,542]
7q33	*NUP205*	NUP205	Regulates transport between the cytoplasm and nucleus	[543]
8q22	*TM7SF4*	DC-STAMP	Involved in OC cell-cell fusion	[88,544]
10p13	*OPTN*	OPTN	Negatively regulates OC differentiation, involved in NF-κB signalling and autophagy	[545,546]
14q32	*RIN3*	RIN3	Involved in vesicular trafficking between the Golgi apparatus and the plasma membrane	[547,548]
15q24	*PML*	PML	Involved in regulating TGF-β signalling, cell growth, apoptosis and cell senescence	[549,550]
18q21	*TNSRSF11A*	RANK	Interacts with RANKL and induces OC differentiation	[56,57,551]

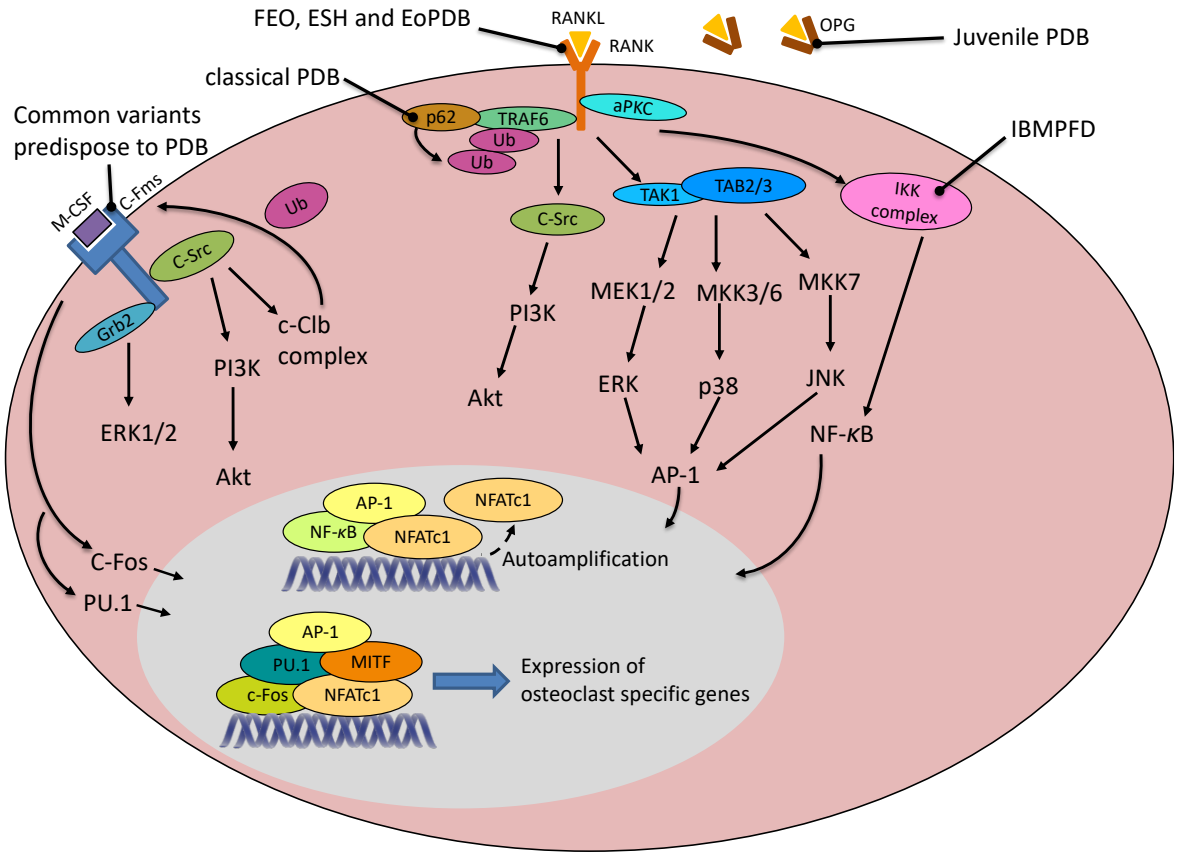

Figure 1.9: Components of the RANKL-RANK-NFκB signalling pathway that are implicated in the pathogenesis of PDB and rare PDB-like syndromes. Mutations or polymorphisms identified in the respective osteoclastogenic genes either disrupt the protein degradation system or promote OC differentiation by enhancing the NF-κB signalling, therefore causing classical PDB or rare PDB-like syndromes. FEO, familial expansile osteolysis; ESH, expansile skeletal hyperphosphatasia; EoPDB, early onset familial Paget's disease; IBMPFD, inclusion body myopathy with early onset Paget's disease of bone and fronto-temporal dementia.

1.6.2.5 Management of PDB

Currently, there is no cure for PDB, however pharmacological therapy using bisphosphonates is recommended for bone pain due to active PDB[552]. Pain management using analgesics and surgical intervention may also be indicated to relieve symptoms and complication caused by PDB. According to current recommendations[552], the treatment aims to control bone pain rather than supress bone turnover.

Bisphosphonates

Among different types of bisphosphonates, ZA is the gold standard for PDB due to its high potency, prolonged duration of action, rapid normalisation of bone turnover markers and a favourable effect on pagetic pain. Reduced bone turnover allows the replacement of poorly mineralised woven bone with normal lamellar bone and the healing of radiologic lesions[553]. ZA is typically administered intravenously as a single infusion at a dose of 5 mg and is the most potent drug in which its therapeutic effect can be sustained for at least 6 years[554]

Risedronate is another treatment option. Risedronate for treatment of PDB is given orally at a daily dose of 30 mg for 2 months. The patients are required to take it first thing in the morning after an overnight fast and wait for a minimum of 30 minutes before having breakfast to achieve adequate absorption and to prevent common adverse effects such as dyspepsia. Risedronate has been shown to be effective in relieving pain and in normalising ALP[555-557].

Two randomised, double-blind, controlled trials of 6 months duration were conducted to compare the efficacy between a single 15 minutes infusion of ZA at 5 mg and 30 mg of oral risedronate for 2 months showed superiority of ZA over risedronate in terms of faster and more profound normalisation of ALP (which lasted for a longer period of time), and an improved quality of life in the ZA group compared to the risedronate group[558]. A subsequent study has shown that the patients who received ZA had an over 90% chance of not relapsing for at least 6.5 years[554]. Nevertheless, so far there is no strong evidence that either therapy is able to prevent the development of complications of PDB[529].

1.6.2.6 Animal models of PDB

In order to investigate the genetic versus the environmental aspect of PDB, groups of investigators have generated transgenic mice via genetic modification.

Kurihara *et al.* showed that targeted measles virus nucleocapsid gene (MVNP) to cells in the OC lineage (linked to the *TRAP* promoter) in transgenic mice increases the OC number and OC nuclearity formed in marrow cultures, in response to 1,25-$(OH)_2D_3$, but not in response to RANKL[559]. Furthermore, 29% of 12-month-old mice had abnormal morphology of cancellous bone in at least 2 vertebrae out of 4 examined, with significant increased OC and osteoblast perimeters accompanied by increase in bone volume, trabecular width and Tb.N compared with WT controls[559]. A remarkable increase in the amount of woven bone was observed in the MVNP transgenic mice as well, suggesting that targeted expression of MVNP in OCs is sufficient to induce bone phenotype that resembles to a degree PDB[559]. This study supports the notion for a potential viral cause of PDB.

Moreover, Kurihara *et al.* from the same laboratory generated transgenic mice that express human $p62^{P392L}$ (linked to the murine *TRAP* promoter) in OC precursors and OCs[560]. OC precursors obtained from these transgenic mice were hyper-responsive to RANKL and TNF-α, resulting in enhanced NF-κB signalling[560]. This was accompanied by an increased number of OCs and progressive bone loss[560]. Moreover, the OC perimeter was found to be increased, and the cancellous bone volume, trabecular width and number were decreased based on the histomorphometric evaluation[560]. Nevertheless, increase in the responsivity to 1,25-$(OH)_2D_3$, in osteoblast number and perimeter as seen in PDB were not observed in this study[560]. In addition, nuclear inclusions were absent in OCs from these transgenic mice as well[560]. Therefore, these findings were suggested to indicate that the expression of $p62^{P392L}$ in OCs may be insufficient to induce PDB-like phenotype in mice, thus arguing against the genetic aetiology of PDB. However, Kurihara *et al.* did not examine long bones for lesions using μCT and the histology was only performed on vertebrae for the purpose of histomorphometry, thus pagetic-like lesions may have been missed.

In contrast, our group generated the mouse model of PDB by introducing the p62 P394L mutation (equivalent to the P392L mutation in humans) into the germline. These mice

carrying the P394L mutation ($p62^{P394L}$) begin to exhibit focal osteolytic lesions detectable by μCT at 8 months of age, and the phenotype continues developing over the life course at least until 12 months of age[253]. Focal cortical thickening and bone expansion is present in the affected bones[253]. Moreover, these lesions are characterised by excessive and disorganised bone remodelling with increased numbers of OCs, numbers of nuclei per OC, and increased bone formation, leading to the accumulation of woven bone[253]. Furthermore, nuclear inclusions are seen in pagetic-like OCs by electron microscopy and there is evidence for dysregulated autophagy in the OC lineage[253]. Finally, ZA prevents the development of the pagetic-like lesions in the $p62^{P394L}$ mice mimicking the treatment effect of ZA in established PDB in humans[561], which validates this mouse model of PDB and provides evidence for the genetic aetiology of PDB.

The discrepancy of findings between the germline knock-in and OC-specific transgenic model is difficult to explain, however μCT was not used for lesion detection as already mentioned and there have been other methodological differences. Interestingly, a previous independent study conducted by Hiruma *et al.* which generated a similar mouse model to the $p62^{P394L}$ described above, carrying the same germline mutation revealed that the RANKL expression of marrow stromal cells was increased, thereby enhancing OC differentiation[562]. Nevertheless, neither pagetic OCs nor focal pagetic lesions were found in these mice on screening using histology[562], which is explained by the focality of the lesions and the necessity of μCT to first identify the lesions and then verify them by targeted histology.

P62 deletion leads to impaired osteoclastogenesis *in vitro* and *in vivo*[563], and to mature-onset obesity and insulin resistance[317]. Surprisingly, the $p62^{-/-}$ mouse model was reported recently by Zach *et al.* (whilst my work was in progress)[357] to show Paget's disease-like small intra-cortical osteolytic lesions in the distal femoral diaphysis at the age of 21 months on TRAP-stained bone sections[357]. This was accompanied by increased OC number, increased multi-nucleation status and sensitivity to RANKL in bone morrow-derived stem cells *in vitro*, elevated levels of bone turnover, and pronounced accumulation of adipocytes in the bone marrow[357]. However, their study lacks a detailed bone phenotype analysis by μCT.

1.7 Aims

Both p38 and p62 play an important role in OC differentiation. In ageing, OC differentiation is increased, and OCs are hyperactive. However, the underlying causal mechanism remains unknown. The overall aim of this project was to understand the role of p38 in the differentiation of OCs with ageing and the role of p62 on age-related bone loss. The specific aims were:

1. Determine the role of p38 and MAPK signalling pathway in age-related increased osteoclastogenesis
2. Understand the role of p38 and autophagy during osteoclastogenesis in ageing
3. Determine the effect of p62 deletion on age-related bone loss

Chapter 2: Materials and methods

2.1 Reagents

Table 2.1 List of reagents

Reagent	Catalogue number	Company
alpha-minimum essential medium (α-MEM)	32571	Life Technologies, USA
Accutase	A1110501	Fisher Scientific, USA
Analine Blue	415049	Sigma Aldrich, UK
Anti-beta Actin antibody [AC-15]	ab6276	Abcam, UK
Anti-FAM48A/P38IP	SAB4200382	Sigma Aldrich, UK
Anti-LC3 pAb	PM036	MBL, Japan
Anti-NFAT2 antibody	ab25916	Abcam
ATG9A rabbit Polyclonal antibody	26276-1-AP	Proteintech, USA
$CaCl_2 \cdot 2H_2O$	223506	Sigma Aldrich, UK
Calcein Blue	M1255	Sigma Aldrich, UK
Chameleon Duo Pre-stained Protein Ladder	928-60000	LI-COR Biosciences, UK
Chloroform	C2432	Sigma Aldrich, UK
Di-butyl phthalate	524980	Sigma Aldrich, UK
DMSO	0231	VWR, USA
Ethanol (histology)	A405P-4	Fisher Scientific, USA
EvoScript Universal cDNA Master	07912455001	Roche, Switzerland
Fetal Bovine Serum	S13871S1810	Biowest, USA
Goat anti-Rabbit IgG (H+L) Cross-Adsorbed Secondary Antibody, Alexa Fluor (AF) 488	A-11008	Fisher Scientific, USA
Goat anti-Mouse IgG (H+L) Cross-Adsorbed Secondary Antibody, AF594	A-11072	Fisher Scientific, USA
Goat anti-Mouse IgG (H+L) Cross-Adsorbed Secondary Antibody, AF594	A-11005	Fisher Scientific, USA
Hydrochloric acid	320331	Scientific Laboratory Supplies, UK
IκBα (L35A5) Mouse mAb (Amino-terminal Antigen)	4814	Cell Signaling Technology, USA
Intercept® (TBS) blocking buffer	(TBS)927-50010	LI-COR Biosciences, UK

IRDye® 680RD Goat anti-Mouse IgG Secondary Antibody	926-68070	LI-COR Biosciences, UK
IRDye® 680RD Goat anti-Rabbit IgG Secondary Antibody	926-68071	LI-COR Biosciences, UK
IRDye® 800CW Goat anti-Mouse IgG Secondary Antibody	926-32210	LI-COR Biosciences, UK
IRDye® 800CW Goat anti-Rabbit IgG Secondary Antibody	926-32211	LI-COR Biosciences, UK
LightCycler 480 probes master	04887301001	Roche, Switzerland
MCSF	cyt-439	Prospec, Israel
MEK-3/6 (B-1)	sc-136982	Santa Cruz Biotechnology, USA
Methoxyethyl acetate (MEA)	109886	Honeywell, USA
Methyl methacrylate (MMA)	1955909	Sigma Aldrich, UK
$MgCl_2 \cdot 6H_2O$	M2670	Sigma Aldrich, UK
Mouse IgG	I-2000	Vector Laboratories, USA
NaCl	S7653	Sigma Aldrich, UK
$NaHCO_3$	S8875	Sigma Aldrich, UK
Na_2HPO_4	S0876	Sigma Aldrich, UK
Naphtol ASBI-phosphate	N2125	Sigma Aldrich, UK
Normal goat serum blocking solution, 2.5%	S-1012	Vector Laboratories, USA
p38α/β (A-12)	sc-7972	Santa Cruz Biotechnology, USA
p38 MAPK (D13E1) XP® Rabbit mAb	8690	Cell Signaling Technology, USA
p44/42 MAPK (Erk1/2) (3A7) Mouse mAb	9107	Cell Signaling Technology, USA
Paraformaldehyde (PFA)		Sigma Aldrich, UK
PBS	D8537	Sigma Aldrich, UK
Phospho- IκBα (Ser32) (14D4) Rabbit mAb	2859	Cell Signaling Technology, USA
Phospho-MKK3 (Ser189)/MKK6 (Ser207) (D8E9) Rabbit mAb	12280	Cell Signaling Technology, USA
Phospho-p38 MAPK (Thr180/Tyr182) (28B10) Mouse mAb	9216	Cell Signaling Technology, USA

Phospho-p44/42 MAPK (Erk1/2) (Thr202/Tyr204) (D13.14.4E) XP® Rabbit mAb	4370	Cell Signaling Technology, USA
Phospho-SAPK/JNK (Thr183/Tyr185) (G9) Mouse mAb	9255	Cell Signaling Technology, USA
Phosphotungstic acid	P4006	Sigma Aldrich, UK
PhosSTOP phosphatase inhibitor cocktail	04906837001	Roche, Switzerland
Protease inhibitor	P8340	Sigma Aldrich, UK
Quick Start™ Bradford protein assay	500-0207	Bio-Rad, UK
Rabbit IgG	I-1000	Vector Laboratories, USA
RANKL	cyt-320	Prospec, Israel
RNeasy Micro kit	74004	Qiagen, Germany
SAPK/JNK Rabbit Ab	9525	Cell Signaling Technology, USA
SQSTM1/p62 Antibody	5114	Cell Signaling Technology, USA
Tris base	T6066	Sigma Aldrich, UK
Tris HCl	T3253	Sigma Aldrich, UK
Triton X-10	T6878	Rohn & Haas Company, Germany
Trizol	79306	Qiagen, Germany
Tween 20	P7949	Sigma Aldrich, UK
VECTASHIELD® Antifade Mounting Medium	H1200	Vector Laboratories, USA
Xylene	X0250	Fisher Scientific, USA

2.2 General

2.2.1 Animals

Bone samples from transgenic *p62*$^{-/-}$ and *p62*^{P394L} and wild type control mice on a C57Bl6 background were obtained from a research team of Dr. Daniela Merlotti and Prof. Luigi Gennari (University of Siena, Italy), and Dr. Simone Cenci and Dr. Maria Materozzi (at the time PhD student, Università Vita-Salute San Raffaele, Milano, Italy) as part of a collaboration. Mice (C57Bl6) used for Chapter 3 and 4 were housed in a pathogen-free facility at the University of Liverpool. All procedures were in accordance with the Animals (Scientific Procedures) Act 1986 and the EU Directive 2010/63/EU and approved by Animal Welfare and Ethical Review Body (AWERB) at the University of Liverpool. *p62*$^{-/-}$ and *p62*^{P394L} mice were generated from heterozygous breeding. Control mice were littermates or age- and sex-matched mice on the same C57Bl6 background. A subset of *p62*$^{-/-}$, *p62*^{P394L} and WT mice received two intraperitoneal (IP) injections of calcein (200-500 µL IP injection of 2 mg/mL) 2 and 5 days (at 6 months of age), or 2 and 7 days (at >12 months of age) days before euthanising (for details please see Chapter 5's method section).

2.2.2 µCT analysis

Left hind limbs of WT, *p62*$^{-/-}$ and p*62*^{P394L} mice at 6, 9-11 and 18-month-old were harvested and fixed overnight in Neutral buffered formalin in Milan. The samples were stored in 70% ethanol and shipped to Liverpool. µCT analysis was performed using a Skyscan 1272 system (Bruker, Belgium). For assessment of bone morphometry, left distal femurs of the animals free of most soft tissue, were scanned at the following parameters: X-ray source voltage 50 kV, source current 200 µA, Al 0.5 mm filter, image pixel size 4.5 µm, rotation step 0.3° over 180°, no frame averaging and no camera binning. Images were reconstructed using Skyscan NRecon software. Trabecular bone parameters were measured using Skyscan CTAn software in a stack of 200 slices immediately proximal to the growth plate of femurs. To screen for the presence of focal lesions, the entire left limbs were scanned at the following parameters: X-ray source voltage 50 kV, source current 200 µA, Al 0.5 mm filter, image pixel size 9.0 µm, rotation step 0.5° over 180°, no frame averaging and 2 x 2 binning. Assessment of lesions was conducted in a blinded fashion to the genotype of animals.

2.3 Tissue culture

2.3.1 Bone marrow extraction and culture of BMMs, POCs and OCs

Bone marrow was obtained from 3-4-month and 12-14-month-old C57Bl6 female mice. After culling the animals via rising concentration of carbon dioxide, they were skinned, and the hind limbs were removed. A scalpel was used to scrape the bones in order to remove all the soft tissue. Tibias and femurs were separated followed by the removal of epiphyses. A 27-gauge hypodermic needle was used to ensure the opening of each extremity of the bone shaft. Each bone was placed into a 500 μL (small) Eppendorf containing a hole in the bottom of the tube which has been perforated beforehand. The small Eppendorf was placed in a 1.5 mL (large) Eppendorf containing 125 μL of α–MEM supplemented with 10% fetal bovine serum and 1% Pen-Strep (complete α–MEM). The Eppendorfs were centrifuged in a Sigma 1-14 Microfuge at 800 g for 3 minutes. This resulted in the bone marrow to be flushed out of the bones in the small Eppendorfs and collected in the large Eppendorfs. The pellets in the large Eppendorfs were resuspended and transferred to a 10 cm petri dish containing 10 mL of complete α–MEM supplemented with 100 ng/mL of MCSF. The cells were incubated at 37°C in a humidified 5% CO_2 atmosphere for 3 days to allow the attachment of the cells. The medium was removed, and the cells were washed with phosphate buffered saline (PBS) after 3 days of incubation, in order to remove the non-adherent cells. Fresh complete α–MEM supplemented with 100 ng/mL of MCSF was added for culturing the cells into BMMs. The cells were left to grow until confluent with medium change performed every 3 days.

For cell seeding, the medium was removed from the petri dishes containing confluent BMMs, and the BMMs were washed twice with PBS. It was followed by the addition of 2.5 mL of Accutase per dish and the incubation of cells at 37°C in a humidified 5% CO_2 atmosphere for 3 minutes for cell detachment. The petri dishes were tapped in order to ensure most of the cells were released. Subsequently, 5.5 mL of medium was added to the petri dish, and the cells were washed thoroughly with the dish inclined. All the content of the petri dish was transferred to a 15 mL tube and centrifuged in a Sigma 1-14 Microfuge at 300 g for 3 minutes. The supernatant was discarded, and the pellet was resuspended by flicking bottom of the tube, and 5 mL of complete α–MEM was then added to the cell suspension. Cells were counted using a TC20 automated cell counter (Bio-Rad, USA).

For RANKL time and dose response assay, the BMMs was seeded to 6-well plates at density of $0.5x10^6$ cells/well and incubated at 37°C in a humidified 5% CO_2 atmosphere in complete α–MEM supplemented with 100 ng/mL of MCSF. To obtain POCs, BMM cultures were cultured for another 48 hours with 100 ng/mL of RANKL (Prospec, Israel) and 25 ng/mL of MCSF (Prospec, Israel). To obtain non-resorbing and resorbing OCs, BMM cultures were cultured on plastic and HA-coated plates respectively, for another 120 hours with 100 ng/mL of RANKL (Prospec, Israel) and 25 ng/mL of MCSF (Prospec, Israel) (**Figure 2.1**).

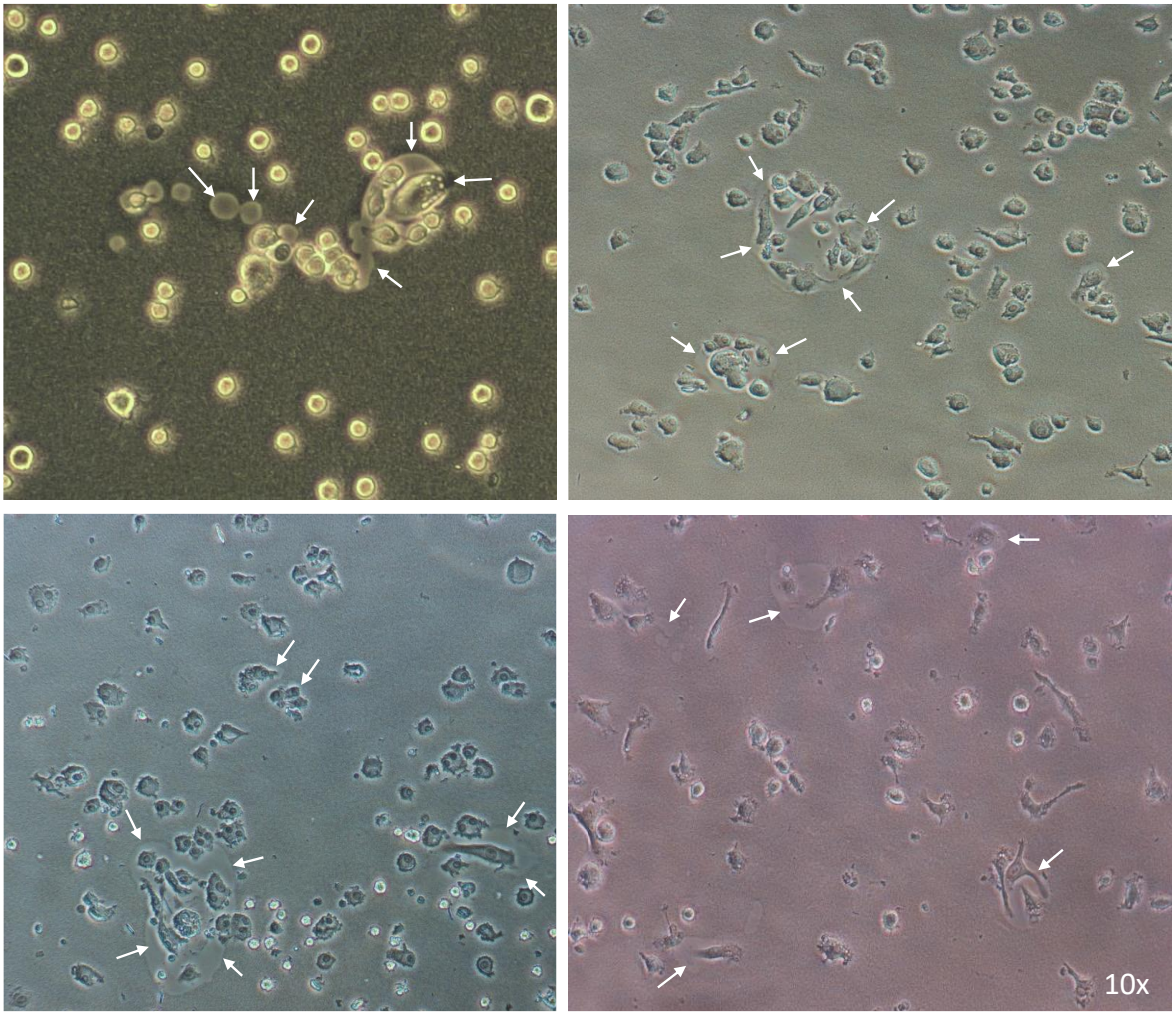

Figure 2.1: Resorbing OCs cultured on HA-coated plates. The OCs were seen actively resorbing the HA coating. White arrows indicate the resorption areas.

2.3.2 Culture of cells on HA-coated coverslips

Coverslips in 12-well plates were coated with HA using the technique described by ten Harkel *et al*[564]. The plate coating procedure was divided into 2 steps: pre-calcification and crystal growth. During the pre-calcification step, the ingredients for the respective solutions were prepared as per **Table 2.2**, to make 3x supersaturated Simulated Body Fluid (SBF) solution.

Table 2.2: Composition of 3x supersaturated SBF solution.

Solution	Ingredient
1. Buffer	12.1 g Tris base 82 mL 1M HCl
2. Calcium	24 g NaCl 0.9 g $MgCl_2 \cdot 6H_2O$ 1.2 g $CaCl_2 \cdot 2H_2O$
3. Phosphate	0.6 g $NaHCO_3$ 1.1 g Na_2HPO_4

First, the buffer solution was made by dissolving Tris base and 1 M HCl in MilliQ water to a total volume of 2 L with a final pH of 7.4. Next, the ingredients of calcium solution as per **Table 2.2** were dissolved in 500 mL of the buffer solution made in the first step. The same step was repeated for phosphate solution. The calcium solution and phosphate solution were mixed to make 3x SBF solution.

The coverslips in the 12-well plates wells were sterilised with 70% ethanol for 20 minutes prior to the addition of 3x SBF solution. It was then followed by washing the coverslips with PBS for three times in order to remove the ethanol. The 3x SBF solution was filtered with a 0.22 μm Minisart® syringe filter before pipetting 1 mL/well into 12-well plates containing coverslips. 12-well plates containing coverslips were incubated at room temperature with the 3x SBF solution for 3 days with solution change performed every day. After the 3-day incubation period, the plates were washed thoroughly five times with MilliQ water.

In the crystal growth step, the ingredients were prepared as per **Table 2.3**, to make CPS solution.

Table 2.3: Composition of CPS solution.

Solution	Ingredient
CPS	8.0 g NaCl 0.59 g $CaCl_2 \cdot 2H_2O$ 0.32 g Na_2HPO_4 6.05 g Tris

The ingredients for CPS solution were dissolved in 800 mL of MilliQ water. The pH of the solution was adjusted to 7.4 using 1M HCl, followed by the addition of 200 mL MilliQ water to a total volume of 1000 mL. The CPS solution was filtered with a 0.22 μm Minisart® syringe filter before pipetting 1 mL/well into the 12-well plates containing pre-coated coverslips. 12-well plates containing pre-coated coverslips were incubated at room temperature with the CPS solution for 3 days. A coarse crystallised layer can be seen deposited on the coverslips when the coating process was completed.

After 3-days of incubation period, the CPS solution was removed, and the wells were washed with 1 mL of 70% ethanol per well for 5 minutes, to ensure the entire well was sterilised. The ethanol was then removed, and the plates were left in the hood to dry for 30 minutes, followed by washing twice with warm PBS. The plates were ready to use after the washing step. For storage and future use purpose, the plates were dried overnight in an incubator at 37°C in a humidified 5% CO_2 atmosphere. Subsequently, the plates were kept and sealed individually in self-seal sterilisation pouches (Granton Medical, UK).

2.4 Molecular analysis

2.4.1 RNA extraction

For RNA extraction, BMMs were plated on 6-well plates at density of $6x10^5$ cells/well and cultured in complete α–MEM supplemented with 100 ng/mL of MCSF until confluent. To generate POCs and OCs, the BMMs were cultured further in complete α–MEM supplemented with 25 ng/mL of MCSF and 100 ng/mL of RANKL for another 2 days and 5 days respectively.

RNA extraction was performed using the RNeasy Micro kit (Qiagen, Germany) according to the manufacturer's instruction. Medium was removed from all wells and the cells were washed gently once with 500 μL of PBS. In order to lyse the cells, 700 μL of Qiazol was added to each well. Cell lysates were collected by scraping the wells using cell scraper, and all the content was transferred into pre-labelled Eppenfdorfs. The lysates were vortexed for 1 minute in order to homogenise the samples followed by incubation at room temperature for 5 minutes. 140 μL of chloroform was added to each sample and the tubes shaken vigorously for 15 seconds. Next, the samples were incubated at room temperature for 2-3 minutes and centrifuged at 12,000 g in a cooled centrifuge (Eppendorf 5415R, Marshall Scientific) at 4°C and for 15 minutes. The upper aqueous phase (approximately 350 μL) was transferred to a new pre-labelled Eppendorf. 1.5 times the volume in the Eppendorf (approximately 525 μL) of 100% ethanol was added and mixed thoroughly by pipetting up and down. 700 μL of each sample (including any precipitate) was transferred into the spin columns provided by the kit and centrifuged at room temperature and 8,000 g for 15 seconds. The flow-through was discarded and the procedure was repeated if there were any remaining samples. 500 μL of Buffer RPE was added, and the spin columns centrifuged at 8,000 g at room temperature for 15 seconds. The flow-through was again discarded. Another 500 μL of Buffer RPE was again added and centrifuged at room temperature and 8,000 g for 2 minutes. The spin columns containing RNA were transferred to a new 1.5 mL collection tube. And 30 μL of RNase-free water was added directly onto the membrane of the spin columns. The collection tubes together with the spin columns were centrifuged at room temperature and 8,000 g for 1 minute. Finally, RNA yields were assessed by using the NanoDrop 2000™ spectrophotometer (Thermo Fisher Scientific, USA). The RNA samples were then stored at -80°C for future use.

2.4.2 cDNA synthesis

After quantifying the RNA yields, cDNA was synthesised using the EvoScript Universal cDNA Master (Roche, Switzerland) according to the manufacturer's instruction. All reagents were vortexed and centrifuged briefly before setting up the reactions. To a PCR reaction tube, the following were added: 1 μg of RNA sample, 4 μL of 5x concentrated Reaction buffer and PCR grade water, to a final volume of 18 μL. The tubes were mixed well, centrifuged briefly and incubated for 5 minutes at room temperature. After the incubation, 2 μL of 10x concentrated Enzyme mix was added and mixed gently. Finally, the tubes were placed in a SimpliAmp Thermal Cycler (Thermo Fisher, USA) and reverse transcription was conducted as per **Table 2.4**.

Table 2.4: Reverse transcription protocol performed on SimpliAmp Thermal Cycler.

Step	Temperature	Duration
1	42°C	15 minutes
2	85°C	5 minutes
3	64°C	15 minutes
4	4°C	∞

2.4.3 Real-time quantitative PCR

For gene expression studies, LightCycler 480 probes master (Roche, Switzerland) was used. Individual master mix for each gene of interest was prepared as follows:

Table 2.5: Ingredient list of real time-quantitative polymerase chain reaction (RT-qPCR) master mix.

Reagent	Volume for 1 sample
Probes Master (2x)	5 μL
Forward primer	0.4 μL
Reverse primer	0.4 μL
Probe	0.2 μL
Water	3 μL

After the master mixes were prepared, for each sample 9 μL of master mix and 1 μL of cDNA was added to a well in a 96-well PCR plate in triplicate, making up a total reaction volume of 10 μL. All qPCR reactions were performed using the Lightcycler 480 (Roche, Switzerland), using the Mono Color Hydrolysis Probe/UPL protocol at the following settings:

Table 2.6: RT-qPCR run program.

Step	Cycle(s)	Temperature	Time
Pre-incubation	1	95°C	10 minutes
Amplification	45	95°C	10 seconds
		60°C	30 seconds
		72°C	1 second
Cooling	1	40°C	30 seconds

CT values were then obtained using LightCycler® 480 software and gene expression relative to HMBS (housekeeping gene chosen based on a study by Stephens *et al*[565]) was calculated. All primer-probe sets (**Table 2.7**) used were pre-validated by the lab group.

Table 2.7: Primer-probe sets.

Primer	Forward (5'-3')	Reverse (5'-3')	Probe
HMBS	TCCCTGAAGGATGTGCCTAC	AAGGGTTTTCCCGTTTGC	79
Atp6v0d2	ATGTGGACCATGGCTACCTG	TCCGTGGTCTGGAGATGAAT	75

2.4.4 Preparation of cell lysates for Western blotting

After the RANKL time or dose response assay (for details please see Chapter 3's method section), the media was removed, and the 6-well plates were placed on ice. The cells in each well were washed with 2 mL of cold PBS in order to stop the phosphorylation cascades. The PBS was then removed and the cells in each well were lysed with 100 μL of lysis buffer (containing radioimmunoprecipitation assay (RIPA) buffer, PhosSTOP phosphatase inhibitor cocktail (Roche, Switzerland) and protease inhibitor (Sigma Aldrich, UK) on ice followed by the collection of lysates into pre-labelled Eppendorfs. The lysates were centrifuged at 4°C, and maximum speed for 10 minutes. The supernatant was transferred into pre-labelled Eppendorfs. The samples were then stored at -20°C for future use.

2.4.5 BCA protein assay

Cells were lysed as described above in **Subsection 2.4.4**, and the protein concentration was determined by Bicinchoninic Acid (BCA) protein assay. The cell lysates were thawed and vortexed. 10 μL of bovine serum albumin (BSA) standards (Bio-Rad, UK) at seven pre-diluted concentrations (0.125, 0.25, 0.5, 0.75, 1.0, 1.5 and 2.0 mg/mL) was loaded in duplicate onto a 96-well plate. Samples were then loaded at 1:5 dilution in water in duplicate. Mixture of bicinchoninic acid solution (**A**) and copper II sulfate pentahydrate 4% solution (**B**) from Sigma Aldrich BCA protein assay kit (UK) was made up in a 15 mL falcon tube at 1:50 dilution. 200 μL of the mixture was added to each well after mixing. The 96-well plate was covered with transparent sticky foil and incubated at 37°C for 15 minutes. Next, the plate was loaded into the SPECTROstar *Nano* microplate reader (BMG Labtech, UK) to measure absorption at 562 nm and protein concentration determined using the standard curve.

2.4.6 Western blotting

30 μg of proteins and 5x sample loading buffer at 1:4 dilution was pipetted into pre-labelled Eppendorfs, vortexed. Next, the lid of Eppendorfs was pierced using a needle, and the proteins denaturated heating in a heat block at 95°C for 5 minutes. The samples were then cooled on ice for 2 minutes and spun down at 4°C and maximum speed for 3 minutes in a centrifuge (Eppendorf 5415R, Marshall Scientific). 5 μL of Chameleon Duo Pre-stained Protein Ladder (LI-COR Biosciences, UK) and the denaturated protein samples were loaded into 10% Criterion™ TGX™ Precast Midi Protein Gel (Bio-Rad, UK), and ran at 300 V, 400 mAH for approximately 20 minutes. The proteins were then transferred from the gel to a Immun-Blot® low fluorescence PVDF membrane (Bio-Rad, UK) via a semi-dry Trans-Blot Turbo Transfer System (Bio-Rad, UK) at 25 volts and 2.4 amps for 7 minutes. The PVDF membranes were blocked with Intercept® (TBS) blocking buffer (LI-COR Biosciences, UK) on a shaker for 1 hour at room temperature. It was followed by three washes with TBST for 15 minutes each. The membranes were incubated in respective primary antibodies at recommended dilution in Intercept® (TBS) blocking buffer (LI-COR Biosciences, UK) overnight at 4°C on a shaker. After the antibody incubation, the membranes were washes three times for 15 minutes in TBST. The membranes were then probed with secondary antibodies goat α-rabbit AF680/800 and goat α-mouse AF680/800 (LI-COR Biosciences) at 1:10000 dilution for 1 hour at room temperature on a shaker and washed three times for 15 minutes with TBST. The membranes were visualised using the Odyssey CLx imaging system (LI-COR Biosciences, UK) and analysed with Image Studio lite (LI-COR Biosciences, UK).

2.4.7 Immunostaining

For immunostaining, the HA-coated coverslips in 12-well plates were incubated with fetal bovine serum (FBS) (Gibco, Thermo Fisher Scientific, USA) at 37°C in a humidified 5% CO_2 atmosphere for 1 hour prior to cell plating. Next, 100 μL of BMMs at density of $1x10^5$ was pipetted on to the coverslip and incubated for 1 hour for cell attachment. The remaining 900 μL of complete α–MEM containing 25 ng/mL of MCSF and 100 ng/mL of RANKL to generate mature OCs. The cells were incubated at 37°C in a humidified 5% CO_2 atmosphere with medium change performed every 3 days.

Resorbing OCs cultured on HA-coated coverslips in 12-well plates were fixed with 4% PFA or ice-cold ethanol (depending on the protein of interest to probe) for 10 minutes and washed with PBS for 2 minutes after removing the complete α-MEM. The cells were permeabilised with PBS containing 0.1% Triton for 10 minutes and blocked with 2.5% normal goat serum blocking solution (Vector Laboratories, USA) for 1.5 hours. For optimisation, the cells were first probed with different dilutions (within the range of recommendation) of primary antibodies to determine the optimal.

After optimisation, the cells were probed with primary antibodies at optimised dilutions for 1 – 3 hours or overnight at room temperature or at 4°C. Mouse IgG or Rabbit IgG were used as negative controls depending on the animal species of primary antibodies. The cells were then washed three times with PBS containing 0.1% Tween for 10 minutes each. The cells were continued to probe with Goat anti-Rabbit IgG (H+L) Cross-Adsorbed Secondary Antibody, AF488 or Goat anti-Mouse with Alexa Fuor 594 (Fisher Scientific, USA) at 1:200 dilutions for 60 minutes at room temperature if the primary antibodies were not conjugated with any fluorophores. The washing step was again repeated, and the primary and secondary antibodies probing steps were also repeated if there was other protein of interests on the same coverslips. After completing probing with all the antibodies of interests, the cell nuclei were stained with DAPI (stock solution at 1 mg/mL) diluted in PBS at 1:1000 dilutions for 5-10 minutes. The cells were washed once with PBS containing 0.1% Tween and mounted onto glass slides with VECTASHIELD® Antifade Mounting Medium (Vector Laboratories, USA), followed by the sealing of the circumference of coverslips using nail varnish. Finally, the cells were visualised using a Zeiss LSM 800 Confocal microscope.

2.5 Histology

2.5.1 Bone histomorphometry

Left hind limbs of the mice were harvested and fixed overnight in Neutral buffered formalin in Milan. The samples were stored in 70% ethanol and shipped to us. After μCT analysis, the femurs were processed with Leica ASP300 tissue processor (Leica Microsystems, UK) and dehydrated through a series of alcohol washes and cleared in xylene (**Table 2.8**). Samples were then infiltrated with a mixture of 88.99% methyl methacrylate (MMA), 10% di-butyl phthalate, 1% Perkadox 16 and 0.01% Tinogard at 4°C under vacuum for 7 days.

Subsequently, Teflon embedding blocks were filled with the mixture described above and the samples were placed in the wells. The wells were then sealed with air-tight lids and the blocks were left to polymerise in a water bath at 30°C at least overnight until polymerisation was completed. The lids were removed and embedding rings were attached to the blocks by adding a mixture of two parts of yellow cold-curing resin powder and one part of Technovit mounting media. The blocks were left to harden for at least 48 hours before sectioning at 5 μm on a Leica RM2265 motorised microtome (Leica Microsystems, UK) fitted with a tungsten steel D-profile knife. The sections were mounted on to Leica X-tra slides, covered with kissol film, and placed under pressure with a slide-press in a dry incubator at 37°C for 48 hours. The above procedures were based on a protocol described by van 't Hof *et al*[566].

Table 2.8: Dehydration steps.

Step	Solution in basket	Processing time
1	70% Ethanol	30 minutes
2	80% Ethanol	2 hours
3	96% Ethanol	2 hours
4	100% Ethanol	3 hours
5	100% Ethanol	3 hours
6	Xylene	1 hour
7	Xylene	12 hours

2.5.1.1 TRAP staining

The following procedures were based on the method described by Chappard *et al*[567] and van 't Hof *et al*[566]. For analysis of osteoclastic bone resorption, the sections were stained for TRAP. The sections were deplasticised in 3 changes of 2-methoxyethyl acetate (MEA), cleared in two changes of Xylene and taken through a decreasing alcohol series to water (**Table 2.9**). The sections were incubated at 37°C for up to 2 hours in a staining solution of naphtol ASBI-phosphate (1.4 mg/mL) and fast red (1.4 mg/mL) in a 0.2 M acetate buffer (pH 5.2) containing 50 mM sodium tartrate. After staining the sections with TRAP, they were washed in two changes of distilled water and counterstained for 15 minutes using 0.33 g/L Aniline blue and 6 g/L phosphotungstic acid in water, and briefly washed in three changes of water. Finally, the sections were coverslipped using Apathy's serum and imaged with a Zeiss Axio Scan.Z1 slide scanner (Carl Zeiss Ltd., UK) in brightfield mode by using 10x lens together with a colour camera, resulting in an isotropic pixel size of 0.442 μm. The TRAP stain analysis was performed using a custom in-house developed image analysis program based on ImageJ, available at https://www.liverpool.ac.uk/ageing-and-chronic-disease/bone-hist/, developed by Prof. Rob van 't Hof[566].

The software was written in Java using the Netbeans development environment, and image analysis routines were based on ImageJ and publicly available at http://www.liverpool.ac.uk/ageing-and-chronic-disease/bone-hist/ (developed by Prof. Rob van 't Hof).

Table 2.9: Deplasticising steps.

Step	Solution in basket	Processing time
1	MEA	20 minutes
2	MEA	20 minutes
3	MEA	20 minutes
4	Xylene	10 minutes
5	Xylene	10 minutes
6	100% Ethanol	2 minutes
7	100% Ethanol	2 minutes
8	80% Ethanol	1 minute
9	70% Ethanol	1 minute
10	50% Ethanol	1 minute
11	Distilled water	1 minute

2.5.1.2 Calcein staining

For analysis of bone formation, the sections were stained in 0.1% Calcein Blue (pH 8) for 3 minutes without being deplasticised. The sections were washed three times in water, dehydrated through a decreasing alcohol series, cleared in xylene and coverslipped using the automatic coverslipper of a Leica auto stainer. The sections were then visualised with the Zeiss Axio Scan.Z1 slide scanner (Carl Zeiss Ltd., UK) with a 20x lens using filter sets for DAPI and calcein, and a Zeiss Axioscan506 monochrome camera and a 20x lens, resulting in an isotropic pixel size of 0.227 μm. The histomorphometric analysis of bone formation was performed using a custom in-house developed image analysis program based on ImageJ, available at https://www.liverpool.ac.uk/ageing-and-chronic-disease/bone-hist/, developed by Prof. Rob van 't Hof[566].

The software was written in Java using the Netbeans development environment, and image analysis routines were based on ImageJ and publicly available at http://www.liverpool.ac.uk/ageing-and-chronic-disease/bone-hist/ (developed by Prof. Rob van 't Hof).

Chapter 3: Role of p38 and other RANKL-induced signalling molecules in osteoclastogenesis with ageing

3.1 Introduction

Bone remodelling is a finely tuned process involving concerted actions of OCs and osteoblasts in coupled bone resorption and formation. Imbalance of the coordinated efforts, in favour of resorption, results in diseases such as osteoporosis, which is the most common age-related metabolic bone disorder. It is characterised by generalised bone deterioration in terms of architecture and low bone mass. Osteoporotic bone is weaker and fragile due to decreased trabecular bone volume and the conversion of plate-like structure into rod-like structure[568], thus, prone to fracture. The incidence and risk of osteoporosis fragility fractures are predicted to increase worldwide as the population ages.

RANKL expressed on the surface of mostly osteocytes, and partially osteoblasts and stromal cells, binds to RANK on POC and OC surface. The binding of RANKL to RANK recruits the TRAF6-p62-aPKC complex, which in turn activates the MAPK signal transduction pathway and IKK phosphorylation followed by NF-κB activation.

MAPK pathways are three-tiered cascades comprised of three components: MAPK, MKK and MEKK and responsible for transducing extracellular stimuli into specific intracellular responses[187]. Upon stimulation, MEKKs, which are serine/threonine protein kinases, phosphorylate and activate MKKs, which in turn dually phosphorylate the tyrosine and serine/threonine residues of MAPKs[192]. Single threonine and single tyrosine residues Thr^{180}/Tyr^{182}, Thr^{202}/Thy^{204} and Thr^{183}/Tyr^{185} of p38, ERK and JNK respectively, are phosphorylated by the specific MKKs[187]. The MAPK pathways are deactivated through dephosphorylation of the threonine or tyrosine residue by phosphatases such as DUSPs[193]. With the availability of MAPK inhibitors, SB203580 and PD98059 for instance, which inhibit p38 and ERK respectively, several studies have shown that MAPKs play a pivotal role in different stages of osteoclastogenesis (as described in detail in Chapter 1)[51,196,199,202]. Duration, intensity and isoform specificity of MAPK activation determine the distinct cell fates of proliferation or differentiation in OC progenitors[188].

Interestingly, p62 was revealed to be the first p38 regulating protein which binds to p38 via the domain corresponding to 173-182 and enhances p38 activity[320,569]. Reduced p62 expression with ageing has been shown in mice[570] and this could directly affect the p38 signalling pathway. Mutations of *p62/SQSTM1* at the UBA domain are associated with PDB, which is the second most common age-related metabolic bone disease after osteoporosis and is due to abnormal and hyperactive OCs[571]. However, to my knowledge no mutations of p62 associated with PDB are known to affect the p62-p38 interaction.

It has been reported that OC formation was increased in ageing in both humans[572] and mice[440,573], and that the OCs from aged mice are hypersensitive to RANKL[561]. However, the intrinsic factors enhancing osteoclastogenesis and hypersensitivity in ageing are incompletely understood. Previous pilot experiments (Reverse Phase Protein Arrays (RPPA)) suggested that the p38 MAPK activation was increased in murine BMMs in ageing after stimulation with RANKL (van 't Hof lab group, unpublished). In this part of my project, my aim was to determine the role of MAPKs including the upstream regulator and the downstream targets in the age-related increased osteoclastogenesis.

3.2 Methods

Bone marrow was harvested from the long bones of 3-4-month and 12-14-month-old C57Bl6 female mice and BMMs and POCs were differentiated as described in Chapter 2. Prior to RANKL time or dose response assays, BMMs or POCs were serum starved for 3 hours.

For the time response assay, 100 ng/mL of RANKL or 2 ng/mL of TNF-α was used to stimulate BMMs or POCs for 5, 10, 15, 20 and 30 minutes to analyse phosphorylation of p38 MAPK, ERK and JNK. For assessment of IκB and MKK3/6 phosphorylation, the BMMs were stimulated with the same concentration of RANKL for 5, 10, 15, 30 and 60 minutes. In the experiment with LPS, 100 ng/mL of RANKL or 2 ng/mL of LPS were used to stimulate BMMs and POCs for 15 minutes. For the dose response assay, 10, 30, 100 ng/mL of RANKL was used to stimulate BMMs. The cells were lysed, and 30 μg of proteins was loaded for Western blotting as described in Chapter 2. After the blocking step, the membranes were probed with the primary antibodies for P-p38, p38, P-ERK, ERK, P-JNK, JNK, phosphorylated- IκB, IκB, phosphorylated-

MKK3/6 (P-MKK3/6) or MKK3/6 (Cell Signaling Technology) at 1:1000 dilution, or β-actin at 1:5000 dilution. The membranes were incubated and proceeded as described in Chapter 2. The same procedures were repeated to probe with second primary antibodies under the same conditions (except probing for β–actin which only required 1 hour at room temperature).

For gene expression studies, BMMs were stimulated with 100 ng/mL of RANKL and 25 ng/mL of M-CSF for 0, 48 and 120 hours, and the RNA was extracted. Next Generation Sequencing (NGS) was then performed in Oxford with high quality, undegraded RNA for all samples after assessing the samples on a TapeStation system. The results of NGS were validated by using qPCR. For further details, please refer to Chapter 2.

For immunostaining experiments, BMMs, POCs and OCs from young and aged mice were fixed with 4% PFA and subjected to immunostaining using standard protocols described in Chapter 2. After the blocking step, primary antibody for NFATc1 (Abcam) was added into 2.5% Goat serum (Vector Laboratories, Inc.) at 1:200 dilution and the cells were probed at room temperature for 1 hour. Secondary antibody Goat α-rabbit AF488 (Thermo Fisher Scientific) was added into 2.5% Goat serum at 1:200 dilution. Nuclei of the cells were stained with DAPI diluted in PBS at 1:1000 dilution for 5 – 10 minutes followed by the mounting of cells onto glass slides with VECTASHIELD® Antifade Mounting Medium with DAPI (Vector Laboratories, USA) and visualised with Zeiss Confocal LSM 800. For further details, please refer to Chapter 2.

3.3 Results

3.3.1 RANKL-mediated MAPK phosphorylation of BMMs in ageing

In order to investigate if MAPK (p38, ERK and JNK) are responsible for increased osteoclastogenesis in ageing, I conducted RANKL stimulation time response assay in BMMs from young and aged mice to quantify the MAPK phosphorylation status using Western blot.

I first studied the phosphorylation of p38 MAPK. Upon RANKL stimulation, p38 MAPK was activated and showed an increase in P-p38 level. The level of P-p38 reached the peak after 15 minutes of stimulation, followed by a gradual decrease. Without the RANKL stimulation, P-p38 in BMMs from both young and aged mice were at the same basal level after starvation. However, the level of P-p38 in BMMs from aged mice was higher than that of young mice after stimulating with RANKL for 5, 10, 15, 20 and 30 minutes, indicating increased p38 MAPK phosphorylation in BMMs from aged mice (**Figure 3.1 A-C**).

In order to quantify P-p38, area under the curve (AUC) of p38 phosphorylation and maximum phosphorylation were calculated. BMMs from aged mice show a significant increase of 93% compared to the BMMs from young mice (N=4, $p<0.001$) **(Figure 3.1 D**). Also, the maximum phosphorylation of p38 is 78% higher at 15 minutes in BMMs from aged mice (N=4, $p<0.05$) (**Figure 3.1 E**).

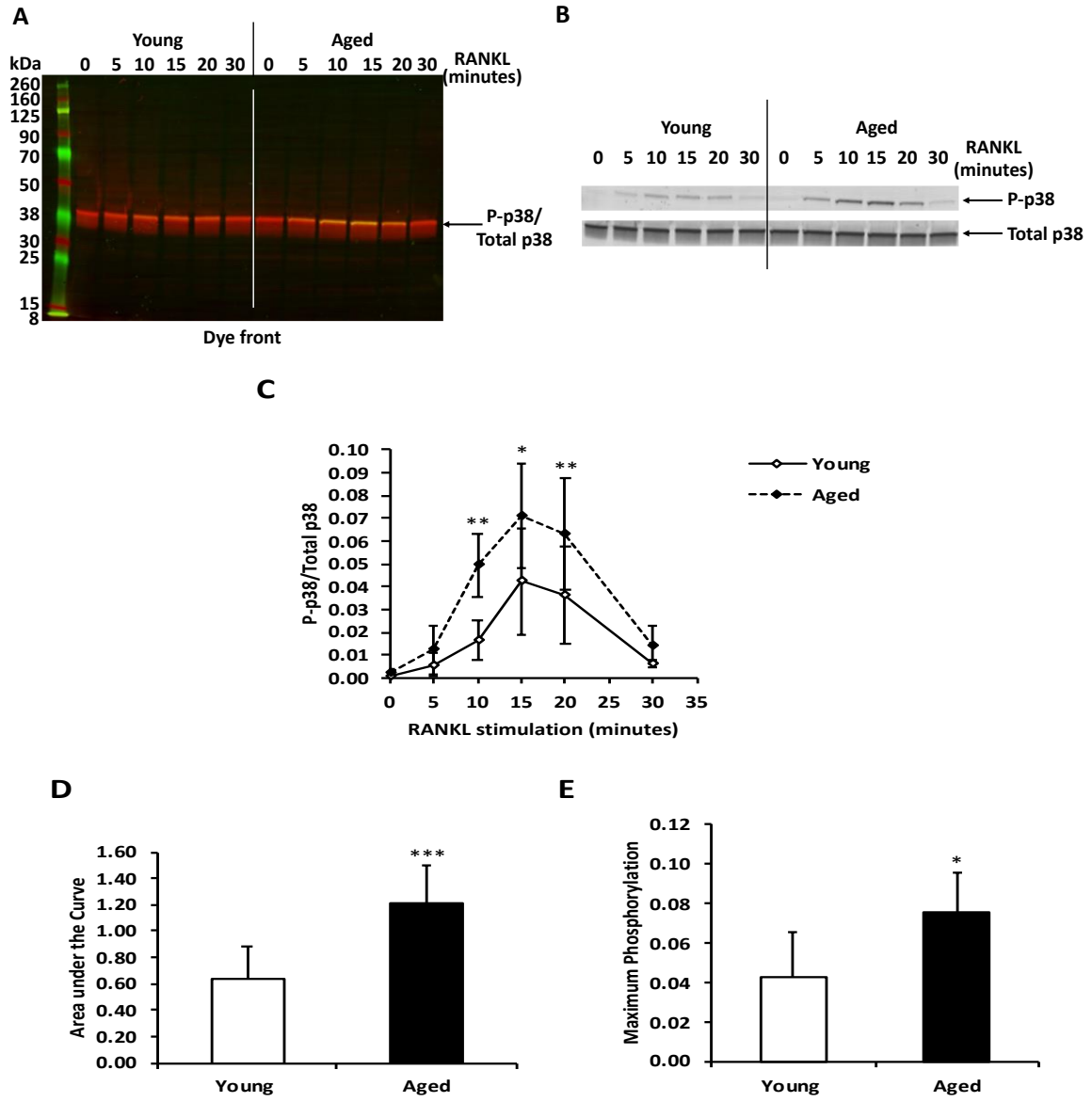

Figure 3.1: Western blot analysis of p38 MAPK phosphorylation in BMMs from young and aged mice in RANKL time response assay. Serum-starved BMMs (isolated from 3-4-month and 12-14-month-old C57Bl6 female mice) cultured with 100 ng/mL of MCSF were stimulated with 100 ng/mL of RANKL for the indicated time points. Representative western blot of p38 phosphorylation in RANKL time response assay in colour with both 680 and 800 channels shown together (**A**) and the same blot in black/white with individual channels shown separately (**B**). Quantification of P-p38 shows the activation of p38 in response to RANKL stimulation (**C**). AUC (**D**) and maximum phosphorylation (**E**) reveal that BMMs from aged mice have a significantly higher p38 phosphorylation than young BMMs (N=4). Total p38 was used for normalisation. The expected molecular weight for P-p38 and Total p38 MAPK is 38 kDa. Data are shown as means ±SD. Unpaired two-tailed Student's *t* test was used to determine if the level of p38 phosphorylation was significantly different between BMMs from young and aged mice. Significance is denoted by *p<0.05, **p<0.01, ***p<0.001.

Since phosphorylation of p38 MAPK in BMMs with ageing is found to be increased in a time-dependent manner after stimulating with RANKL, I then performed a RANKL dose response assay to assess the difference in sensitivity to RANKL between BMMs from aged versus young mice.

P38 MAPK was activated in response to RANKL in a dose-dependent manner (**Figure 3.2 A-C**). There was no significant difference in the p38 MAPK phosphorylation between BMMs from young and aged mice in response to increasing doses of RANKL (**Figure 3.2 C**). AUC of p38 phosphorylation and maximum phosphorylation also show similar results (**Figure 3.2 D and E**). Of note, the BMMs from aged mice in the dose response assay when stimulated with 100 ng/mL of RANKL for 15 minutes gave rise to a much lower level of P-p38 (0.05) compared to that in the time response assay (0.07) (**Figure 3.1 C and 3.2 C**).

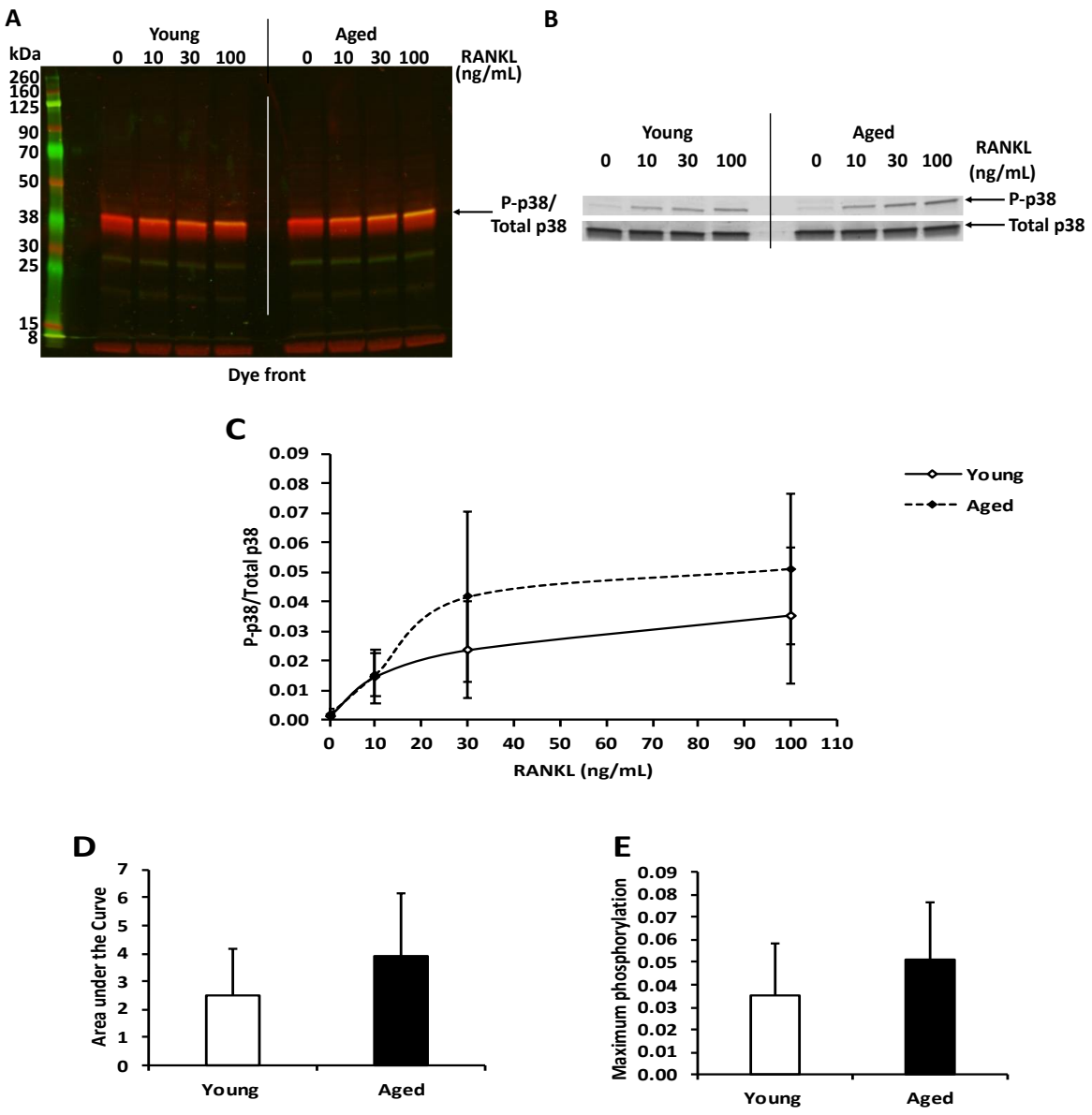

Figure 3.2: Western blot analysis of p38 MAPK phosphorylation in BMMs from young and aged mice in RANKL dose response assay. BMMs obtained from 3-4-month and 12-14-month-old C57Bl6 mice and cultured with 100 ng/mL of M-CSF were stimulated with indicated concentrations of RANKL for 15 minutes. Representative western blot of p38 phosphorylation in RANKL dose response assay in colour with both 680 and 800 channels shown together (**A**) and the same blot in black/white with individual channels shown separately (**B**). Quantification of P-p38 shows a gradual elevation with increasing doses of RANKL and reaches a plateau in BMMs from both young and aged mice (**C**). AUC (**D**) and maximum phosphorylation (**E**) reveal that BMMs from aged mice have a higher p38 phosphorylation than that of young mice but insignificant (N=3). Total p38 was used for normalisation. The expected molecular weight for P-p38 and Total p38 MAPK is 38 kDa. Data are shown as means ±SD. Unpaired two-tailed Student's *t* test was used to determine if the level of p38 phosphorylation was significantly different between BMMs from young and aged mice.

ERK, as another member of MAPK, was activated in response to RANKL stimulation, peaked at 15 minutes and returned to baseline by 30 minutes. No significant difference was observed in the level of P-ERK between BMMs from young and aged mice after stimulating with RANKL at 10-, 15- and 20-minute time points (**Figure 3.3 A-C**). Nevertheless, AUC of ERK phosphorylation showed a significant increase of 34% (N=3, $p<0.05$) (**Figure 3.3 D**), while the maximum phosphorylation of ERK has no difference (**Figure 3.3 E**). Hence, the result overall shows a marginally increased ERK phosphorylation in BMMs from aged mice as compared to BMMs from young mice.

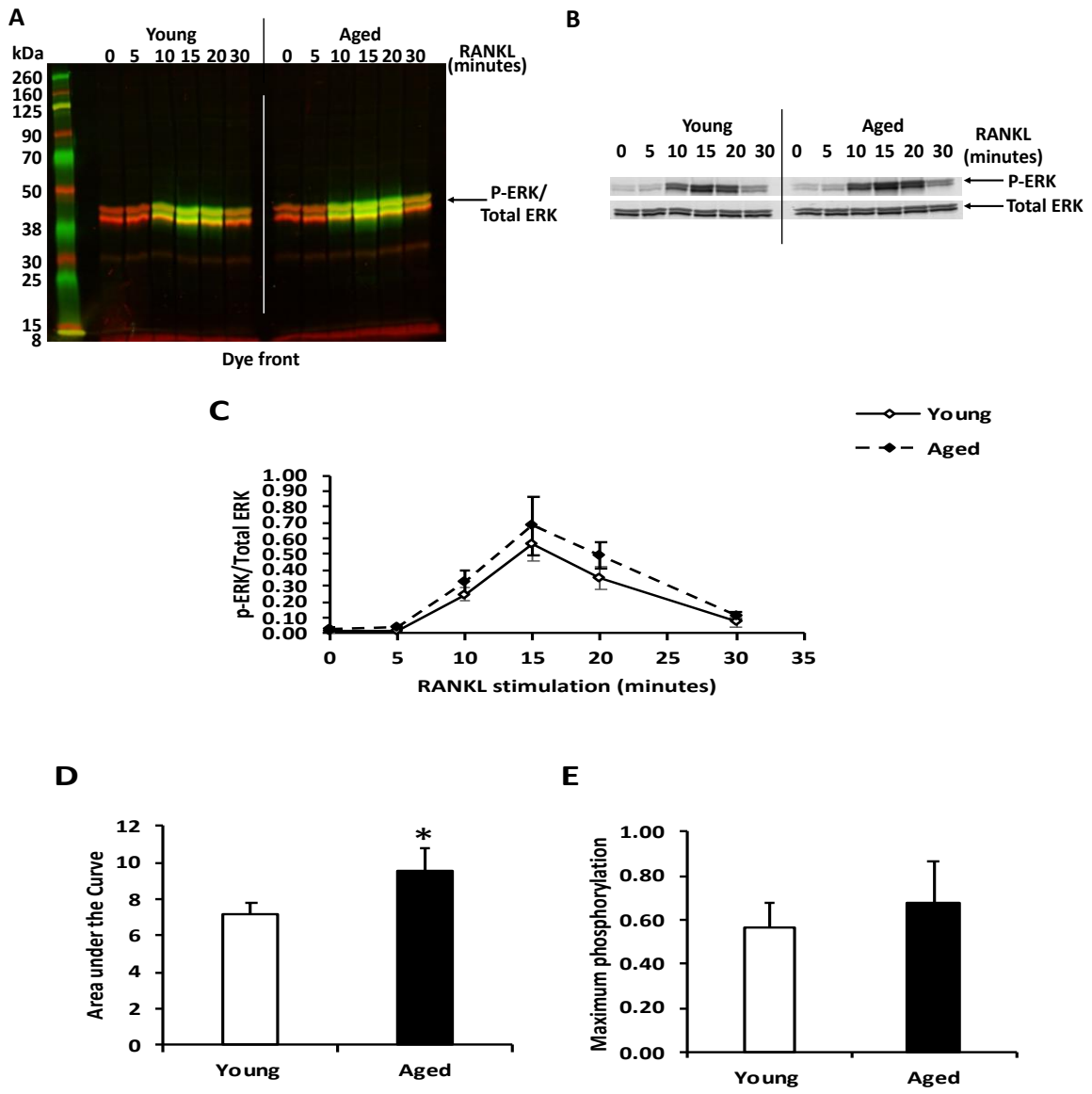

Figure 3.3: Western blot analysis of ERK phosphorylation in BMMs from young and aged mice in RANKL time response assay. Serum-starved BMMs (isolated from 3-4-month and 12-14-month-old C57Bl6 female mice) cultured with 100 ng/mL of MCSF were stimulated with 100 ng/mL of RANKL for the indicated time points. Representative western blot of ERK phosphorylation in RANKL time response assay in colour with both 680 and 800 channels shown together (**A**) and the same blot in black/white with individual channels shown separately (**B**). Quantification of P-ERK shows the activation of ERK in response to RANKL stimulation (**C**). AUC (**D**) reveals that BMMs from aged mice have a slight but significant increase in ERK phosphorylation as compared to BMMs from young mice (N=4), while maximum phosphorylation (**E**) shows no significant difference. Total ERK was used for normalisation. The expected molecular weight for P-ERK and Total ERK is 44/42 kDa. Data are shown as means $\pm$SD. Unpaired two-tailed Student's *t* test was used to determine if the level of ERK phosphorylation was significantly different between BMMs from young and aged mice. Significance is denoted by *$p<0.05$.

Since phosphorylation of ERK in ageing is found to be marginally increased in a time-dependent manner after stimulating with RANKL, I then performed a RANKL dose response assay to assess the difference in sensitivity to RANKL between BMMs from young and aged mice.

Similar to p38 MAPK, ERK was activated in response to RANKL in a dose-dependent manner (**Figure 3.4 A-C**). There was no significant difference in the ERK phosphorylation between BMMs from young and aged mice in response to increasing doses of RANKL (**Figure 3.4 C**). AUC of ERK phosphorylation and maximum phosphorylation also show similar results (**Figure 3.4 D and E**). Of note, the aged BMMs in the dose response assay when stimulated with 100 ng/mL of RANKL for 15 minutes gave rise to a much higher level of P-ERK (1.4) compared to that in the time response assay (0.7) (**Figure 3.3 C and 3.4 C**).

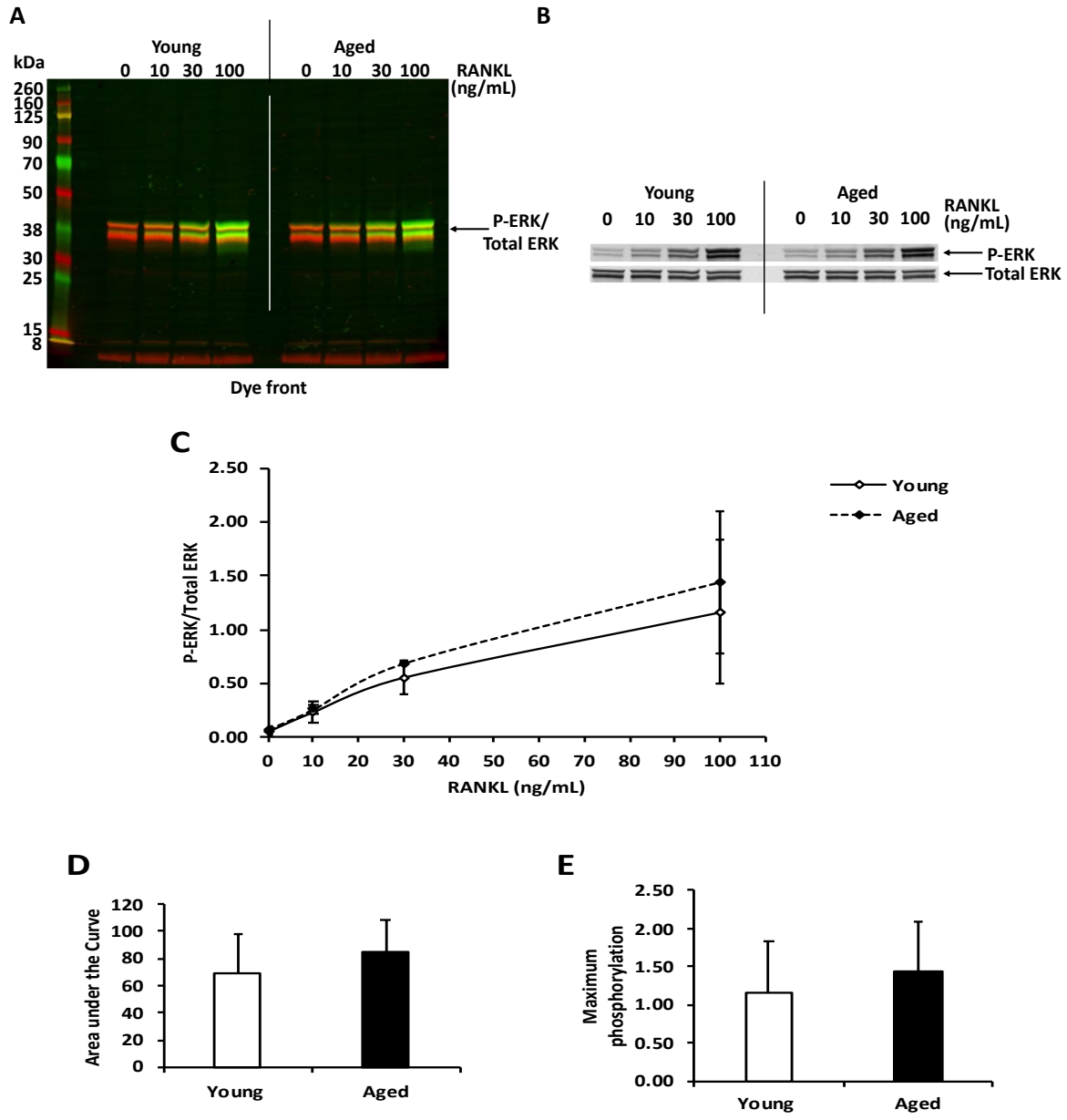

Figure 3.4: Western blot analysis of ERK phosphorylation in BMMs from young and aged mice in RANKL dose response assay. BMMs obtained from 3-4-month and 12-14-month-old C57Bl6 mice and cultured with 100 ng/mL of M-CSF were stimulated with indicated concentrations of RANKL for 15 minutes. Representative western blot of ERK phosphorylation in RANKL dose response assay in colour with both 680 and 800 channels shown together (**A**) and the same blot in black/white with individual channels shown separately (**B**). Quantification of P-ERK shows a gradual elevation with increasing doses of RANKL in BMMs from both young and aged mice (**C**). AUC (**D**) and maximum phosphorylation quantifications (**E**) reveal that there is no significant difference between BMMs from aged versus young mice (N=3). Total ERK was used for normalisation. The expected molecular weight for P-ERK and Total ERK is 44/42 kDa. Data are shown as means ± SD. Unpaired two-tailed Student's *t* test was used to determine if the level of ERK phosphorylation was significantly different between BMMs from young and aged mice.

JNK, another member of MAPK, like p38 and ERK was activated in response to RANKL stimulation. However, JNK stimulation peaked at 20 minutes and then decreased to a level higher than at baseline. There was no significant difference in the JNK phosphorylation between young and aged BMMs in response to increasing doses of RANKL (**Figure 3.5 A-C**). AUC of JNK phosphorylation and maximum phosphorylation quantification also showed similar results (**Figure 3.5 D and E**). Thus, the result overall did not show differential JNK phosphorylation in BMMs from both young and aged mice.

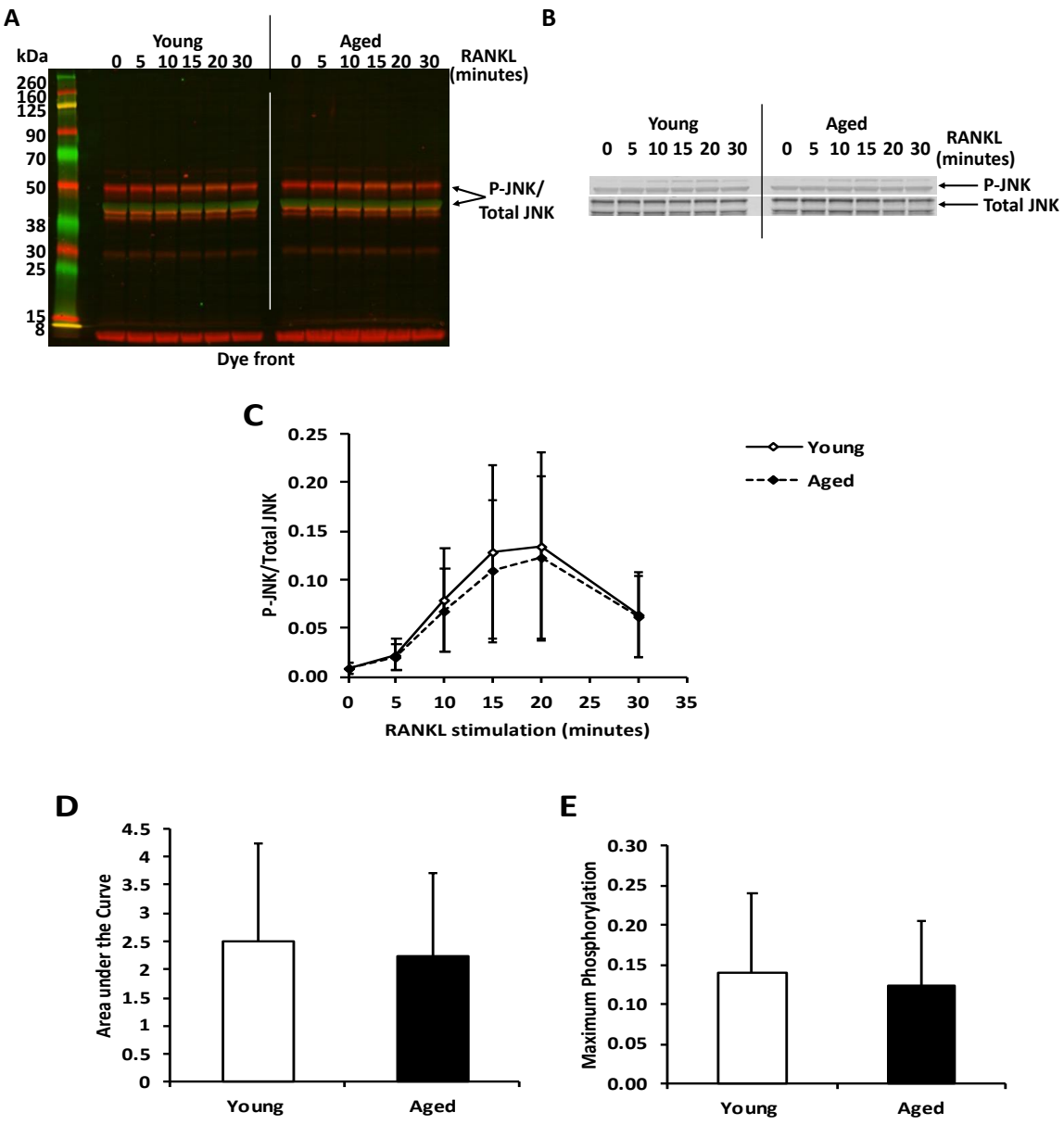

Figure 3.5: Western blot analysis of JNK phosphorylation in BMMs from young and aged mice in RANKL time response assay. Serum-starved BMMs (isolated from 3-4-month and 12-14-month-old C57Bl6 female mice) cultured with 100 ng/mL of M-CSF were stimulated with 100 ng/mL of RANKL for the indicated time points. Representative western blot of JNK phosphorylation in RANKL time response assay in colour with both 680 and 800 channels shown together (**A**) and the same blot in black/white with individual channels shown separately (**B**). Quantification of P-JNK shows the activation of JNK in response to RANKL stimulation (**C**). Both the AUC (**D**) and maximum phosphorylation (**E**) reveal that BMMs from both young and aged mice have the same level of JNK activation (N=3). Total JNK was used for normalisation. The expected molecular weight for P-JNK and Total JNK is 54/46 kDa. Data are shown as means ±SD. Unpaired two-tailed Student's *t* test was used to determine if the level of JNK phosphorylation was significantly different between BMMs from young and aged mice.

3.3.2 RANKL-mediated MAPK phosphorylation of POCs in ageing

In the previous section, I showed that RANKL stimulation causes an increase in p38 MAPK and ERK phosphorylation in aged BMMs. As the binding of RANKL to RANK induces osteoclast differentiation, I wanted to ask if p38 MAPK and ERK phosphorylation are increased in POCs due to ageing. Therefore, I performed similar RANKL stimulation assays to determine RANKL effect on MAPK stimulation in POCs in ageing.

RANKL failed to induce p38 MAPK (**Figure 3.6 A, B and E)** and ERK (**Figure 3.6 C, D and F)** phosphorylation in both young and aged POCs. The level of Total p38 MAPK and ERK were unchanged with and without the RANKL treatment throughout the experimental period. This suggests that the RANKL-RANK interaction for MAPK phosphorylation is essential for the early stage of osteoclastogenesis, and it is possible that the phosphorylation system may be activated via different pathway in the later phase of differentiation.

As I have found no difference in JNK phosphorylation between BMMS derived from aged versus young mice, as described in the previous section, I did not assess for similar differences in POCs.

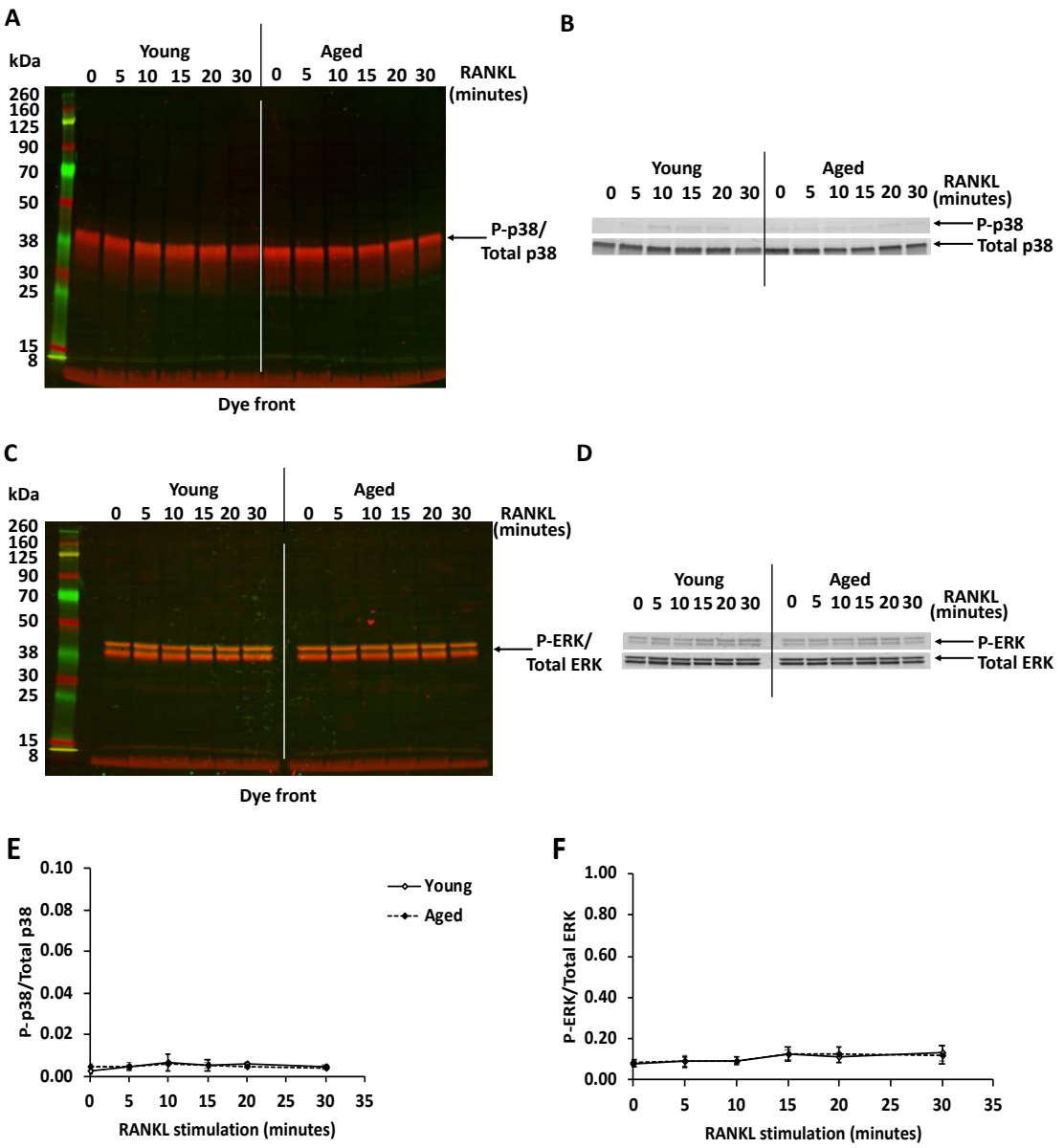

Figure 3.6: Western blot analysis of p38 MAPK and ERK phosphorylation in POCs from young and aged mice in RANKL time response assay. BMMs obtained from 3-4-month and 12-14-month-old C57Bl6 female mice and cultured with 25 ng/mL of M-CSF and 100 ng/mL of RANKL for 48 hours to obtain POCs, were stimulated with 100 ng/mL of RANKL for the indicated time points. Representative western blot of p38 phosphorylation (**A and B**) and of ERK phosphorylation (**C and D**) in colour with both 680 and 800 channels shown together and the same blot in black/white with individual channels shown separately. Quantification of the P-p38 and P-ERK show no activation of p38 (**E**) and ERK (**F**) in POCs from both young and aged mice (N=4). Total p38 and Total ERK were used for normalisation. The expected molecular weight for P-p38 and Total p38 MAPK is 38 kDa and 44/42 kDa for P-ERK and Total ERK. Data are shown as means ±SD. Unpaired two-tailed Student's *t* test was used to determine if the level of p38 and ERK phosphorylation was significantly different between POCs from young and aged mice.

Apart from RANKL, LPS, the toll-like receptor 4 (TLR4) ligand as well as a bacterial pathogenic factor, has been shown to induce OC formation and promote OC survival[199,574-576]. Hence, I conducted another stimulation assay by using LPS in order to have a positive control for ERK phosphorylation in OC precursors. Rather than stimulating for 5 different time points, the young and aged POCs were only stimulated for 15 minutes which is the time point when the maximum phosphorylation is reached in MCSF-dependent BMMs.

Similar to POCs treated with RANKL, p38 MAPK was not phosphorylated in POCs treated with LPS (**Figure 3.7 A, B and E**). These results confirmed my findings described earlier (**Figure 3.6 A, B and E**).

Surprisingly, ERK phosphorylation was significantly induced when POCs were treated either with RANKL or LPS (**Figure 3.7 C, D and F**). The level of P-ERK in POCs from aged mice was higher than in the POCs from young mice after stimulating either with RANKL or LPS for 15 minutes. These results indicate that p38 MAPK and ERK may be stimulated through different pathways in POCs. Moreover, ERK phosphorylation in response to RANKL is significantly higher in POCs from aged versus young mice.

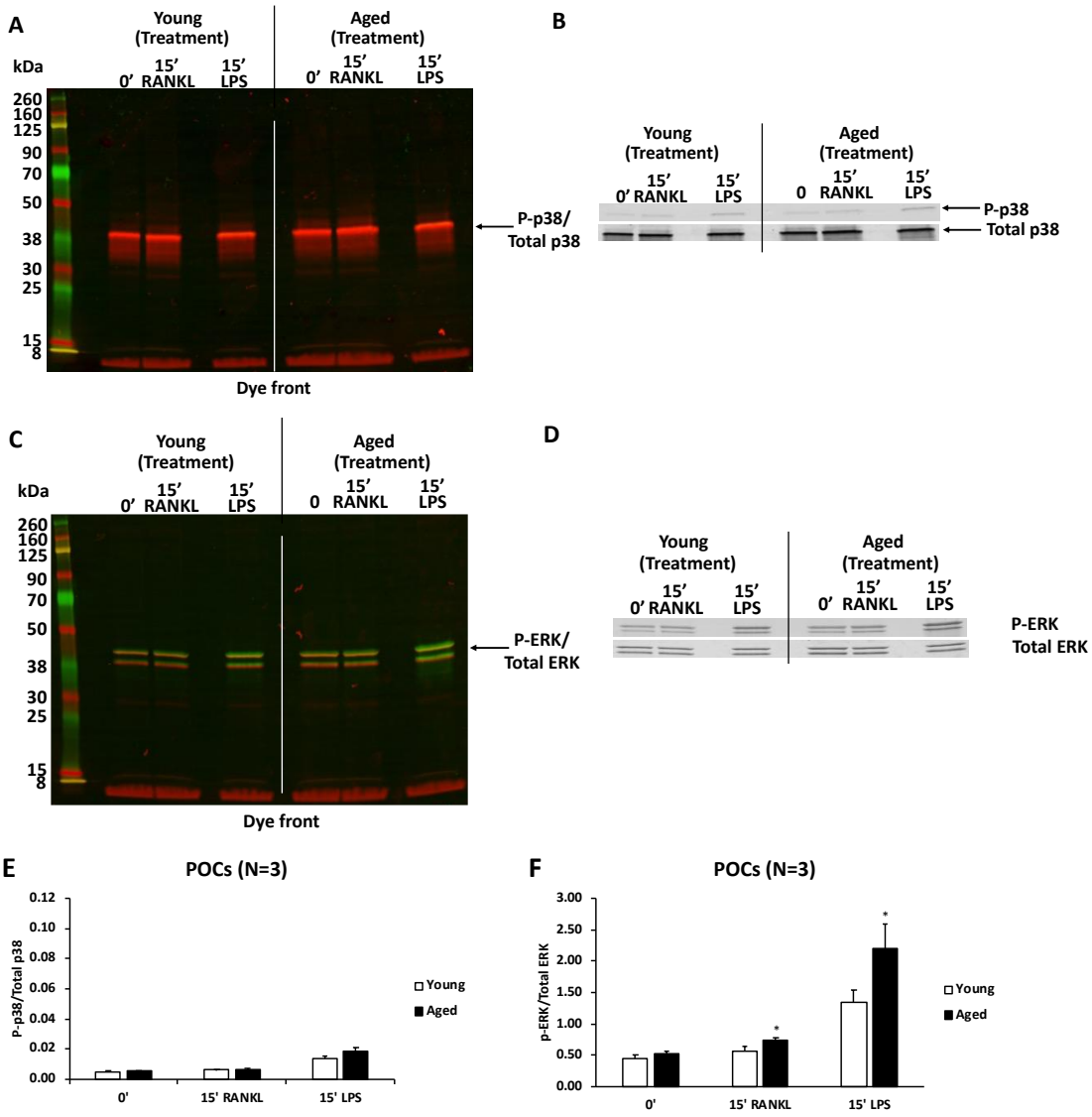

Figure 3.7: Western blot analysis of p38 MAPK and ERK phosphorylation in POCs from young and aged mice in RANKL or LPS stimulation assays. Serum-starved POCs prepared from BMMs isolated from 3-4-month and 12-14-month-old C57Bl6 female mice and cultured with 25 ng/mL of M-CSF and 100 ng/mL of RANKL for 48 hours, were stimulated with 100 ng/mL of RANKL or 2 ng/mL of LPS for 15 minutes. Representative western blot of p38 phosphorylation (**A and B**) and of ERK phosphorylation (**C and D**) in POCs from young and aged mice in colour with both 680 and 800 channels shown together and the same blot in black/white with individual channels shown separately. Quantification of the respective phosphorylated proteins show almost none or low level of p38 MAPK activation (**E**) and a significantly higher level of ERK activation in both the RANKL- and LPS-treated POCs from the aged mice than in the young ones (**F**) (N=3). Total p38 and total ERK were used for normalisation. The expected molecular weight for P-p38 and Total p38 MAPK is 38 kDa and is 44/42 kDa for P-ERK and Total ERK. LPS, lipopolysaccharide; POCs, pre-osteoclasts. Data are shown as means ±SD. Unpaired two-tailed Student's *t* test was used to determine if the level of p38 and ERK phosphorylation was significantly different between POCs from young and aged mice. Significance is denoted by *p<0.05.

3.3.3 TNF-α-mediated p38 MAPK phosphorylation of BMMs in ageing

LPS induces BMMs and fibroblasts to produce TNF-α which is a pro-inflammatory cytokine that is involved in the pathogenesis of bone resorption induced by inflammation and is able to promote OC formation and activation[206]. The circulating levels of TNF-α are increased in ageing due to increased inflammatory activity[577,578]. Thus, I performed a stimulation assay using TNF-α as the stimulant to assess for differences between p38 phosphorylation in BMMs with ageing.

p38 MAPK was activated upon TNF-α stimulation (**Figure 3.8 A-C**). The level of P-p38 reached the peak after 15 minutes of stimulation, followed by a gradual decrease. However, unlike after RANKL stimulation, there was no significant difference between BMMs derived from aged versus young mice (**Figure 3.8 C-E**). As I have previously shown that out of the MAPKs, p38 shows the highest differential response to RANKL with ageing, and due to time constraints, I did not proceed to examine the effect of TNF-α on the remaining MAPKs.

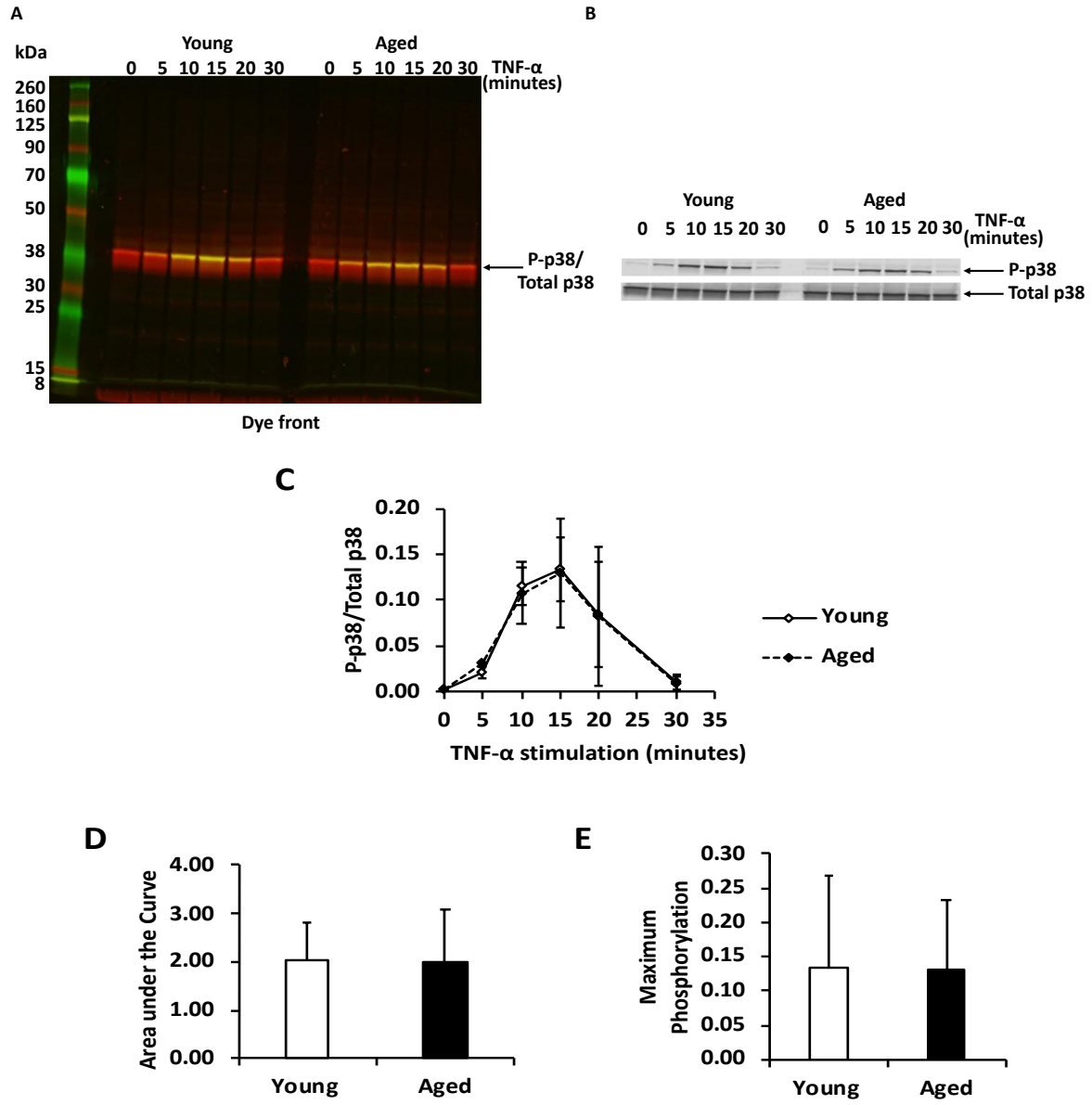

Figure 3.8: Western blot analysis of p38 MAPK phosphorylation in BMMs from young and aged mice in TNF-α time response assay. Serum-starved BMMs (isolated from 3-4-month and 12-14-month-old C57Bl6 female mice) cultured with 100 ng/mL of M-CSF were stimulated with 2 ng/mL of TNF-α for the indicated time points. Representative western blot of p38 phosphorylation in TNF-α time response assay in colour with both 680 and 800 channels shown together (**A**) and the same blot in black/white with individual channels shown separately (**B**). Quantification of P-p38 shows a gradual elevation, peak at 15 minutes and decline subsequently in BMMs from both young and aged mice (**C**). AUC (**D**) and maximum phosphorylation (**E**) reveal that both BMMs have the same level of p38 activation when stimulated with TNF-α (N=3). Total p38 was used for normalisation. The expected molecular weight for P-p38 and Total p38 MAPK is 38 kDa. Data are shown as means ±SD. Unpaired two-tailed Student's *t* test was used to determine if the level of p38 phosphorylation was significantly different between BMMs from young and aged mice.

3.3.4 RANKL-mediated upstream MKK phosphorylation of BMMs in ageing

To investigate if upstream MKK (please refer to **Chapter 1's Figure 1.3**) is responsible for the increase in p38 MAPK and ERK phosphorylation in ageing, the phosphorylation status of MKK3/6 in a RANKL stimulation time response assay in BMMs from young and aged mice was detected using Western blot.

Upon RANKL stimulation, the level of P-MKK3 and P-MKK6 was very similar in BMMs from both young and aged mice. The results show no significant difference in MKK3 and MKK6 phosphorylation between BMMs from aged versus young mice (**Figure 3.9**). This indicates that the increased p38 MAPK and ERK phosphorylation is not due to increased MKK3/6 phosphorylation and may be caused by other upstream (e.g TRAF6 and TAB1) or downstream (e.g DUSPs) regulators which ought to be further studied.

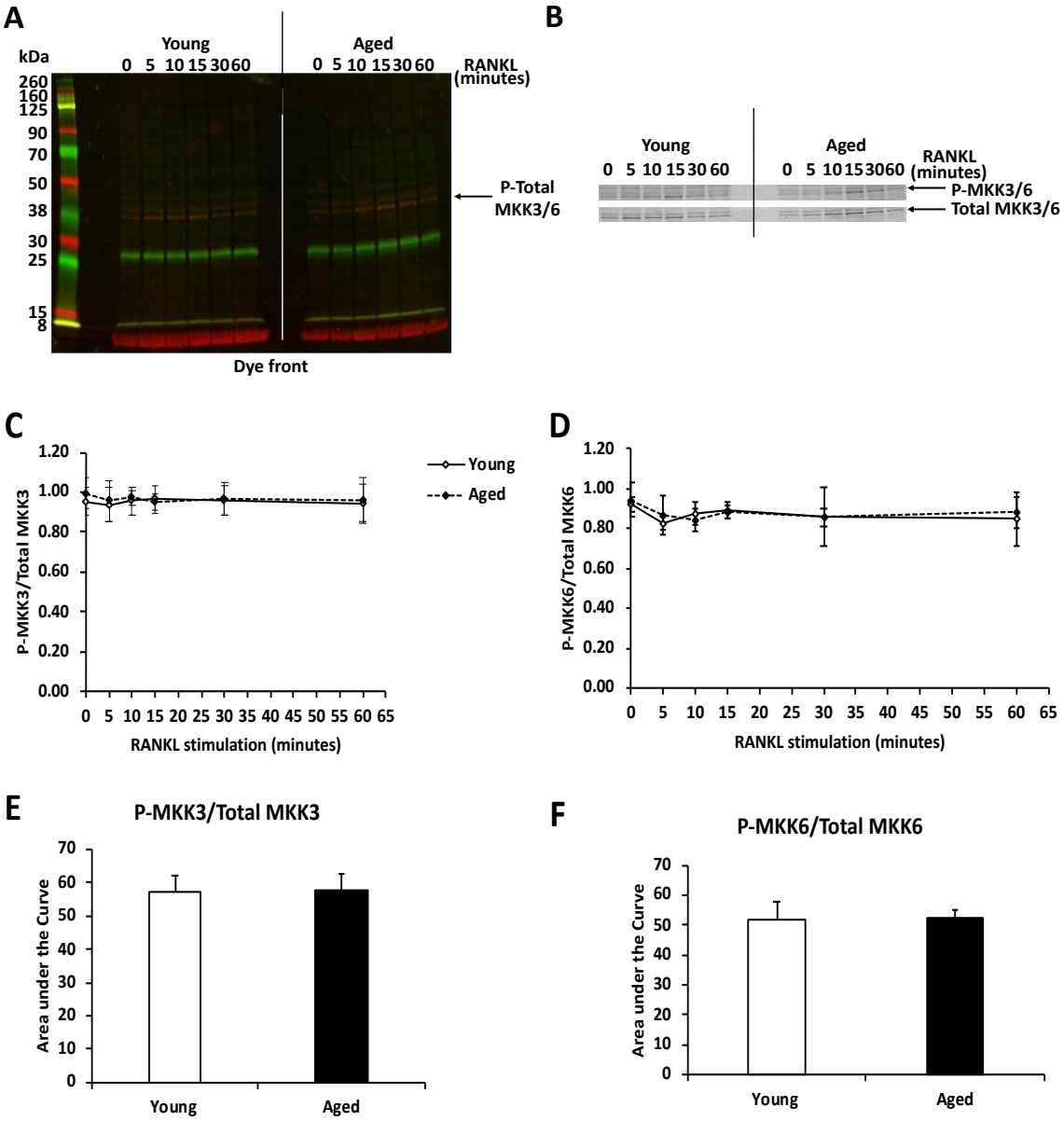

Figure 3.9: Western blot analysis of MKK3/6 phosphorylation in BMMs from young and aged mice in RANKL time response assay. Serum-starved BMMs (isolated from 3-4-month and 12-14-month old C57Bl6 female mice) cultured with 100 ng/mL of M-CSF were stimulated with 100 ng/mL of RANKL for the indicated time periods. Representative western blot of MKK3/6 phosphorylation in RANKL time response assay in colour with both 680 and 800 channels shown together (**A**) and the same blot in black/white with individual channels shown separately (**B**). Quantification of P-MKK3 and P-MKK6 shows no difference between BMMs from aged versus young mice (**C & D**). AUC (**E & F**) reveals that BMMs from aged versus young mice have no differential MKK3 and MKK6 activation (N=3). Total MKK3 or MKK6 were used for normalisation. The expected molecular weight for P-MKK3/6 and Total MKK3/6 is 40/38 kDa. Data are shown as means ±SD. Unpaired two-tailed Student's *t* test was used to determine if the level of MKK3/6 phosphorylation was significantly different between BMMs from young and aged mice.

3.3.5 RANKL-mediated NF-κB signalling of BMMs in ageing

NF-κB is a major transcription factor and its activation triggers the induction of NFATc1 transcription which is a master regulator of OC differentiation and fusion[50,88,579]. IκBα binds to and sequesters NF-κB in the cytoplasm, inhibiting it from translocating to the nucleus and regulating gene expression[580]. The phosphorylation of IκBα by IKKβ targets IκBα to the ubiquitin-proteasome pathway, resulting in the dissociation of IκBα from NF-κB[61]. NF-κB is no longer bound to IκBα and can translocate into the nucleus, where it activates response genes[61]. Therefore, I performed Western blotting following RANKL stimulation time response assay in BMMs from young and aged mice to determine if there are differences in IκBα phosphorylation, which would indirectly inform about the role NF-κB plays in increased osteoclastogenesis in ageing.

Upon 5 minutes of RANKL stimulation, P-IκBα reached the peak followed by returning to the basal level (**Figure 3.10 A-C**), indicating the targeting of P-IκBα for degradation. On the other hand, total IκB declined and reached the lowest level after 10 to 15 minutes of RANKL stimulation, followed by an increase in BMMs from both young and aged mice (**Figure 3.10 A, B and E**). AUC of IκBα phosphorylation showed no difference between BMMs from aged versus young mice (**Figure 3.10 D and F**). This indicates that NF-κB may not be responsible for increased osteoclastogenesis in ageing.

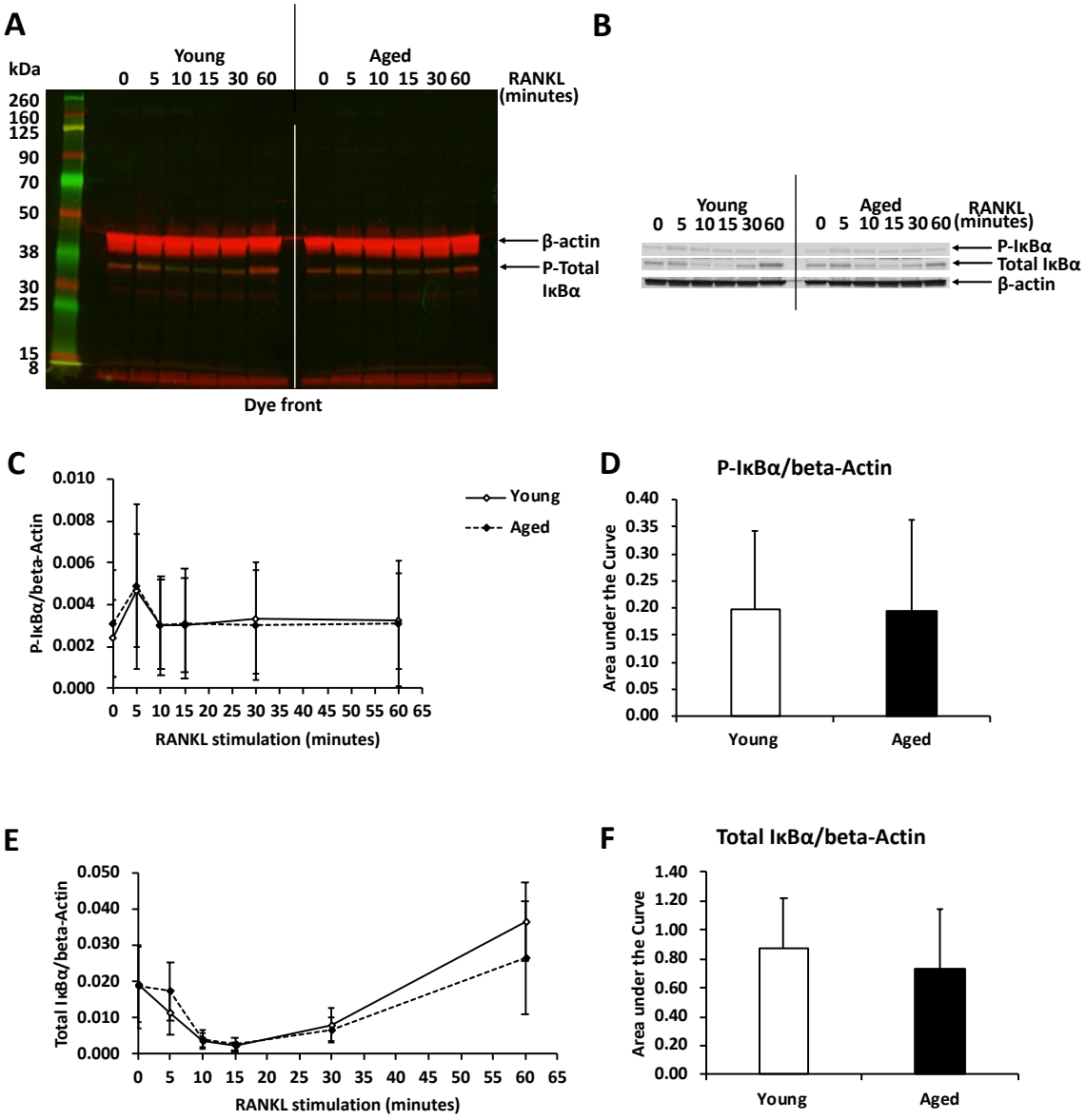

Figure 3.10: Western blot analysis of IκBα phosphorylation in BMMs from young and aged mice in RANKL time response assay. Serum-starved BMMs (isolated from 3-4-month and 12-14-month-old C57Bl6 female mice) cultured with 100 ng/mL of M-CSF were stimulated with 100 ng/mL of RANKL for the indicated time points. Representative western blot of IκB phosphorylation in RANKL time response assay in colour with both 680 and 800 channels shown together (**A**) and the same blot in black/white with individual channels shown separately (**B**). Quantification of P-IκBα and Total IκBα show the phosphorylation status of IκBα in response to RANKL stimulation in BMMs from both young and aged mice (**C and E**). AUC reveals no significant difference in IκB phosphorylation between BMMs from aged versus young mice (N=3) (**D & F**). β-actin was used for normalisation. The expected molecular weight for P-IκBα and Total IκBα is 40/39 kDa and is 42 kDa for β-actin. Data are shown as means ±SD. Unpaired two-tailed Student's *t* test was used to determine if the level of IκBα phosphorylation was significantly different between BMMs from young and aged mice.

3.3.6 RANKL-mediated expression of OC-related genes in ageing (next-generation RNA sequencing)

Due to the discovery of increased p38 MAPK and ERK phosphorylation in BMMs in ageing, I wanted to ask if the MAPK downstream targets are increased as well, which in turn could contribute to the increased osteoclastogenesis in ageing. Hence, I analysed the next-generation RNA sequencing data to study the expression of genes related to osteoclastogenesis in BMMs, POCs and OCs from young and aged mice. I concentrated on *Nfkb1*, *Nfkb2, Mmp9, Acp5, Atp6v0d2* and *Plekhm1* due to their role in OC differentiation and osteoclastic bone resorption.

Nfkb1 and *Nfkb2* are the two members of the NF-κB family, which encodes the protein p105 and p100 that serve as the precursors of p50 and p52 respectively[581]. Upon proteasomal degradation of NF-κB1 p105 and NF-κB2 p100, p50 and p52 are generated and subsequently translocate into the nucleus to induce the expression of their target genes such as *c-fos* and *NFATc1*, which play an important role in OC differentiation (please refer to **Chapter 1's Figure 1.3**). The gene expression of *Nfkb1* and *Nfkb2* showed no difference between BMMs from young and aged mice. When BMMs were differentiated into POCs in response to 48 hours of RANKL stimulation, the gene expression of *Nfkb1* and *Nfkb2* was significantly increased in POCs from aged mice compared to that of young ones (N=4, $p<0.01$). Upon 120 hours of RANKL stimulation, POCs were differentiated into mature OCs, and showed no difference in the gene expression of *Nfkb1* and *Nfkb2* between OCs from aged versus young mice (**Figure 3.11 A and B**).

Furthermore, pleckstrin homology domain-containing family M member 1 (encoded by *Plekhm1*) which is involved in OC vesicular trafficking[582,583], and matrix metalloproteinase 9 (MMP-9) which is predominantly expressed by OCs and plays a role in regulating osteoclastic activity[584,585], showed a similar result (**Figure 3.11 C and D**). The expression of *Plekhm1* (N=4, $p<0.01$) and *Mmp9* (N=4, $p<0.05$) are higher in POCs from aged mice compared to that of young mice, and no significant difference was observed between BMMs and mature OCs from aged versus young mice.

Moreover, the expression of *Acp5* (encodes TRAP) which is an OC marker, and *Atp6v0d2,* the OC-specific proton pump was upregulated (**Figure 3.11 E and F**). In addition, it was observed that the *Atp6v0d2* expression was already higher in BMMs from aged mice than that of the young ones. Based on these data, it is possible that the upregulation of those OC-related genes may be part of the reason of increased osteoclastogenesis in ageing. However, the result needs to be validated with qPCR.

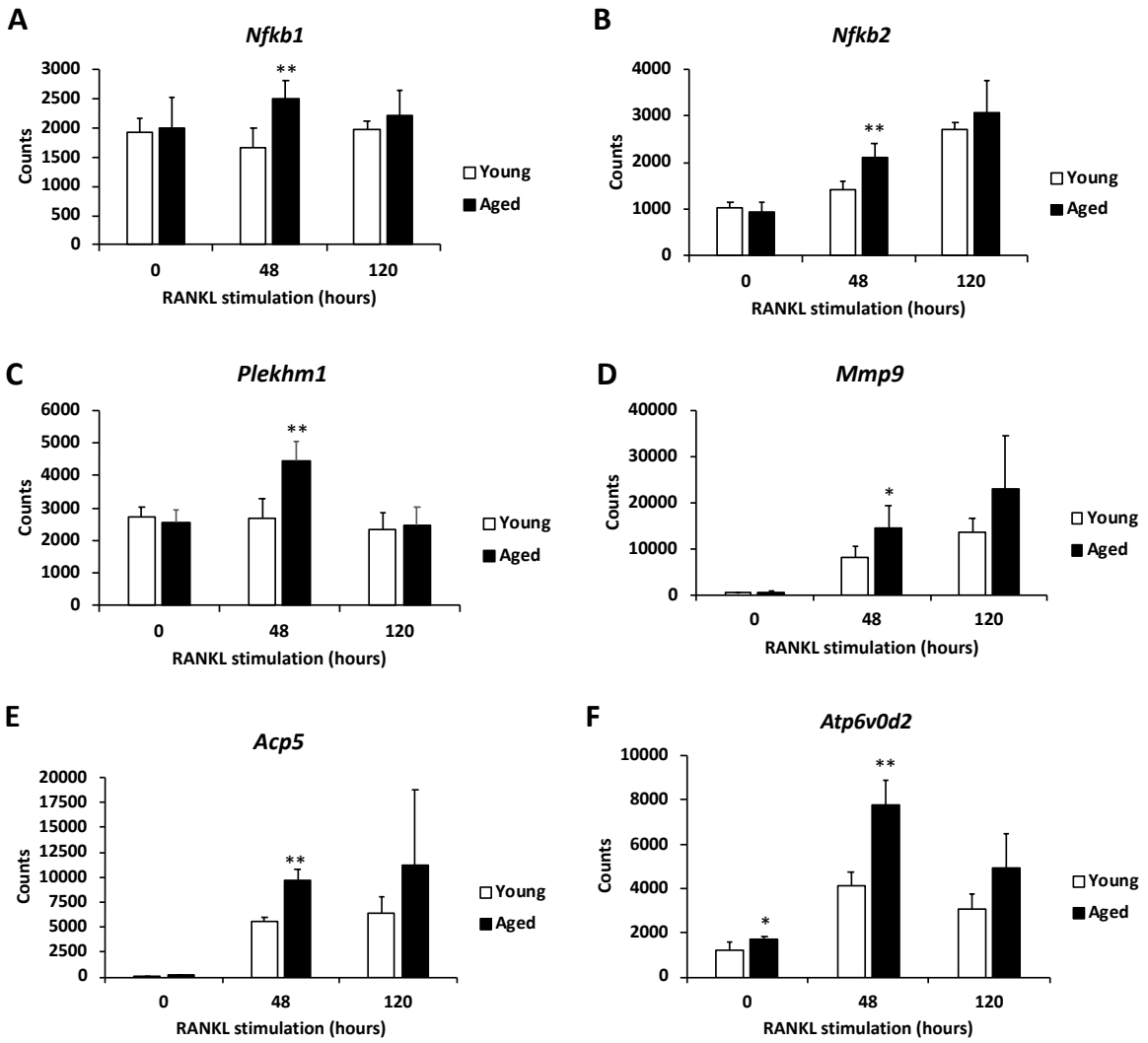

Figure 3.11: NGS data analysis of osteoclastogenic gene expression in BMMs, POCs and OCs from young and aged mice. BMMs were obtained from 3-month and 14-month-old C57Bl6 mice and cultured with 25 or 100 ng/mL of M-CSF and with 100 ng/mL of RANKL or without for indicated periods to obtain POCs (48 hours of RANKL) and OCs (120 hours of RANKL). Analysis of next-generation RNA sequencing shows a significant upregulation of osteoclastogenesis-related genes *Nfkb1* (**A**), *Nfkb2* (**B**), *Plekhm1* (**C**), *Mmp9* (**D**), *Acp5* (**E**) and *Atp6v0d2* (**F**) after 48 hours of RANKL stimulation in POCs derived from aged versus young mice (N=4). Data are shown as means ±SD. Unpaired two-tailed Student's *t* test was used to determine if the osteoclastogenic gene expression was significantly different between BMMs, POCs and OCs from young and aged mice. Significance is denoted by *p<0.05, **p<0.01.

As the phosphorylation of p38 MAPK and ERK in BMMs was found to be increased in ageing, I wanted to further explore the underlying reasons that caused the increase. As mentioned previously in **Sub-section 3.3.4**, the downstream regulators of MAPKs such as DUSPs could be one of the factors that caused increased p38 MAPK and ERK phosphorylation, and thus, I analysed the next-generation RNA sequencing data to study the gene expression of dual-specificity MAPK phosphatases in BMMs, POCs and OCs from young and aged mice.

Dual-specificity MAPK phosphatases (MKPs/DUSPs) are responsible for dephosphorylating both tyrosine and serine/threonine residues of MAPKs[586]. Each DUSP has different substrate specificity and displays preference for one or more of the MAPKs based on the interaction of kinase interacting motifs (KIMs) within the amino terminal region with the common domain (CD) of MAPKs[586]. DUSP1 prefers JNK and p38 MAPK over ERK[587-589], while DUSP3 prefers ERK and JNK with no activity towards p38 MAPK[590-592]. In addition, DUSP4 preferentially dephosphorylates ERK and JNK with little activity towards p38 MAPK[593], and DUSP9 prefers ERK over p38 MAPK with no activity towards JNK[594,595].

The gene expression of *Dusp1* (**Figure 3.12 A**)*, Dusp3* (**Figure 3.12 B**)*, Dusp4* (**Figure 3.12 C**) and *Dusp9* (**Figure 3.12 D**) showed no difference between the young and aged BMMs (RANKL stimulation at 0 hour). When BMMs were differentiated into POCs in response to 48 hours of RANKL stimulation, gene expression of the four *Dusps* was significantly increased in the aged POCs compared to the young POCs ($N=4$, $p<0.01$). Upon 120 hours of RANKL stimulation, POCs were differentiated into mature OCs, and showed no difference in the gene expression of the four *Dusps* genes between OCs from aged versus young mice.

These data indicate that the increased p38 MAPK and ERK phosphorylation in BMMs with ageing is not due to downregulation of their specific phosphatases. Moreover, the results on the upregulation of the gene expression of all four *Dusp* in aged POCs needs to be validated with qPCR.

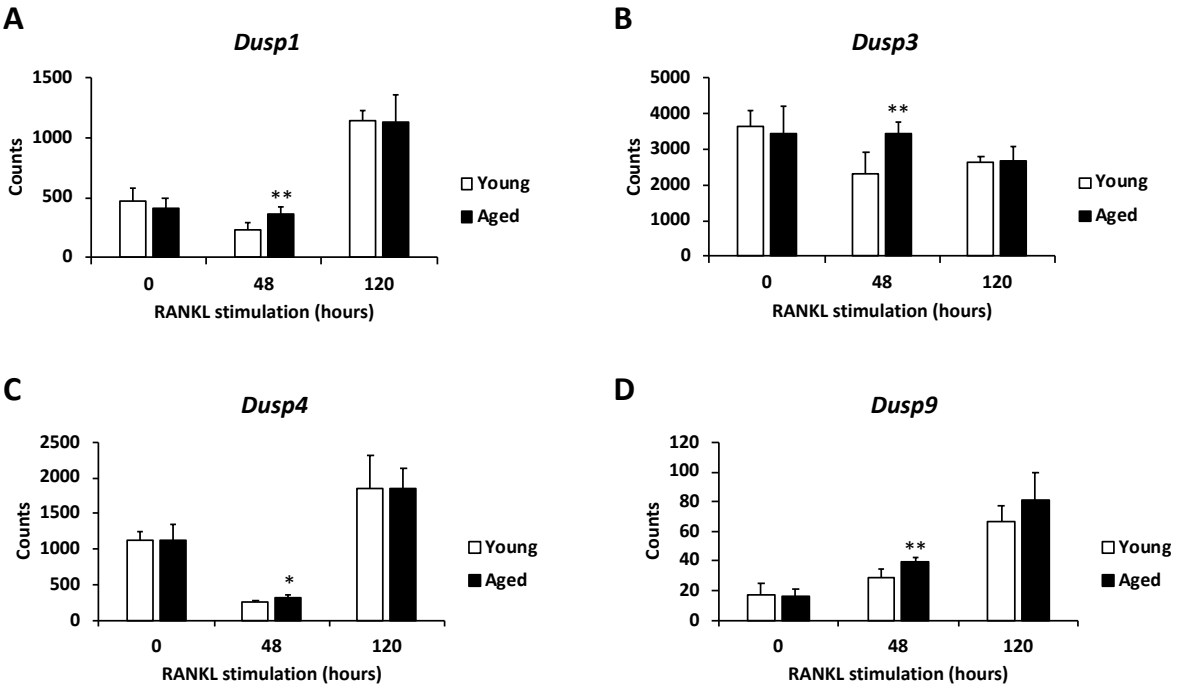

Figure 3.12: NGS data analysis of gene expression of dual-specificity MAPK phosphatases in BMMs, POCs and OCs from young and aged mice. BMMs were obtained from 3-month and 14-month-old C57Bl6 mice and cultured with 25 or 100 ng/mL of M-CSF and with 100 ng/mL of RANKL or without for indicated periods to obtain POCs (48 hours of RANKL) and OCs (120 hours of RANKL). Analysis of next-generation RNA sequencing shows a significant upregulation of phosphatase genes *Dusp1* (**A**), *Dusp3* (**B**), *Dusp4* (**C**) and *Dusp9* (**D**) after 48 hours of RANKL stimulation in POCs derived from aged versus young mice (N=4). Data are shown as means ±SD. Unpaired two-tailed Student's *t* test was used to determine if the gene expression of *Dusps* was significantly different between BMMs, POCs and OCs from young and aged mice. Significance is denoted by *p<0.05, **p<0.01.

3.3.7 RANKL-mediated expression of OC-related genes in ageing (analysed by using qPCR)

In the previous sub-section, the gene expression of *Atp6v0d2* was discovered to be increased in BMMs and POCs from aged mice via next-generation RNA sequencing analysis. I validated the result with the assistance of an Honours project student, Ellie McConachie.

Similar to the next-generation RNA sequencing analysis, RT-qPCR analysis has shown that the gene expression of *Atp6v0d2* in BMMs and POCs from aged mice was significantly higher than that of young mice. Upon 120 hours of RANKL stimulation, the *Atp6v0d2* expression continued to be increased in OCs derived from aged versus young mice (**Figure 3.13**). These data suggest that the RANKL-specific increase in p38 MAPK and ERK phosphorylation enhances *Atp6v0d2* causing increased osteoclastogenesis in ageing.

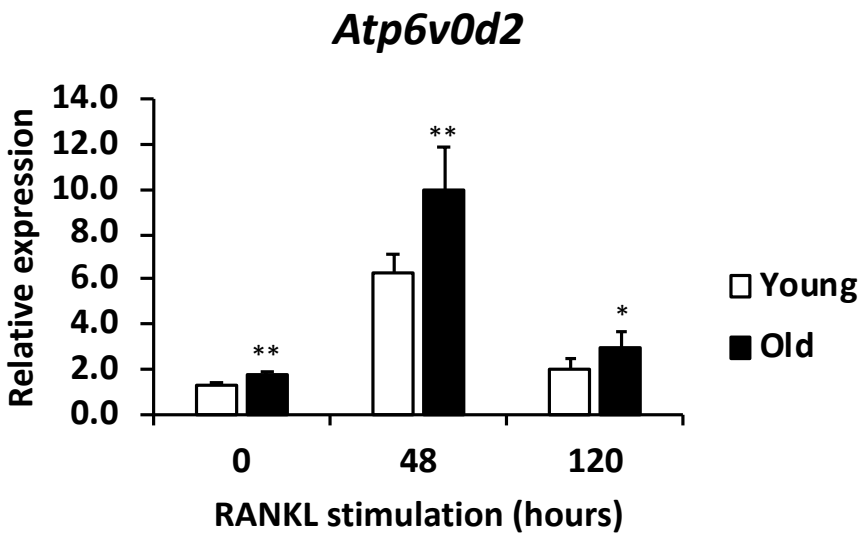

Figure 3.13: RT-qPCR analysis of *Atp6v0d2* in BMMs, POCs and OCs from young and aged mice. BMMs were obtained from 3-month and 14-month-old C57Bl6 mice and cultured with 25 or 100 ng/mL of M-CSF and with 100 ng/mL of RANKL or without for indicated periods to obtain POCs (48 hours of RANKL) and OCs (120 hours of RANKL). Analysis of relative expression to housekeeping gene *Hmbs* shows a significant upregulation of *Atp6vod2* after 0, 48 and 120 hours of RANKL stimulation in BMMs, POCs and OCs derived from aged versus young mice, respectively (N=3). Data are shown as means ±SD. Unpaired two-tailed Student's *t* test was used to determine if the gene expression of *Atp6v0d2* was significantly different between BMMs, POCs and OCs from young and aged mice. Significance is denoted by *p<0.05, **p<0.01.

3.3.8 RANKL-mediated expression of NFATc1 in OCs in ageing (analysed by using immunostaining)

NFATc1 is known to be the target of p38 in T cells[596] and the association of NFATc1 and PU.1 along with p38 regulates the expression of *CTSK* during osteoclastogenesis[51]. NFATc1 also induces OC fusion by upregulating *ATP6v0d2* and *DC-STAMP*[88]. Therefore, I performed immunostaining in BMMs, POCs and OCs from young and aged mice to detect NFATc1 expression, to establish if NFATc1 increases due to increased p38 MAPK phosphorylation in BMMs from aged mice, resulting in enhanced osteoclastogenesis in ageing.

The nuclear expression of *NFATc1* was upregulated in response to the RANKL stimulation for 48 and 120 hours in POCs and OCs derived from both young and aged mice (**Figure 3.14 A**). There is a trend of increased nuclear *NFATc1* expression in POCs from aged mice upon 48 hours of RANKL stimulation (**Figure 3.14 B**). However, the result needs to be validated by repeating the experiment for at least two to three times, or by performing Western blotting.

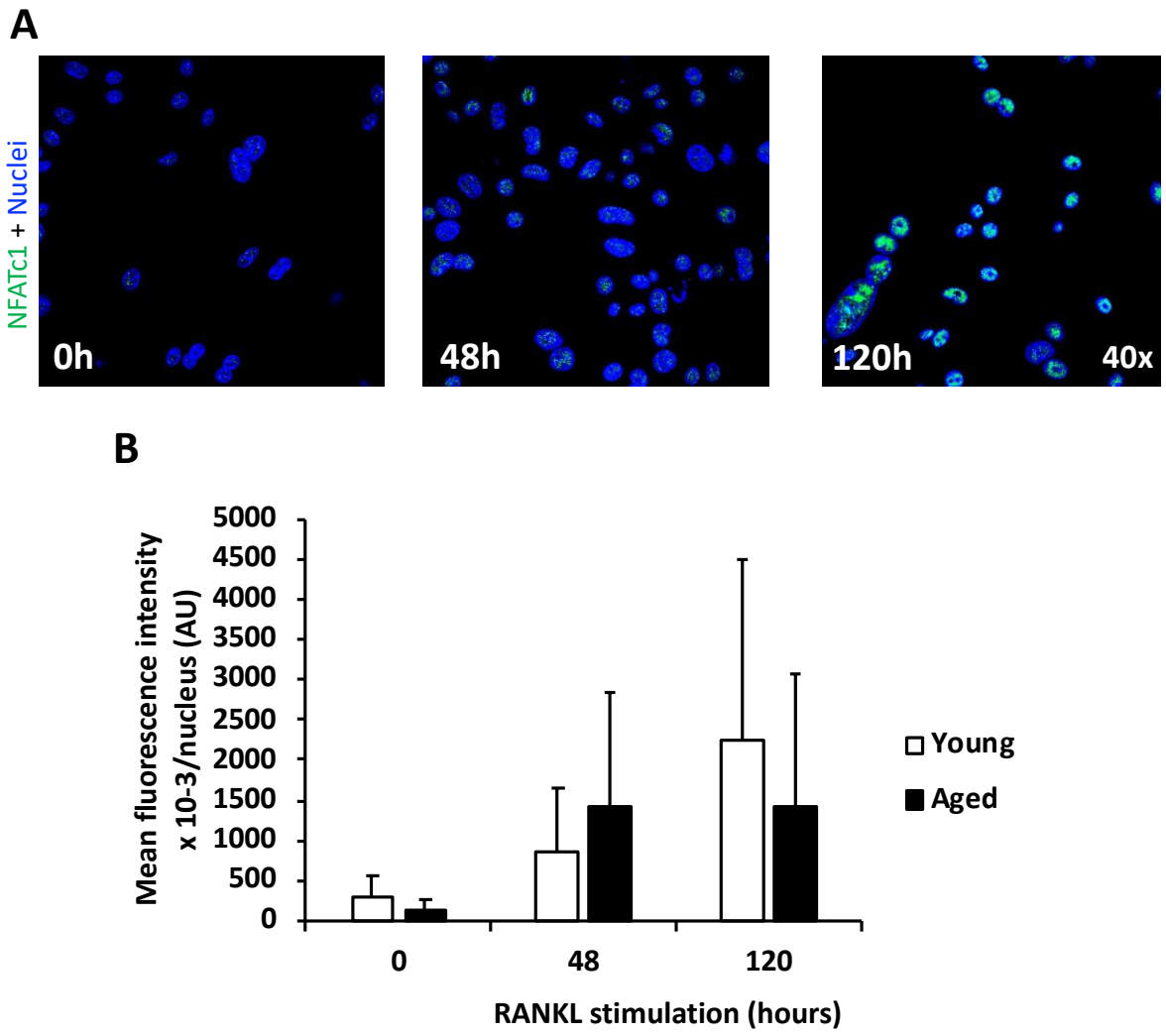

Figure 3.14: Immunostaining analysis of nuclear NFATc1 expression in BMMs, POCs and OCs from young and aged mice. BMMs were obtained from 3-month and 14-month-old C57Bl6 mice and cultured with 25 or 100 ng/mL of M-CSF and with 100 ng/mL of RANKL or without for indicated periods to obtain POCs (48 hours of RANKL) and OCs (120 hours of RANKL). Representative confocal microscopy images (**A**) of BMMs (0h), POCs (48h) and OCs (120h) from young mice. Quantification of mean fluorescence intensity (**B**) shows no difference between BMMs, POCs and OCs derived from aged versus young mice (N=1). 200-300 of cells per group were used in the quantification. Data are shown as means ±SD. Unpaired two-tailed Student's *t* test was used to determine if the nuclear NFATc1 expression was significantly different between BMMs, POCs and OCs from young and aged mice.

3.4 Discussion

Osteoporosis and PDB are the two most common age-related metabolic bone disorders. Osteoporosis is caused by generalised increase of osteoclastic bone resorption and decrease of osteoblastic bone formation, while PDB is due to focally increased bone resorption and formation[597,598]. Although significant advances have been made in the understanding of the genetic background of these two very different conditions , many questions remain unanswered. Indeed, the exact molecular mechanism underlying the increased OC activity in osteoporosis and PDB is not entirely clear.

To understand age-related changes in MAPK phosphorylation in relation to increased OC differentiation and activity, I performed western blot to quantifify the MAPK phosphorylation status in BMMs from young and aged mice upon RANKL stimulation. I found enhanced phosphorylation of p38 MAPK in BMMs from aged mice compared to that of young mice, which may explain increased osteoclastogenesis in ageing (**Figure 3.1**). I also found P-ERK to be slightly elevated with marginal significance in BMMs from aged mice but not JNK (**Figure 3.3 and 3.5**). The findings have been summarised in **Table 3.1.**

Table 3.1: Summary of the presence or absence of changes in gene or protein expression in BMMs, POCs, and OCs derived from young and aged mice.

Cell types	Changes in the gene expression							Changes in the protein expression									
								RANKL							LPS		TNF-α
								Time-response					Dose-response				
	Nfkb 1/2	*Plekhm1*	*Mmp9*	*Acp5*	*Atp6v0 d2* (by NGS)	*Atp6v0 d2* (by qPCR)	*Dusp 1/3/ 4/9*	P38	ERK	JNK	MKK 3/6	IκBα	P38	ERK	P38	ERK	P38
BMMs	-	-	-	-	+	+	-	+	+	-	-	-	-	-			-
POCs	+	+	+	+	+	+	+	-	-						-	+	
OCs	-	-	-	-	-	+	-										

All three main families of MAPKs take part in regulating the transmission of intracellular signalling for cell survival, proliferation and differentiation in response to stress and cytokines[599]. MAPK activation determines the transition between OC precursor proliferation and differentiation[188]. p38 MAPK and ERK are crucial in OC differentiation while ERK and JNK are essential in OC differentiation and survival[224,491,600].

It has also been reported that age-related bone loss in mice is associated with increased OC progenitor pool and osteoclastogenesis[440,573]. Another study has further showed that p38 MAPK regulates the proliferation and differentiation of OC progenitors in an age-dependent manner[197]. Therefore, the increase in p38 MAPK and ERK phosphorylation in BMMs from aged mice but not JNK may be the underlying reason that more OC precursors are differentiated in ageing, and results in an increased OC precursor pool.

Moreover, p38 MAPK and ERK bind to p62, which is the key regulator of autophagy, via p38 binding site (p38BS) and PB1 respectively[77,320]. By interacting with p38 MAPK and ERK, p62 is able to regulate p38 activities in a substrate-specific manner, as well as modulating adipogenesis and obesity[58,320]. In addition, P392L mutation at the UBA domain of p62 is associated with PDB[77] (will be discussed in detail in Chapter 5). Furthermore, P-p38 inhibits autophagy by directly competing with mAtg9 and binding with p38IP, p38 MAPK is activated and the dispersion of mAtg9 to the cell periphery is inhibited (please refer to **Chapter 1's Figure 1.8**)[354,601]. As a result, p38IP binds with P-p38 with a higher affinity, which inhibits autophagy[354,601] (will be discussed in detail in Chapter 4). Together with the findings in this study, it could be speculated that increased p38 MAPK phosphorylation may lead to an increase in the interaction between P-p38 and p38IP, and a decrease in the interaction between p38IP and mAtg9 in ageing (**Figure 3.15**).

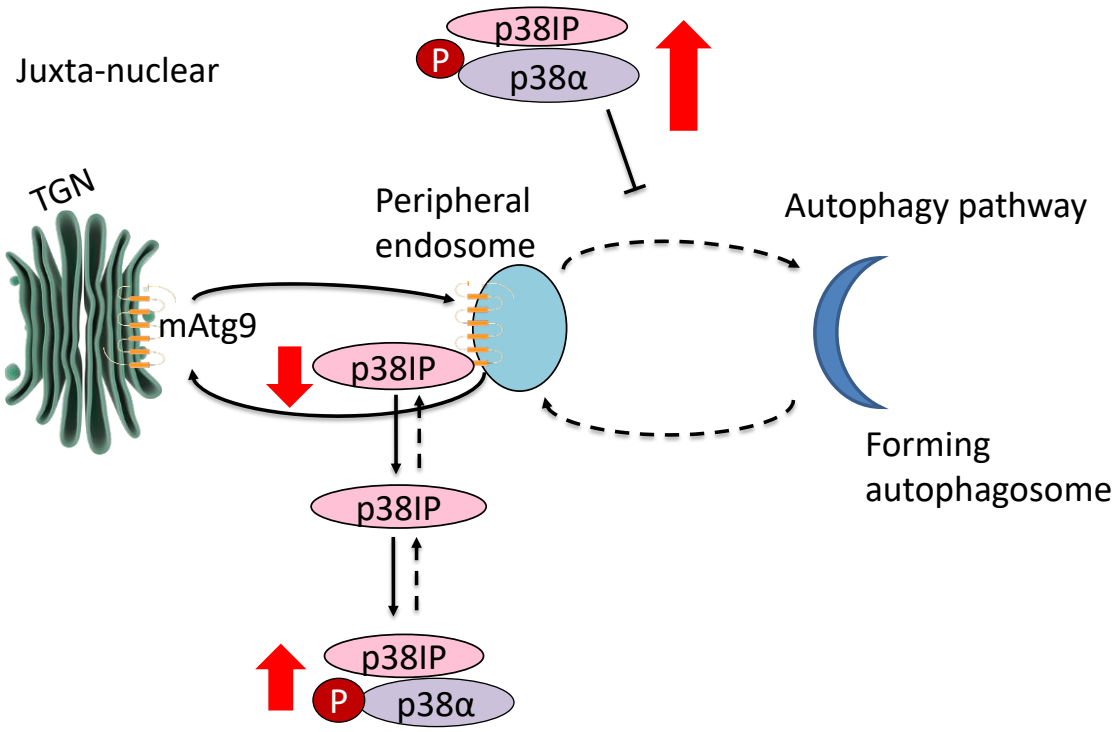

Figure 3.15: Hypothetical changes in the p38-p38IP-mAtg9 interaction in ageing. Increased p38 MAPK phosphorylation may lead to enhanced p38-p38IP interaction and reduced p38IP-mAtg9 interaction, thus inhibition of autophagy.

Furthermore, dose response assay was conducted to examine the sensitivity of BMMs in response to RANKL in ageing. The results show no difference in the p38 MAPK and ERK phosphorylation between BMMs from aged versus young mice with increasing dosage of RANKL (N=3) (**Figure 3.2 and 3.4**). Of note, the magnitude of p38 MAPK activity in dose response assay was relatively lower than that in time response assay when the BMMs derived from aged mice were stimulated with 100 ng/mL of RANKL for 15 minutes. In contrast, the magnitude of ERK activity in time response assay was relatively lower than that in dose response assay when the BMMs derived from aged mice were stimulated with 100 ng/mL of RANKL for 15 minutes. Although there were at least three replicates per assay, however the magnitude of MAPK activity may be affected due to different batches of BMMs that were used.

Unlike in BMMs, p38 MAPK and ERK were not phosphorylated in POCs upon RANKL stimulation **(Figure 3.6)** in keeping with the findings of Li *et al.* that showed no p38 MAPK

phosphorylation in mature OCs[199]. Thus it has been suggested that p38-mediated signal transduction is essential for induction of RANKL-induced OC differentiation, but not for the OC function[199].

The higher level of P-p38 in BMMs from aged mice could be due to enhanced activation of the upstream signalling molecules, MKK3/6 which phosphorylate p38 MAPK. To investigate the protein expression level of P-MKK3/6, the blots were probed with respective antibodies, using the total MKK3/6 as the normalisation protein. Surprisingly, the result showed no difference in the ratio of P-MKK3/6 to total MKK3/6 between young and aged BMMs **(Figure 3.9).**

Another explaination would be a reduced rate of dephosphorylation in ageing. The MAPK pathways are a three-tiered kinase cascade in which their activation involves sequential phosphorylation whereas deactivation requires dual-specificity threonine/tyrosine (Thr/Tyr) protein phosphatases (DUSPs)[602]. The duration and intensity of MAPK activation are pivotal factors of physiological outcome in cells, OC differentiation in this case[603]. It is tightly regulated and does not simply switch off without the regulation of DUSPs on the negative feedback and crosstalk mechanisms of MAPK activity[603]. The MAPK pathway output reflects the balance between the activity of upstream pathway components and the negative modulatory mechanism[602]. With the results of enhanced p38 MAPK phosphorylation without disparity in MKK3/6 phosphorylation, it is possible that there could be an alteration in DUSPs which inactivate the P-p38 MAPK by removing the phosphate groups from either the threonine residue or tyrosine residue or both. As the addition of phosphate groups on both the residues is necessary for their activation, removal of either residue is sufficient for inactivation[602,604].

Generally, DUSPs have been categorised into three subgroups based on sequence homology, substrate selectivity and subcellular localisation[602]. First of which are mitogen- and stress-inducible MKPs located in the nucleus that includes DUSP1/MKP-1, DUSP2 (PAC1), DUSP4/MKP-2 and DUSP5. DUSP1 is identified as a negative regulator of p38 MAPK and DUSP2 is predominantly expressed in hematopoietic tissues (OCs are hematopoietic-origin) and is more specific targetting of ERK than p38 MAPK[193,605]. DUSP6/MKP-3, DUSP7/MKP-X

and DUSP9/MKP-4 are being classed as the second group localising in the cytoplasm and are specific to ERK[602]. DUSP8 (M3/6), DUSP10/MKP-5 and DUSP16/MKP-7 make up the final group which can be found both in the nucleus and cytoplasm[604,606]. The last group of MKPs has high specificity to P38 MAPK and JNK but not ERK while DUSP 10/MKP-5 is present exclusively in liver and skeletal muscle[607-611]. Therefore, the increased in p38 MAPK phosphorylation in BMMs with ageing may be due to a severe disruption in the Type I and III of DUSPs which are more specific to p38 MAPK whereas a moderate alteration in the Type II for the slight enhanced ERK phosphorylation.

In this study, the analysis of next-generation RNA sequencing data shows no difference in the expression of *Dusp1, Dusp3, Dusp4* and *Dusp9* between BMMs from aged versus young mice. However, the expression of all four *Dusps* were significantly higher in POCs from aged mice compared to that of young mice (**Figure 3.12**). This could partly be the reason why p38 MAPK and ERK phosphorylation was not detected in POCs by using Western blot when stimulated with RANKL (**Figure 3.6**). Furthermore, no difference in the expression of *Dusp2, Dusp5, Dusp6, Dusp7, Dusp8, Dusp10* and *Dusp16* between BMMs, POCs and mature OCs derived from aged versus young mice was observed (data not shown).

NF-κB is another pathway downstream of TRAF6 upon RANKL stimulation and is also one of the key players critical for OC survival, fusion and function[64,612,613]. The recruitment of TRAF6-p62-aPKC complex intitiates the phosphorylation of the IKK complex, thereby phosphorylating IκBα and subsequently targeting it for degradation through the ubiquitin-proteosome system (UPS)[563,614,615]. In consequence, the inactive NF-κB is no longer retained by IκB in the cytoplasm and is released to become active and translocate into the nucleus to activate the transcription of osteoclastogenic target genes. To investigate if NF-κB causes enhanced osteoclastogenesis and OC acitivity in ageing, the blots were probed for P-IκB. No difference in the ratio of P- IκB or Total IκB to β-actin between young and aged BMMs was found implying that there is no changes in IκB phosphorylation and degradation, and thus NF-κB activation followed by its nuclear translocation (**Figure 3.10**).

On the other hand, the next-generation RNA sequencing data analysis showed a higher expression of *Nfkb1* and *Nfkb2* in POCs from aged mice compared to that of young mice

(**Figure 3.11**). Increased NF-κB activation is associated with age-related systemic low grade inflammation and may contribute to enhanced osteoclastogenesis that could lead to osteoporosis[579,616]. Based on the findings, it is possible that the upregulation of *NF-κB* expression in POCs derived from aged mice favors the onset of age-related increase in OC formation and activity, which in turn leads to bone loss and skeletal ageing. Nevertheless, luciferase reporter assays to measure NF-κB activity in BMMs, POCs and OCs derived from young and aged mice may need to be conducted for verification.

P38 MAPK is activated by MKK3/6 (upstream) and undergoes dual phosphorylation at Thr and Tyr residues prior to phosphorylating its downstream transcription factors such as activating transcription factor 2 (ATF2), MITF and NFATc1[51,199,211,617], which in turn induces the expression of function-related genes, *Ctsk, Acp5, Atp6v0d2 and DC-STAMP*[88]. Increased p38 MAPK phosphorylation in ageing may elevate those downstream molecules as well, resulting in enhanced OC differentiation. Apart from that, p38 MAPK signalling pathway is also involved in the regulation of RANKL-induced MMP-9 activity, which is a type IV collagenase that is predominantly expressed in OCs and takes part in degradation of extracellular matrix[618].

Next-generation RNA sequencing data showed a statistically significant increase in the expression of *Mmp9, Atp6v0d2* and *Acp5* in POCs from aged mice compared to that of young mice (**Figure 3.11**). The result of *Atp6v0d2* was verified by qPCR and the expression of *Atp6v0d2* was observed to be increased in BMMs, POCs and OCs derived from aged mice when compared to cells derived from young mice (**Figure 3.13**). However, preliminary data of NFATc1 expression indicate no difference between BMMs, POCs and OCs from aged versus young mice (N=1) (**Figure 3.14**).

Atp6v0d2 was expressed at a low level in the unstimulated BMMs, followed by an increase in response to RANKL stimulation for 48 hours, when the cells begin to differentiate into mononuclear TRAP-positive POCs and subsequently fuse into multinucleated OCs (**Figure 3.11**). Concordantly, *Acp5* expression was undetected initially but elevated drastically upon 48 hours of RANKL stimulation where the cells have reached POCs stage (**Figure 3.11**).

As mentioned before, p38 MAPK and ERK were not activated in POCs when stimulated with RANKL. In order to have a positive control for ERK phosphorylation in OC precursors, LPS was used to stimulate the BMMs and POCs alongside with RANKL for 15 minutes which is the duration for the phosphorylation to achieve the peak. Although RANKL failed to induce p38 MAPK and ERK phosphorylation in POCs, I found that LPS does phosphorylate ERK in POCs and OCs (late stage of differentiation)[199]. Besides that, it also induces MKK3/6 and ATF2 phosphorylation which are the upstream and downstream signals of p38 in POCs but not OCs[199]. Surprisingly, it revealed that the ERK phosphorylation was significantly enhanced by 39% in POCs from aged mice (**Figure 3.7**). This implies that p38 MAPK and ERK may be activated through different pathway in POCs.

TNF-α is also known to be a stimulator of osteoclastogenesis. In addition, the production of circulating pro-inflammatory cytokines is increased in ageing, one of which is TNF-α[203,619]. To study if TNF-α response in BMMs also increases with ageing, BMMs were stimulated with TNF-α to trigger the MAPK phosphorylation. No difference was observed between the young and aged BMMs (**Figure 3.8**). Taken together, it suggests that increased osteoclastogenesis in ageing may be caused by the RANKL-mediated enhancement in p38 MAPK phosphorylation.

As a result, it suggests that the age-related enhanced osteoclastogenesis is caused by an increase in RANKL-mediated p38 phosphorylation and marginally in ERK phosphorylation, which both regulate OC differentiation (**Figure 3.16**). This lead to increased expression of *Nfkb1, Nfkb2, Plekhm1, Mmp9, Atp6v0d2* and *Acp5* that plays a role in OC differentiation, fusion and function. Further studies are needed to determine on how the elevated p38 phosphorylation leads to higher expression of *Nfkb1, Nfkb2, Plekhm1, Mmp9, Atp6v0d2* and *Acp5* in ageing, and how the p38 MAPK phosphorylation is induced in later stages of OC differentiation. Besides that, the underlying reason that caused the increase in p38 MAPK and ERK phosphorylation is yet to be discovered as well.

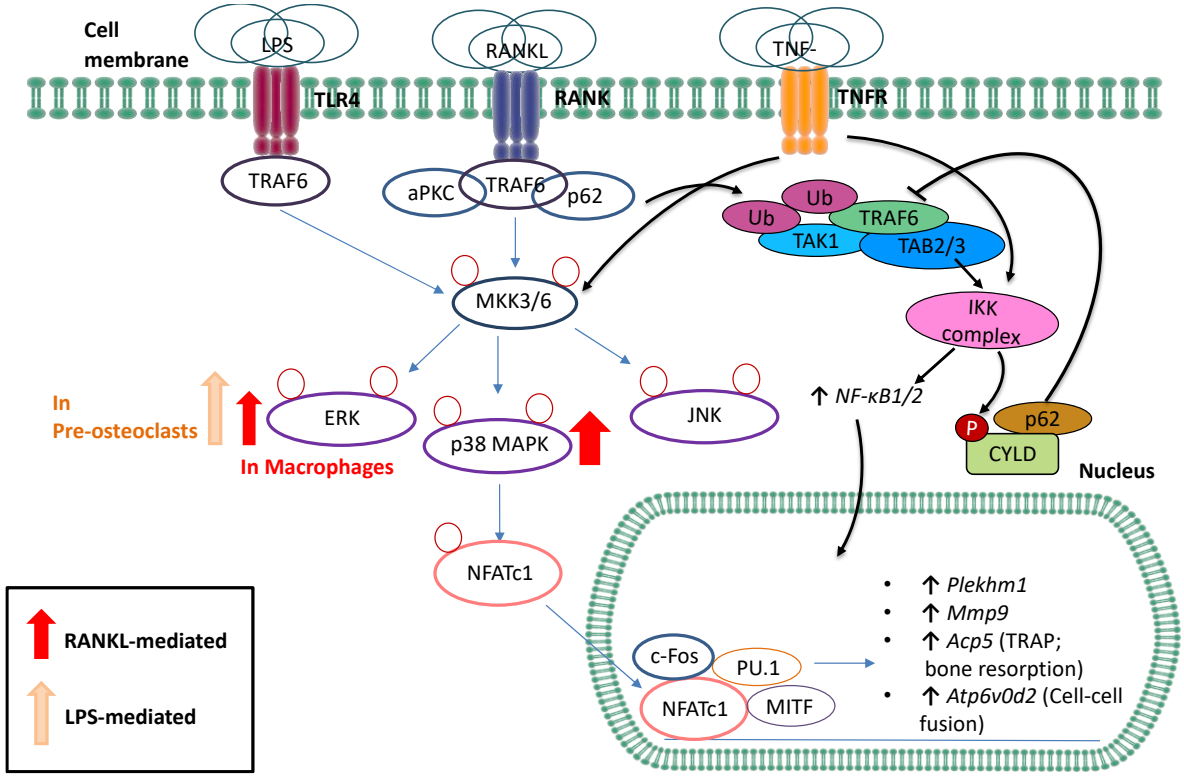

Figure 3.16: Changes in the signalling pathways in BMMs and POCs derived from aged mice (compared to young mice) during osteoclastogenesis. In ageing, RANKL-mediated p38 and ERK phosphorylation are increased (marginally in the latter) during osteoclast differentiation. This leads to enhanced expression of osteoclastogenic genes. ERK phosphorylation is also increased upon LPS stimulation. TNF-α does not induce differential activation in MAPK signalling pathway.

Chapter 4: Role of p38 and autophagy during osteoclastogenesis in ageing

4.1 Introduction

Autophagy is a major catabolic process that acts as a quality control mechanism in order to maintain cellular homeostasis which is essential for cell development and function. Decreased autophagic activity has been known to be one of the hallmarks of ageing[620,621]. Defective autophagosome formation and clearance could be caused by the failure of autophagosome-lysosome fusion, reduced lysosomal proteolysis, accumulation of undegraded macromolecules within lysosomes, or signalling-mediated deregulation of autophagy, which in turns lead to the low rate of protein degradation[622,623].

Growing evidence suggests an essential non-autophagic role of autophagy-related proteins in osteoclastic bone resorption. LC3-II was demonstrated to be involved in the regulation of OC secretion and osteoclastic bone resorption[36]. It was showed that LC3 lipidation which required the presence of Atg5, Atg7 and Atg4B was essential for the resorptive activity of OCs, the lysosomal secretion at the RB and the transport of LC3 itself to the RB[36]. When Atg5 or Atg7 was absent or the dominant negative mutant of Atg4B was expressed in the OCs, which results in the inhibition of LC3 conversion, reduced bone pit excavation, mislocalised CtsK and inhibited LC3 trafficking to the RB were observed[36]. Similar results were obtained when $Atg5^{K130R}$ which is a mutant form of Atg5 that is not conjugated to Atg12 was expressed in OCs[36].

Moreover, mAtg9 traffics between the TGN, peripheral endosomes and autophagosomes[624,625], and competes with p38α for p38IP interaction depending on nutrient status[354] (please refer to **Chapter 1's Figure 1.8**). In full medium, mAtg9 is localised at and trafficking between TGN and peripheral endosomes, where it binds to p38IP with a lower affinity[354,601,625]. However, upon starvation, the juxta-nuclear pool of mAtg9 is diminished. At the same site, p38IP binds to mAtg9 with a higher affinity due to dephosphorylation of p38, and travels to forming autophagosomes in a complex and colocalises with LC3 (autophagosome marker), facilitating autophagy[354,625].

My findings described in Chapter 3 show that the p38 phosphorylation is increased in aged BMMs in a RANKL-specific manner which could explain increased osteoclastogenesis and hyperactivity of OCs in ageing. As mentioned above, P-p38 plays an inhibitory role in autophagy. Therefore, this study aims to examine the changes in the autophagy pathway in osteoclastogenesis in relation to ageing.

4.2 Methods

Bone marrow was harvested from the long bones of 3-4-month and 12-14-month-old C57Bl6 female mice and cultured for BMMs, POCs and resorbing OCs as described in Chapter 2.

For gene expression studies, BMMs were stimulated with 100 ng/mL of RANKL and 25 ng/mL of M-CSF for 0, 48 and 120 hours, and the RNA was extracted. NGS was then performed in Oxford (**Figure 4.1**).

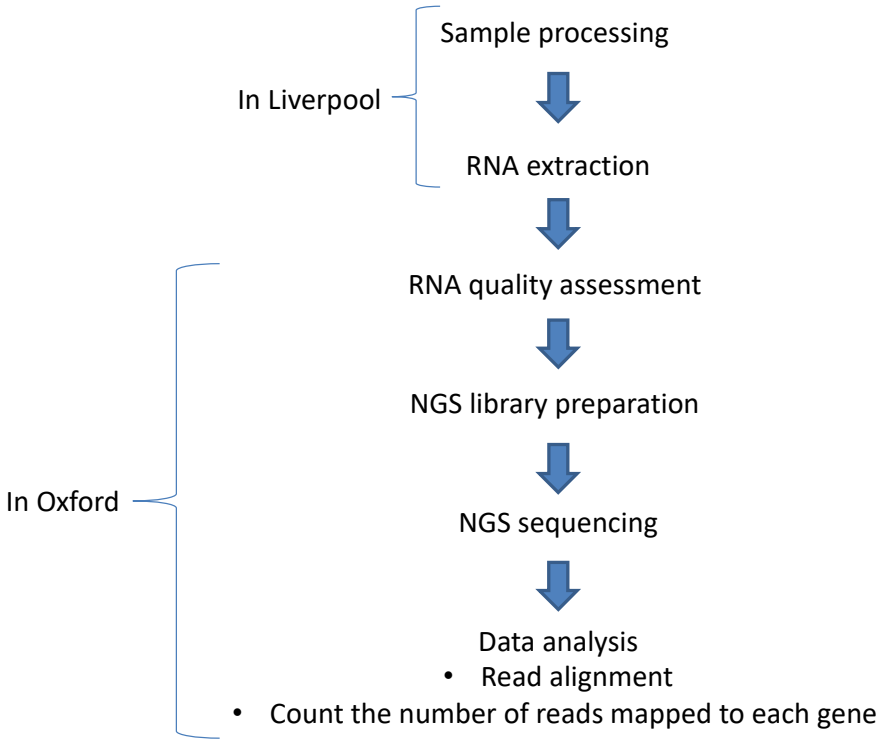

Figure 4.1: NGS data analysis pipeline. Following the sample processing and RNA extraction in Liverpool, the RNA quality was assessed on a TapeStation system. Libraries were then prepared and the samples were sequenced on an Illumina Nextseq 500 system. Reads were demultiplexed and aligned to the GRCm38.86 using HISAT2. Mapped reads were counted using Feature Counts with the Ensembl GRCm38.86 gtf used as reference. Counts were made at the exon level and summarised to the gene level.

For autophagic flux assay, BMMs, POCs and resorbing OCs were treated with 100 nM of bafilomycin B_1 (dissolved in dimethyl sulfoxide, DMSO) for 4 hours in order to inhibit autophagy by blocking V-ATPase-mediated acidification of lysosomes[626,627]. Same concentration of DMSO was used as a control.

Bicinchoninic acid (BCA) protein assay and Western blotting were conducted using standard protocols described in Chapter 2. After the blocking step, primary antibodies for LC3 (MBL International Corporation), p62 (Cell Signaling Technology) p38IP (Sigma) or β-Actin (Abcam) was added into the Odyssey blocking buffer (LI-COR Biosciences) at 1:1000 dilution and blots were probed overnight at 4°C with agitation, except for β-Actin which was diluted at 1:5000 and the blot probed for 1 hour at room temperature with agitation. For the western blot analysis of LC3 and p62 level, LC3 was first probed followed by β-Actin and p62 (**Figure 4.5, 4.6 and 4.7**).

Secondary antibodies: goat α-rabbit AF800 and goat α-mouse AF680 (LI-COR Biosciences) were added into the Odyssey blocking buffer containing 0.1 % Tween 20 at 1:10,000 dilution and blots probed for 1 hour at room temperature with agitation and protection from light.

The resorbing OCs on HA-coated coverslips in 12-well plates were fixed with 4% PFA and subjected to immunostaining using standard protocol described in Chapter 2.

To optimise the immunostaining, primary antibodies were diluted in 2.5% Goat serum (Vector Laboratories, Inc.) at the suggested range of 1:50 – 1:500 and the cells were immunostained for recommended duration (1 – 3 hours or overnight) and temperature (room temperature or 4°C), based on the respective product datasheets. The optimal dilution, duration and temperature for each antibody were summarised in **Table 4.1**. The standard protocol of immunostaining was performed as described in Chapter 2. Fluorescence images of young and aged cells were obtained using confocal microscope (Zeiss LSM 800) equipped with a 40x oil objective, and visualised under the same settings, along with the negative control. P-p38 was not included due to weak signal and transient p38 activation.

Table 4.1: Antibodies were used at different dilutions and conditions in the immunostaining.

Primary antibody	Conjugation	Dilution	Incubation period	Secondary antibody	Company
p38	AF546	1:50	O/N at 4°C	-	Santa Cruz Biotechnology
LC3	-	1:500	1h at RT	Goat anti-rabbit AF488/AF594	MBL International Corporation
p38IP	-	1:500	1.5h at RT	Goat anti-rabbit AF488	Sigma-Aldrich
Atg9a	-	1:50	1.5h at RT	Goat anti-rabbit AF488	Proteintech

RT, room temperature; O/N, overnight

Note: Atg9a is equivalent to mATG9 (mentioned previously in Chapter 1).

4.3 Results

4.3.1 Autophagy regulation of BMMs, POCs and mature OCs in ageing

To study how the expression of autophagy-related genes and proteins changes in BMMs, POCs and mature OCs from young and aged mice during ageing in bone homeostasis, I first analysed the data obtained from NGS, and then performed Western blotting in subsequent experiments. From the huge NGS dataset, *p38, p38IP, Atg9a, LC3b, Sqstm1, Atg5, Atg4B, Atg12* and *Atg7* were selected due to their role in autophagy and in regulating the generation of OC RB, lysosomal secretion and OC activity as mentioned in Chapter 1 and Section 4.1.

Gene expression quantification based on NGS showed that the *p38, LC3b, p38IP, Atg9a,* and *SQSTM1* were expressed at a similar level in BMMs from young and aged mice, and no significant differences were detected (**Figure 4.2**).

However, the expression of the genes mentioned above was upregulated in POCs from aged mice, compared to that of young mice. The upregulation of *p38, p38IP* and *Atg9a* expression in POCs from aged mice suggests that the interaction of p38-p38IP and p38IP-Atg9a were in equilibrium under full medium condition, therefore inhibiting autophagy. Nevertheless, the expression of *LC3b* and *SQSTM1,* which encode for LC3b and p62 (the autophagosome marker and autophagy adaptor respectively) was increased in POCs from aged mice as well. It is tempting to speculate that the observed increase in *LC3b* and *Sqstm1* genes is compensatory.

Previous study has reported increased synthesis of LC3b during OC maturation[359]. Hence, increased expression of both the autophagy-related genes may be due to the involvement in non-autophagy events that contribute to the enhanced osteoclastogenesis in ageing. Nonetheless, the results were yet to be validated by qPCR.

Similar to BMMs, no significant differences in the gene expression of *p38, LC3b, p38IP, Atg9a,* and *SQSTM1* were detected between mature OCs from aged versus young mice.

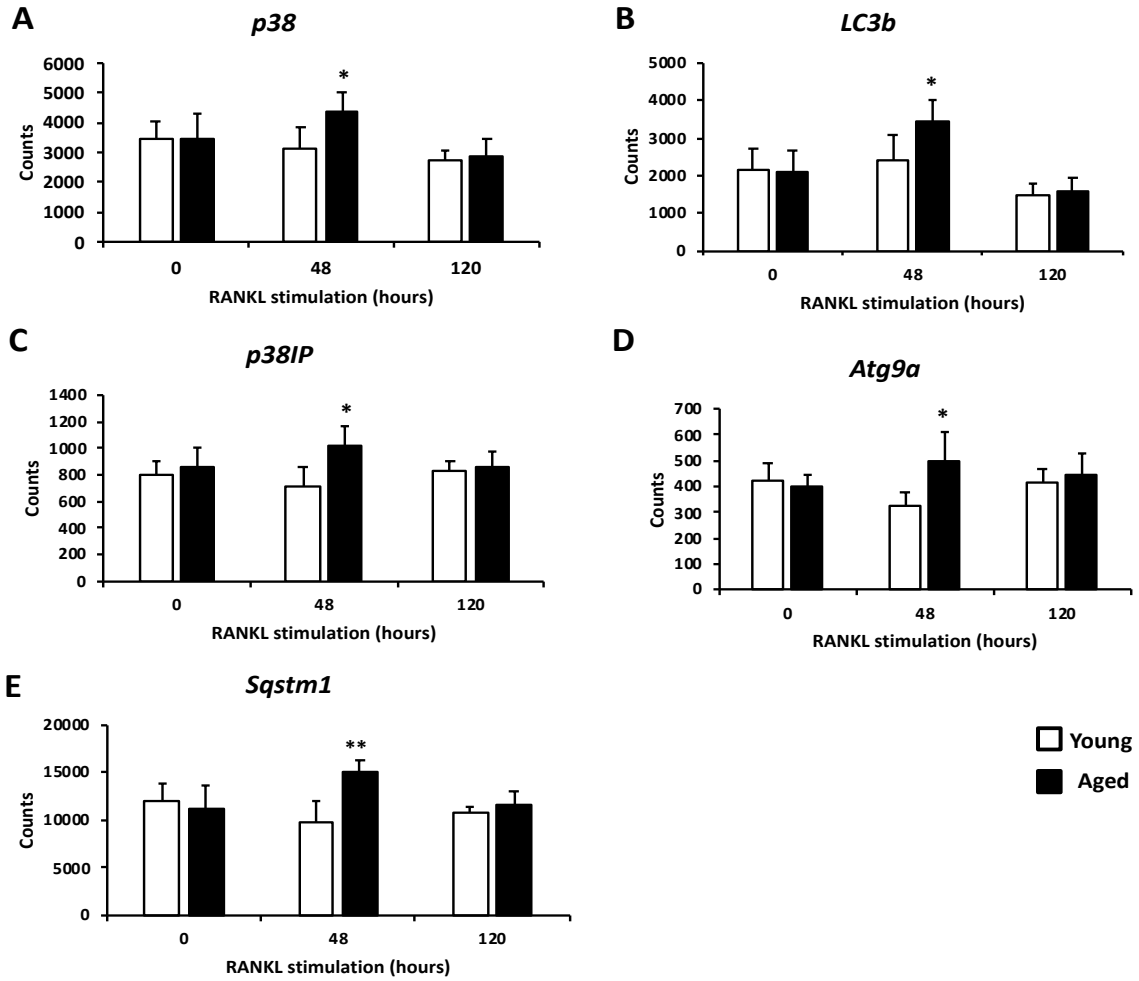

Figure 4.2: NGS data analysis of selected autophagic gene expression in BMMs, POCs and mature OCs from young and aged mice. Cells were prepared from BMMs isolated from 3-month and 14-month-old C57Bl6 mice and cultured on plastic with 25 or 100 ng/mL of M-CSF and 100ng/mL of RANKL for indicated periods. Cells were lysed and subjected to next-generation RNA sequencing analysis. The analysis shows an upregulation of *p38* (**A**), *LC3b* (**B**), *p38IP* (**C**), *Atg9a* (**D**), and *Sqstm1* (**E**) in aged POCs upon 48 hours of RANKL stimulation (N=4). Data are shown as means ±SD. Unpaired two-tailed Student's *t* test was used to determine if the selected autophagic gene expression was significantly different between BMMs, POCs and OCs from young and aged mice. Significance is denoted by *p<0.05, **p<0.01.

It was showed that *Atg5, Atg12, Atg4B* and *Atg7* genes were expressed at a similar level in BMMs from young and aged mice, and no significant differences were detected (**Figure 4.3**).

Interestingly, the expression of *Atg5, Atg12, Atg4B* and *Atg7* genes which are all involved in the formation of the RB, fusion of secretory lysosomes with the RB and bone resorption activity, were upregulated in POCs differentiated from aged mice (**Figure 4.3**). This suggests that the RB generation and lysosomal secretion may be enhanced, which could possibly explain why OC differentiation and activity are increased in ageing. However, these results have yet to be validated by qPCR.

Similar to BMMs, no significant differences in the gene expression of *Atg5, Atg12, Atg4B* and *Atg7* were detected between mature OCs from aged versus young mice.

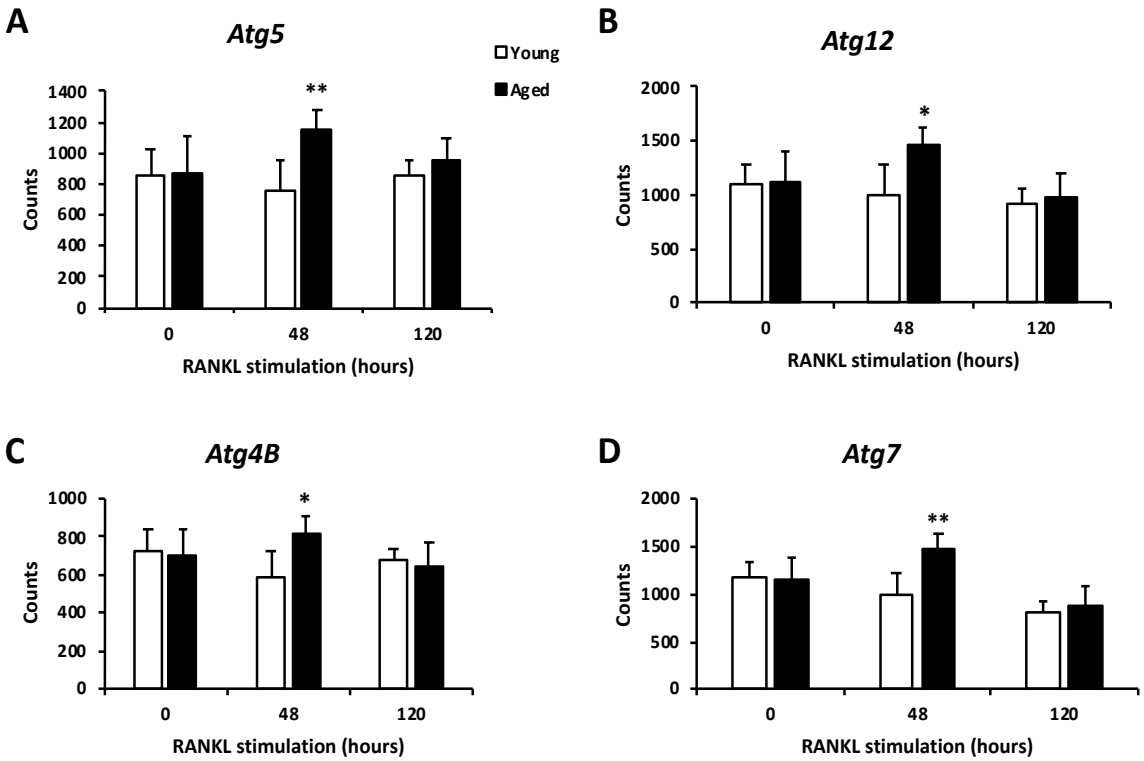

Figure 4.3: NGS data analysis of selected autophagic gene expression in BMMs, POCs and mature OCs from young and aged mice. Cells were prepared from BMMs isolated from 3-month and 14-month-old C57Bl6 mice and cultured on plastic with 25 or 100 ng/mL of M-CSF and 100ng/mL of RANKL for indicated periods. Cells were lysed and subjected to next-generation RNA sequencing analysis. The analysis shows an upregulation of *Atg5* (**A**), *Atg12* (**B**), *Atg4B* (**C**), and *Atg7* (**D**) in aged POCs upon 48 hours of RANKL stimulation (N=4). Data are shown as means ±SD. Unpaired two-tailed Student's *t* test was used to determine if the selected autophagic gene expression was significantly different between BMMs, POCs and OCs from young and aged mice. Significance is denoted by *p<0.05, **p<0.01.

As the preliminary data of NGS analysis showed an upregulation in *p38IP* expression in POCs from aged mice, it was expected that the protein expression would be increased as well. Therefore, I performed Western blotting to determine if there is a difference in the protein expression between BMMs and POCs from aged versus young mice.

Surprisingly, I could not detect a significant difference in the expression of p38IP protein in BMMs and POCs from aged versus young mice (**Figure 4.4**).

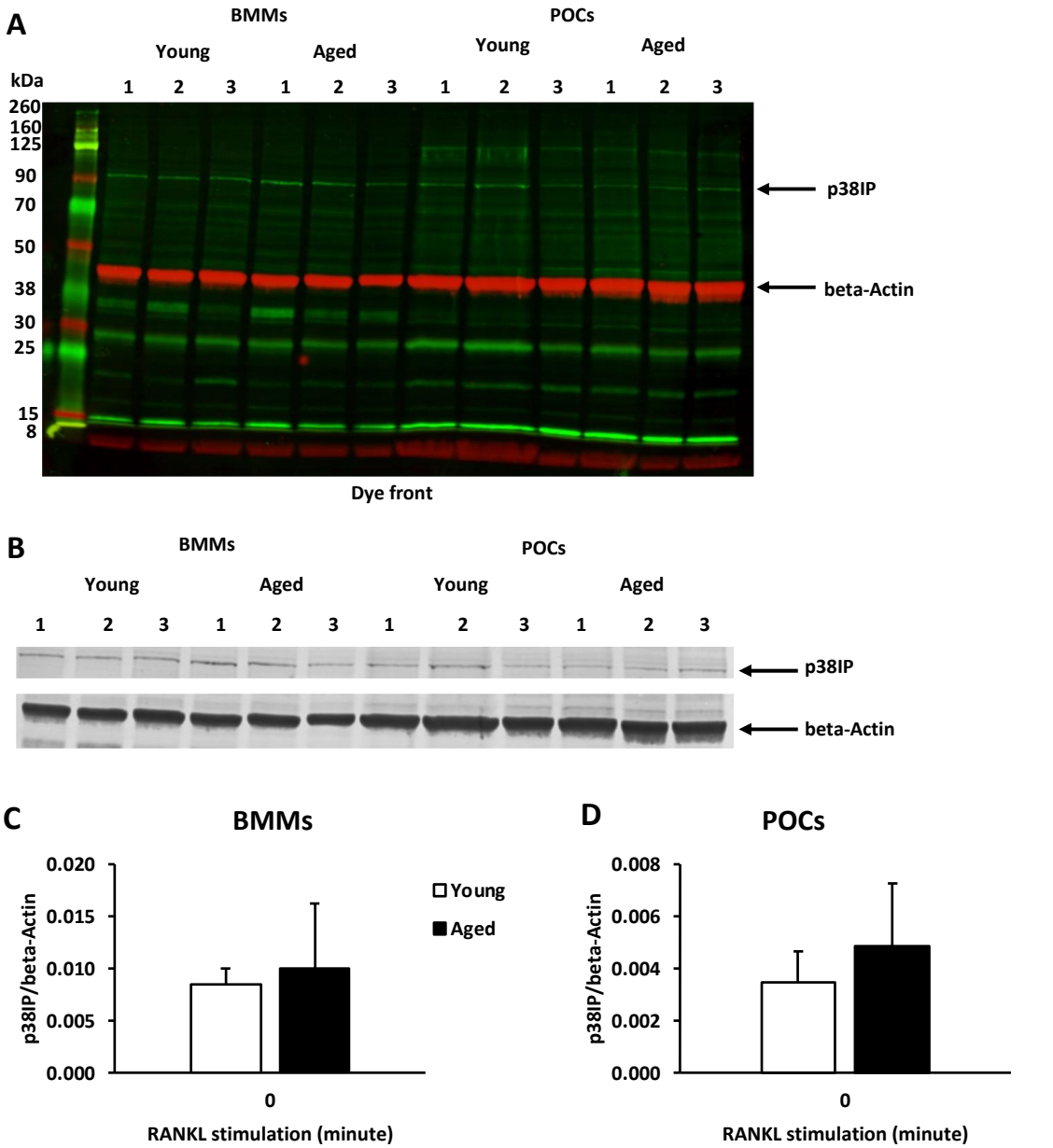

Figure 4.4: Western blot analysis of p38IP level in BMMs and POCs from young and aged mice. POCs were differentiated from BMMs of 3-4-month-old and 12-14-month-old female mice and cultured with 25 ng/mL of M-CSF and 100ng/mL of RANKL for 48 hours. Western blot of p38IP in colour with both 680 and 800 channels shown together (**A**) and the same blot in black/white with individual channels shown separately (**B**). Quantification of p38IP/β-actin shows no difference between young and aged BMMs (**C**) and POCs (**D**) (N=3). β-actin was used for normalisation. The expected molecular weight for p38IP is 95 kDa. Data are shown as means ±SD. Unpaired two-tailed Student's *t* test was used to determine if the level of p38IP was significantly different between BMMs and POCs from young and aged mice.

4.3.2 Autophagic flux of BMMs, POCs and resorbing OCs in ageing

The findings in **Sub-section 4.3.1** showed an upregulation in the autophagic genes in POCs (but not in OCs) differentiated from aged versus young mice. However, the OC differentiation was performed on plastic, therefore fully resorbing OCs were not obtained. Therefore, I conducted LC3 and p62 turnover assays to determine if there is a difference in autophagy flux between BMMs, POCs and resorbing OCs from young and aged mice cultured on HA-coated layer.

BMMs were treated with lysosomal inhibitor, Bafilomycin B_1 which inhibits autophagy, and as a result, LC3-II was observed to be accumulated (**Figure 4.5 A & B**). LC3-II accumulation in both young and aged BMMs was twofold higher in the presence of Bafilomycin B_1 (and statistically significant when compared to the absence of Bafilomycin B_1, $p<0.01$ and $p<0.05$, respectively), indicating that the effect of the inhibitor has taken place (**Figure 4.5 C**). However, there was no significant difference in the LC3-II (**Figure 4.5 C**) or p62 level (**Figure 4.5 D**) between young and aged BMMs, indicating a similar level of autophagy flux in BMMs in ageing.

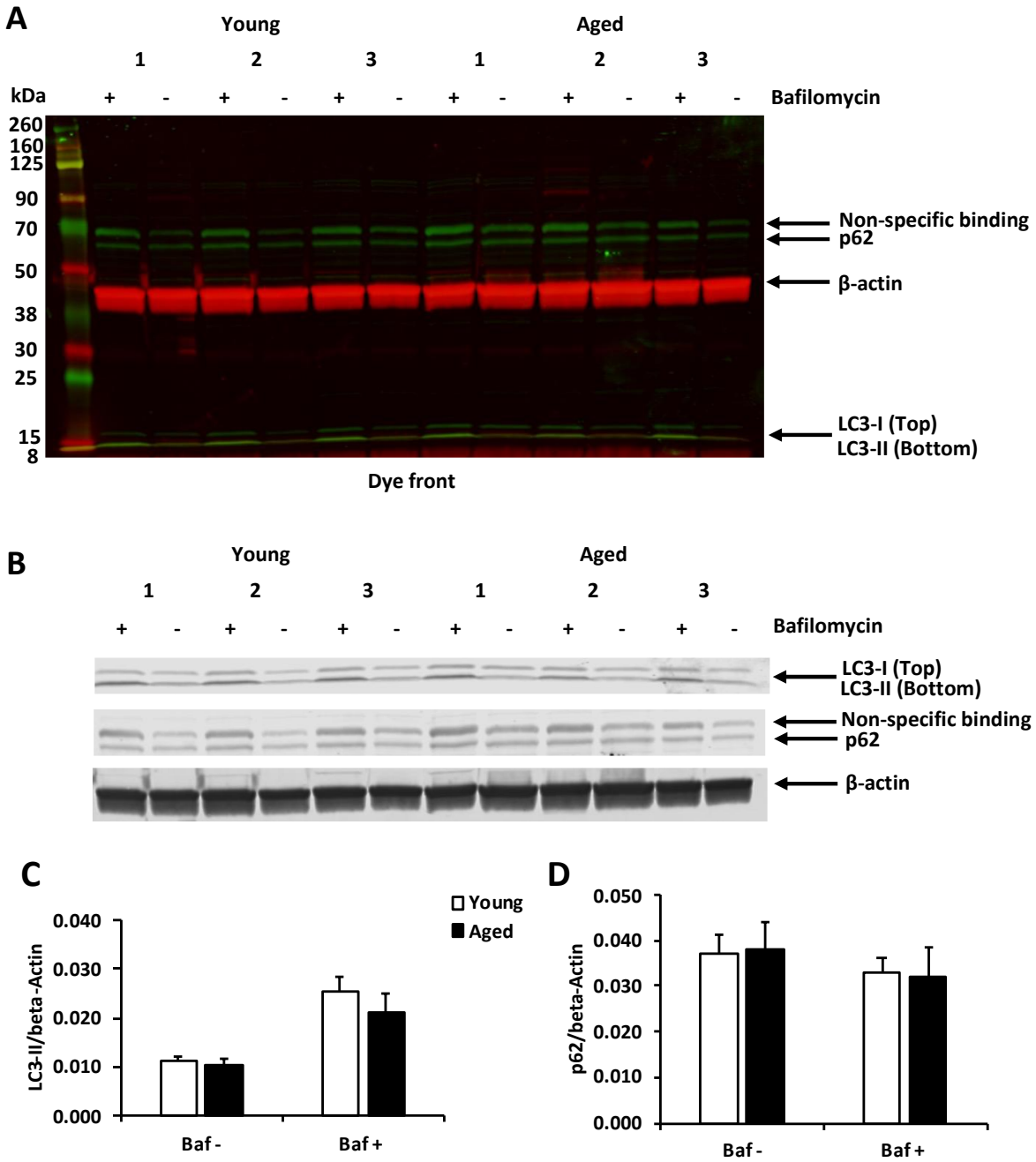

Figure 4.5: Western blot analysis of LC3 and p62 level in BMMs from young and aged mice. BMMs isolated from 3-4-month-old and 12-14-month-old C57Bl6 female mice and cultured with 100 ng/mL of M-CSF on HA-coated coverslips in 12-well plates were treated with 100 nM of bafilomycin B_1 for 4 hours. Western blot of LC3 and p62 in colour with both 680 and 800 channels shown together (**A**) and the same blot in black/white with individual channels shown separately (**B**). Quantification of LC3-II/β-actin (**C**) and p62/ β-actin **(D**) shows no difference between young and aged BMMs (N=3). The expected molecular weight for LC3-II and LC3-I is 14/16 kDa, and of p62 is 62 kDa. Data are shown as means ±SD. Unpaired two-tailed Student's *t* test was used to determine if the level of LC3-II and p62 was significantly different between BMMs from young and aged mice.

Increased amount of LC3-II in young and aged POCs with Bafilomycin B_1 was statistically significant compared to those without Bafilomycin B_1 ($p<0.01$ and $p<0.05$, respectively). Unlike in the BMMs, a significantly higher level of LC3-II was observed in POCs derived from aged mice when compared to that of young mice before and after the treatment with Bafilomycin B_1, suggesting increased autophagic flux with ageing (**Figure 4.6 A-C**). However, there was no significant difference in p62 level between POCs from aged vs young mice. (**Figure 4.6 D**). This result suggests an increase in autophagic flux during OC differentiation with ageing.

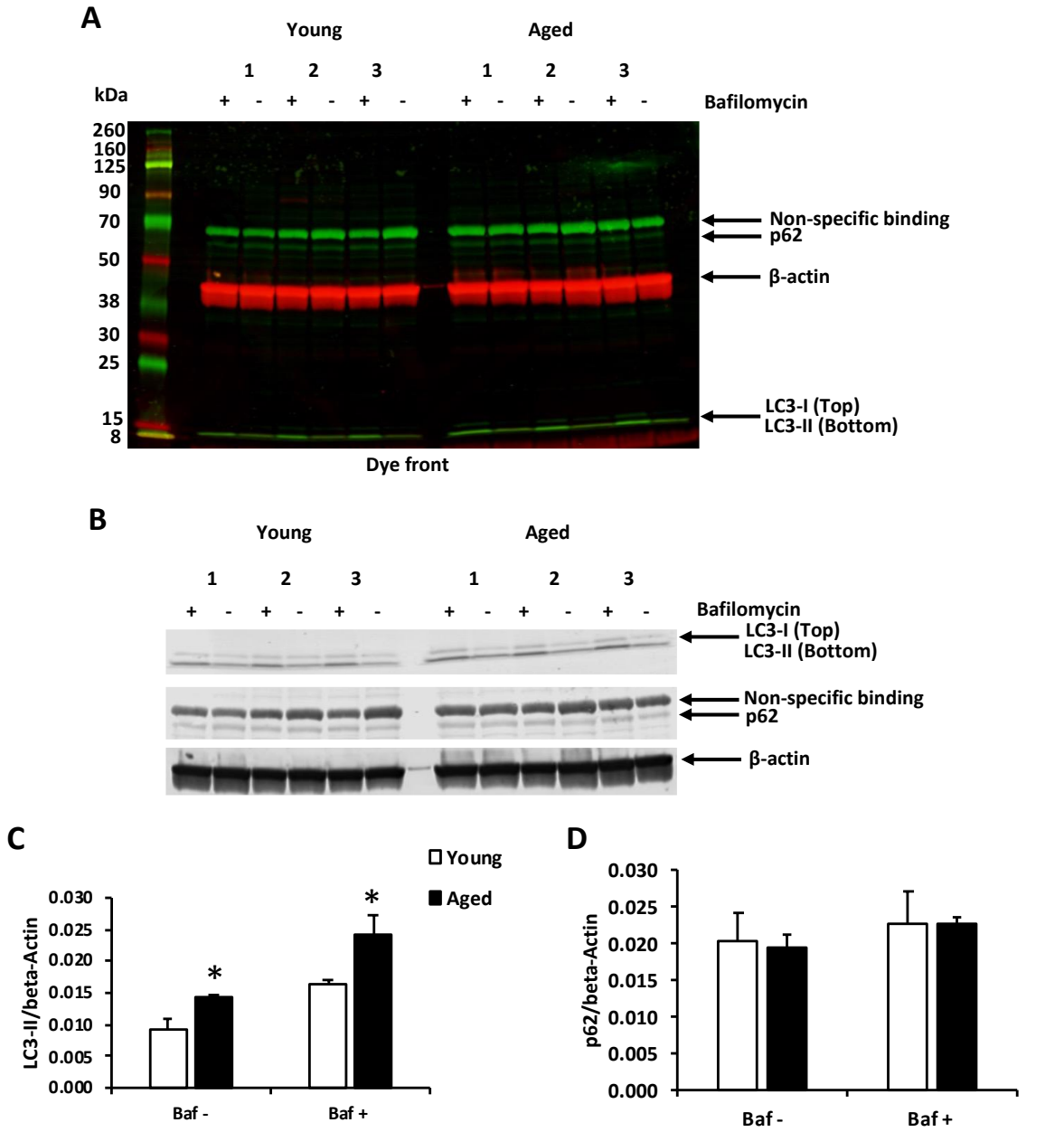

Figure 4.6: Western blot analysis of LC3 and p62 level in POCs from young and aged mice. POCs were differentiated from BMMs of 3-4-month-old and 12-14-month-old female mice and cultured with 25 ng/mL of M-CSF and 100 ng/mL of RANKL for 48 hours on HA-coated coverslips in 12-well plates. The POCs were treated with 100 nM of bafilomycin B_1 for 4 hours. Western blot of LC3 and p62 in colour with both 680 and 800 channels shown together (**A**) and the same blot in black/white with individual channels shown separately (**B**). Quantification of LC3-II/β-actin (**C**) displays a significantly higher level of lipidated LC3 in the aged POCs than the young, in the presence of bafilomycin (N=3). p62/ β-actin **(D)** shows no difference between young and aged BMMs. The expected molecular weight for LC3-II and LC3-I is 14/16 kDa, and of p62 is 62 kDa. Data are shown as means ±SD. Unpaired two-tailed Student's *t* test was used to determine if the level of LC3-II and p62 was significantly different between POCs from young and aged mice. Significance is denoted by *p<0.05.

The difference in the amount of LC3-II was statistically significant between the presence and absence of Bafilomycin B_1 in young and aged POCs ($p<0.05$ and $p<0.001$. respectively). Interestingly, there was no significant difference in the level of LC3-II or p62 between resorbing OCs from aged versus aged mice (**Figure 4.7**), indicating a similar level of autophagy in resorbing OCs in ageing.

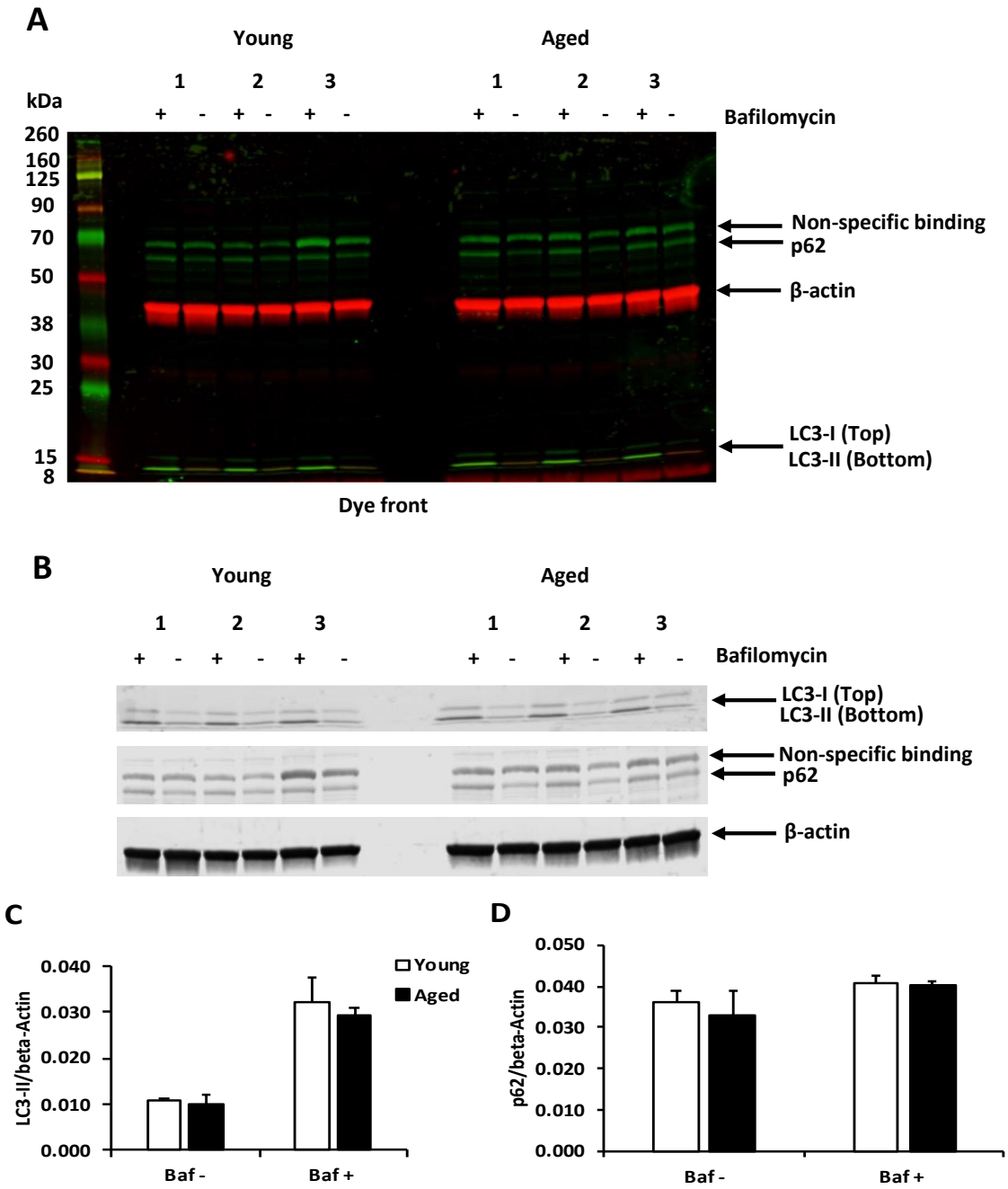

Figure 4.7: Western blot analysis of LC3 and p62 level in resorbing OCs from young and aged mice. OCs were differentiated from BMMs of 3-4-month-old and 12-14-month-old female mice and cultured with 25 ng/mL of M-CSF and 100 ng/mL of RANKL for 120 hours on HA-coated coverslips in 12-well plates. The cells were treated with 100 nM of bafilomycin B_1 for 4 hours. Western blot of LC3 and p62 in colour with both 680 and 800 channels shown together (**A**) and the same blot in black/white with individual channels shown separately (**B**). Quantification of LC3-II/β-actin (**C**) and p62/ β-actin **(D**) show no difference between young and aged BMMs (N=3). The expected molecular weight for LC3-II and LC3-I is 14/16 kDa, and of p62 is 62 kDa. Data are shown as means ±SD. Unpaired two-tailed Student's *t* test was used to determine if the level of LC3-II and p62 was significantly different between OCs from young and aged mice.

4.3.3 Localisation of autophagy-related proteins regulated by p38 MAPK in resorbing OCs in ageing

The findings in **Sub-section 4.3.1 and 4.3.2** showed increased expression of autophagic genes (*p38, p38IP, Sqstm1, LC3b, Atg9a, Atg5, Atg4B, Atg12* and *Atg7*), and protein (LC3-II) in POCs but not in OCs differentiated from aged mice. Therefore, I wanted to determine if the above-mentioned differential gene and protein expression in POCs with ageing affected the p38-p38IP-Atg9a pathway in relation to LC3 in resorbing OCs. Thus, I performed immunostaining to study the localisation and colocalisation of LC3, Atg9a and p38IP with p38 in resorbing OCs differentiated from young and aged mice.

Under basal conditions, LC3 appears as punctate structures and the majorly localises in the nuclei with only a small pool scattered in the cytoplasm (**Figure 4.8 A-D**). It has been shown that the LC3 is localised in both the nucleus and the cytoplasm when cells are grown in full medium[628]. Furthermore, the nuclear pool of LC3 is a reservoir for the cytoplasmic pool and is vital for starvation-induced autophagosome formation[628,629]. The quantification of immunofluorescence signal intensity shows increased nuclear and cytoplasmic LC3 in resorbing OCs derived from aged mice compared to that of young mice (**Figure 4.8 E**). Based on the role of LC3 in the secretory component of osteoclastic bone resorption, it is tempting to speculate that more LC3 has localised to the RB as aged OCs resorb more.

On the other hand, the level of p38 in the cytoplasm displays a significant increase in resorbing OCs derived from aged mice which echoes with my findings in Chapter 3 (**Figure 4.8 F**). Partial colocalisation can be observed in the cytoplasm, however, there is no alteration in ageing (**Figure 4.8 G**).

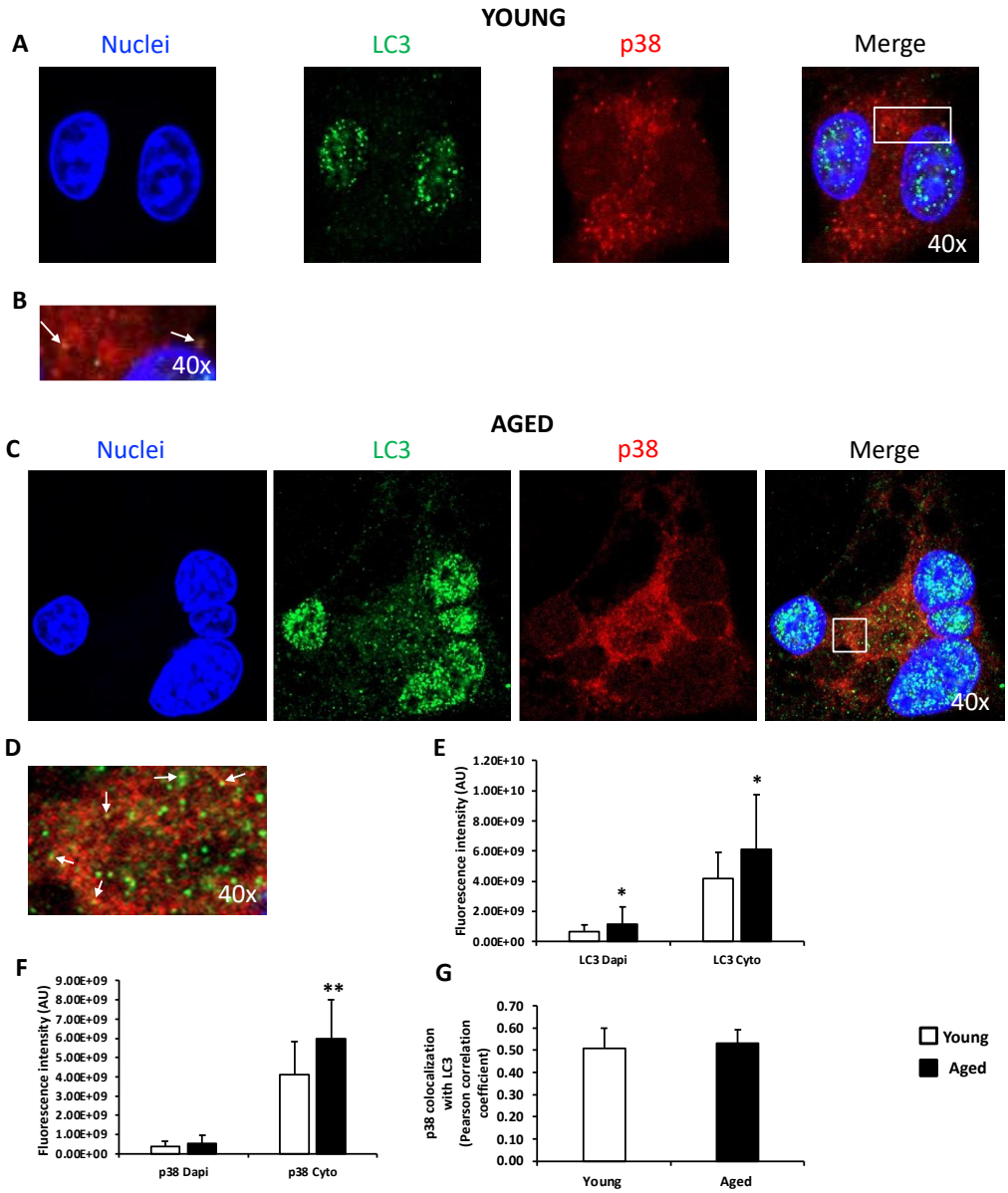

Figure 4.8: Localisation of LC3 and p38 in resorbing OCs from young and aged mice. OCs were differentiated from BMMs of 3-4-month-old and 12-14-month-old female mice and cultured on HA-coated coverslips in 12-well plates with 25 ng/mL of M-CSF and 100 ng/mL of RANKL for 120 hours. Representative fluorescence images of young (**A**) and aged (**C**) resorbing OC immunostained with DAPI, anti-LC3, anti-p38 conjugated to AF546 and merge. White box shows partial colocalisation between p38 and LC3 (yellow) that is enlarged in the panels below (**B and D**). Quantification of immunofluorescence signal intensity of nuclear and cytosolic LC3 (**E**) and p38 (**F**) (15-20 OCs pulled from 3 young and aged mice were analysed). Colocalisation analysis of p38 with endogenous LC3 in young and aged resorbing OCs (**G**) using Z-stack confocal images as represented in (**A-D**). Data are shown as means ±SD. Unpaired two-tailed Student's *t* test was used to determine if the level of LC3 and p38 in the nucleus and the cytoplasm was significantly different between OCs from young and aged mice. Significance is denoted by $p<0.05$, $^{**}p<0.01$.

I then looked at the localisation of LC3 to the RB in relation to p38. The sealing zone of resorbing OCs (indicated with red arrows) was seen (**Figure 4.9**). Unfortunately, I had difficulty visualising the fluorescently labelled LC3 (with AF594) and p38 (with AF546) at the RB due to the limited selection of fluorophores. The excitation of AF594 using a 594 nm laser also produced excitation of AF546, although to a lesser degree. This results in the bleed-through or crossover of fluorescence emission, as the spectral profiles of the fluorophores were overlapped. However, either LC3 or p38 or both can be seen localised at the RB.

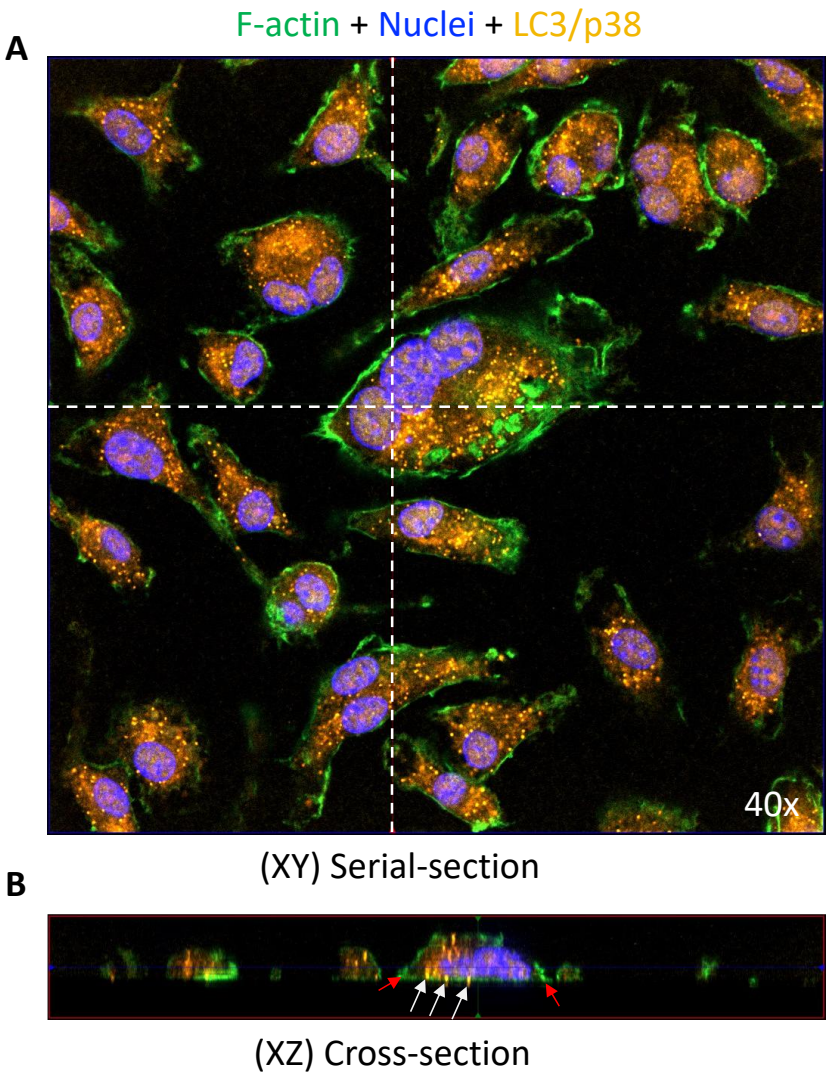

Figure 4.9: Visualisation of LC3 and/or p38 localised at the RB of resorbing OCs derived from young mice. OCs were differentiated from BMMs of 3-4-month-old female mouse and cultured on HA-coated coverslips in 12-well plates with 25 ng/mL of M-CSF and 100 ng/mL of RANKL for 120 hours. Images represent confocal planes of fluorescent channels merged together. XY = top view (**A**), XZ = side view (**B**). Red arrows indicate the sealing zone and white arrows indicate LC3 and/or p38.

In light of my western blot findings suggesting increased autophagy flux (**Figure 4.6**) in POCs with ageing, and increased LC3 nuclear and cytoplasmic staining in normal conditions in resorbing OCs with ageing, I asked how treatment with bafilomycin would affect LC3 cellular distribution with ageing.

At baseline, when the resorbing OCs from both young and aged mice were treated with DMSO as a control, punctate LC3 staining is seen in the nucleus with only a small pool scattered in the cytoplasm, which echoes with the findings in **Figure 4.8**. Upon 4 hours of bafilomycin treatment, LC3 is seen to be distributed into the cytoplasm (**Figure 4.10 A**).

When the bafilomycin is absent, the signal intensities of cytoplasmic LC3 but not nuclear LC3 is increased in resorbing OCs in ageing (**Figure 4.10 C**). This may suggest that in ageing there is a relative distribution of LC3 from the cytoplasm to the RB, however I was unable to confirm it due to difficulties visualising the RB and time constraints.

Similarly, the intensity of p38 signal in the cytoplasm but not in the nucleus is significantly higher in resorbing OCs differentiated from aged mice in the absence of bafilomycin, while no difference can be observed when the inhibitor is present (**Figure 4.10 B**). This indicates increased total p38 MAPK expression in ageing, which is in concordant with my findings in Chapter 3.

Intriguingly, the addition of bafilomycin gives rise to giant and hypernucleated OCs with the maximum nuclei number of 27 (**Figure 4.10 A & D**). This suggests that the bafilomycin treatment promotes rapid cell fusion and multinucleation of OCs.

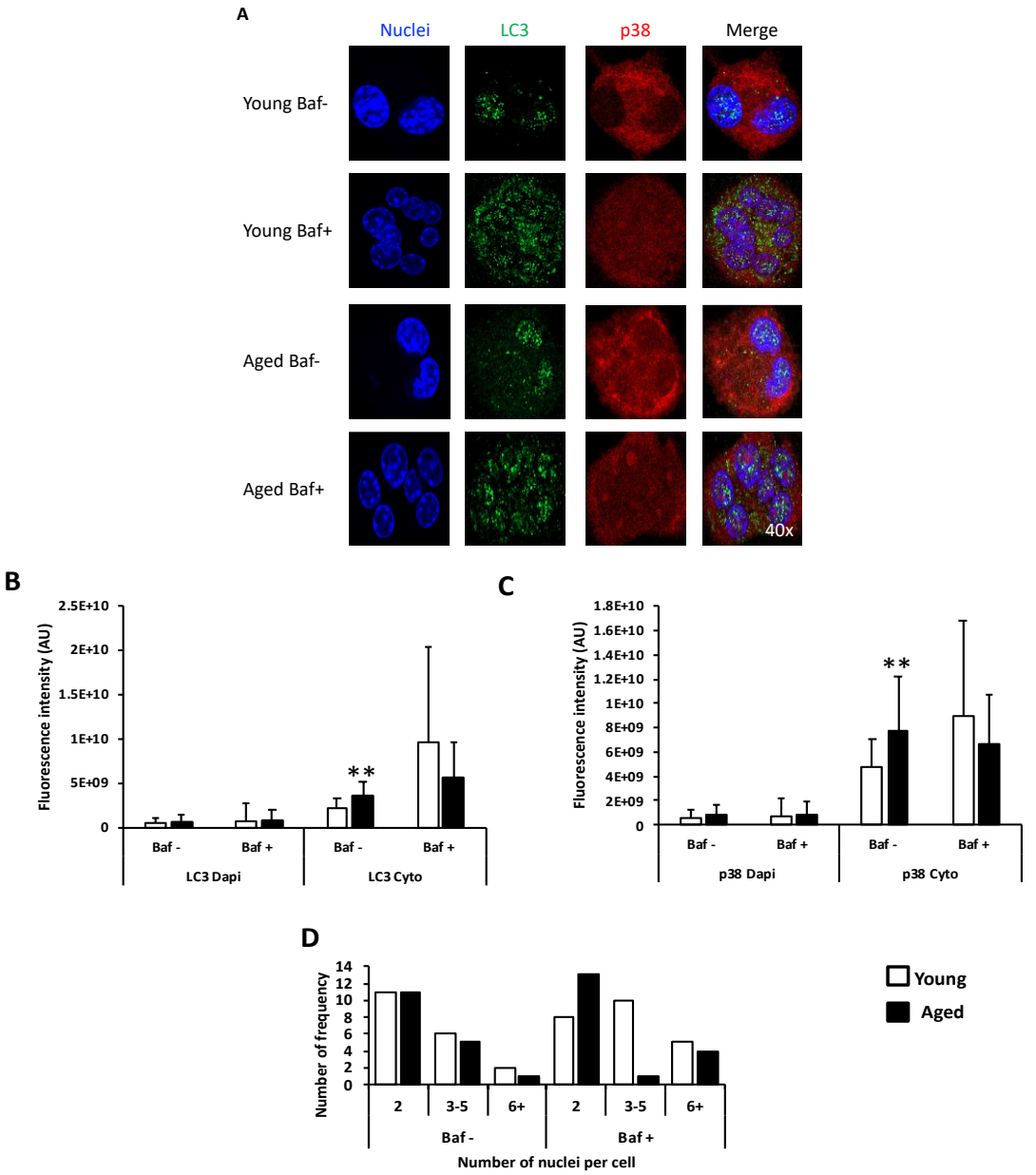

Figure 4.10: Localisation of LC3 and p38 in resorbing OCs from young and aged mice with and without bafilomycin. OCs were differentiated from BMMs of 3-4-month-old and 12-14-month-old female mice and cultured on HA-coated coverslips in 12-well plates with 25 ng/mL of M-CSF and 100 ng/mL of RANKL for 120 hours. The cells were treated or not with 100 nM of bafilomycin B_1 for 4 hours. Representative fluorescence images of an aged resorbing OC immunostained with DAPI, anti-LC3, anti-p38 conjugated to AF546 and merge (**A**). Quantification of immunofluorescence signal intensity of nuclear and cytosolic LC3 (**B**) and p38 (**C**) in the presence and absence of bafilomycin (24-25 OCs pulled from 3 young and aged mice were analysed). Frequency distribution of the nuclear number per cell with and without bafilomycin (**D**). Data are shown as means ±SD. Unpaired two-tailed Student's *t* test was used to determine if the level of LC3 and p38 in the nucleus and the cytoplasm was significantly different between OCs from young and aged mice. Significance is denoted by **p<0.01.

Similar to the LC3 immunostaining, Atg9a displays as punctate structures and the majorly is localised in the nucleus with only a small pool scattered in the cytoplasm under basal conditions (**Figure 4.11 A-D**). However, this is unexpected because mAtg9 which is equivalent to Atg9a was reported to traffic between juxta-nuclear region and cell periphery[354,601,625]. The use of different antibodies may explain the discrepancies. Besides that, the nuclei were not immunostained using DAPI in the reported studies, the TGN was immunostained using the marker TGN46 instead. Hence, my finding may suggest a novel role of Atg9a in nuclei of resorbing OCs.

The quantification of the immunofluorescence signal intensity indicates no difference in nuclear and cytoplasmic Atg9a and p38 between resorbing OCs from aged versus young mice (**Figure 4.11 F &G**). Partial colocalisation can be observed in the cytoplasm, however there is no alteration in ageing (**Figure 4.11 E**). p38 MAPK competes with Atg9a for p38IP when inhibiting autophagy, therefore, no significant colocalisation level between the two is expected.

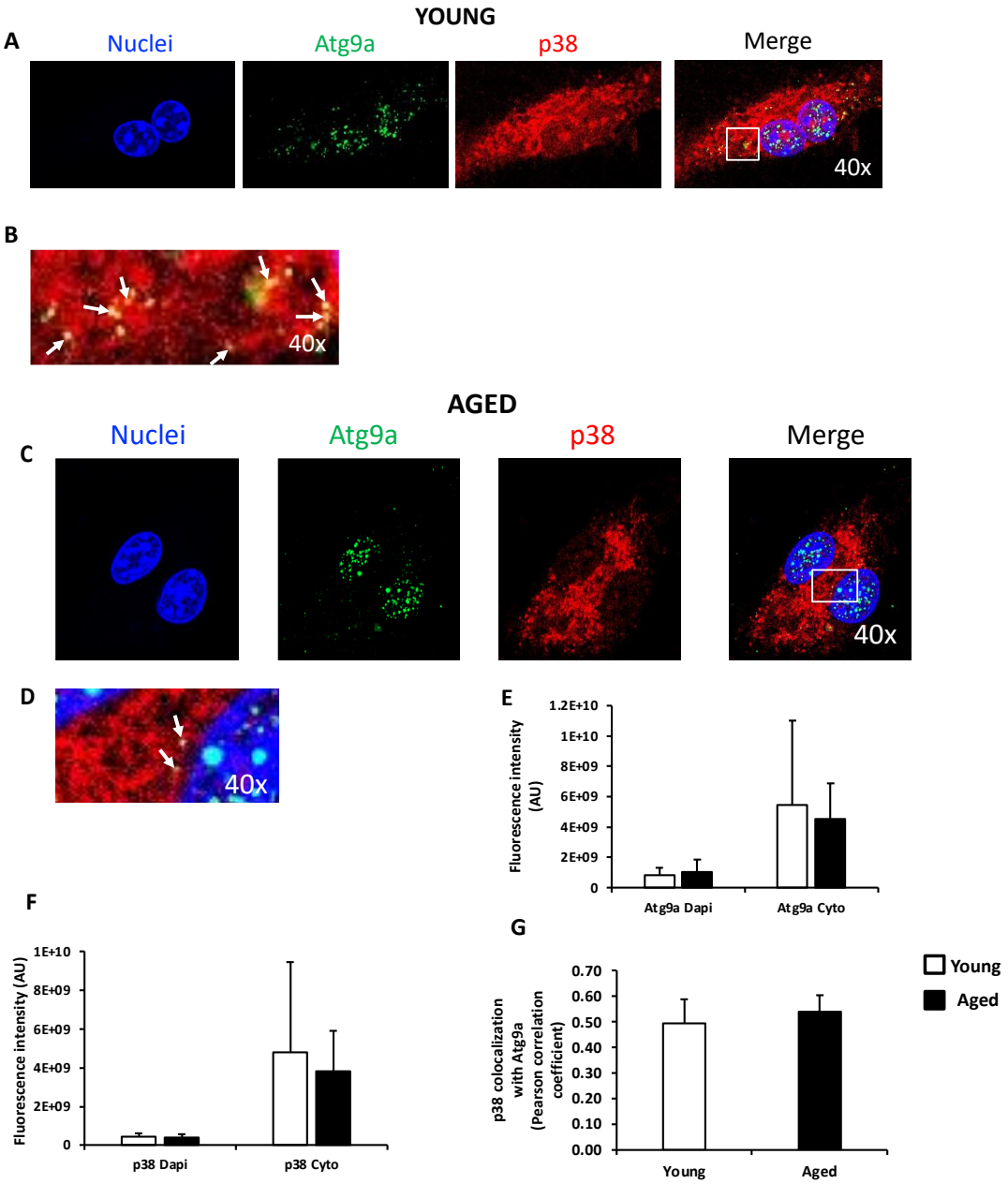

Figure 4.11: Localisation of Atg9a and p38 in resorbing OCs from young and aged mice. OCs were differentiated from BMMs of 3-4-month-old and 12-14-month-old female mice and cultured on HA-coated coverslips in 12-well plates with 25 ng/mL of M-CSF and 100 ng/mL of RANKL for 120 hours. Representative fluorescence images of young (**A**) and aged (**C**) resorbing OC immunostained with DAPI, anti-Atg9a, anti-p38 conjugated to AF546 and merge. White box shows partial colocalisation between p38 and Atg9a (yellow) that is enlarged in the panel below (**B and D**). Quantification of immunofluorescence signal intensity of nuclear and cytosolic Atg9a (**E**) and p38 (**F**) (13-14 OCs pulled from 3 young and aged mice were analysed). Assessment of colocalisation between p38 and Atg9a in young and aged resorbing OCs (**G**) using Z-stack confocal images as represented in (**A-D**). Data are shown as means ± SD. Unpaired two-tailed Student's *t* test was used to determine if the level of Atg9a and p38 in the nucleus and the cytoplasm was significantly different between OCs from young and aged mice.

I then looked at the distribution of p38 in relation to p38IP. As expected, p38IP punctate staining can be observed in the nucleus and cytoplasm (**Figure 4.12 A-D**). The quantification of immunofluorescence signal intensity indicates no difference in nuclear and cytoplasmic p38IP and p38 between resorbing OCs from aged versus young mice (**Figure 4.12 F & G**). Partial colocalisation can be observed in the cytoplasm, however there is no alteration in ageing (**Figure 4.12 E**). Of note, p38 exhibits a higher degree of colocalisation to p38IP than Atg9a (**Figure 4.12 H)**. This is in agreement with the findings from Webber and Tooze[354,601].

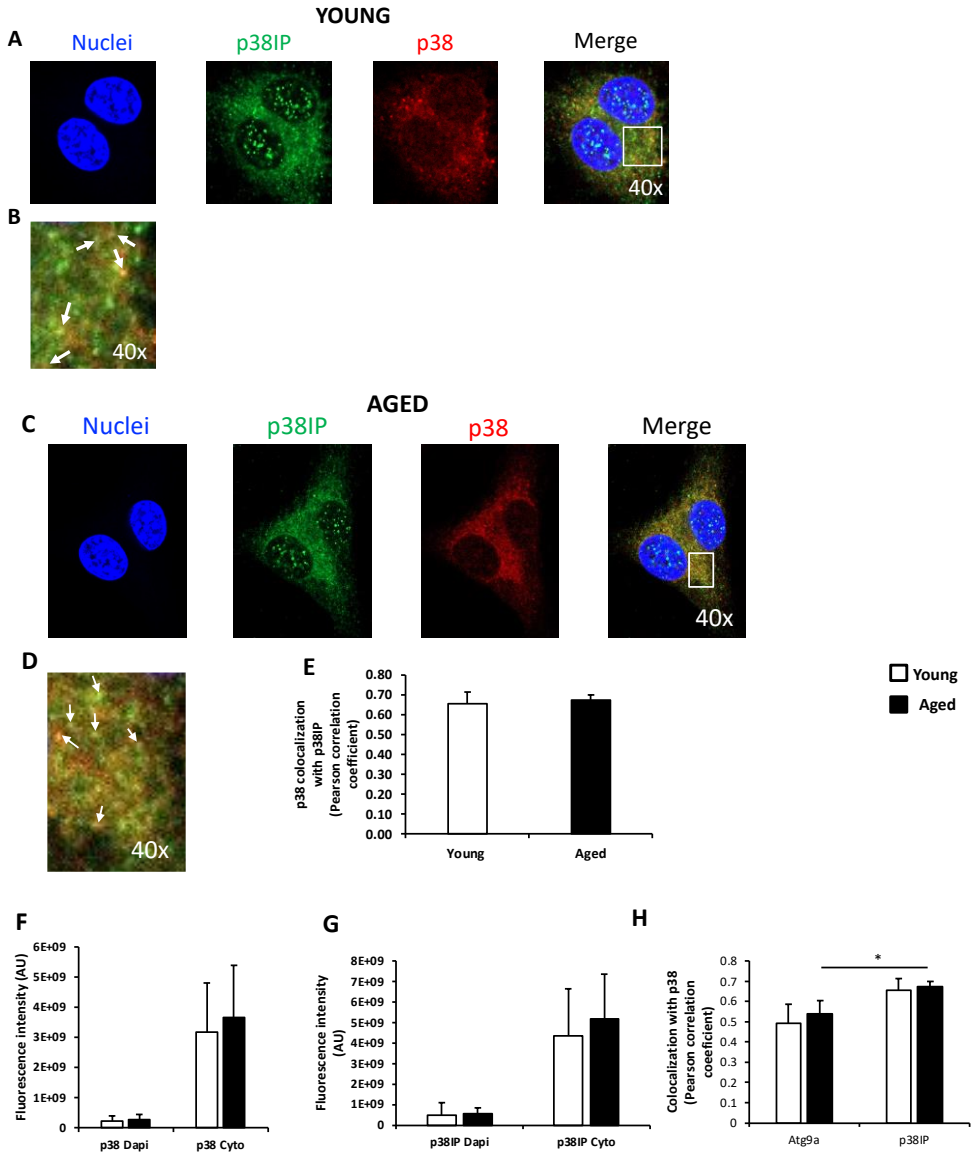

Figure 4.12: Localisation of p38IP and p38 in resorbing OCs from young and aged mice. OCs were differentiated from BMMs of 3-4-month-old and 12-14-month-old female mice and cultured on HA-coated coverslips in 12-well plates with 25 ng/mL of M-CSF and 100 ng/mL of RANKL for 120 hours. Representative fluorescence images of young (**A**) and aged (**C**) resorbing OC immunostained with DAPI, anti-p38IP, anti-p38 conjugated to AF546 and merge. White box shows partial colocalisation between p38 and p38IP (yellow) that is enlarged in the panel below (**B and D**). Quantification of immunofluorescence signal intensity of nuclear and cytosolic p38IP (**E**) and p38 (**F**) (16-20 OCs pulled from 3 young and aged mice were analysed). Assessment of colocalisation between p38 and p38IP in young and aged resorbing OCs (**E**) using Z-stack confocal images as represented in (**A-D**). Comparison between the colocalisation of p38 and Atg9a, p38IP or LC3 in pulled aged versus young OCs (**H**). Data are shown as means ±SD. Unpaired two-tailed Student's *t* test was used to test for significant differences in the level of p38IP and p38 in the nucleus and the cytoplasm between OCs from young and aged mice, as well as to test for significant differences in p38 colocalisation between Atg9a and p38IP. Significance is denoted by *p<0.05.

4.4 Discussion

It is generally accepted that ageing is associated with a reduction in autophagy. Compromised autophagy and impaired aggregate clearance contribute to metabolic disorders, neurodegenerative diseases such as Alzheimer's disease, and cancer[630-632]. Age-related decline of autophagy has been reported in several tissues such as the liver[633], kidney[634], pancreatic islets[635] and skeletal muscle[636]. The autophagic activity in osteocytes was showed to be reduced during ageing[637], however it is not known in osteoblasts and OCs.

To understand age-related changes in autophagy in relation to increased osteoclast activity[16,380], I first analysed the NGS data of autophagy-related gene expression in BMMs, POCs and mature OCs from young and aged mice. Interestingly, the expression of selected autophagic genes (*p38, p38IP, Sqstm1, LC3b, Atg9a, Atg5, Atg12, Atg4B* and *Atg7*) was significantly upregulated in aged POCs (**Figure 4.2 and 4.3**). The work of DeSelm and colleagues has showed that Atg5 and Atg7 are essential for the conversion of LC3-I to LC3-II and OC activity[36]. Specific knockdown of Atg5 or Atg7 results in the inhibition of LC3-I to LC3-II conversion[36]. Moreover, LC3-II along with Atg5 and Atg4B affect the maturation of OCs, fusion of secretory lysosomes with the RB and osteoclastic resorption activity[36,359]. Furthermore, Atg5 acts upstream of Rab7, which is a protein associated with late endosomes or lysosomes. They are both involved in the regulation of lysosomal secretion and mediate the RB formation[36,638]. Atg5-deficient OCs mislocalised Rab7 in which its downregulation led to defective bone resorption caused by impaired F-actin ring formation and the inhibition of polarisation[36,639]. Taken together, my findings suggest enhanced non-canonical autophagy during osteoclastogenesis in ageing which primes the OCs for maturation. However, the results of NGS data analysis are yet to be verified using qPCR.

Subsequently, I performed Western blotting using bafilomycin-treated cells to investigate autophagic flux. Bafilomycin B_1 blocks autophagy by inhibiting the proton pumping V-ATPase to attenuate acidification and the fusion between autophagosomes and lysosomes[640,641], and thereby induces LC3-II accumulation. The level of LC3-II was increased in both young and aged cells at all three stages of osteoclastogenesis after the addition of bafilomycin, indicating the

treatment was in effect (**Figure 4.5, 4.6 and 4.7**). Upon bafilomycin treatment, the lipidated LC3 level was significantly increased in aged as compared to young POCs, suggesting increased autophagic flux (**Figure 4.6**). LC3 has been shown to involve in both autophagy and lysosomal secretion, therefore, it is possible that the two pathways cross over at the level of LC3 regulation[642]. LC3 is conjugated either to the autophagosomal membrane to be involved in autophagy or to be transferred to the RB for promoting lysosomal secretion[36,642].

On the other hand, the level of p62 protein expression was not significantly different at any stage of osteoclastogenesis despite increased *Sqstm1* expression in NGS in POCs (**Figure 4.5, 4.6 and 4.7**). My findings are in contrast with the work of Zhu and colleagues, which showed increased levels of p62 proteins after 24 hours of bafilomycin treatment in osteoclast-like cells (OCLs) derived from $RAW^{264.7}$ cell line[641]. Primary cells were used in my study and the cells were treated with bafilomycin for 4 hours, which could explain the discrepancy.

Other than Western blotting, I performed immunostaining to examine differences in the localisation of selected autophagy-related proteins in aged versus young resorbing OCs. Under basal conditions, the level of cytoplasmic p38, nuclear LC3 and cytoplasmic LC3 were increased in aged resorbing OCs compared to the young ones (**Figure 4.8**). As previously mentioned, LC3 is involved in the regulation of OC secretion, this finding suggests that enhanced OC activity in ageing may be due to increased LC3 localisation at the RB. F-actin and LC3 staining would be needed to visualise the localisation of LC3 at the RB of resorbing OCs, which due to time constraints and limited selection of fluorophores I was unable to perform (**Figure 4.9**).

Besides affecting the acidification of the extracellular space by acting on the V-ATPase inserted in the RB of OCs and therefore inhibiting bone resorption, bafilomycin also impacts endocytic trafficking from the RB[38]. Therefore, I treated the aged and young resorbing OCs with bafilomycin in order to stop the autophagic flux and quantify the intracellular proteins of interest. Increased cytoplasmic p38 signal intensity in the aged resorbing OCs was observed in the absence of Bafilomycin B_1 (**Figure 4.10**). This finding is echoed by the observation in Chapter 3 showing increased p38 MAPK phosphorylation in aged BMMs upon RANKL stimulation. However, I did not find increased p38 MAPK activation in OC precursors or OCs

in keeping with previous reports[199]. Due to the transient activation of p38 MAPK and a weak P-p38 signal which I observed while trying to optimise the immunostaining (data not shown), immunostaining for P-p38 was not performed. In contrast, Wu and colleagues have discovered increased p38 MAPK after bafilomycin treatment in colon cancer cells[643]. The outcome could be cell-specific, hence, further studies would be required to investigate the activation status of p38 MAPK in aged resorbing OCs in the presence of bafilomycin and/or a proteasome inhibitor as p38α is known to be degraded by the proteasome[644].

Similar to cytoplasmic p38, the level of cytoplasmic LC3 was increased in the aged resorbing OCs when bafilomycin was absent (**Figure 4.10**). Furthermore, LC3 localised to the dispersed punctate structures scattered throughout the cytoplasm after the addition of Bafilomycin B_1 as compared with the control, indicating autophagy inhibition. Due to the limited selection of fluorophores, unfortunately I was unable to label the F-actin ring, which is used to visualise the RB, therefore could not determine LC3's localisation to the RB.

Moreover, the data analysis from NGS revealed significant upregulation of *p38IP* and *Atg9a* in the aged POCs (**Figure 4.2**). Nevertheless, when I looked at the protein level of p38IP at the basal level under RANKL-unstimulated condition using Western blotting (**Figure 4.4**), no significant difference between young and aged BMMs and POCs was observed. Apart from that, the immunostaining of p38IP and Atg9a in resorbing OCs showed no difference as well (**Figure 4.11 & 4.12**). This may be due to the post-transcriptional regulation, especially in the aged POCs. Due to time constraints, I was unable to study p38IP in resorbing OCs by Western blotting which is needed for further investigation.

The analysis shows a higher colocalization level between p38 and p38IP compared to Atg9a, (**Figure 4.12**), which is in agreement with the work from Webber and Tooze[354]. However, they also showed that it is the activated form of p38 MAPK, P-p38 which binds to p38IP with a greater affinity than mAtg9, leading to a low basal rate of autophagy[354]. Decreased P-p38 caused by reduced amino acid level during starvation, results in a lower affinity of p38IP for dephosphorylated p38 and favours binding Atg9[354]. Subsequently, mAtg9-p38IP complex traffics from peripheral endosomes to forming autophagosomes, thereby increasing autophagy[354,601]. Unlike Webber who used HEK293A and HeLa cell lines, I used murine OCs.

As mentioned in Chapter 3, p38 MAPK phosphorylation is not seen in mature OCs upon RANKL stimulation[199]. This leads to the question of whether p38IP acts differently in murine OCs compared to cell lines and binds to the p38 MAPK regardless of the phosphorylation status. Again, the colocalisation of Atg9a and p38IP unfortunately could not be examined as both the antibodies were yielded from the same animal species and only a limited selection of fluorophores was available. Moreover, as colocalisation may not truly represent the presence of physical interaction between the proteins, fluorescence resonance energy transfer (FRET) microscopy would be needed, which was beyond the scope of my project[645].

Taken together, my data suggest that the age-related increased osteoclastogenesis may be also due to enhanced non-canonical autophagy, apart from the increased RANKL-induced p38 phosphorylation, marginally in ERK phosphorylation and *Atp6v0d2* expression (results from Chapter 3). Despite the inability to validate the analysis of NGS data using qPCR due to time constrains, the data analysis of NGS is still informative and sheds light on the directions where further studies are warranted. Epigenetics, the localisation of LC3 and/or p38 at the RB, the effect of bafilomycin on the murine OCs in terms of OC size, cytoplasm growth and nuclear area, immunoprecipitation of p38-p38IP-Atg9a, and endocytic traffic, in ageing all warrant further investigation in order to have a better understanding of the mechanisms underlying the age-related increased osteoclastogenesis.

Chapter 5: Role of p62 in age-related bone loss

5.1 Introduction

p62 possesses multiple interaction domains and takes part in forming multimeric signalling complexes. It is intimately involved in cell signalling, protein turnover and trafficking[70]. P62 serves as a functional link between RANKL and TRAF6-mediated NF-κB activation, and thus plays an important role in osteoclastogenesis[70].

Also, p62 as the selective autophagy adaptor, directly binds to polyubiquitinated proteins interacting with the UBA domain, sequesters the ubiquitinated cargos into inclusion bodies via the PB1 domain and shuttles them for degradation via either proteasome pathway or autophagy. Those two domains regulate p62 self-oligomerisation which is crucial for the formation and degradation of ubiquitinated protein aggregates as well as the conformational change of p62 into filamentous helical scaffold which exposes PB1 domain and LIR domain for polymerisation and interaction with LC3 in phagophore membrane development[646]. The ZZ domain binds N-degrons which induces p62-LC3 interaction and redirects the N-end rule substrates to the autophagy pathway[646]. Alteration of p62 expression has been shown to impair signal transduction and lead to defective autophagy[70].

PDB-associated mutations of *p62/SQSTM1* have been identified to be clustered around or within the UBA domain[647]. The most common mutation of p62 associated with PDB is a C→T transversion at position 1215 in *SQSTM1/p62* exon 8 which causes a proline to leucine substitution at residue 392 (P392L) mutation[77,530,531].

After osteoporosis, PDB is the second most common metabolic bone disorder associated with ageing. It is characterised by focally disorganised and excessive bone turnover with OC precursors that are hyper-responsive to osteoclastogenic factors such as RANKL and TNF-α[560]. Pagetic OCs are larger in size with more nuclei and enhanced ability to resorb bone[70,253]. The *p62^{P394L}* mutation has been reported to increase osteoclastogenesis and RANKL-RANK -mediated signalling by reducing CYLD activity[648] and upregulating NFATc1 expression in POCs[563,648], resulting in prolonged NF-κB signalling and enhanced osteoclastogenesis, eventually inducing the activated stage of OCs[571]. P394L mutation in the UBA domain of a full-

length p62 leads to a loss of function in the binding affinity for poly-ubiquitin chains[647]. This alteration of ubiquitin chain binding by p62 is believed to be important for the development of PDB[356].

The association of p62 mutations with PDB was made in 2002[530,531], but to prove the causative effect of P392L mutation, Daroszewska *et al.* developed a mouse model with equivalent P394L mutation which developed pagetic-like lesions. This point mutation in the UBA domain of p62 was shown to be sufficient to cause a Paget's disease-like disorder in aged mice, which is characterised by focal bone lesions observed predominantly in the long bones, increased osteoclastic bone resorption and osteoblastic bone formation with woven bone and nuclear inclusion bodies within hypernucleated OCs[253]. Interestingly, *p62^{P394L}* mice with ageing were observed to have increased osteoclastogensis in association with accelerated bone loss in the long bones paired with increased pre-osteoclast sensitivity to RANKL with ageing *in vitro*[561].

As previous findings have shown that p62 serves as scaffold in the RANK- NF-κB signalling pathway and *p62^{P394L}* OC precursors with ageing are hyperactive towards RANKL, it is possible that the OCs would be less active if p62 was knocked-down or deleted. Consequently, lack of p62 activity could potentially have a protective effect on age-related bone loss. Thus, I hypothesised that p62 deletion would attenuate osteoclastogenesis *in vivo* and attenuate age-related bone loss. Therefore, in this part of my project I studied the *in vivo* effects of p62 deletion in bone. I compared the bone phenotype of *p62$^{-/-}$* mice with both wildtype (WT) and *p62^{P394L}* mice and investigated the effect of ageing on bone in these mice.

5.2 Methods

Long bones (left femur and tibia per mouse) of *p62*$^{-/-}$, *p62*^{P394L} and wild type (WT) mice, all on the C57BL/6 background were kindly provided by the research team: Dr. Daniela Merlotti and Prof. Luigi Gennari (University of Siena, Italy), and Dr. Simone Cenci and Dr. Maria Materozzi (at the time PhD student, Università Vita-Salute San Raffaele, Milano, Italy) as part of a collaboration. Mice were generated and genotyped as previously described[303,562]. All mice were born and kept under pathogen-free conditions. Homozygous *p62*$^{-/-}$ and *p62* $^{P394L/P394L}$ mice were obtained by either crossing two *p62*$^{+/-}$ or two *p62*$^{WT/P394L}$ mice. *p62*$^{-/-}$, *p62*^{P394L} and WT mice (6- and 18-month-old) received two injections of calcein (200-500 µL IP injection of 2 mg/mL) 2 and 5 days (at 6 months of age), or 2 and 7 days (at >12 months of age) days before euthanising (**Figure 5.1**). The subset of mice that received calcein injection are summarised in **Table 5.1**. Left legs were harvested, fixed overnight in PFA (4%) and stored in 70% ethanol. The above-described procedures were conducted in Milan and the samples shipped to us.

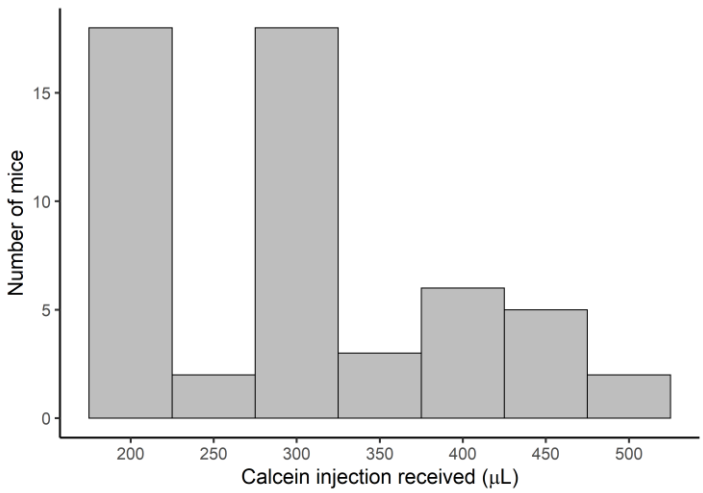

Figure 5.1: Frequency distribution of the mice that received different injection volume of calcein.

Table 5.1 Number of mice that received calcein injection by age, gender and genotype.

Genotype	Male		Female	
	6-month-old	18-month-old	6-month-old	18-month-old
WT	7	5	6	4
p62$^{-/-}$	7	5	8	7
p62^{P394L}	1	2	0	2

To access the effect of p62 deletion on bone morphometry, bones were scanned by micro-computed tomography (µCT) at 4.5 µm resolution for the distal femurs and 9.0 µm resolution to access for the focal lesions, considering known Pagetic-like phenotype of the *p62^{P394L}* mice[253,561]. The µCT was performed using a Skyscan 1272 (Bruker, Belgium) and trabecular morphometry was analysed as per standard protocol described in Chapter 2. Measurements of *p62$^{-/-}$* and *p62^{P394L}* were compared to those of the WT.

After µCT analysis, the left femurs were processed for MMA embedding as described in Chapter 2. For the analysis of bone resorption, MMA embedded sections of the left femurs which are summarised in **Table 5.2** were stained for TRAP, followed by the counterstaining using Aniline Blue to visualise OCs and bone respectively, adapted from Chappard *et al.*[567] (for details please see Chapter 2). To image the TRAP-stained sections, Zeiss Axio Scan.Z1 slide scanner was used with a 10x lens together with a colour camera resulting in an isotropic pixel size of 0.442 µm and analysed using the TrapHisto software developed by Van 't Hof *et al.*[566] .

Table 5.2 Number of left femurs that were processed for TRAP stain.

Genotype	Male			Female		
	6-month-old	9-11-month-old	18-month-old	6-month-old	9-11-month-old	18-month-old
WT	15	5	12	13	0	10
***p62*$^{-/-}$**	13	3	5	13	0	4
***p62*^{P394L}**	3	2	8	5	0	5

For the analysis of bone formation, MMA embedded sections of the left femurs of mice that received calcein injections (summarised in **Table 5.1**) were stained with Calcein Blue (Sigma). Calcein labels newly formed bone, whereas the calcein blue counterstain labels mineralised bone. The sections were then visualised using the Zeiss Axio Z1 slide scanner with a monochrome camera and a 20x lens resulting in an isotropic pixel size of 0.227 µm. The images were analysed by using the CalceinHisto software developed by Van 't Hof *et al.*[566].

Statistical analysis was performed using one-way analysis of variance (ANOVA) with Dunnett's post hoc test, unpaired two-tailed Student's *t* test and Chi-squared test as indicated.

5.3 Results

5.3.1 Body weight of young and aged male and female *p62*$^{-/-}$ and *p62*^{P394L} mice

As loss of p62 leads to mature-onset obesity in mice over the life course and body weight can be negatively associated with bone volume (as high-fat diet–induced obesity in mice results in bone loss)[317,649], I first analysed the weight of the WT, *p62*$^{-/-}$ and *p62*^{P394L} mice. The number of mice for which the body weight was analysed is summarised in **Table 5.3**.

There was no difference in body weight between WT and *p62*^{P394L} mice at any age. Female *p62*$^{-/-}$ mice had higher body weight compared to WT mice, and this difference increased with age **(Figure 5.2)**. Body weight also increased in males at 6 and 9-11 months of age, however no significant difference was seen at 18 months.

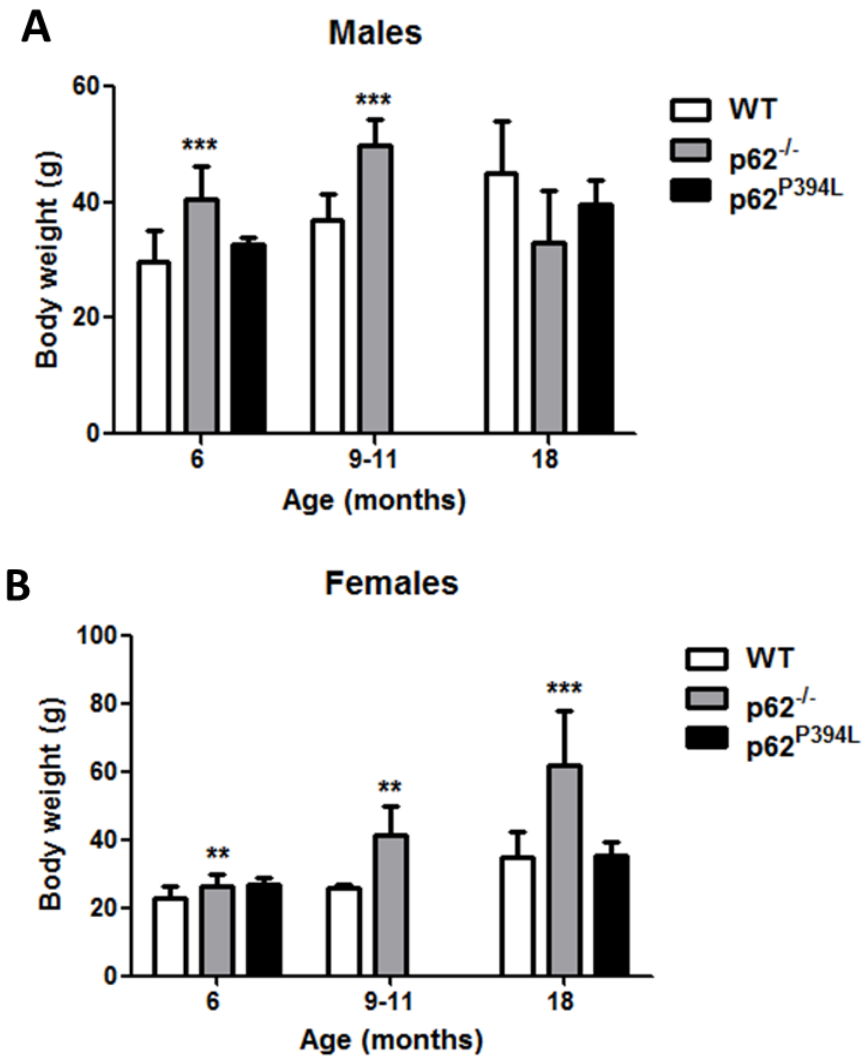

Figure 5.2: Body weight of 6, 9-11 and 18-month-old male and female WT, *p62*$^{-/-}$ and *p62*^{P394L} mice. Male **(A)** and female **(B)** *p62*$^{-/-}$ mice gained weight with ageing with the exception of 18-month-old male mice. No significant difference in weight change was observed in *p62*^{P394L} mice. Sample number is summarised in Table 5.3. Data are shown as means ±SD. One-way ANOVA with Dunnett's post hoc test was used to test for significant differences in body weight of 6, 9-11 and 18-month-old male and female WT, *p62*$^{-/-}$ and *p62*^{P394L} mice. Significance compared to WT is denoted by **p<0.01, ***p<0.001.

Table 5.3: Demographics of mice by age, gender and genotype. The number of mice for which the body weight was available.

Months	Males			Females		
	WT	*p62*$^{-/-}$	*p62*^{P394L}	WT	*p62*$^{-/-}$	*p62*^{P394L}
6	16	16	4	15	16	5
9-11	7	6	2	5	5	2
18	14	7	4	12	10	6

5.3.2 Bone morphometry in male *p62*$^{-/-}$ and *p62*^{P394L} mice during ageing

In order to study the effect of p62 deletion on the bone phenotype in ageing, I used µCT for morphometric analysis of the distal femurs of 6-, 9-11- and 18-month-old male WT, *p62*$^{-/-}$ and *p62*^{P394L} mice, as per **Table 5.4**.

With ageing, both *p62*$^{-/-}$ and WT male mice lost bone, however the bone loss was much more pronounced in the aged WT compared to the aged *p62*$^{-/-}$ **(Figure 5.3 and 5.4)**. At 6-months of age, WT, *p62*$^{-/-}$ and *p62*^{P394L} mice show no difference. However, at 9-11-month-old, *p62*$^{-/-}$ mice started to show a decreased reduction in bone volume per tissue volume (BV/TV) and Tb.N, and a lower increase in trabecular pattern factor (Tb.Pf) and structural model index (SMI) compared to WT mice. Tb.Pf is an inverse index of trabecular connectivity in which a lower Tb.Pf indicates better connected trabecular structure and a higher Tb.Pf signifies a more disconnected structure. SMI is used to measured plate- or rod-like geometry in trabecular bone with the SMI value of 0 indicates plate-like structure and 3 indicates rod-like structure. A similar, but more pronounced difference was observed in 18-month-old *in p62*$^{-/-}$ mice. Overall, the age-related morphometry changes in the phenotype are summarised in **Table 5.5**.

These results demonstrate that male *p62*$^{-/-}$ mice at 9-11 and 18-month-old have a high bone volume phenotype versus WT due to an increase in Tb.N, and this leads to an increase in trabecular connectivity **(Figure 5.4 A-F)**. With ageing, male *p62*$^{-/-}$ mice showed a higher bone density with more trabeculae, greater connectivity and structural integrity within the trabecular structure, and more 'plate-like' trabeculae, which are stronger than 'rod-like' trabeculae in comparison to that of WT mice **(Figure 5.4)**.

No significant difference was observed at any age between WT and *p62*^{P394L} mice which may be due to low numbers of *p62*^{P394L} mice at 6- months of age (N=4). In addition, due to the very low number of *p62*^{P394L} mice at 9-11-month-old (N=2), data on these mice are not included in **Figure 5.3** and **Table 5.5**.

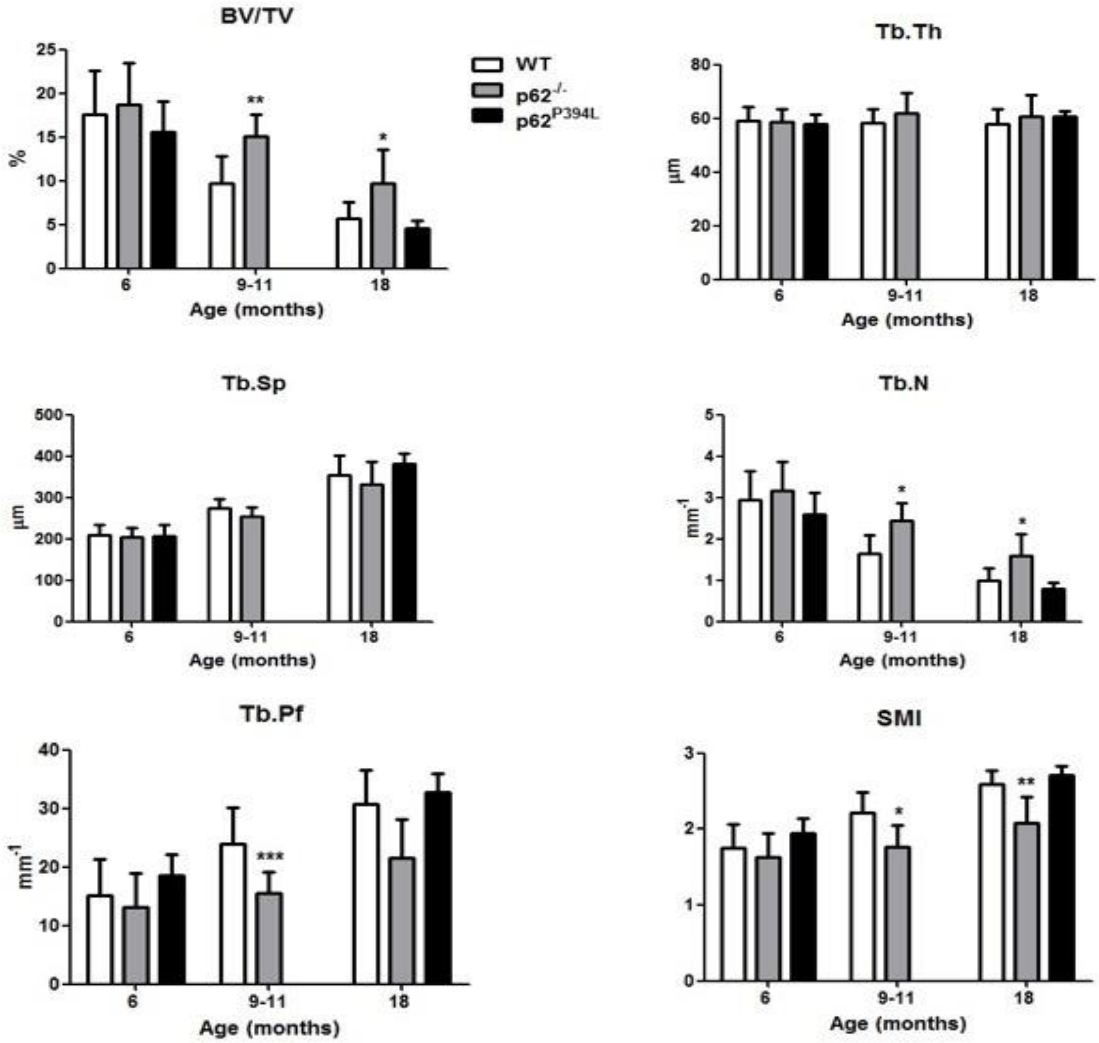

Figure 5.3: Trabecular morphometry of distal femurs of 6, 9-11 and 18-month-old male WT, *p62*$^{-/-}$ and *p62*^{P394L} mice. Distal femurs of 6, 9-11 and 18-month-old male *p62*$^{-/-}$ (N=16, N=6 and N=7, respectively), *p62*^{P394L} (N=4, N=2 and N=4, respectively) and WT (N=16, N=7 and N=14, respectively) were scanned *ex vivo* with µCT at 4.5 µm resolution. BV/TV, bone volume per tissue volume; Tb.Th, trabecular thickness; Tb.Sp, trabecular separation; Tb.N, trabecular number; Tb.Pf, trabecular pattern factor; SMI, structural model index. Data are shown as means ±SD. Unpaired two-tailed Student's *t* test and one-way ANOVA with Dunnett's post hoc test were used to test for significant differences in bone parameters of 6, 9-11 and 18-month-old male WT, *p62*$^{-/-}$ and *p62*^{P394L} mice. Significance compared to WT is denoted by *p<0.05, **p<0.01, ***p<0.001.

Table 5.4: Demographics of male mice by age and genotypes used for the morphometric analysis.

Months	WT	*p62*$^{-/-}$	*p62*^{P394L}
6	16	16	4
9-11	7	6	2
18	14	7	4

Table 5.5: Reduced age-related bone loss in male *p62*$^{-/-}$ mice. Age-related changes in bone parameters (expressed as % change from the same genotype at 6 months of age) are shown as mean ±SD. *p62*$^{-/-}$ or *p62*^{P394L} was compared to WT. *p62*^{P394L} mice aged 9-11 months were not included due to a very low number (N=2). Unpaired two-tailed Student's *t* test and one-way ANOVA with Dunnett's post hoc test were used to test for significant differences in age-related changes in bone parameters of male WT, *p62*$^{-/-}$ and *p62*^{P394L} mice. Significant difference between *p62*$^{-/-}$ versus WT is denoted by *p<0.05, **p<0.01, ***p<0.001.

	9-11-month-old		18-month-old		
	WT (N=7)	***p62*$^{-/-}$ (N=6)**	**WT (N=14)**	***p62*$^{-/-}$ (N=7)**	***p62*^{P394L} (N=4)**
BV/TV (%)	-50.28% ± 13.15%	**- 24.08% ± 12.29%****	- 67.86% ± 10.63%	**- 49.04% ± 20.10%***	- 73.30% ± 3.61%
Tb.Th (µm)	- 1.05% ± 8.87%	**+ 5% ± 13.27%**	- 1.60% ± 8.95%	**+ 3.35% ± 13.18%**	+ 4.86% ± 3.78%
Tb.Sp (µm)	+ 31.95% ± 10.30%	**+ 25.75% ± 11.03%**	+ 69.92% ± 23.50%	**+ 64.29% ± 27.91%**	+ 85.35% ± 11.29%
Tb.N (mm^{-1})	- 45.04% ± 14.56%	**- 24% ± 12.88%***	- 67.14% ± 10.31%	**- 51.00% ± 16.44%***	- 81.55% ± 12.57%
Tb.Pf (mm^{-1})	+ 77.37% ± 25.26%	**+ 10.93% ± 25.13%*****	+ 93.47% ± 36.49%	**+ 53.51% ± 46.36%**	+ 29.62% ± 86.43%
SMI	+ 32.91% ± 11.29%	**+ 9.79% ± 18.73%***	+ 50.62% ± 10.35%	**+ 30.08% ± 21.55%****	+ 44.57% ± 5.22%

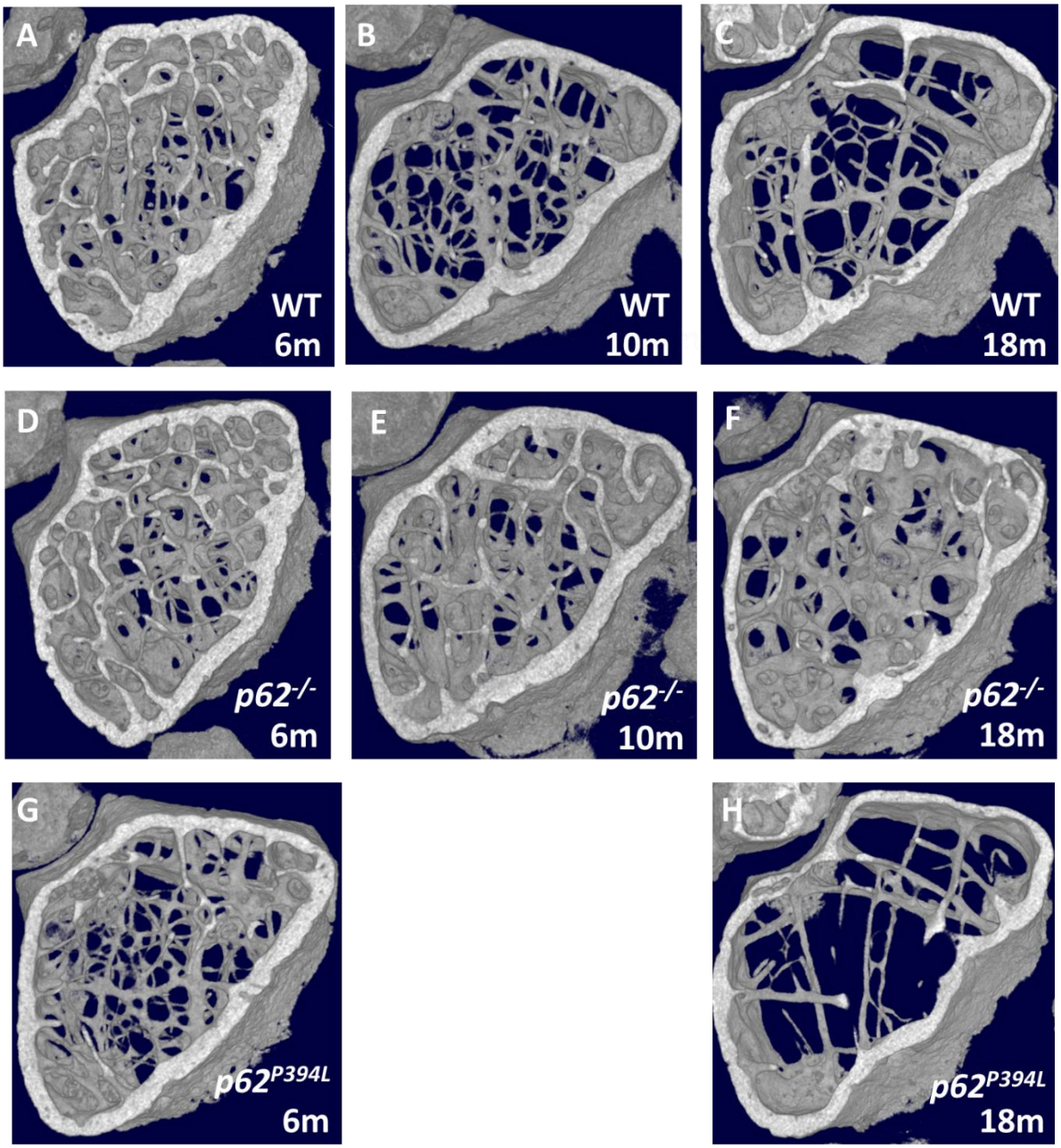

Figure 5.4: Representative cross-sectional images of 3D µCT reconstructions of whole bone from femurs of 6, 9-11 and 18-month-old male WT, *p62*$^{-/-}$ and *p62*^{P394L} mice. The 3D cross-sections show altered trabecular bone architecture and higher bone volume in *p62*$^{-/-}$ compared to WT with ageing **(A-F)**. *p62*^{P394L} shows no difference when compared to WT with ageing which may be due to low numbers of mice at 6- and 18-months of age (N=4 and N=4, respectively) **(G-H)**.

5.3.3 Bone morphometry in female *p62*$^{-/-}$ and *p62*^{P394L} mice during ageing

Certain bone diseases such as osteoporosis and PDB exhibit gender differences in prevalence[650]. Therefore, I used μCT to also examine the femurs of 6-, 9-11- and 18-month-old female WT, *p62*$^{-/-}$ and *p62*^{P394L} mice, as per **Table 5.6**.

Unlike the 6-month-old male *p62*$^{-/-}$ mice, the age-matched female *p62*$^{-/-}$ mice exhibit significantly higher BV/TV versus WT ($p<0.05$) (**Figure 5.5**). This indicates that the p62 deletion already affects the bone morphometry of female mice at 6 months of age. There is a trend for reduction in the bone loss in 9-11-month-old female *p62*$^{-/-}$ mice compared to the age-matched WT however, the lack of significance may be due to a small sample number (N=5). Similar to the results obtained for 18-month-old male *p62*$^{-/-}$ mice, the bone loss was reduced in the 18-month-old female *p62*$^{-/-}$ mice, with higher BV/TV and Tb.N compared to the age-matched WT **(Figure 5.5 and 5.6)**. Overall, the age-related morphometry changes in the phenotype are shown in **Table 5.7**.

These results demonstrate that *p62*$^{-/-}$ female mice at 18-months of age have high bone volume phenotype versus WT due to an increase in Tb.N **(Figure 5.6 A-F)**. With ageing, female *p62*$^{-/-}$ mice showed a higher bone density with more trabeculae and structural integrity within the trabecular structure in comparison to that of WT mice **(Figure 5.5)**.

No significant difference was observed between WT and *p62*^{P394L} mice at any age. The lack of significant difference between WT and *p62*^{P394L} mice at 6-month-old may be due to low numbers of *p62*^{P394L} mice (N=5). In addition, due to very low number of *p62*^{P394L} mice at 9-11-month-old (N=2), the data is not included in **Figure 5.5** and **Table 5.7**.

Unexpectedly, pagetic-like lesions were observed in some of the *p62*$^{-/-}$ 18-month-old animals, therefore data from affected bones (N=3) have been removed from this analysis and will be discussed in **Sub-section 5.3.8.**

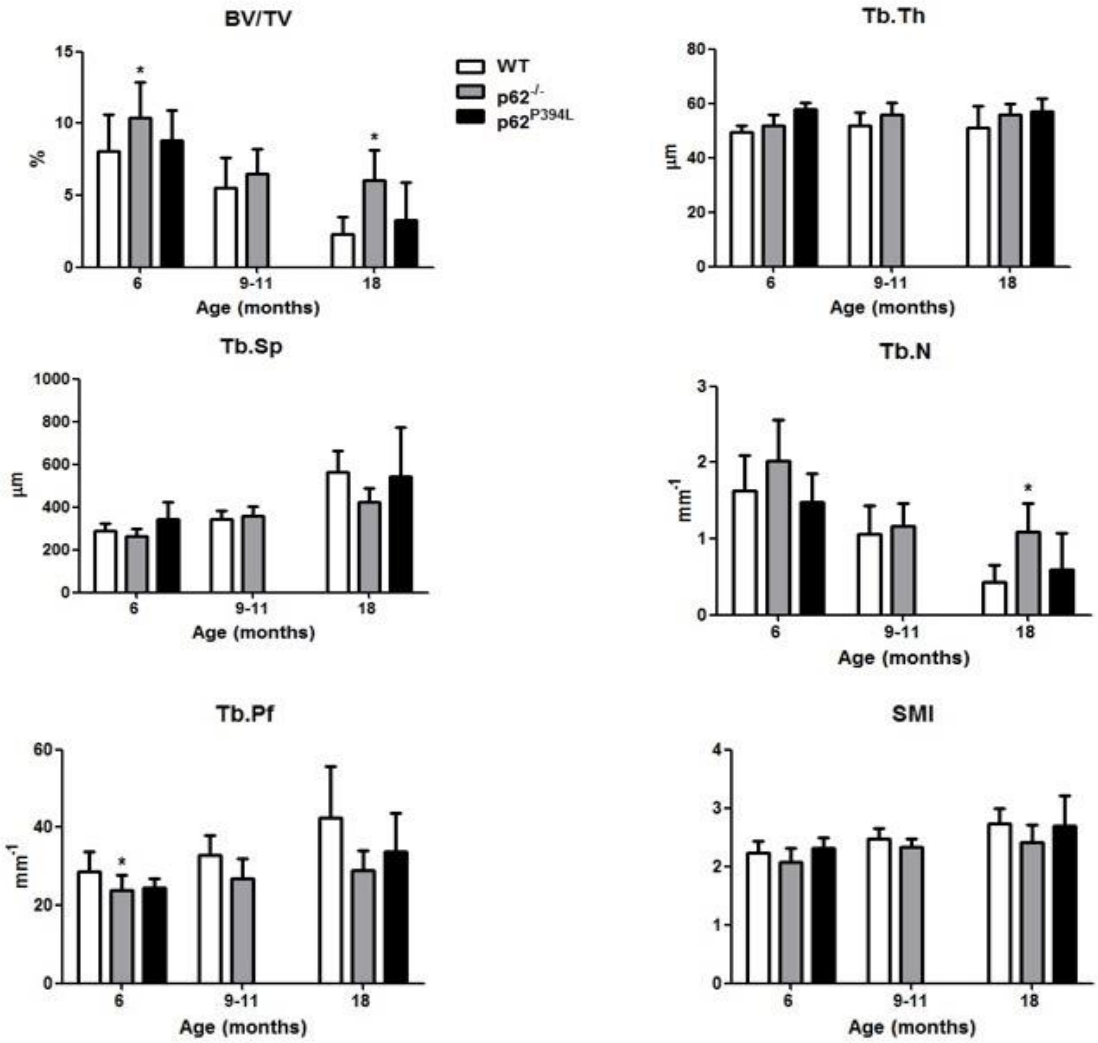

Figure 5.5: Trabecular morphometry of distal femurs of 6, 9-11 and 18-month-old female WT, *p62*$^{-/-}$ and *p62*^{P394L} mice. Distal femurs of 6, 9-11 and 18-month-old female *p62*$^{-/-}$ (N=16, N=5 and N=7, respectively), *p62*^{P394L} (N=5, N=2 and N=6, respectively) and WT (N=15, N=5 and N=12, respectively) were scanned *ex vivo* with µCT at 4.5 µm resolution. BV/TV, bone volume per tissue volume; Tb.Th, trabecular thickness; Tb.Sp, trabecular separation; Tb.N, trabecular number; Tb.Pf, trabecular pattern factor; SMI, structural model. Data are shown as means ±SD. Unpaired two-tailed Student's *t* test and one-way ANOVA with Dunnett's post hoc test were used to test for significant differences in bone parameters of 6, 9-11 and 18-month-old female WT, *p62*$^{-/-}$ and *p62*^{P394L} mice. Significance compared to WT is denoted by *p<0.05.

Table 5.6: Demographics of female mice by age and genotypes used for the morphometric analysis.

Months	WT	*p62*$^{-/-}$	*p62*^{P394L}
6	15	16	5
9-11	5	5	2
18	12	7	6

Table 5.7: Reduced age-related bone loss in female *p62*$^{-/-}$ mice. Age-related changes in bone parameters (expressed as % change from the same genotype at 6 months of age) are shown as mean ±SD. *p62*$^{-/-}$ or *p62*^{P394L} was compared to WT. *p62*^{P394L} mice aged 9-11 months were not included due to a very low number (N=2). Unpaired two-tailed Student's *t* test and one-way ANOVA with Dunnett's post hoc test were used to test for significant differences in age-related changes in bone parameters of female WT, *p62*$^{-/-}$ and *p62*^{P394L} mice. Significant difference between *p62*$^{-/-}$ versus WT is denoted by *p<0.05.

	9-11-month-old		18-month-old		
	WT (N=5)	***p62*$^{-/-}$ (N=5)**	**WT (N=12)**	***p62*$^{-/-}$ (N=7)0**	***p62*^{P394L} (N=6)**
BV/TV (%)	- 40.87% ± 18.17%	**- 30.74% ± 9.71%**	- 69.96% ± 14.30%	**- 48.62% ± 16.96%***	- 76.00% ± 17.67%
Tb.Th (µm)	+ 4.76% ± 9.97%	**+ 8.13% ± 8.50%**	+ 2.96% ± 16.91%	**+ 6.41% ± 8.77%**	- 1.33% ± 8.19%
Tb.Sp (µm)	+ 18.54% ± 15.12%	**+ 36.94% ± 17.91%**	+ 95.21% ± 36.28%	**+ 72.00% ± 39.65%**	+ 58.41% ± 66.36%
Tb.N (mm^{-1})	- 34.49% ± 22.35%	**- 42.46% ± 15.31%**	- 73.28% ± 14.88%	**- 51.63% ± 24.28%***	- 60.53% ± 31.56%
Tb.Pf (mm^{-1})	+ 14.84% ± 17.84%	**+ 12.72% ± 20.37%**	+ 31.47% ± 61.65%	**+ 8.76% ± 43.22%**	+ 35.39% ± 38.91%
SMI	+ 10.47% ± 8.73%	**+ 12.17% ± 6.76%**	+ 22.83% ± 11.57%	**+ 19.87% ± 18.04%**	+ 16.27% ± 22.45%

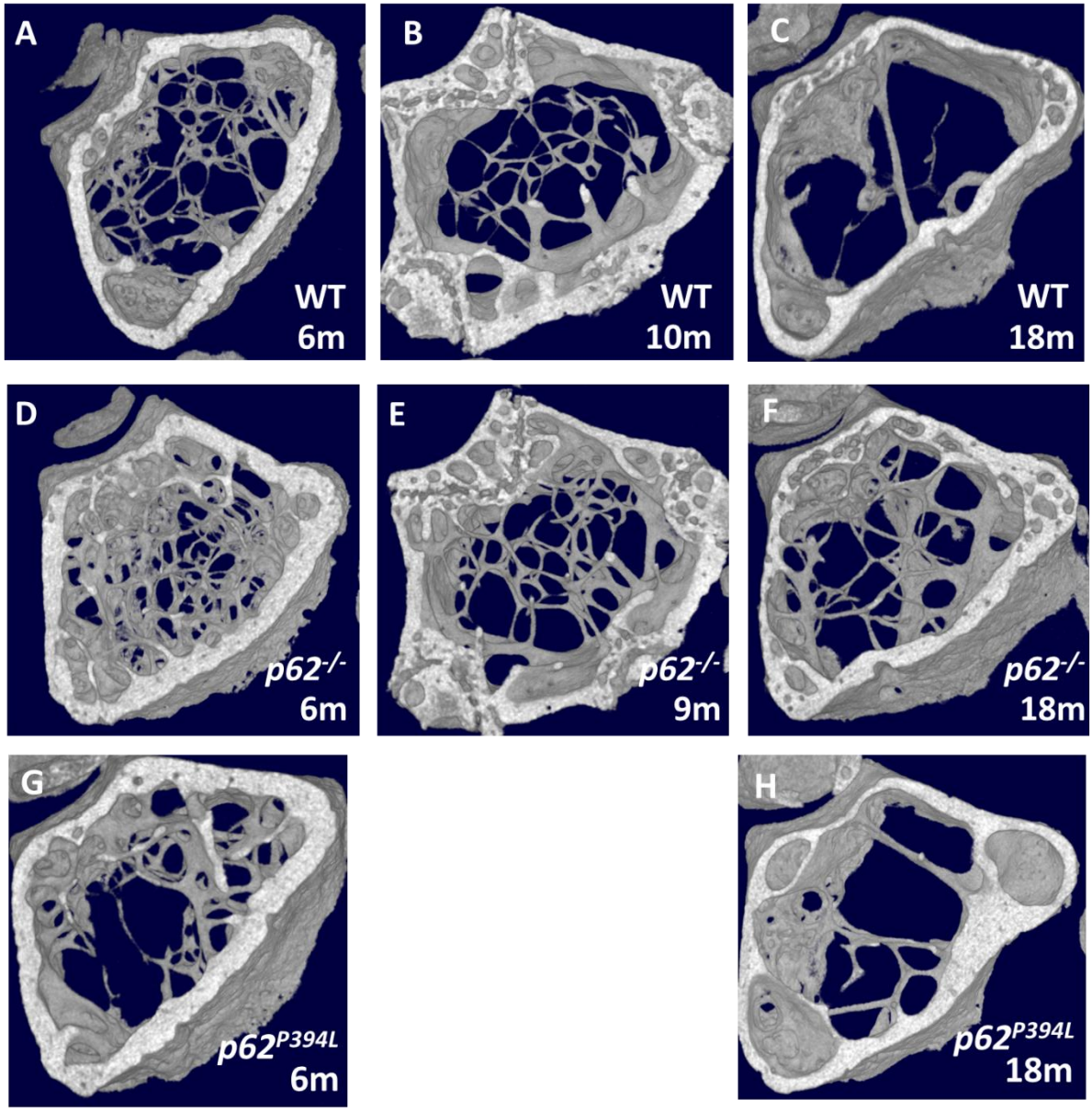

Figure 5.6: Representative cross-sectional images of 3D µCT reconstructions of whole bone from femurs of 6, 9-11 and 18-month-old female WT, *p62*$^{-/-}$ and *p62*^{P394L} mice. The 3D cross-sections show altered trabecular bone architecture and higher bone volume in *p62*$^{-/-}$ compared to WT with ageing **(A-F)**. *p62*^{P394L} shows no difference when compared to WT with ageing which may be due to low numbers of mice at 6-month-old (N=5) **(G-H)**.

5.3.4 Bone resorption histomorphometry in male *p62*$^{-/-}$ and *p62*^{P394L} mice during ageing

The findings obtained using µCT suggest that the protective effect on age-related bone loss caused by the deletion of p62 may be due to a decrease in bone resorption. RANKL-RANK interaction recruits TRAF6[599] and activates the osteoclastogenic transcription factors, particularly NF-κB and NFATc1[651]. P62 is known as one of the key players which link RANKL and TRAF6-mediated NF-κB activation. Therefore, it is possible that the loss of p62 would result in lower OC formation or activity. To detect bone-resorbing OCs, I performed TRAP stain on the femurs of 6, 10 and 18-month-old male WT, *p62*$^{-/-}$ and *p62*^{P394L} mice, as per **Table 5.8**.

6 and 10-month-old male *p62*$^{-/-}$ mice consistently showed reduced osteoclast surface per bone surface (Oc.S/BS) and number of osteoclasts per bone surface (N.Oc/BS) (**Figure 5.7 and Figure 5.8**). *p62*$^{-/-}$ mice at 18-month-old showed a trend of reduction, however, the lack of significance may be due to insufficient sample size (N=5). No significant difference was observed between WT and *p62*^{P394L}. Histomorphometric age-related changes in phenotype are shown in **Table 5.9**. This indicates that the impact of p62 deletion on the osteoclastogenesis in male mice is already present at 6 months of age and continues over the life course at least until 10 months of age. These data are in keeping with reduced osteoclastogenesis in male *p62*$^{-/-}$ mice, thereby lower bone resorption. Due to the very low number of *p62*^{P394L} mice at 9-11-month-old (N=2), data on these mice are not included in **Figure 5.7** and **Table 5.9**.

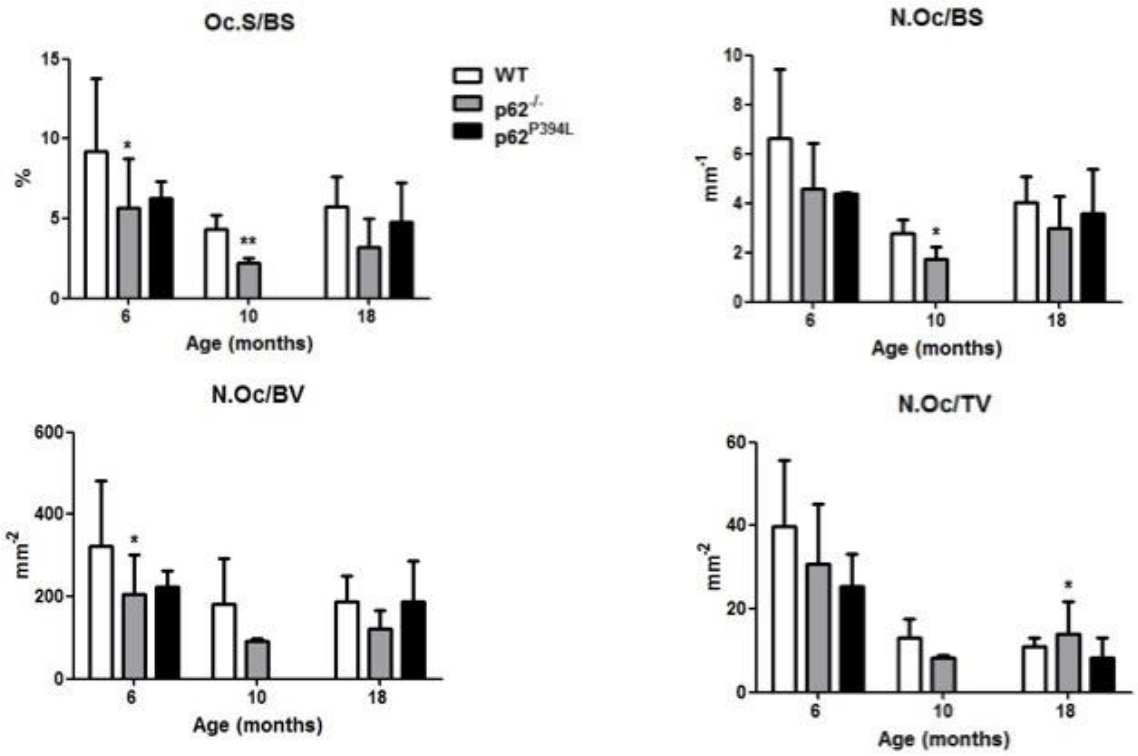

Figure 5.7: Histomorphometric quantification of OCs in 6, 10 and 18-month-old male WT, *p62*$^{-/-}$ and *p62*^{P394L} mice. MMA embedded sections of the distal femurs of 6, 10 and 18-month-old male *p62*$^{-/-}$ (N=13, N=3 and N=5, respectively), *p62*^{P394L} (N=3, N=2 and N=8, respectively) and WT (N=15, N=5 and N=12, respectively) were TRAP stained for histomorphometric analysis. Oc.S/BS, osteoclast surface per bone surface; N.Oc/BS, number of osteoclasts per bone surface; N.Oc/BV, number of osteoclasts per bone volume; N.Oc/TV, number of osteoclasts per tissue volume. Data are shown as means $\pm$ SD. Unpaired two-tailed Student's *t* test and one-way ANOVA with Dunnett's post hoc test were used to test for significant differences in OC parameters in 6, 9-11 and 18-month-old male WT, *p62*$^{-/-}$ and *p62*^{P394L} mice. Significance compared to WT is denoted by *p<0.05, **p<0.01.

Table 5.8: Demographics of male mice by age and genotypes used for the histomorphometric analysis.

Months	WT	*p62*$^{-/-}$	*p62*^{P394L}
6	15	13	3
10	5	3	2
18	12	5	8

Table 5.9: The changes of OC number in distal femurs of male *p62$^{-/-}$*, *p62^{P394L}* and WT mice at 10 and 18 months of age in comparison to 6 months of age. Age-related changes in OC parameters (expressed as % change from the same genotype at 6 months of age) are shown as means ±SD. *p62$^{-/-}$* or *p62^{P394L}* was compared to WT. Unpaired two-tailed Student's *t* test and one-way ANOVA with Dunnett's post hoc test were used to test for significant differences in age-related changes in OC parameters of male WT, *p62$^{-/-}$* and *p62^{P394L}* mice. Significant difference between *p62$^{-/-}$* versus WT is denoted by *p<0.05, **p<0.01.

	10-month-old		18-month-old		
	WT (N=5)	***p62$^{-/-}$* (N=3)**	**WT (N=12)**	***p62$^{-/-}$* (N=5)**	***p62^{P394L}* (N=8)**
Oc.S/BS (%)	- 56.88% ± 4.62%	**- 60.28% ± 5.02%****	- 52.82% ± 10.85%	**- 43.96% ± 31.56%**	- 20.91% ± 41.40%
N.Oc/BS (mm^{-1})	- 58.06% ± 8.09%	**- 61.51% ± 10.91%***	- 31.46% ± 25.32%	**- 34.07% ± 28.15%**	- 17.24% ± 42.51%
N.Oc/BV (mm^{-2})	- 43.47% ± 34.31%	**- 55.06% ± 3.07%**	- 37.55% ± 23.77%	**- 41.23% ± 22.98%**	- 20.98% ± 44.82%
N.Oc/TV (mm^{-2})	- 66.85% ± 11.18%	**- 73.42% ± 2.11%**	- 70.19% ± 8.43%	**- 45.86% ± 24.95%***	- 42.29% ± 78.87%

Note: There were no *p62^{P394L}* mice aged 10 months available.

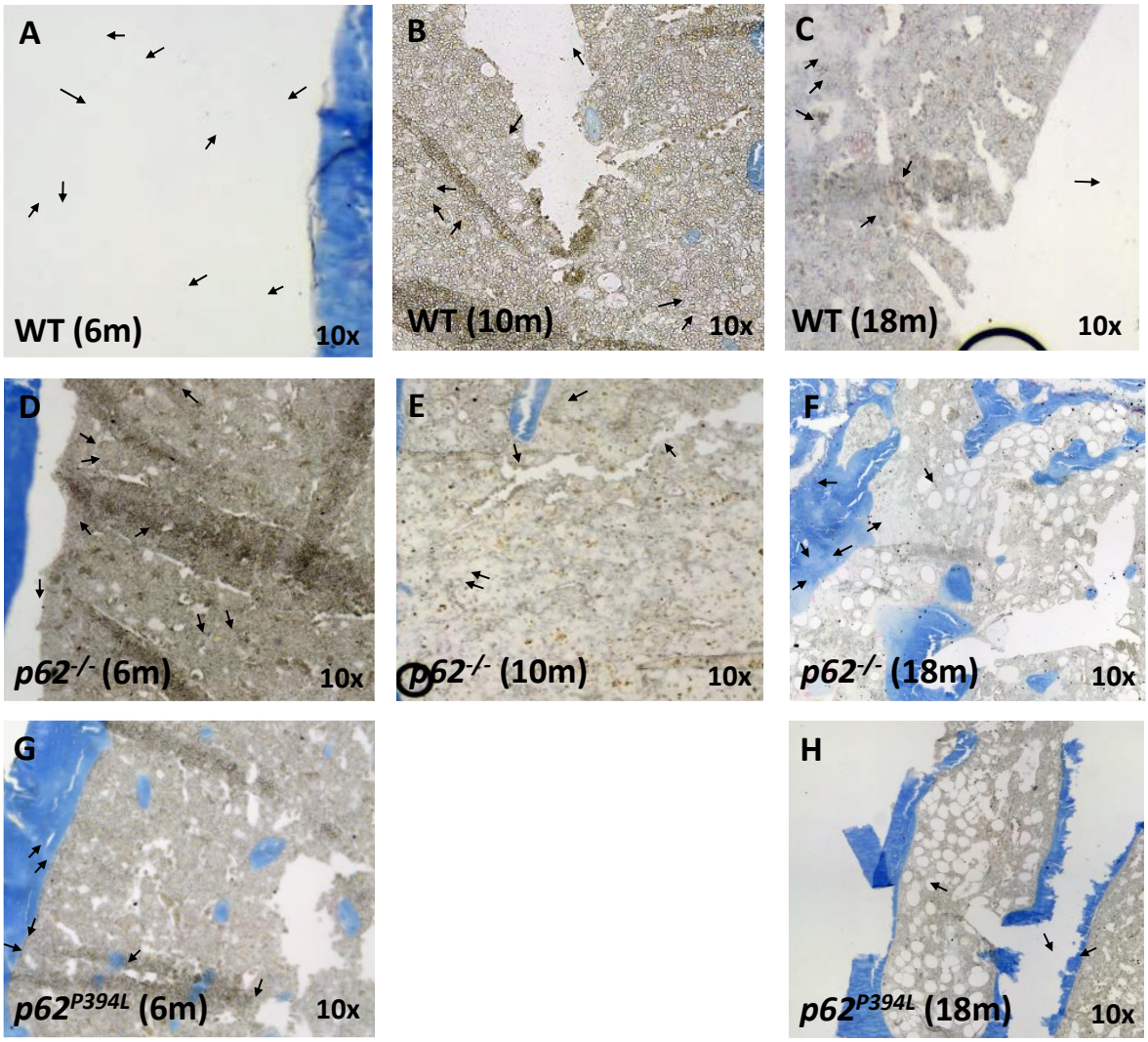

Figure 5.8: Aniline Blue and TRAP staining of distal femurs of 6, 10 and 18-month-old male WT, *p62*$^{-/-}$ and *p62*^{P394L} mice. The TRAP staining demonstrates a lower number of OCs in the *p62*$^{-/-}$ mice with ageing **(D-F)** compared to the WT mice **(A-C)**, with OCs (stained red) indicated by arrows. No significant difference was observed in 6 and 18-month-old *p62*^{P394L} mice which may be due to low numbers of 6-month-old mice (N=3) **(G-H)**.

5.3.5 Bone resorption histomorphometry in female *p62*$^{-/-}$ and *p62*^{P394L} mice during ageing

I also performed TRAP stain on the femurs of 6 and 18-month-old female WT, *p62*$^{-/-}$ and *p62*^{P394L} mice, as per **Table 5.10**. Similar to male *p62*$^{-/-}$ mice, female *p62*$^{-/-}$ mice at 6-months of age showed reduced Oc.S/BS, N.Oc/BS and N.Oc.BV ($p<0.01$) compared to WT mice. *p62*$^{-/-}$ mice at 18-months of age show no significant difference, which may be due to insufficient sample size (N=4), as 3 samples had to be removed because of the observation made of the presence of pagetic-like lesions at the distal femurs which will be discussed in **Sub-section 5.3.8**.

On the other hand, female *p62*^{P394L} mice at 6-months of age also show reduced N.Oc/BS and N.Oc.BV ($p<0.05$) (**Figure 5.9 and 5.10**) compared to WT mice. With ageing, *p62*^{P394L} mice at 18-months display increased Oc.S/BS ($p<0.05$) and N.Oc/BS ($p<0.01$). This implies increased OC differentiation is in accordance with previous findings[561].

Histomorphometric age-related changes in phenotype are shown in **Table 5.11**. This indicates that the impact of p62 deletion on the osteoclastogenesis in female mice is present at 6 months of age. Nevertheless, more sample size of *p62*$^{-/-}$ mice is required at 18-months of age to quantify changes in OC differentiation.

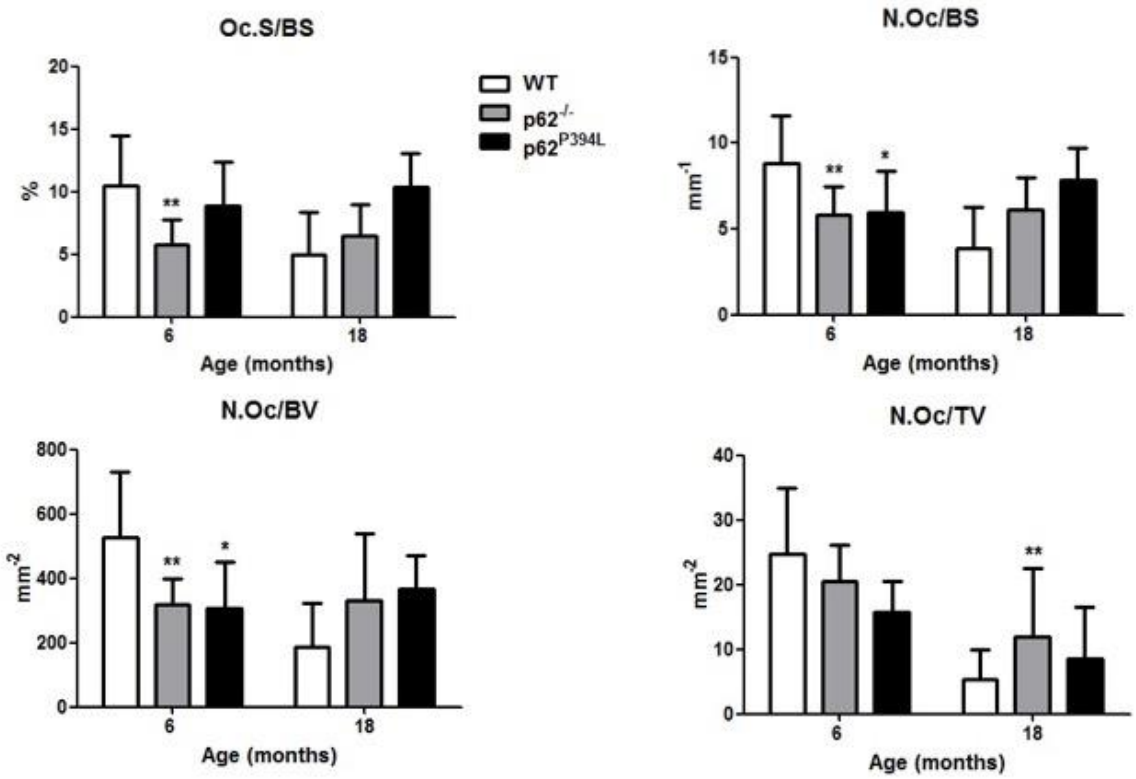

Figure 5.9: Histomorphometric quantification of OCs in 6 and 18-month-old female WT, *p62*$^{-/-}$ and *p62*^{P394L} mice. MMA embedded sections of the distal femurs of 6 and 18-month-old female *p62*$^{-/-}$ (N=13 and N=4, respectively), *p62*^{P394L} (N=5 and N=5, respectively) and WT (N=13 and N=10, respectively) were TRAP stained for histomorphomtric analysis. Oc.S/BS, osteoclast surface per bone surface; N.Oc/BS, number of osteoclasts per bone surface; N.Oc/BV, number of osteoclasts per bone volume; N.Oc/TV, number of osteoclasts per tissue volume. Data are shown as means ±SD. One-way ANOVA with Dunnett's post hoc test was used to test for significant differences in OC parameters in 6 and 18-month-old female WT, *p62*$^{-/-}$ and *p62*^{P394L} mice. Significance compared to WT is denoted by *p<0.05, **p<0.01.

Table 5.10: Demographics of female mice by age and genotypes used for the histomorphometric analysis.

Months	WT	*p62*$^{-/-}$	*p62*^{P394L}
6	13	13	5
18	10	4	5

Table 5.11: The changes of OC number in distal femurs of female WT, *p62*$^{-/-}$ and *p62*^{P394L} mice at 18 months of age in comparison to 6 months of age. Age-related changes in OC parameters (expressed as % change from the same genotype at 6 months of age) are shown as means ±SD. 18-month-old *p62*$^{-/-}$ or *p62*^{P394L} was compared to WT. One-way ANOVA with Dunnett's post hoc test was used to test for significant differences in age-related changes in OC parameters of female WT, *p62*$^{-/-}$ and *p62*^{P394L} mice. Significant difference between *p62*^{P394L} versus WT is denoted by *p<0.05, **p<0.01.

	18-month-old		
	WT (N=10)	***p62*$^{-/-}$ (N=4)**	***p62*^{P394L} (N=5)**
Oc.S/BS (%)	- 32.43% ± 54.64%	**+ 11.18% ± 37.75%**	-8.13% ± 49.96%*
N.Oc/BS (mm^{-1})	- 39.10% ± 46.72%	**- 2.07% ± 27.07%**	+ 4.66% ± 52.16%**
N.Oc/BV (mm^{-2})	- 49.83% ± 41.09%	**- 12.65% ± 56.15%**	- 4.40% ± 50.28%
N.Oc/TV (mm^{-2})	- 76.28% ± 17.78%	**- 16.94% ± 55.11%****	- 55.37% ± 44.72%

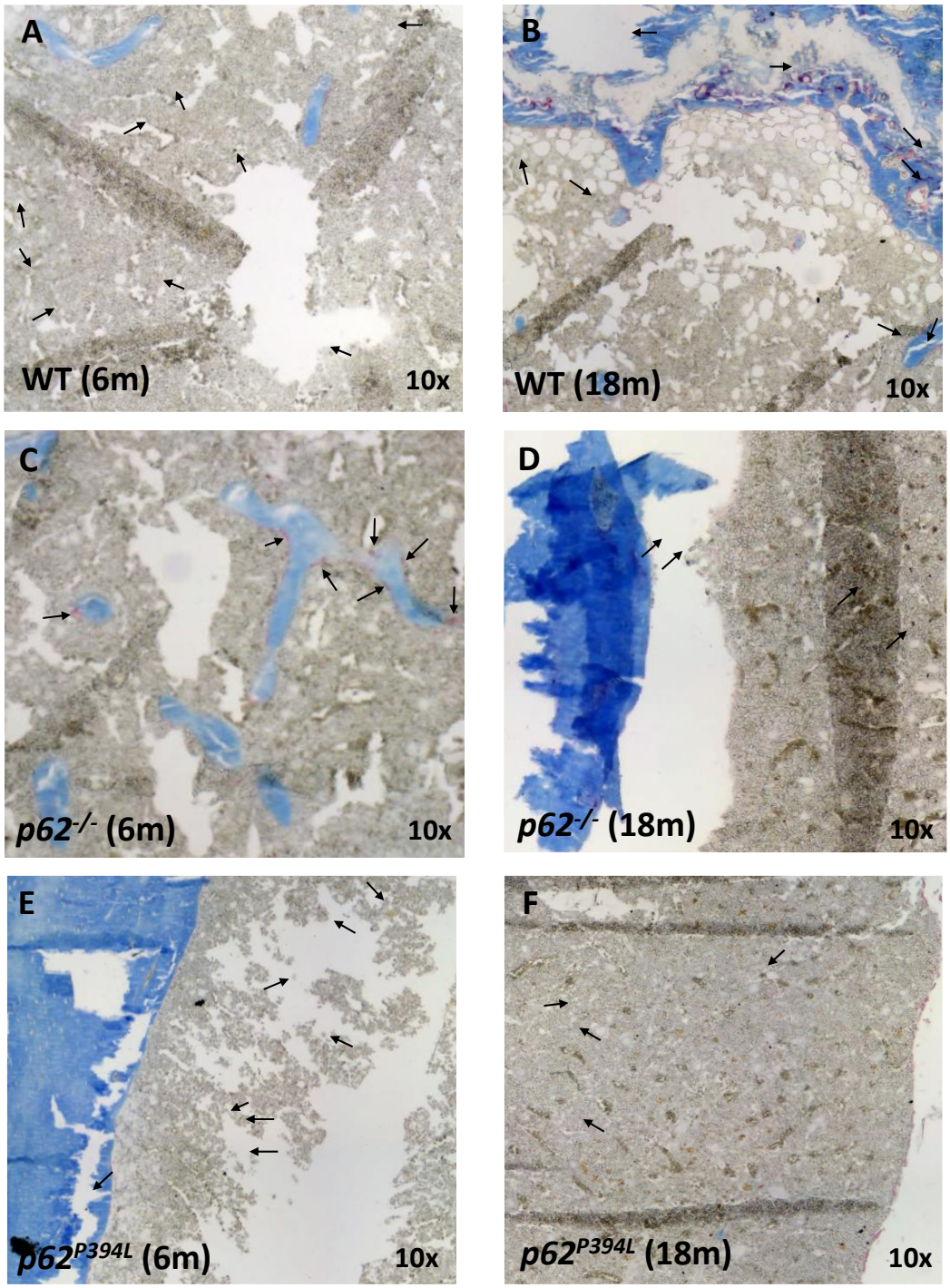

Figure 5.10: Aniline Blue and TRAP staining of distal femurs of 6 and 18-month-old female WT, *p62*$^{-/-}$ and *p62*^{P394L} mice. The TRAP staining shows no changes in the number of OCs in the *p62*$^{-/-}$ mice with ageing **(C and D respectively)**, and an increase in the number of OCs in *p62*^{P394L} mice with ageing **(E and F respectively)** when compared to that of the WT mice **(A and B respectively)**, with OCs (stained red) indicated by arrows.

5.3.6 Bone formation histomorphometry in male *p62*$^{-/-}$ and *p62*^{P394L} mice during ageing

Apart from lower bone resorption, the protective effect on age-related bone loss caused by the deletion of p62 may be also due to an increase in bone formation. To assess the rate of osteoblastic bone formation, I analysed calcein double staining on subset of the distal femurs of 6 and 18-month-old male WT and *p62*$^{-/-}$ mice, as per **Table 5.12**.

With ageing, both male *p62*$^{-/-}$ and WT mice have reduced rate of bone formation, however the reduction was less pronounced in the 18-month-old *p62*$^{-/-}$ compared to the age-matched WT **(Figure 5.11 and 5.12).** This indicates that male *p62*$^{-/-}$ mice with ageing have a higher rate of osteoblastic bone formation as compared to the WT with ageing.

In the distal femur, *p62*$^{-/-}$ mice at 6-months show no difference versus WT. At 18-months, *p62*$^{-/-}$ versus WT mice exhibit significantly increased BV/TV ($p<0.05$) and mineralising apposition rate (MAR) ($p<0.05$). This was accompanied by a significant increase in bone formation rate per bone surface (BFR/BS) ($p<0.05$). Overall, the age-related morphometric changes in the phenotype are shown in **Table 5.13**. Calcein double labelling showed less pronounced reduction of double label surface in *p62*$^{-/-}$ with ageing compared to WT mice **(Figure 5.12 A-D)**. Due to the very low number of *p62*^{P394L} mice at 6- and 18-month-old (N=1, N=2, respectively), data on these mice are not included in **Figure 5.11** and **Table 5.13**.

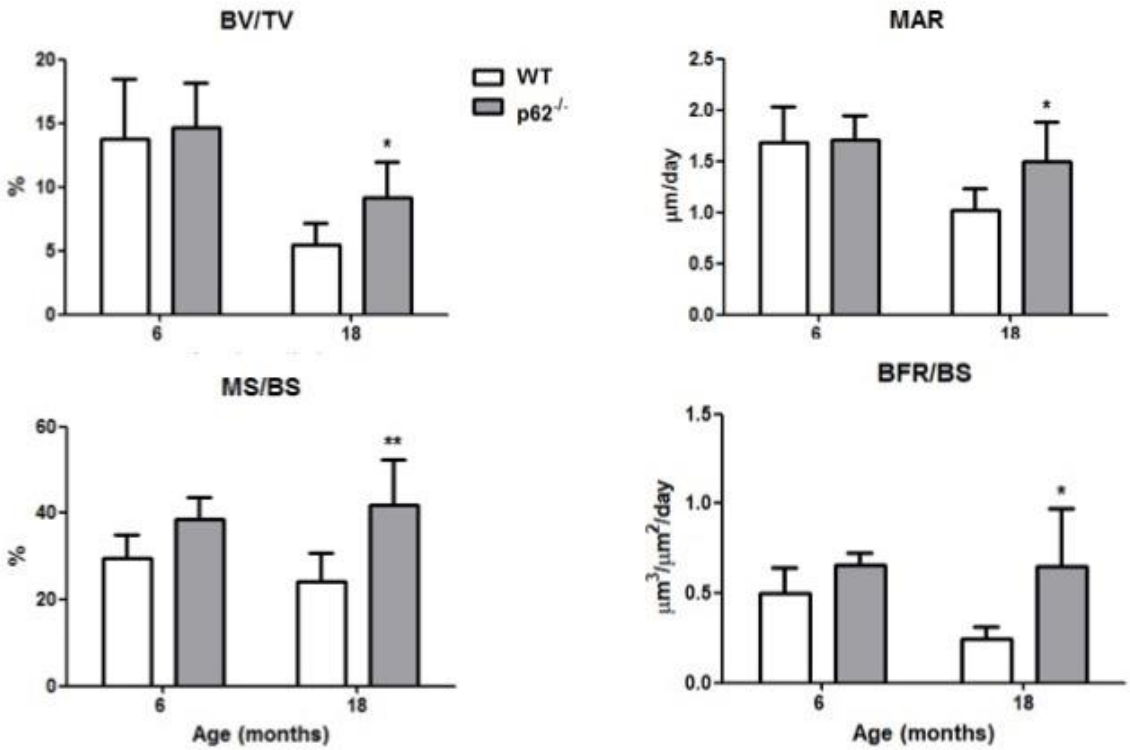

Figure 5.11: Dynamic histomorphometric analysis of bone formation in 6 and 18-month-old male WT and *p62*$^{-/-}$ mice. MMA embedded sections of the distal femurs of 6 and 18-month-old male *p62*$^{-/-}$ (N=7 and N=5, respectively) and WT (N=7 and N=5, respectively) were stained with Calcein Blue for dynamic histomorphometric analysis. BV/TV, bone volume per tissue volume; MAR, mineralising apposition rate; MS/BS, mineralising surface per bone surface; BFR/BS, bone formation rate per bone surface. Data are shown as means ±SD. Unpaired two-tailed Student's *t* test was used to test for significant differences in bone formation parameters in 6 and 18-month-old male WT and *p62*$^{-/-}$ mice. Significance compared to WT is denoted by *p<0.05.

Table 5.12: Demographics of male mice by age and genotypes used for the dynamic histomorphometric analysis.

Months	WT	*p62*$^{-/-}$
6	7	7
18	5	5

Table 5.13: The changes of bone formation rate in distal femurs of male WT and *p62*$^{-/-}$ mice at 18 months of age in comparison to 6 months of age. Age-related changes in bone formation parameters (expressed as % change from the same genotype of 6 months of age) are shown as means ±SD. *p62*$^{-/-}$ was compared to WT. Unpaired two-tailed Student's *t* test was used to test for significant differences in age-related changes in bone formation parameters of male WT and *p62*$^{-/-}$ mice. Significant difference between *p62*$^{-/-}$ versus WT is denoted by *p<0.05.

	18-month-old	
	WT (N=5)	***p62*$^{-/-}$ (N=5)**
BV/TV (%)	- 60.29% ± 12.56%	**- 37.69% ± 18.94%***
MAR (µm/day)	- 39.09% ± 12.06%	**- 12.59% ± 22.87%***
MS.BS (%)	- 17.97% ± 22.44%	**+ 8.25% ± 27.37%**
BFR/BS (µm^3/µm^2/day)	- 50.47% ± 13.13%	**- 0.86% ± 48.83%***

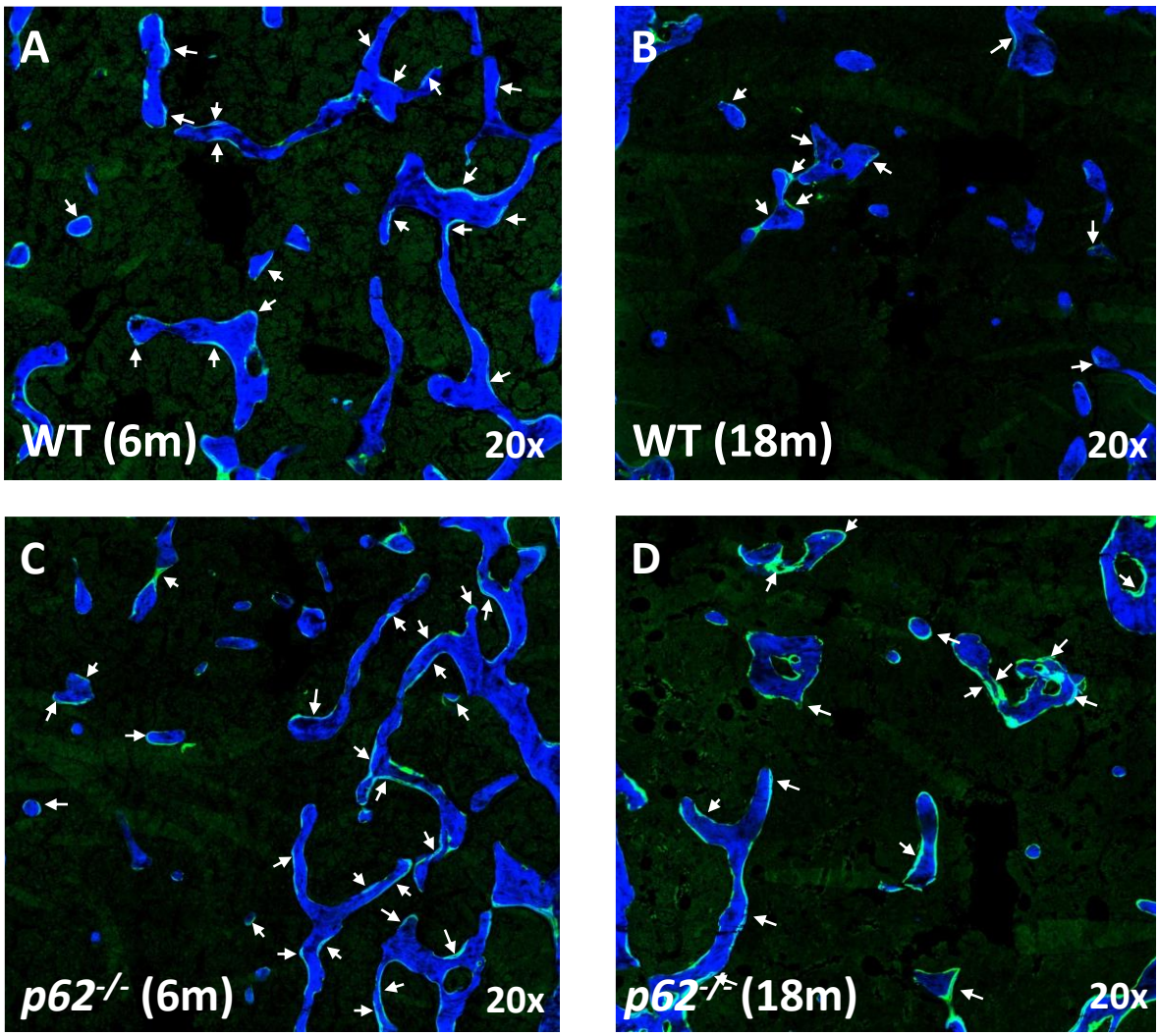

Figure 5.12: Fluorescent microscopy of distal femurs of 6 and 18-month-old male WT and *p62*$^{-/-}$ mice. Age-related decrease in trabecular bone counterstained with calcein blue is seen in both WT (**A and B**) and *p62*$^{-/-}$ (**C and D**). The calcein double-labelling of bone surfaces (green) indicated by arrows shows increased bone formation rate in *p62*$^{-/-}$ compared to WT mice at 18 months of age compared to WT mice with ageing.

5.3.7 Bone formation histomorphometry in female *p62*$^{-/-}$ and *p62*^{P394L} mice during ageing

I also performed calcein double staining on the femurs of 6 and 18-month-old female WT and *p62*$^{-/-}$ mice, as per **Table 5.14**. Unlike in the male *p62*$^{-/-}$ mice, there were no significant differences in any of the histomorphometric parameters in the female *p62*$^{-/-}$ versus WT mice at 6 or 18 months of age (**Figure 5.13 and 5.14, Table 5.15**). This is not surprising as 3 samples from 18-month-old *p62*$^{-/-}$ mice had to be removed because of the observation made of the presence of Pagetic-like lesions at the distal femurs which will be discussed in **Sub-section 5.3.8**, leaving only four femurs for this analysis.

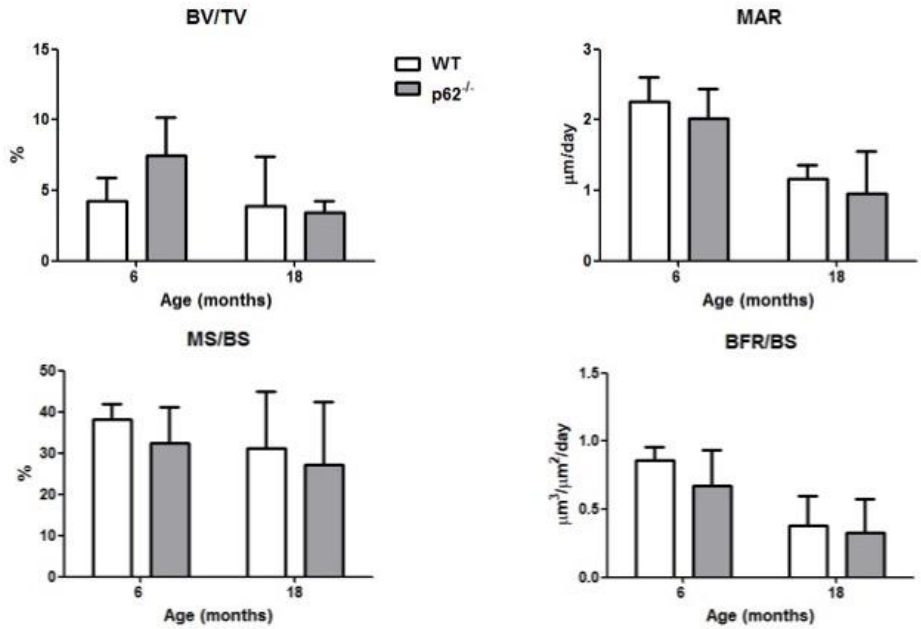

Figure 5.13: Dynamic histomorphometric analysis of bone formation in 6 and 18-month-old female WT and *p62*$^{-/-}$ mice. MMA embedded sections of the distal femurs of 6 and 18-month-old female *p62*$^{-/-}$ (N=8 and N=4, respectively) and WT (N=6 and N=4, respectively) were stained with Calcein blue for dynamic histomorphometric analysis. BV/TV, bone volume per tissue volume; MAR, mineralising apposition rate; MS/BS, mineralising surface per bone surface; BFR/BS and bone formation rate per bone surface. Data are shown as means ±SD. Unpaired two-tailed Student's *t* test was used to test for significant differences in bone formation parameters in 6 and 18-month-old female WT and *p62*$^{-/-}$ mice.

Table 5.14: Demographics of female mice by age and genotypes used for the dynamic histomorphometric analysis.

Months	WT	*p62*$^{-/-}$
6	6	8
18	4	4

Table 5.15: The changes of bone formation rate in distal femurs of female WT and *p62*$^{-/-}$ mice at 18 months of age in comparison to 6 months of age. Age-related changes in bone formation parameters (expressed as % change from the same genotype of 6 months of age) are shown as means ±SD. *p62*$^{-/-}$ was compared to WT. Unpaired two-tailed Student's *t* test was used to test for significant differences in age-related changes in bone formation parameters of female WT and *p62*$^{-/-}$ mice. 3 samples from the 18-month-old *p62*$^{-/-}$ mice had to be removed, thus N=4.

	18-month-old	
	WT (N=4)	***p62*$^{-/-}$ (N=4)**
BV/TV (%)	- 47.92% ± 22.87%	**- 54.13% ± 11.51%**
MAR (µm/day)	- 48.59% ± 8.85%	**- 52.32% ± 29.68%**
MS.BS (%)	- 17.82% ± 35.91%	**- 15.93% ± 46.77%**
BFR/BS ($\mu m^3/\mu m^2$/day)	- 55.66% ± 24.93%	**- 51.02% ± 36.14%**

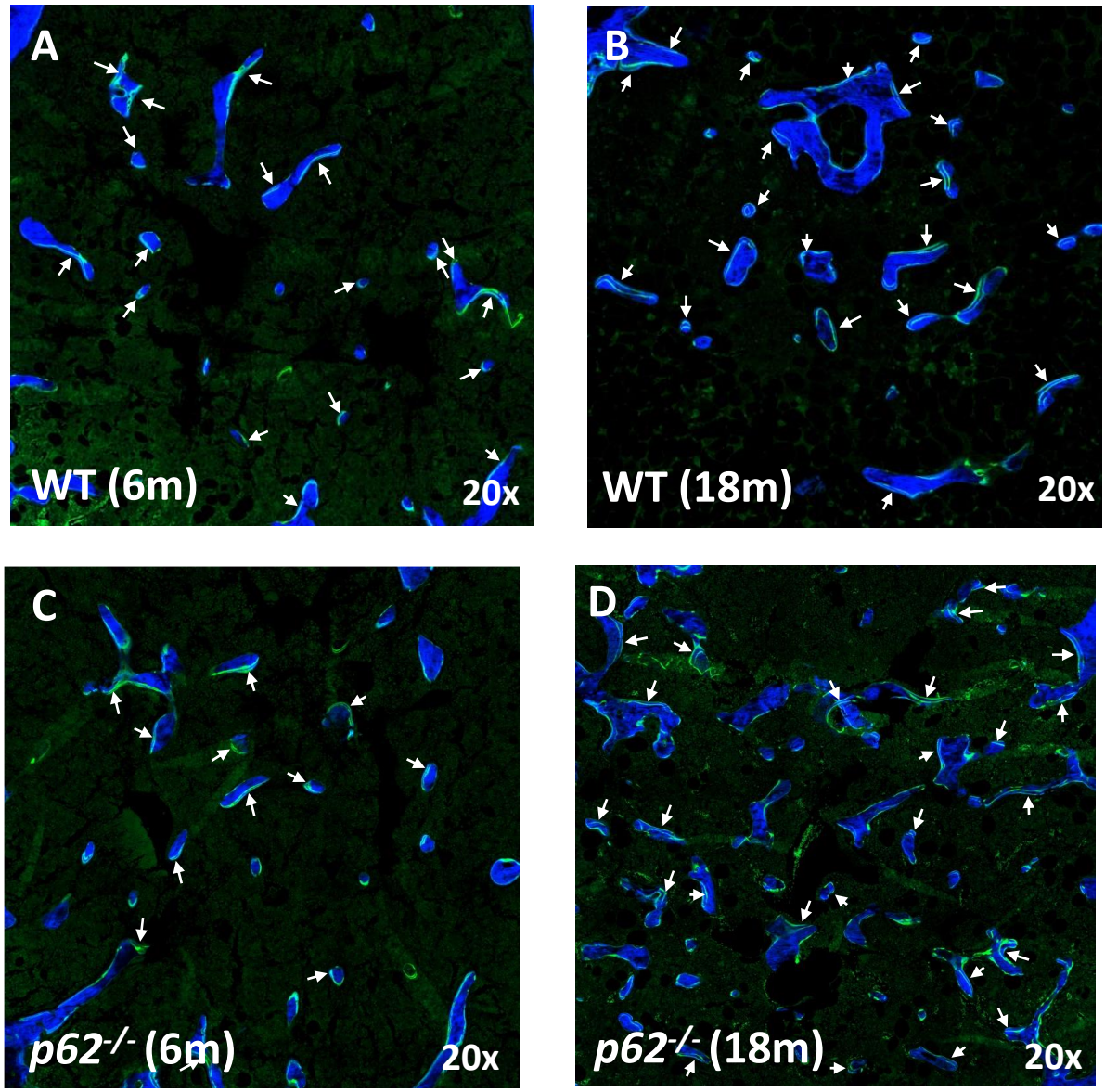

Figure 5.14: Fluorescent microscopy of distal femurs of 6 and 18-month-old female WT and *p62*$^{-/-}$ mice. Age-related decrease in trabecular bone counterstained with calcein blue is seen in both WT (**A and B**) and *p62*$^{-/-}$ (**C and D**). The calcein double-labelling of bone surfaces (green) indicated by arrows shows no difference in the rate of bone formation in *p62*$^{-/-}$ compared to WT mice at 18 months of age.

5.3.8 Development of Pagetic-like skeletal lesions in aged *p62*$^{-/-}$ mice

While investigating the effect of p62 deletion on bone morphometry and histomorphometry in ageing, unexpectedly Pagetic-like lesions were observed on µCT in some of the 18-month-old animals. Therefore, mice in which the analysed area was affected by the lesions were removed from the previous analysis in **Sub-section 5.3.3, 5.3.5 and 5.3.7** and were analysed in this sub-section. In PDB, lesions could be present and distributed at multiple sites with different severity[253]. Due to the lack of experience, the lesion identification and prevalence shown in **Table 5.16** was performed together with my supervisors.

Lesions visualised by 3D µCT reconstruction shown in **Figure 5.15 B, E and H** were observed to be located at the lesser trochanter of femur and distal femur close to the growth plate in *p62*$^{-/-}$ mice. Cross-sectional analysis of the reconstructed lesions revealed disorganised and highly trabecularised bone structure, and osteolytic lesions within the trabecular compartment in *p62*$^{-/-}$ mice **(Figure 5.15 H and L)**. **Figure 5.15** shows the most severely affected femur of *p62*$^{-/-}$ mice. On the 2D sections, whole cortex is thickened in the *p62*$^{-/-}$ **(Figure 5.15 M).** Overall, *p62*^{P394L} is less affected compared to *p62*$^{-/-}$.

Table 5.16: Prevalence of lesions in *p62*$^{-/-}$ and *p62*^{P394L}. Left hind legs of the mice were analysed by µCT at 9 µm, and Pagetic-like lesions were counted per mouse. Chi-squared test was used to test the prevalence of lesions in *p62*$^{-/-}$ and *p62*^{P394L}. The chi-square test indicates that lesions are more prevalent in *p62*$^{-/-}$ than *p62*^{P394L} ($\chi^2 = 18.17$, d.f. = 2, $P < 0.0001$).

	WT	KO	KI
Lesions	0	11	8
No lesions	18	5	9

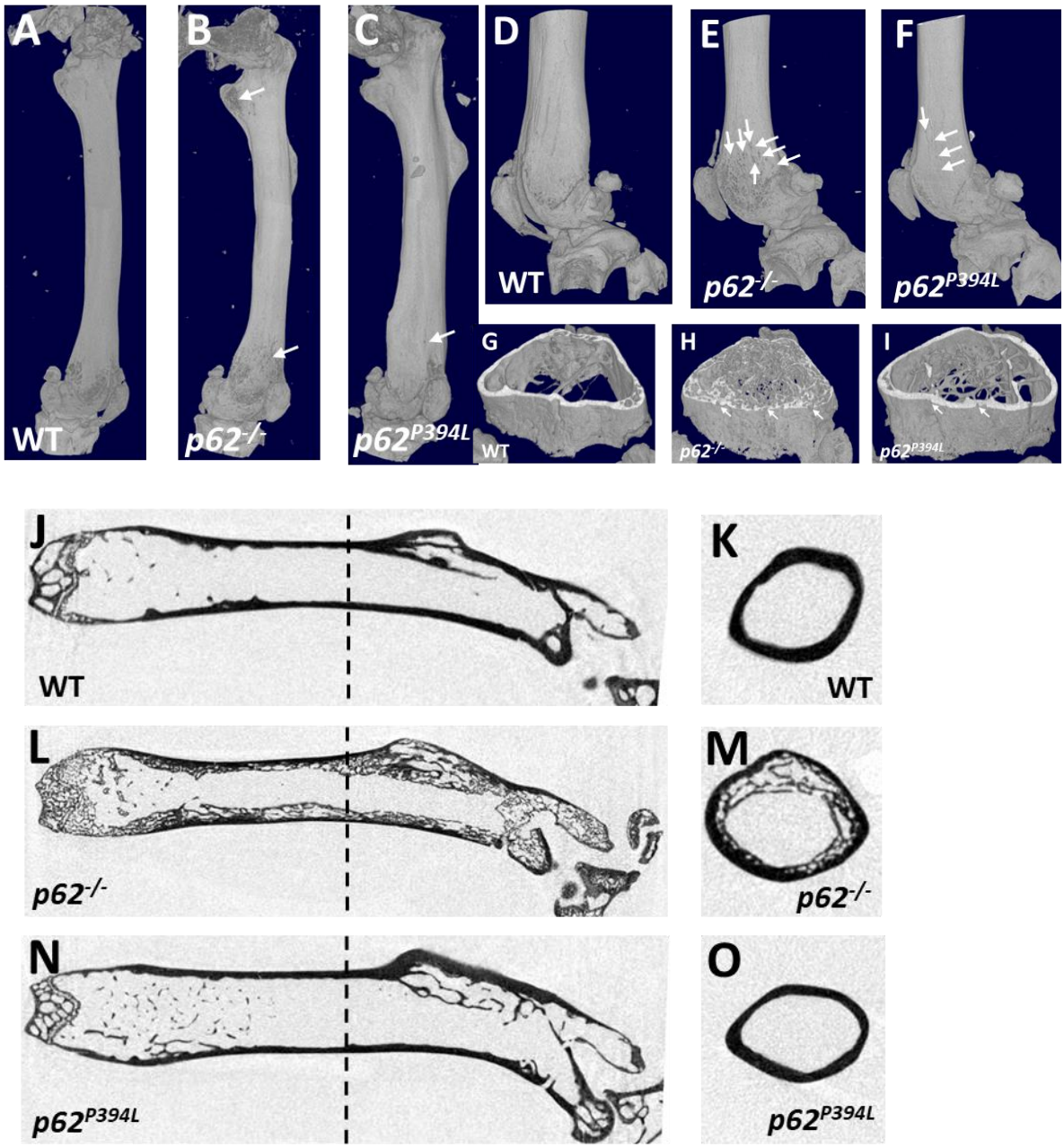

Figure 5.15: μCT analysis of femurs from 18-month-old *p62*$^{-/-}$, *p62*^{P394L} and WT mice. μCT analysis with 3D reconstruction of the full length, the distal femur and proximal tibia of a female WT mouse **(A and D)**, a female *p62*$^{-/-}$ mouse **(B and E)** and a male *p62*^{P394L} mouse **(C and F)** showing multiple focal osteolytic lesions penetrating the cortex (arrows). **(G-I)** Cross-section from (D) to (F). Longitudinal μCT section of the femur from a WT mouse **(J)**, a *p62*$^{-/-}$ mouse **(L)** and a *p62*^{P394L} mouse **(N)** showing mixed osteosclerotic and osteolytic lesions at proximal and distal femur in the *p62*$^{-/-}$ mouse (**L**). In this cross-section, there are no apparent lesions seen in the *p62*^{P394L} mouse (**N**). **(K)**, **(M)** and **(O)** Cross-sections from the femorae of the same animals taken at the level of the broken line seen in (J), (L) and (N).

Histological analysis of bone lesions identified by µCT showed significantly increased number of OCs within the bone lesion on TRAP stain **(Figure 5.16 B and D)**. There was a 15-fold increase in N.Oc/TV ($p<0.001$) within the focal lesion when compared to the WT. Moreover, the size of OCs within the lesion appears to be larger than that of the WT **(Figure 5.16 B)**.

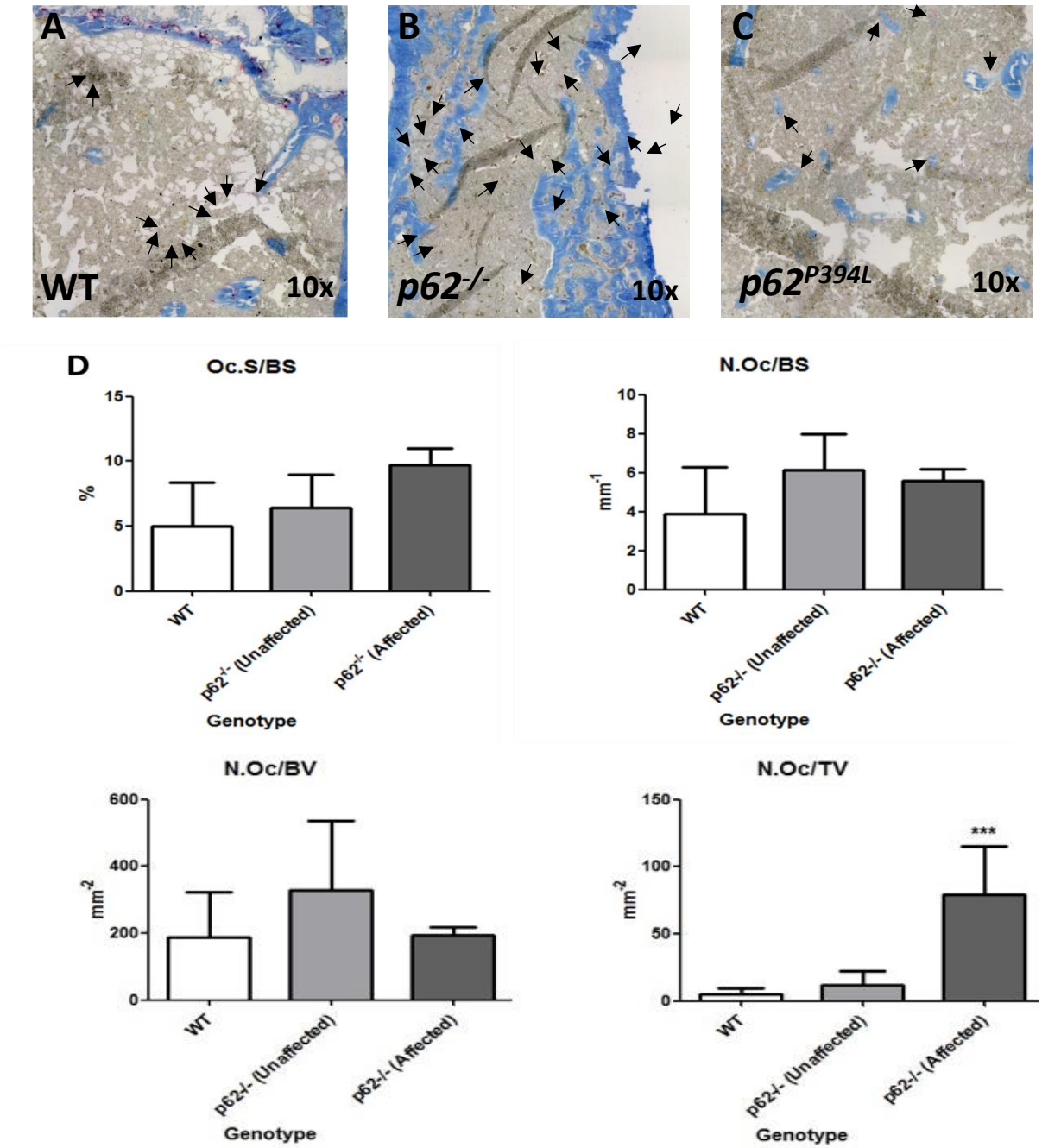

Figure 5.16: Histomorphometric analysis of focal lesions from 18-month-old female *p62$^{-/-}$* mice. Aniline Blue and TRAP stain of distal femurs from 18-month-old WT **(A)**, ***p62$^{-/-}$*** (affected by lesions) **(B)** and *p62^{P394L}* **(C)**, with OCs (TRAP-stained red) indicated by arrows. Histological analysis **(D)** of the distal femurs of 18-month-old *p62$^{-/-}$* (affected by lesions) (N=3), *p62$^{-/-}$* (unaffected by lesions) (N=4**)** and WT (N=10). Due to insufficient samples of *p62^{P394L}* with lesions, quantification cannot be done. Oc.S/BS, osteoclast surface per bone surface; N.Oc/BS, number of osteoclasts per bone surface; N.Oc/BV, number of osteoclasts per bone volume; N.Oc/TV, number of osteoclasts per tissue volume. Data are shown as means ±SD. One-way ANOVA with Dunnett's post hoc test was used to test for significant differences in OC parameters in 18-month-old female WT and *p62$^{-/-}$* mice. Significance compared to WT is denoted by ***p<0.001.

Histomorphometric analysis showed an increased bone formation as detected by calcein double labelling in the lesion compared to the WT **(Figure 5.17 B)**. There was a 7 and 3-fold increase in BV/TV ($p<0.001$), and BFR/BS ($p<0.05$) respectively within the focal lesion when compared to the WT. In addition, *p62*$^{-/-}$ **(Figure 5.17 B)** seems to have had more excess bone formation than P394L **(Figure 5.17 C)** within the lesions, however this was not formally quantified.

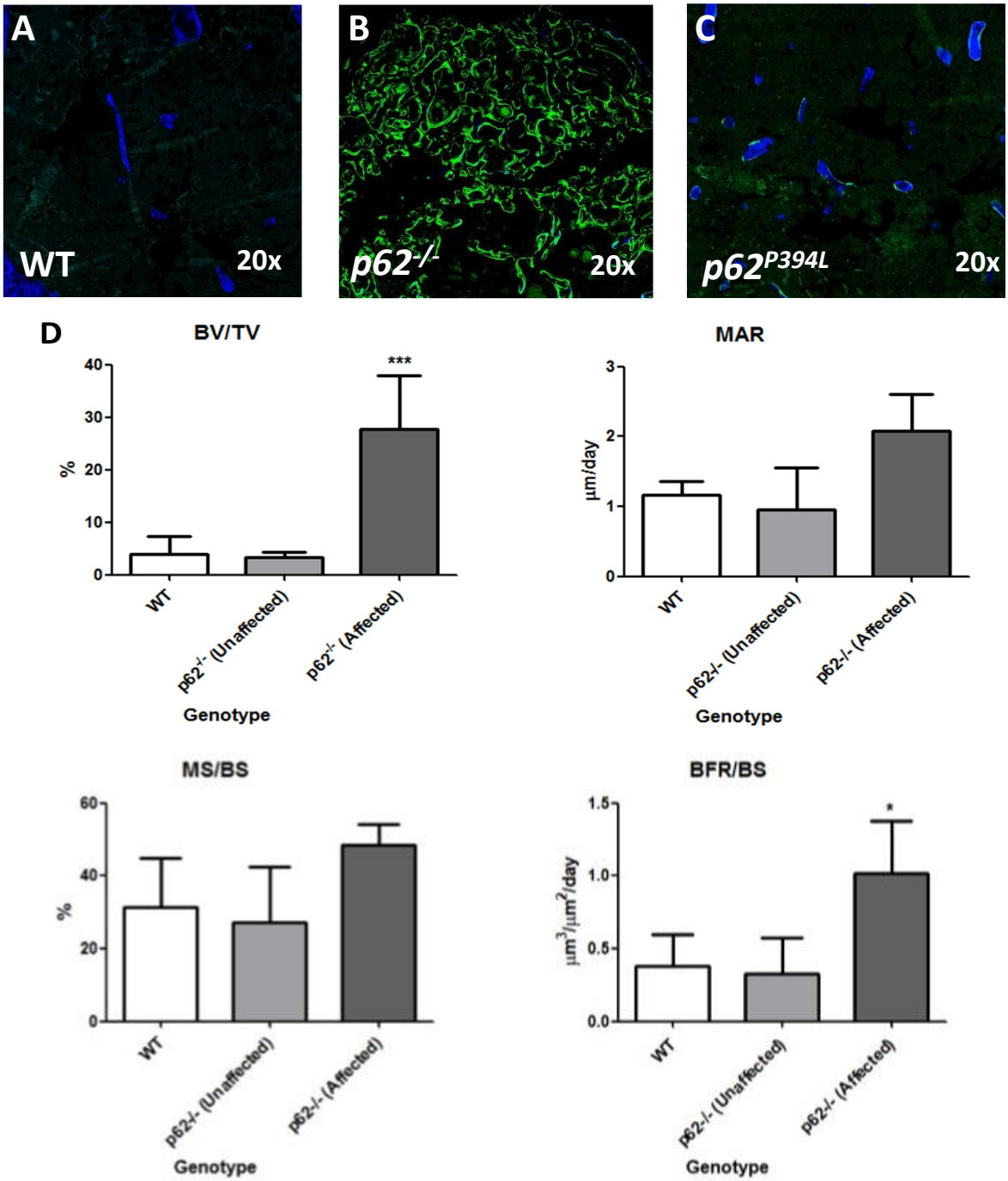

Figure 5.17: Dynamic histomorphometric analysis of focal lesions from 18-month-old female *p62*$^{-/-}$ mice. Fluorescent microscopy of distal femurs from 18-month-old WT **(A)**, *p62*$^{-/-}$ (affected by lesions) **(B)** and *p62*^{P394L} (affected by lesions) **(C)** mice with calcein double-labelling of bone surfaces (green) indicated by arrows and Calcein blue counterstain. Histological analysis (**D**) of the femurs of 18-month-old *p62*$^{-/-}$ (affected by lesions) (N=3), *p62*$^{-/-}$ (unaffected by lesions) (N=4) and WT (N=4). Due to insufficient samples of *p62*^{P394L} with lesions, quantification cannot be done. Data are shown as means ± SD. One-way ANOVA with Dunnett's post hoc test was used to test for significant differences in bone formation parameters in 18-month-old female WT and *p62*$^{-/-}$ mice. Significance compared to WT is denoted by *p<0.05, ***p<0.001.

5.4 Discussion

Growing lines of evidence point to a significant role of p62 in bone metabolism, especially after the discovery of p62 mutations contributing to PDB which is a late-onset skeletal disorder. While most of the studies are focused on the role of p62 in the pathogenesis of PDB, little is known about the influence of p62 deletion on bone metabolism, particularly in ageing. Durán and colleagues reported that 6-8-week-old p62-deficient mice manifested impaired osteoclastogenesis and increased bone volume in response to parathyroid hormone-related protein (PTHrP, which is a calciotropic hormone and stimulates osteoclastogenesis), however, statistical analysis data supporting this claim were not provided[563]. In contrast, Zach and colleagues argue that p62 acts as a negative regulator of osteoclastogenesis[357].

In order to understand how the deletion of p62 alters the bone phenotype in ageing, I first assessed the femurs of 6, 9-11 and 18-month-old WT and *p62*$^{-/-}$, male and female mice. I showed that p62 deficiency was associated with reduced age-related bone loss and with less microarchitectural deterioration of bone in both male and female mice, as compared to the WT **(Figure 5.3 - 5.6)**. These µCT data are supported by the results obtained in histomorphometric analysis in which the loss of p62 with ageing leads to lower bone resorption (**Figure 5.7 - 5.10**), and higher bone formation **(Figure 5.11 - 5.14)**. Although there was no significant difference in the bone volume of male *p62*$^{-/-}$ mice at 6 months of age in comparison to the WT, reduced OC surface and number was found **(Figure 5.3 and 5.4, 5.7 and 5.8)**. The dynamic histomorphometric analysis of bone formation in female *p62*$^{-/-}$ mice at all ages display no significant difference in all parameters **(Figure 5.13)**, however this could be explained by limited number of data points, thus reduced statistical power.

My findings contrast with the work of Agas *et al.*, which showed the inhibition of PTH-induced bone remodelling and impaired bone turnover due to p62 deletion[652]. They reported that the OC and osteoblast differentiation, as well as the activity of osteoblasts were reduced *in vivo*, indicating lower bone turnover caused by decreased *Runx2* protein synthesis in *p62*$^{-/-}$ mice compared to WT[652]. In addition, the osteogenic effects for PTH such as osteoblast proliferation, increase of RANKL and Runx2 synthesis, and ALP activity, were abolished in primary calvarial osteoblasts from *p62*$^{-/-}$ mice[652]. The discrepancies could be caused by different age of animals used and the location where the measurements of structural

parameters were taken. Agas *et al.* were using young animals (8-9-week-old), whereas I used mice between 6 and 18 months of age. Therefore, Agas's analysis reflects changes in rapidly growing young mice, whereas I focused on adult bone homeostasis and the effect of ageing. Interestingly, my findings of reduced OC parameters in 6-month-old male mice are in keeping with similar findings of Agas *et al.* in young mice[652].

While I was working on the morphometric analysis of *p62*$^{-/-}$ mice over the life course, surprisingly, we discovered pagetic-like lesions in 18-month-old male and female *p62*$^{-/-}$ mice **(Figure 5.15)**. Within these lesions, I found remarkably increased bone turnover as compared to the unaffected bone on histology **(Figure 5.16 and 5.17)**. These findings echoed the work of Zach *et al.* revealed that p62 deletion leads to a Paget's disease-like bone phenotype in mice reported in 2018, while I was working on my project[357]. However, they observed only small intra-cortical lesions, which they found on histology in two aged (21-month-old) mice. Apart from that, they also showed increased bone turnover by demonstrating dense trabecular network and enhanced TRAP activity via Haemotoxylin & Eosin (H&E), TRAP and Safranin O staining, in association with significantly increased level of C-telopeptide of type I collagen (CTX-1) and procollagen type I N propeptide (PINP) in the serum of 21-month-old female *p62*$^{-/-}$ mice[357]. Nevertheless, a proper histomorphometric analysis is absent in their paper.

Although Zach *et al.* found a trend for higher bone density in 15-month-old *p62*$^{-/-}$ mice accompanied with a significant increase in Tb.N and separation, the findings of increased BV/TV just fell below the statistical significance which may have been due to limited sample number (N=4). The findings in my study have shown that both male and female *p62*$^{-/-}$ mice with ageing have a significantly increased bone volume due to an increase in the Tb.N, therefore lower Tb.Pf and more 'plate-like' trabeculae, which are stronger than 'rod-like' trabeculae. Moreover, the report of Zach's research lacks histomorphometric quantification of OCs and dynamic histomorphometric analysis of bone formation. In my study, I have demonstrated that the protective effect of p62 deletion on age-related bone loss is partly due to lower bone resorption which already started at 6 months of age and continued over the life course, at least until 18 months of age. This observation is accompanied by higher bone formation in 18-month-old male *p62*$^{-/-}$ mice which must be contributing to the phenotype. No

significant difference was found in the bone formation of female *p62*$^{-/-}$ mice at 18 months of age, however this is likely due to limited sample numbers (N=4), as 3 female *p62*$^{-/-}$ mice had to be removed from the analysis because of the presence of pagetic-like lesions in the distal femurs.

As mentioned before, Zach and colleagues did observe the presence of small PDB-like intra-cortical osteolytic lesions in the distal diaphysis femurs of 21-month-old *p62*$^{-/-}$ mice (N=2) in TRAP-stained bone sections, however without any supportive histomorphometric or µCT analysis. In contrast, large pagetic-like osteolytic lesions in *p62*$^{-/-}$ mice, which seemed to be more severely affected than the *p62*^{P394L} mice, were observed in my study using µCT, accompanied by significantly increased N.Oc/TV and bone formation rate, indicating excessive bone turnover.

It is interesting to note that p62 deletion with ageing overall impairs osteoclastogenesis in unaffected bone, but osteoclastogenesis is increased within pagetic-like lesions. Aged WT OC precursors have an increased sensitivity towards RANKL and enhanced osteoclastogenesis *in vitro*[561]. This phenomenon is even more pronounced in POCs from the p62 mouse model of Paget's disease (*p62*^{P394L})[561]. In PDB, OCs are primarily affected, exhibiting morphological abnormalities and becoming hyperactive, causing a focal increase in osteoclastic bone resorption, which is the characteristic of the initial lesion in the disorder[653]. This in turn induces excessive bone formation by morphologically normal, but hyperactive osteoblasts, resulting in focally accelerated bone turnover[653]. Hiruma *et al.* reported that the P394L *SQSTM1/p62* mutation causes the osteoclastogenic potential of the bone microenvironment to be increased[562]. However, in order to assess if the OCs within the lesions in 18-month-old *p62*$^{-/-}$ mice appeared to be morphologically similar to the pagetic OCs, haematoxylin and eosin (H&E) staining is required, which due to time constraints, I have not been able to perform.

The pagetic-like lesions observed in this study seem to be at the mixed lytic/sclerotic phase in which intense bone remodelling takes place, supported by the observation of an increased number of OCs and significantly enhanced bone formation within the pagetic-like lesions. However, many lesions in the *p62*$^{-/-}$ mice exhibited exuberant bone formation (as compared to *p62*^{P394L}-lesions) on µCT. Hence, there is a possibility that some lesions in p62-deficient

aged mice may have transformed into osteosarcoma. Furthermore, tumor-suppressor miR-16 is a negative regulator of the p62 transcript[654]. miR-16 was observed to be downregulated in PDB but discovered to have an increased expression in PDB-associated osteosarcoma, compared to non-transformed pagetic bone lesions[655]. It has been proposed that miR-16-mediated silencing of *SQSTM1* disables the cell protection against oxidative stress-induced oncogenesis[655]. Therefore, cells with gradual loss of *SQSTM1* may be prone to developing cancer, including osteosarcoma. Thus, it is plausible that lack of p62 in the osteoblast lineage cells eventually may lead to development of osteosarcoma.

Based on the results of this study, together with the findings of Daroszewska and colleagues who showed that *p62^{P394L}* is associated with accelerated age-related bone loss[561], lead me to question the role of p62 in regulating osteoblasts with ageing. The results obtained in this study suggest that p62 negatively regulates osteoblastogenesis. In line with the work of Rodriguez and colleagues, the *p62$^{-/-}$* mice gained significantly more weight with ageing compared to the WT **(Figure 5.2)**[317]. As high-fat diet induced obesity in mice results in bone loss[649], the weight gain of *p62$^{-/-}$* does not explain the bone protective effect of deleting p62.

Taken together, my results indicate that the p62-deficient mice are protected from age-related bone loss through lower bone resorption and higher bone formation. However, these mice developed pagetic-like lesions characterised by excessive bone remodelling with increased numbers of OCs and increased osteoblastic activity. Nevertheless, whether the lesions only present in old age or already start to appear at an earlier age, such as 10-month-old *p62$^{-/-}$* mice is yet to be investigated. Furthermore, much of the p62-related studies, particularly on PDB, focused on OCs, whereas my findings indicate that the effect of p62 (or lack of it) on osteoblast differentiation ought to be researched as well. Indeed, it would be most interesting to elucidate the role of p62 in PDB-associated osteosarcoma, given the florid lesions in *p62$^{-/-}$*. In addition, further studies are also required to understand how p62 deletion affects autophagy, as the expression of autophagy-related genes was found to be increased in OC precursors from *p62^{P394L}* mice[253], and the interplay between p62 and p38 with ageing, considering my findings from Chapter 3.

Chapter 6: Summary and Discussion

Osteoporosis, which is the most common age-related metabolic bone disorder, is characterised by increased bone remodelling that favours osteoclastic bone resorption and unchanged or diminished osteoblastic bone formation. Such imbalance between bone resorption and formation results in decreased bone mass, especially in elderly women after menopause[572,656]. It has been suggested that the increase in osteoclastogenic potential of bone marrow cells and OC differentiation in ageing is the primary factor causing the reduced bone mass[443,572]. Several studies have reported similar observations in 12- and 24-month-old mice in which increased RANKL-induced OC formation and enhanced sensitivity to cytokines such as recombinant granulocyte-macrophage-colony stimulating factor (rGM-CSF) was observed in the aged mice[440,561,573]. However, little is known about the molecular mechanism underlying the cause of increased OC differentiation in ageing.

Here I have shown that p38 MAPK and p62 have a role in age-related increased osteoclastogenesis. Firstly, I have demonstrated enhanced p38 MAPK and (marginally) ERK phosphorylation in aged BMMs (isolated from 12-14-month-old mice) in a RANKL-specific manner, as compared to that of 3-4-month-old mice, suggesting p38 (and ERK) contribution to increased osteoclastogenesis in ageing upon RANKL-RANK interaction. This is supported by the work of Cong *et al.* which showed increased p38 MAPK activation in bone marrow monocytes isolated from 6-month-old mice compared to that of 2.5-month-old mice[197]. These results indicate that phosphorylation of p38 MAPK may begin to increase in 6-month-old mice. Moreover, an increase in p38 phosphorylation in aged mice and rats has been demonstrated in other tissues such as brain and kidneys[657,658]. Previous studies have reported that RANKL-induced activation of TAK1, and MKK3/6 leads to increased p38 phosphorylation[195]. On the other hand, p38 MAPK regulates feedback control of TAK1 which is vital for OC differentiation, by phosphorylating TAB1/2[195,231,659,660]. As my study has determined no differential MKK3/6 activation in BMMs differentiated from young and aged mice, TAK1 activation may be affected by the upregulated p38 phosphorylation due to the feedback regulation, which warrants further investigation.

Furthermore, elevation of P-p38 and P-ERK level was not observed in the later stages of cell differentiation (POCs and OCs) upon RANKL stimulation, showing increased phosphorylation only at the early stage of osteoclastogenesis. This observation is in accordance with the observation of Huang *et al.* and Li *et al.* which have shown p38 MAPK activation only in macrophages (an early phase of OC differentiation), but not in mature OCs[195,199]. Interestingly, I observed increased level of P-ERK in POCs differentiated from aged mice when treated with LPS. However, in this project I primarily focused on RANKL-RANK signalling pathway, thus LPS-TLR4 signalling pathway was not further explored.

As enhanced p38 MAPK activation was observed in aged BMMs, this led me to question the cause of increased phosphorylation in ageing. DUSP regulates MAPK activities in terms of spatiotemporal profiles, duration and magnitude by dephosphorylating and inactivating the signalling molecules[661]. By analysing the data obtained from next-generation RNA sequencing, I found that the expression of *Dusp 1, 3, 4* and *9* did not change in BMMs with ageing. However, I found upregulation of *Dusp 1, 3, 4* and *9* expression in POCs differentiated from aged mice, which could in part explain the inactivation of p38 MAPK and ERK in the later stages of cell differentiation.

Moreover, on next-generation RNA sequencing the expression of *Nfkb1/2, Plekhm1, Mmp9, Atp6v0d2,* and *Acp5* which are the genes that are highly expressed during OC differentiation was found to be increased in POCs differentiated from aged mice. Furthermore, increased expression of autophagy-related genes such as *LC3b, p38IP, Atg9a, Sqstm1, Atg5, Atg12, Atg4B* and *Atg7* was observed in POCs differentiated from aged mice as well. These pilot data suggest that the autophagy proteins may play non-autophagic role and contribute to enhanced osteoclastogenesis in ageing. In fact, DeSelm *et al.* has reported the involvement of autophagy-related proteins in fusion of secretory lysosomes with the RB, OC maturation and osteoclastic resorption acitivty[36]. Furthermore, DeSelm *et al.* showed that the deletion of Atg5, Atg7 and/or Atg4B in OCs inhibits targeting of LC3 and secretory lysosomes to the RB[36]. This could possibly affect the secretion of lysosomal enzymes such as cathepsin K, thereby dampening bone resorption. Nevertheless, above data generated by NGS have yet to be verified by using qPCR, except for *Atp6v0d2* which has been verified by qPCR. Validating NGS data with qPCR is important because NGS allows researchers to analyse a large number of

genes and provides a broad picture of the results, in contrast qPCR is a more specific, sensitive and targeted method that gives the exact copy number of individual mRNAs, as well as a gold standard method to confirm an observation.

The expression of *Atp6v0d2* was increased in BMMs, POCs and mature OCs differentiated from aged mice. Atp6v0d2 and dendritic cell-specific transmembrane protein (DC-STAMP) are key fusion-mediating molecules which are induced by NFATc1, the master regulator of RANKL-induced OC differentiation[88,544,662]. It has been reported that the deletion of *Atp6v0d2* or *DC-STAMP* results in increased bone mass, leading to the development of osteopetrosis, due to impaired OC fusion[544,663]. Moreover, knockdown of *Atp6v0d2* that localised at the RB impairs extracellular acidification of OCs, therefore decreased bone resorption, showing its role as an OC-specific proton pump[664]. Taken together, it could be speculated that enhanced p38 MAPK phosphorylation leads to an increase in NFTAc1 activation, followed by the upregulation in *Atp6v0d2* expression.

However, the detection of NFATc1 expression in BMMs from yound and aged mice, by using western blotting was very poor due to its low expression at early stage of OC differentiation. Therefore, I performed immunofluorescence staining, which revealed that the NFATc1 expression level increased across different stages of osteoclastogenesis in response to the RANKL stimulation, as well as its nuclear translocation, which echoed the findings of Takayanagi *et al.*[84]. Furthermore, NFATc1 displayed a trend for increased expression in pre-OCs differentiated from aged mice compared with that of young. Unfortunately, this result was obtained from only one mouse and replicates are required. I also attempted immunofluorescence staining for Atp6v0d2 localisation, which however was inconclusive due to the limited selection of fluorophores available.

In addition to the findings reported by DeSelm *et al.*, which demonstrated non-autophagic roles of autophagy proteins in OC maturation and function, increasing evidence points to the involvement of autophagy in maintaining bone remodeling. Indeed, its dysregulation is associated with the development of bone disorders such as osteoporosis and PDB[36,253,358,359,665,666]. As overall autophagy in cells decreases with ageing, however more experiments would be required to answer this question.

p38 MAPK has been established to be involved in the regulation of autophagy as well, especially by interacting with Atg9 and its novel binding partner, p38IP[354,667-669]. Whether the regulation is positive or negative, depends on the cell type and stimulus specificity[670]. In human bone osteosarcoma epithelial cells (U2OS line), prolonged p38 MAPK activation induces autophagy by phosphorylating ULK1 kinase, resulting in a protective effect on cancer cells against chemotherapy-induced apoptosis[667]. In contrast, Webber *et al.* showed that P-p38 MAPK inhibits autophagy by interacting with p38IP, constraining p38IP from binding to Atg9 which the interaction is required for autophagy[354,601,670]. Based on the findings obtained in my study, it is possible that increased p38 MAPK phosphorylation in ageing results in the inhibition of autophagy, which in turns reduces antioxidant effects and increases oxidative stress, and thus increased osteoclastogenesis, followed by age-related bone loss. However, enhanced ROS production leads to p38 MAPK activation, as it has previously been reported, indicating the dynamic activation of p38 MAPK[671-673]. Hence, the questions revolving around the signalling pathway upstream of p38 MAPK, p38IP and Atg9 are yet to be solved.

Moreover, I have shown increased lipidated-LC3 (LC3-II) levels in POCs differentiated from aged mice upon Bafilomycin B_1 treatment, which blocks autophagy by inhibiting V-ATPase-mediated autophagosome-lysosome fusion and autolysosome acidification. Chung *et al.* demonstrated that the inflammatory cytokine, interleukin-1 beta (IL-1β) increases the level of LC3-II in secretory lysosomes which secrete CtsK in OC precursors. Moreover, IL-1 synergistically with RANKL activates ERK in a calcium-dependent manner[225]. In addition, LPS is known to activate IL-1β in immune cells[674-676]. Interestingly, I observed enhanced ERK phosphorylation after stimulating with LPS in POCs differentiated from aged mice in my study. It is tempting to speculate that the secretion of CtsK in aged OC precursors is increased, presumably mediated by LC3-II due to enhanced ERK phosphorylation under such mechanism. In support of this notion, $Atg4B^{C74A}$, a dominant negative mutant of Atg4B in which the lipidation of LC3 paralogues is inhibited, impairs LC3 targeting to the RB and disrupts localisation of CtsK within the actin ring, hence, reduced bone pit excavation[36]. Furthermore, LC3 knockdown affects actin ring formation, CtsK release and bone resorption activity of OCs[359]. However, on the basis of my results, I cannot conclude whether the increased level of

LC3-II in POCs with ageing reflects increased secretory lysosomal activity, which is likely or increased autophagy. The latter is less likely.

Of note, the scaffold protein p62 plays an important role in autophagy, and posseses the domains for interaction with p38 and LC3. P62 mutations that cluster around or within the UBA domain are associated with PDB, which is the second most common age-related metabolic bone disorder[530,531]. As mentioned before, the most common mutation of p62 associated with PDB is a C→T transversion at position 1215 in *SQSTM1/p62* exon 8 which causes a proline to leucine substitution at residue 392 (P392L) mutation[77,530,531]. PDB is characterised by focally disorganised and excessive bone turnover with OC precursors that are hyper-responsive to osteoclastogenic factors, resulting in the formation of woven bone[560].

In my study, I have characterised the long bones of young adult (6-month-old) and aged (9-11 and 18-month-old) *p62*$^{-/-}$, *p62*^{P394L} and WT mice, and have shown that p62 deletion has a protective effect on age-related bone loss in mice. The *p62*$^{-/-}$ mice exhibited increased bone volume and Tb.N, better connected trabecular lattices, and more 'plate-like' trabeculae, showing reduced age-related bone loss and with less microarchitectural deterioration of bone in both male and female mice, as compared to the WT. This bone phenotype is associated with lower bone resorption and higher bone formation.

P62 has previously been reported to play an important role in RANKL-induced osteoclastogenesis and bone remodeling[358,563]. As anticipated, the loss of p62 displayed a high bone volume phenotype, which correlates with the findings of Li *et al.* and Duran *et al.* that showed inhibition of osteoclastogenesis in RAW264.7 cells with p62 knocked down, and in p62 knockout mice, respectively[358,563]. In contrast, Zach *et al.* demonstrated enhanced osteoclastogenesis in p62-deficient cells, claiming p62 to be a negative regulator of OC differentiation[357]. Furthermore, Zach *et al.* also reported the presence of small PDB-like intra-cortical osteolytic lesions in the distal diaphysis femurs of 21-month-old *p62*$^{-/-}$ mice (N=2) in TRAP-stained bone sections, however without any supportive histomorphometric or µCT analysis. Their findings are echoed by the observations in my study, in which Pagetic-like lesions were observed on µCT in some of the 18-month-old *p62*$^{-/-}$ animals, while investigating the effect of p62 deletion on bone morphometry and histomorphometry in ageing.

Surprisingly, aged *p62*$^{-/-}$ mice developed mixed osteolytic and osteosclerotic lesions that are much more severe and prevalent than that of *p62*^{P394L} and within the lesions excessive bone remodelling is evident in keeping with a PDB-like phenotype. Thus, the *p62*$^{-/-}$ mouse may be of value in further studies into the role of p62 in PDB, and as such adds to the established *p62*^{P394L} mouse model of PDB.

Taken together, my results have shown that p38 MAPK and p62 play an important role in contributing to age-related osteoclastogenesis. Increased p38 MAPK phosphorylation induced by RANKL enhances *Atp6v0d2* which explains at least to a degree to increased osteoclastogenesis in ageing. Also, p62 deletion has a protective effect on age-related bone loss, resulting in a relatively high bone volume phenotype. However, the underlying reason that causes the increase in p38 MAPK phosphorylation warrants further studies. Moreover, the reason for the upregulation of autophagic genes in aged POCs is yet to be determined. Furthermore, the detailed characterisation of lesions found in aged *p62*$^{-/-}$ mice is required to have a better understanding of the nature of these lesions. Based on the findings of my study, p38 MAPK and p62 may be potential therapeutic targets for treatment of osteoporosis, however further studies of the *p62*$^{-/-}$ are critical before silencing of p62 could be attempted therapeutically for safety reasons.

References

1 Clarke, B. Normal bone anatomy and physiology. *Clin J Am Soc Nephrol* **3 Suppl 3**, S131-139, doi:10.2215/CJN.04151206 (2008).

2 Ng, K. W., Romas, E., Donnan, L. & Findlay, D. M. Bone biology. *Baillieres Clin Endocrinol Metab* **11**, 1-22, doi:10.1016/s0950-351x(97)80473-9 (1997).

3 Romaniuk, A. *et al.* Structural features of bone marrow. *Interv Med Appl Sci* **8**, 121-126, doi:10.1556/1646.8.2016.3.3 (2016).

4 Travlos, G. S. Normal structure, function, and histology of the bone marrow. *Toxicol Pathol* **34**, 548-565, doi:10.1080/01926230600939856 (2006).

5 Nahian, A. & Chauhan, P. R. in *StatPearls* (2020).

6 Spiesz, E. M., Kaminsky, W. & Zysset, P. K. A quantitative collagen fibers orientation assessment using birefringence measurements: calibration and application to human osteons. *J Struct Biol* **176**, 302-306, doi:10.1016/j.jsb.2011.09.009 (2011).

7 Lai, X. *et al.* The dependences of osteocyte network on bone compartment, age, and disease. *Bone Res* **3**, doi:10.1038/boneres.2015.9 (2015).

8 Shapiro, F. & Wu, J. Y. Woven bone overview: structural classification based on its integral role in developmental, repair and pathological bone formation throughout vertebrate groups. *Eur Cell Mater* **38**, 137-167, doi:10.22203/eCM.v038a11 (2019).

9 Florencio-Silva, R., Sasso, G. R., Sasso-Cerri, E., Simoes, M. J. & Cerri, P. S. Biology of Bone Tissue: Structure, Function, and Factors That Influence Bone Cells. *Biomed Res Int* **2015**, 421746, doi:10.1155/2015/421746 (2015).

10 Boskey, A. L. & Coleman, R. Aging and bone. *J Dent Res* **89**, 1333-1348, doi:10.1177/0022034510377791 (2010).

11 doblaré, M., García, J. M. & Gomez-Benito, M. J. Modelling bone tissue fracture and healing: A review. *Engineering Fracture Mechanics* **71**, 1809-1840, doi:10.1016/j.engfracmech.2003.08.003 (2004).

12 Jilka, R. L. The relevance of mouse models for investigating age-related bone loss in humans. *J Gerontol A Biol Sci Med Sci* **68**, 1209-1217, doi:10.1093/gerona/glt046 (2013).

13 Raggatt, L. J. & Partridge, N. C. Cellular and molecular mechanisms of bone remodeling. *J Biol Chem* **285**, 25103-25108, doi:10.1074/jbc.R109.041087 (2010).

14 Frost, H. M. Skeletal structural adaptations to mechanical usage (SATMU): 4. Mechanical influences on intact fibrous tissues. *Anat Rec* **226**, 433-439, doi:10.1002/ar.1092260405 (1990).

15 Kular, J., Tickner, J., Chim, S. M. & Xu, J. An overview of the regulation of bone remodelling at the cellular level. *Clin Biochem* **45**, 863-873, doi:10.1016/j.clinbiochem.2012.03.021 (2012).

16 Kenkre, J. S. & Bassett, J. The bone remodelling cycle. *Ann Clin Biochem* **55**, 308-327, doi:10.1177/0004563218759371 (2018).

17 Nesbitt, S. A. & Horton, M. A. Trafficking of matrix collagens through bone-resorbing osteoclasts. *Science* **276**, 266-269, doi:10.1126/science.276.5310.266 (1997).

18 Salo, J., Lehenkari, P., Mulari, M., Metsikko, K. & Vaananen, H. K. Removal of osteoclast bone resorption products by transcytosis. *Science* **276**, 270-273, doi:10.1126/science.276.5310.270 (1997).

19 Sims, N. A. & Martin, T. J. Coupling the activities of bone formation and resorption: a multitude of signals within the basic multicellular unit. *Bonekey Rep* **3**, 481, doi:10.1038/bonekey.2013.215 (2014).
20 Eriksen, E. F., Melsen, F. & Mosekilde, L. Reconstruction of the resorptive site in iliac trabecular bone: a kinetic model for bone resorption in 20 normal individuals. *Metab Bone Dis Relat Res* **5**, 235-242, doi:10.1016/0221-8747(84)90065-1 (1984).
21 Eriksen, E. F., Gundersen, H. J., Melsen, F. & Mosekilde, L. Reconstruction of the formative site in iliac trabecular bone in 20 normal individuals employing a kinetic model for matrix and mineral apposition. *Metab Bone Dis Relat Res* **5**, 243-252, doi:10.1016/0221-8747(84)90066-3 (1984).
22 Manolagas, S. C. Birth and death of bone cells: basic regulatory mechanisms and implications for the pathogenesis and treatment of osteoporosis. *Endocr Rev* **21**, 115-137, doi:10.1210/edrv.21.2.0395 (2000).
23 Bilgiç, E., Boyacıoğlu, Ö., Gizer, M., Korkusuz, P. & Korkusuz, F. in *Comparative Kinesiology of the Human Body* (eds Salih Angin & Ibrahim Engin Şimşek) 71-90 (Academic Press, 2020).
24 Matsuo, K. Cross-talk among bone cells. *Curr Opin Nephrol Hypertens* **18**, 292-297, doi:10.1097/MNH.0b013e32832b75f1 (2009).
25 Crockett, J. C., Rogers, M. J., Coxon, F. P., Hocking, L. J. & Helfrich, M. H. Bone remodelling at a glance. *J Cell Sci* **124**, 991-998, doi:10.1242/jcs.063032 (2011).
26 Teitelbaum, S. L. Bone resorption by osteoclasts. *Science* **289**, 1504-1508, doi:10.1126/science.289.5484.1504 (2000).
27 Roodman, G. D. Advances in bone biology: the osteoclast. *Endocr Rev* **17**, 308-332, doi:10.1210/edrv-17-4-308 (1996).
28 Kanehisa, J. & Heersche, J. N. Osteoclastic bone resorption: in vitro analysis of the rate of resorption and migration of individual osteoclasts. *Bone* **9**, 73-79, doi:10.1016/8756-3282(88)90106-8 (1988).
29 Arkett, S. A., Dixon, S. J. & Sims, S. M. Substrate influences rat osteoclast morphology and expression of potassium conductances. *J Physiol* **458**, 633-653, doi:10.1113/jphysiol.1992.sp019438 (1992).
30 Hirvonen, M. J., Fagerlund, K., Lakkakorpi, P., Vaananen, H. K. & Mulari, M. T. Novel perspectives on the transcytotic route in osteoclasts. *Bonekey Rep* **2**, 306, doi:10.1038/bonekey.2013.40 (2013).
31 Mulari, M., Vaaraniemi, J. & Vaananen, H. K. Intracellular membrane trafficking in bone resorbing osteoclasts. *Microsc Res Tech* **61**, 496-503, doi:10.1002/jemt.10371 (2003).
32 Saltel, F., Chabadel, A., Bonnelye, E. & Jurdic, P. Actin cytoskeletal organisation in osteoclasts: a model to decipher transmigration and matrix degradation. *Eur J Cell Biol* **87**, 459-468, doi:10.1016/j.ejcb.2008.01.001 (2008).
33 Schachtner, H., Calaminus, S. D., Thomas, S. G. & Machesky, L. M. Podosomes in adhesion, migration, mechanosensing and matrix remodeling. *Cytoskeleton (Hoboken)* **70**, 572-589, doi:10.1002/cm.21119 (2013).
34 Faccio, R. *et al.* Localization and possible role of two different alpha v beta 3 integrin conformations in resting and resorbing osteoclasts. *J Cell Sci* **115**, 2919-2929 (2002).

35 Baron, R. *et al.* Polarized secretion of lysosomal enzymes: co-distribution of cation-independent mannose-6-phosphate receptors and lysosomal enzymes along the osteoclast exocytic pathway. *J Cell Biol* **106**, 1863-1872, doi:10.1083/jcb.106.6.1863 (1988).
36 DeSelm, C. J. *et al.* Autophagy proteins regulate the secretory component of osteoclastic bone resorption. *Dev Cell* **21**, 966-974, doi:10.1016/j.devcel.2011.08.016 (2011).
37 Riihonen, R. *et al.* Membrane-bound carbonic anhydrases in osteoclasts. *Bone* **40**, 1021-1031, doi:10.1016/j.bone.2006.11.028 (2007).
38 Stenbeck, G. & Horton, M. A. Endocytic trafficking in actively resorbing osteoclasts. *J Cell Sci* **117**, 827-836, doi:10.1242/jcs.00935 (2004).
39 Vaaraniemi, J. *et al.* Intracellular machinery for matrix degradation in bone-resorbing osteoclasts. *J Bone Miner Res* **19**, 1432-1440, doi:10.1359/JBMR.040603 (2004).
40 Faccio, R., Novack, D. V., Zallone, A., Ross, F. P. & Teitelbaum, S. L. Dynamic changes in the osteoclast cytoskeleton in response to growth factors and cell attachment are controlled by beta3 integrin. *J Cell Biol* **162**, 499-509, doi:10.1083/jcb.200212082 (2003).
41 Fuller, K. *et al.* Macrophage colony-stimulating factor stimulates survival and chemotactic behavior in isolated osteoclasts. *J Exp Med* **178**, 1733-1744, doi:10.1084/jem.178.5.1733 (1993).
42 Wiktor-Jedrzejczak, W. *et al.* Total absence of colony-stimulating factor 1 in the macrophage-deficient osteopetrotic (op/op) mouse. *Proc Natl Acad Sci U S A* **87**, 4828-4832, doi:10.1073/pnas.87.12.4828 (1990).
43 Kim, J. H. & Kim, N. Signaling Pathways in Osteoclast Differentiation. *Chonnam Med J* **52**, 12-17, doi:10.4068/cmj.2016.52.1.12 (2016).
44 Lee, A. W. & States, D. J. Both src-dependent and -independent mechanisms mediate phosphatidylinositol 3-kinase regulation of colony-stimulating factor 1-activated mitogen-activated protein kinases in myeloid progenitors. *Mol Cell Biol* **20**, 6779-6798, doi:10.1128/mcb.20.18.6779-6798.2000 (2000).
45 Xiong, Y. *et al.* A CSF-1 receptor phosphotyrosine 559 signaling pathway regulates receptor ubiquitination and tyrosine phosphorylation. *J Biol Chem* **286**, 952-960, doi:10.1074/jbc.M110.166702 (2011).
46 Bourette, R. P., Myles, G. M., Choi, J. L. & Rohrschneider, L. R. Sequential activation of phoshatidylinositol 3-kinase and phospholipase C-gamma2 by the M-CSF receptor is necessary for differentiation signaling. *EMBO J* **16**, 5880-5893, doi:10.1093/emboj/16.19.5880 (1997).
47 Mancini, A. *et al.* Identification of a second Grb2 binding site in the v-Fms tyrosine kinase. *Oncogene* **15**, 1565-1572, doi:10.1038/sj.onc.1201518 (1997).
48 Tondravi, M. M. *et al.* Osteopetrosis in mice lacking haematopoietic transcription factor PU.1. *Nature* **386**, 81-84, doi:10.1038/386081a0 (1997).
49 Grigoriadis, A. E. *et al.* c-Fos: a key regulator of osteoclast-macrophage lineage determination and bone remodeling. *Science* **266**, 443-448, doi:10.1126/science.7939685 (1994).
50 Kim, J. H. & Kim, N. Regulation of NFATc1 in Osteoclast Differentiation. *J Bone Metab* **21**, 233-241, doi:10.11005/jbm.2014.21.4.233 (2014).

51 Matsumoto, M. *et al.* Essential role of p38 mitogen-activated protein kinase in cathepsin K gene expression during osteoclastogenesis through association of NFATc1 and PU.1. *J Biol Chem* **279**, 45969-45979, doi:10.1074/jbc.M408795200 (2004).
52 Suda, T. *et al.* Modulation of osteoclast differentiation and function by the new members of the tumor necrosis factor receptor and ligand families. *Endocr Rev* **20**, 345-357, doi:10.1210/edrv.20.3.0367 (1999).
53 Lacey, D. L. *et al.* Osteoprotegerin ligand is a cytokine that regulates osteoclast differentiation and activation. *Cell* **93**, 165-176, doi:10.1016/s0092-8674(00)81569-x (1998).
54 Lum, L. *et al.* Evidence for a role of a tumor necrosis factor-alpha (TNF-alpha)-converting enzyme-like protease in shedding of TRANCE, a TNF family member involved in osteoclastogenesis and dendritic cell survival. *J Biol Chem* **274**, 13613-13618, doi:10.1074/jbc.274.19.13613 (1999).
55 Wong, B. R. *et al.* TRANCE, a TNF family member, activates Akt/PKB through a signaling complex involving TRAF6 and c-Src. *Mol Cell* **4**, 1041-1049, doi:10.1016/s1097-2765(00)80232-4 (1999).
56 Wong, B. R. *et al.* The TRAF family of signal transducers mediates NF-kappaB activation by the TRANCE receptor. *J Biol Chem* **273**, 28355-28359, doi:10.1074/jbc.273.43.28355 (1998).
57 Ye, H. *et al.* Distinct molecular mechanism for initiating TRAF6 signalling. *Nature* **418**, 443-447, doi:10.1038/nature00888 (2002).
58 Moscat, J., Diaz-Meco, M. T. & Wooten, M. W. Signal integration and diversification through the p62 scaffold protein. *Trends Biochem Sci* **32**, 95-100, doi:10.1016/j.tibs.2006.12.002 (2007).
59 Besse, A. *et al.* TAK1-dependent signaling requires functional interaction with TAB2/TAB3. *J Biol Chem* **282**, 3918-3928, doi:10.1074/jbc.M608867200 (2007).
60 Kishida, S., Sanjo, H., Akira, S., Matsumoto, K. & Ninomiya-Tsuji, J. TAK1-binding protein 2 facilitates ubiquitination of TRAF6 and assembly of TRAF6 with IKK in the IL-1 signaling pathway. *Genes Cells* **10**, 447-454, doi:10.1111/j.1365-2443.2005.00852.x (2005).
61 Lallena, M. J., Diaz-Meco, M. T., Bren, G., Paya, C. V. & Moscat, J. Activation of IkappaB kinase beta by protein kinase C isoforms. *Mol Cell Biol* **19**, 2180-2188, doi:10.1128/mcb.19.3.2180 (1999).
62 Shi, J. H. & Sun, S. C. Tumor Necrosis Factor Receptor-Associated Factor Regulation of Nuclear Factor kappaB and Mitogen-Activated Protein Kinase Pathways. *Front Immunol* **9**, 1849, doi:10.3389/fimmu.2018.01849 (2018).
63 Huang, H. *et al.* Induction of c-Fos and NFATc1 during RANKL-stimulated osteoclast differentiation is mediated by the p38 signaling pathway. *Biochem Biophys Res Commun* **351**, 99-105, doi:10.1016/j.bbrc.2006.10.011 (2006).
64 Kobayashi, N. *et al.* Segregation of TRAF6-mediated signaling pathways clarifies its role in osteoclastogenesis. *EMBO J* **20**, 1271-1280, doi:10.1093/emboj/20.6.1271 (2001).
65 Vanhaesebroeck, B. & Alessi, D. R. The PI3K-PDK1 connection: more than just a road to PKB. *Biochem J* **346 Pt 3**, 561-576 (2000).

66 Moon, J. B. *et al.* Akt induces osteoclast differentiation through regulating the GSK3beta/NFATc1 signaling cascade. *J Immunol* **188**, 163-169, doi:10.4049/jimmunol.1101254 (2012).
67 Matsumoto, T. *et al.* Regulation of bone resorption and sealing zone formation in osteoclasts occurs through protein kinase B-mediated microtubule stabilization. *J Bone Miner Res* **28**, 1191-1202, doi:10.1002/jbmr.1844 (2013).
68 Lamothe, B. *et al.* Site-specific Lys-63-linked tumor necrosis factor receptor-associated factor 6 auto-ubiquitination is a critical determinant of I kappa B kinase activation. *J Biol Chem* **282**, 4102-4112, doi:10.1074/jbc.M609503200 (2007).
69 Lamothe, B. *et al.* TRAF6 ubiquitin ligase is essential for RANKL signaling and osteoclast differentiation. *Biochem Biophys Res Commun* **359**, 1044-1049, doi:10.1016/j.bbrc.2007.06.017 (2007).
70 McManus, S. & Roux, S. The adaptor protein p62/SQSTM1 in osteoclast signaling pathways. *J Mol Signal* **7**, 1, doi:10.1186/1750-2187-7-1 (2012).
71 Jin, W. *et al.* Deubiquitinating enzyme CYLD negatively regulates RANK signaling and osteoclastogenesis in mice. *J Clin Invest* **118**, 1858-1866, doi:10.1172/JCI34257 (2008).
72 Wooten, M. W. *et al.* Essential role of sequestosome 1/p62 in regulating accumulation of Lys63-ubiquitinated proteins. *J Biol Chem* **283**, 6783-6789, doi:10.1074/jbc.M709496200 (2008).
73 Hutti, J. E. *et al.* Phosphorylation of the tumor suppressor CYLD by the breast cancer oncogene IKKepsilon promotes cell transformation. *Mol Cell* **34**, 461-472, doi:10.1016/j.molcel.2009.04.031 (2009).
74 Reiley, W., Zhang, M., Wu, X., Granger, E. & Sun, S. C. Regulation of the deubiquitinating enzyme CYLD by IkappaB kinase gamma-dependent phosphorylation. *Mol Cell Biol* **25**, 3886-3895, doi:10.1128/MCB.25.10.3886-3895.2005 (2005).
75 Brummelkamp, T. R., Nijman, S. M., Dirac, A. M. & Bernards, R. Loss of the cylindromatosis tumour suppressor inhibits apoptosis by activating NF-kappaB. *Nature* **424**, 797-801, doi:10.1038/nature01811 (2003).
76 Kovalenko, A. *et al.* The tumour suppressor CYLD negatively regulates NF-kappaB signalling by deubiquitination. *Nature* **424**, 801-805, doi:10.1038/nature01802 (2003).
77 Rea, S. L., Walsh, J. P., Layfield, R., Ratajczak, T. & Xu, J. New insights into the role of sequestosome 1/p62 mutant proteins in the pathogenesis of Paget's disease of bone. *Endocr Rev* **34**, 501-524, doi:10.1210/er.2012-1034 (2013).
78 Simonet, W. S. *et al.* Osteoprotegerin: a novel secreted protein involved in the regulation of bone density. *Cell* **89**, 309-319, doi:10.1016/s0092-8674(00)80209-3 (1997).
79 Matsuo, K. & Irie, N. Osteoclast-osteoblast communication. *Arch Biochem Biophys* **473**, 201-209, doi:10.1016/j.abb.2008.03.027 (2008).
80 Glass, D. A., 2nd *et al.* Canonical Wnt signaling in differentiated osteoblasts controls osteoclast differentiation. *Dev Cell* **8**, 751-764, doi:10.1016/j.devcel.2005.02.017 (2005).
81 Holmen, S. L. *et al.* Essential role of beta-catenin in postnatal bone acquisition. *J Biol Chem* **280**, 21162-21168, doi:10.1074/jbc.M501900200 (2005).
82 Kieslinger, M. *et al.* EBF2 regulates osteoblast-dependent differentiation of osteoclasts. *Dev Cell* **9**, 757-767, doi:10.1016/j.devcel.2005.10.009 (2005).

83 Bucay, N. *et al.* osteoprotegerin-deficient mice develop early onset osteoporosis and arterial calcification. *Genes Dev* **12**, 1260-1268, doi:10.1101/gad.12.9.1260 (1998).
84 Takayanagi, H. *et al.* Induction and activation of the transcription factor NFATc1 (NFAT2) integrate RANKL signaling in terminal differentiation of osteoclasts. *Dev Cell* **3**, 889-901, doi:10.1016/s1534-5807(02)00369-6 (2002).
85 Koga, T. *et al.* Costimulatory signals mediated by the ITAM motif cooperate with RANKL for bone homeostasis. *Nature* **428**, 758-763, doi:10.1038/nature02444 (2004).
86 Humphrey, M. B., Lanier, L. L. & Nakamura, M. C. Role of ITAM-containing adapter proteins and their receptors in the immune system and bone. *Immunol Rev* **208**, 50-65, doi:10.1111/j.0105-2896.2005.00325.x (2005).
87 Shinohara, M. *et al.* Tyrosine kinases Btk and Tec regulate osteoclast differentiation by linking RANK and ITAM signals. *Cell* **132**, 794-806, doi:10.1016/j.cell.2007.12.037 (2008).
88 Kim, K., Lee, S. H., Ha Kim, J., Choi, Y. & Kim, N. NFATc1 induces osteoclast fusion via up-regulation of Atp6v0d2 and the dendritic cell-specific transmembrane protein (DC-STAMP). *Mol Endocrinol* **22**, 176-185, doi:10.1210/me.2007-0237 (2008).
89 Yagi, M. *et al.* Induction of DC-STAMP by alternative activation and downstream signaling mechanisms. *J Bone Miner Res* **22**, 992-1001, doi:10.1359/jbmr.070401 (2007).
90 Vaananen, H. K. *et al.* Evidence for the presence of a proton pump of the vacuolar H(+)-ATPase type in the ruffled borders of osteoclasts. *J Cell Biol* **111**, 1305-1311, doi:10.1083/jcb.111.3.1305 (1990).
91 Georgess, D., Machuca-Gayet, I., Blangy, A. & Jurdic, P. Podosome organization drives osteoclast-mediated bone resorption. *Cell Adh Migr* **8**, 191-204, doi:10.4161/cam.27840 (2014).
92 Luxenburg, C. *et al.* The architecture of the adhesive apparatus of cultured osteoclasts: from podosome formation to sealing zone assembly. *PLoS One* **2**, e179, doi:10.1371/journal.pone.0000179 (2007).
93 Silver, I. A., Murrills, R. J. & Etherington, D. J. Microelectrode studies on the acid microenvironment beneath adherent macrophages and osteoclasts. *Exp Cell Res* **175**, 266-276, doi:10.1016/0014-4827(88)90191-7 (1988).
94 Teti, A. *et al.* Cytoplasmic pH regulation and chloride/bicarbonate exchange in avian osteoclasts. *J Clin Invest* **83**, 227-233, doi:10.1172/JCI113863 (1989).
95 Supanchart, C. & Kornak, U. Ion channels and transporters in osteoclasts. *Arch Biochem Biophys* **473**, 161-165, doi:10.1016/j.abb.2008.03.029 (2008).
96 Baron, R. Polarity and membrane transport in osteoclasts. *Connect Tissue Res* **20**, 109-120, doi:10.3109/03008208909023879 (1989).
97 Nielsen, R. H., Karsdal, M. A., Sorensen, M. G., Dziegiel, M. H. & Henriksen, K. Dissolution of the inorganic phase of bone leading to release of calcium regulates osteoclast survival. *Biochem Biophys Res Commun* **360**, 834-839, doi:10.1016/j.bbrc.2007.06.145 (2007).
98 Arnett, T. R. Extracellular pH regulates bone cell function. *J Nutr* **138**, 415S-418S, doi:10.1093/jn/138.2.415S (2008).

99 Blair, H. C., Kahn, A. J., Crouch, E. C., Jeffrey, J. J. & Teitelbaum, S. L. Isolated osteoclasts resorb the organic and inorganic components of bone. *J Cell Biol* **102**, 1164-1172, doi:10.1083/jcb.102.4.1164 (1986).
100 Van Wesenbeeck, L. *et al.* Involvement of PLEKHM1 in osteoclastic vesicular transport and osteopetrosis in incisors absent rats and humans. *J Clin Invest* **117**, 919-930, doi:10.1172/JCI30328 (2007).
101 Del Fattore, A. *et al.* A new heterozygous mutation (R714C) of the osteopetrosis gene, pleckstrin homolog domain containing family M (with run domain) member 1 (PLEKHM1), impairs vesicular acidification and increases TRACP secretion in osteoclasts. *J Bone Miner Res* **23**, 380-391, doi:10.1359/jbmr.071107 (2008).
102 Zaidi, M., Troen, B., Moonga, B. S. & Abe, E. Cathepsin K, osteoclastic resorption, and osteoporosis therapy. *J Bone Miner Res* **16**, 1747-1749, doi:10.1359/jbmr.2001.16.10.1747 (2001).
103 Aubin, J. E. & Turksen, K. Monoclonal antibodies as tools for studying the osteoblast lineage. *Microsc Res Tech* **33**, 128-140, doi:10.1002/(SICI)1097-0029(19960201)33:2<128::AID-JEMT4>3.0.CO;2-P (1996).
104 Breeland, G., Sinkler, M. A. & Menezes, R. G. *Embryology, Bone Ossification*. (StatPearls Publishing, Treasure Island (FL), 2020).
105 Hatori, M., Klatte, K. J., Teixeira, C. C. & Shapiro, I. M. End labeling studies of fragmented DNA in the avian growth plate: evidence of apoptosis in terminally differentiated chondrocytes. *J Bone Miner Res* **10**, 1960-1968, doi:10.1002/jbmr.5650101216 (1995).
106 Bruder, S. P. & Caplan, A. I. Cellular and molecular events during embryonic bone development. *Connect Tissue Res* **20**, 65-71, doi:10.3109/03008208909023875 (1989).
107 He, X., Semenov, M., Tamai, K. & Zeng, X. LDL receptor-related proteins 5 and 6 in Wnt/beta-catenin signaling: arrows point the way. *Development* **131**, 1663-1677, doi:10.1242/dev.01117 (2004).
108 Schulte, G. & Bryja, V. The Frizzled family of unconventional G-protein-coupled receptors. *Trends Pharmacol Sci* **28**, 518-525, doi:10.1016/j.tips.2007.09.001 (2007).
109 Day, T. F., Guo, X., Garrett-Beal, L. & Yang, Y. Wnt/beta-catenin signaling in mesenchymal progenitors controls osteoblast and chondrocyte differentiation during vertebrate skeletogenesis. *Dev Cell* **8**, 739-750, doi:10.1016/j.devcel.2005.03.016 (2005).
110 Yamaguchi, T. P. Heads or tails: Wnts and anterior-posterior patterning. *Curr Biol* **11**, R713-724, doi:10.1016/s0960-9822(01)00417-1 (2001).
111 Komiya, Y. & Habas, R. Wnt signal transduction pathways. *Organogenesis* **4**, 68-75, doi:10.4161/org.4.2.5851 (2008).
112 Tamai, K. *et al.* LDL-receptor-related proteins in Wnt signal transduction. *Nature* **407**, 530-535, doi:10.1038/35035117 (2000).
113 Hay, E. *et al.* Interaction between LRP5 and Frat1 mediates the activation of the Wnt canonical pathway. *J Biol Chem* **280**, 13616-13623, doi:10.1074/jbc.M411999200 (2005).
114 Hatsell, S., Rowlands, T., Hiremath, M. & Cowin, P. Beta-catenin and Tcfs in mammary development and cancer. *J Mammary Gland Biol Neoplasia* **8**, 145-158, doi:10.1023/a:1025944723047 (2003).

115 Reya, T. & Clevers, H. Wnt signalling in stem cells and cancer. *Nature* **434**, 843-850, doi:10.1038/nature03319 (2005).
116 Harland, R. & Gerhart, J. Formation and function of Spemann's organizer. *Annu Rev Cell Dev Biol* **13**, 611-667, doi:10.1146/annurev.cellbio.13.1.611 (1997).
117 Cavallo, R. A. *et al.* Drosophila Tcf and Groucho interact to repress Wingless signalling activity. *Nature* **395**, 604-608, doi:10.1038/26982 (1998).
118 Roose, J. *et al.* The Xenopus Wnt effector XTcf-3 interacts with Groucho-related transcriptional repressors. *Nature* **395**, 608-612, doi:10.1038/26989 (1998).
119 Gaur, T. *et al.* Canonical WNT signaling promotes osteogenesis by directly stimulating Runx2 gene expression. *J Biol Chem* **280**, 33132-33140, doi:10.1074/jbc.M500608200 (2005).
120 Aberle, H., Bauer, A., Stappert, J., Kispert, A. & Kemler, R. beta-catenin is a target for the ubiquitin-proteasome pathway. *EMBO J* **16**, 3797-3804, doi:10.1093/emboj/16.13.3797 (1997).
121 Kitagawa, M. *et al.* An F-box protein, FWD1, mediates ubiquitin-dependent proteolysis of beta-catenin. *EMBO J* **18**, 2401-2410, doi:10.1093/emboj/18.9.2401 (1999).
122 Semenov, M., Tamai, K. & He, X. SOST is a ligand for LRP5/LRP6 and a Wnt signaling inhibitor. *J Biol Chem* **280**, 26770-26775, doi:10.1074/jbc.M504308200 (2005).
123 Glinka, A. *et al.* Dickkopf-1 is a member of a new family of secreted proteins and functions in head induction. *Nature* **391**, 357-362, doi:10.1038/34848 (1998).
124 Mao, B. *et al.* Kremen proteins are Dickkopf receptors that regulate Wnt/beta-catenin signalling. *Nature* **417**, 664-667, doi:10.1038/nature756 (2002).
125 Hoang, B. H. *et al.* Expression pattern of two Frizzled-related genes, Frzb-1 and Sfrp-1, during mouse embryogenesis suggests a role for modulating action of Wnt family members. *Dev Dyn* **212**, 364-372, doi:10.1002/(SICI)1097-0177(199807)212:3<364::AID-AJA4>3.0.CO;2-F (1998).
126 Hsieh, J. C. *et al.* A new secreted protein that binds to Wnt proteins and inhibits their activities. *Nature* **398**, 431-436, doi:10.1038/18899 (1999).
127 Kubota, T., Michigami, T. & Ozono, K. Wnt signaling in bone metabolism. *J Bone Miner Metab* **27**, 265-271, doi:10.1007/s00774-009-0064-8 (2009).
128 Westendorf, J. J., Kahler, R. A. & Schroeder, T. M. Wnt signaling in osteoblasts and bone diseases. *Gene* **341**, 19-39, doi:10.1016/j.gene.2004.06.044 (2004).
129 Duan, P. & Bonewald, L. F. The role of the wnt/beta-catenin signaling pathway in formation and maintenance of bone and teeth. *Int J Biochem Cell Biol* **77**, 23-29, doi:10.1016/j.biocel.2016.05.015 (2016).
130 Cadigan, K. M. & Peifer, M. Wnt signaling from development to disease: insights from model systems. *Cold Spring Harb Perspect Biol* **1**, a002881, doi:10.1101/cshperspect.a002881 (2009).
131 Veeman, M. T., Axelrod, J. D. & Moon, R. T. A second canon. Functions and mechanisms of beta-catenin-independent Wnt signaling. *Dev Cell* **5**, 367-377, doi:10.1016/s1534-5807(03)00266-1 (2003).
132 Canalis, E., Economides, A. N. & Gazzerro, E. Bone morphogenetic proteins, their antagonists, and the skeleton. *Endocr Rev* **24**, 218-235, doi:10.1210/er.2002-0023 (2003).

133 Urist, M. R. Bone: formation by autoinduction. *Science* **150**, 893-899, doi:10.1126/science.150.3698.893 (1965).
134 Wozney, J. M. *et al.* Novel regulators of bone formation: molecular clones and activities. *Science* **242**, 1528-1534, doi:10.1126/science.3201241 (1988).
135 Yamaguchi, A., Komori, T. & Suda, T. Regulation of osteoblast differentiation mediated by bone morphogenetic proteins, hedgehogs, and Cbfa1. *Endocr Rev* **21**, 393-411, doi:10.1210/edrv.21.4.0403 (2000).
136 Heldin, C. H., Miyazono, K. & ten Dijke, P. TGF-beta signalling from cell membrane to nucleus through SMAD proteins. *Nature* **390**, 465-471, doi:10.1038/37284 (1997).
137 Kawabata, M., Imamura, T. & Miyazono, K. Signal transduction by bone morphogenetic proteins. *Cytokine Growth Factor Rev* **9**, 49-61, doi:10.1016/s1359-6101(97)00036-1 (1998).
138 Liu, F., Ventura, F., Doody, J. & Massague, J. Human type II receptor for bone morphogenic proteins (BMPs): extension of the two-kinase receptor model to the BMPs. *Mol Cell Biol* **15**, 3479-3486, doi:10.1128/mcb.15.7.3479 (1995).
139 Nohno, T. *et al.* Identification of a human type II receptor for bone morphogenetic protein-4 that forms differential heteromeric complexes with bone morphogenetic protein type I receptors. *J Biol Chem* **270**, 22522-22526, doi:10.1074/jbc.270.38.22522 (1995).
140 Rosenzweig, B. L. *et al.* Cloning and characterization of a human type II receptor for bone morphogenetic proteins. *Proc Natl Acad Sci U S A* **92**, 7632-7636, doi:10.1073/pnas.92.17.7632 (1995).
141 Mace, P. D., Cutfield, J. F. & Cutfield, S. M. High resolution structures of the bone morphogenetic protein type II receptor in two crystal forms: implications for ligand binding. *Biochem Biophys Res Commun* **351**, 831-838, doi:10.1016/j.bbrc.2006.10.109 (2006).
142 Wu, M., Chen, G. & Li, Y. P. TGF-beta and BMP signaling in osteoblast, skeletal development, and bone formation, homeostasis and disease. *Bone Res* **4**, 16009, doi:10.1038/boneres.2016.9 (2016).
143 Hoodless, P. A. *et al.* MADR1, a MAD-related protein that functions in BMP2 signaling pathways. *Cell* **85**, 489-500, doi:10.1016/s0092-8674(00)81250-7 (1996).
144 Kretzschmar, M., Liu, F., Hata, A., Doody, J. & Massague, J. The TGF-beta family mediator Smad1 is phosphorylated directly and activated functionally by the BMP receptor kinase. *Genes Dev* **11**, 984-995, doi:10.1101/gad.11.8.984 (1997).
145 Liu, F. *et al.* A human Mad protein acting as a BMP-regulated transcriptional activator. *Nature* **381**, 620-623, doi:10.1038/381620a0 (1996).
146 Chen, G., Deng, C. & Li, Y. P. TGF-beta and BMP signaling in osteoblast differentiation and bone formation. *Int J Biol Sci* **8**, 272-288, doi:10.7150/ijbs.2929 (2012).
147 Afzal, F. *et al.* Smad function and intranuclear targeting share a Runx2 motif required for osteogenic lineage induction and BMP2 responsive transcription. *J Cell Physiol* **204**, 63-72, doi:10.1002/jcp.20258 (2005).
148 Franceschi, R. T. & Xiao, G. Regulation of the osteoblast-specific transcription factor, Runx2: responsiveness to multiple signal transduction pathways. *J Cell Biochem* **88**, 446-454, doi:10.1002/jcb.10369 (2003).

149 Lee, K. S., Hong, S. H. & Bae, S. C. Both the Smad and p38 MAPK pathways play a crucial role in Runx2 expression following induction by transforming growth factor-beta and bone morphogenetic protein. *Oncogene* **21**, 7156-7163, doi:10.1038/sj.onc.1205937 (2002).
150 Hata, A., Lagna, G., Massague, J. & Hemmati-Brivanlou, A. Smad6 inhibits BMP/Smad1 signaling by specifically competing with the Smad4 tumor suppressor. *Genes Dev* **12**, 186-197, doi:10.1101/gad.12.2.186 (1998).
151 Abe, E. *et al.* Essential requirement of BMPs-2/4 for both osteoblast and osteoclast formation in murine bone marrow cultures from adult mice: antagonism by noggin. *J Bone Miner Res* **15**, 663-673, doi:10.1359/jbmr.2000.15.4.663 (2000).
152 Gazzerro, E., Gangji, V. & Canalis, E. Bone morphogenetic proteins induce the expression of noggin, which limits their activity in cultured rat osteoblasts. *J Clin Invest* **102**, 2106-2114, doi:10.1172/JCI3459 (1998).
153 Wan, D. C. *et al.* Noggin suppression enhances in vitro osteogenesis and accelerates in vivo bone formation. *J Biol Chem* **282**, 26450-26459, doi:10.1074/jbc.M703282200 (2007).
154 Balemans, W. & Van Hul, W. Extracellular regulation of BMP signaling in vertebrates: a cocktail of modulators. *Dev Biol* **250**, 231-250 (2002).
155 Brunet, L. J., McMahon, J. A., McMahon, A. P. & Harland, R. M. Noggin, cartilage morphogenesis, and joint formation in the mammalian skeleton. *Science* **280**, 1455-1457, doi:10.1126/science.280.5368.1455 (1998).
156 McMahon, J. A. *et al.* Noggin-mediated antagonism of BMP signaling is required for growth and patterning of the neural tube and somite. *Genes Dev* **12**, 1438-1452, doi:10.1101/gad.12.10.1438 (1998).
157 Anderson, R. M., Lawrence, A. R., Stottmann, R. W., Bachiller, D. & Klingensmith, J. Chordin and noggin promote organizing centers of forebrain development in the mouse. *Development* **129**, 4975-4987 (2002).
158 Kamiya, N. *et al.* Wnt inhibitors Dkk1 and Sost are downstream targets of BMP signaling through the type IA receptor (BMPRIA) in osteoblasts. *J Bone Miner Res* **25**, 200-210, doi:10.1359/jbmr.090806 (2010).
159 Kamiya, N. *et al.* BMP signaling negatively regulates bone mass through sclerostin by inhibiting the canonical Wnt pathway. *Development* **135**, 3801-3811, doi:10.1242/dev.025825 (2008).
160 Salazar, V. S. *et al.* Postnatal ablation of osteoblast Smad4 enhances proliferative responses to canonical Wnt signaling through interactions with beta-catenin. *J Cell Sci* **126**, 5598-5609, doi:10.1242/jcs.132233 (2013).
161 Ueland, T. *et al.* Increased serum and bone matrix levels of transforming growth factor {beta}1 in patients with GH deficiency in response to GH treatment. *Eur J Endocrinol* **165**, 393-400, doi:10.1530/EJE-11-0442 (2011).
162 Yee, J. A., Yan, L., Dominguez, J. C., Allan, E. H. & Martin, T. J. Plasminogen-dependent activation of latent transforming growth factor beta (TGF beta) by growing cultures of osteoblast-like cells. *J Cell Physiol* **157**, 528-534, doi:10.1002/jcp.1041570312 (1993).
163 Oreffo, R. O., Mundy, G. R., Seyedin, S. M. & Bonewald, L. F. Activation of the bone-derived latent TGF beta complex by isolated osteoclasts. *Biochem Biophys Res Commun* **158**, 817-823, doi:10.1016/0006-291x(89)92795-2 (1989).

164 Crane, J. L. & Cao, X. Bone marrow mesenchymal stem cells and TGF-beta signaling in bone remodeling. *J Clin Invest* **124**, 466-472, doi:10.1172/JCI70050 (2014).
165 Pfeilschifter, J. & Mundy, G. R. Modulation of type beta transforming growth factor activity in bone cultures by osteotropic hormones. *Proc Natl Acad Sci U S A* **84**, 2024-2028, doi:10.1073/pnas.84.7.2024 (1987).
166 Dallas, S. L., Rosser, J. L., Mundy, G. R. & Bonewald, L. F. Proteolysis of latent transforming growth factor-beta (TGF-beta)-binding protein-1 by osteoclasts. A cellular mechanism for release of TGF-beta from bone matrix. *J Biol Chem* **277**, 21352-21360, doi:10.1074/jbc.M111663200 (2002).
167 Bonewald, L. F. & Dallas, S. L. Role of active and latent transforming growth factor beta in bone formation. *J Cell Biochem* **55**, 350-357, doi:10.1002/jcb.240550312 (1994).
168 Tang, Y. *et al.* TGF-beta1-induced migration of bone mesenchymal stem cells couples bone resorption with formation. *Nat Med* **15**, 757-765, doi:10.1038/nm.1979 (2009).
169 Noda, M. & Camilliere, J. J. In vivo stimulation of bone formation by transforming growth factor-beta. *Endocrinology* **124**, 2991-2994, doi:10.1210/endo-124-6-2991 (1989).
170 Carreira, A. C., Alves, G. G., Zambuzzi, W. F., Sogayar, M. C. & Granjeiro, J. M. Bone Morphogenetic Proteins: structure, biological function and therapeutic applications. *Arch Biochem Biophys* **561**, 64-73, doi:10.1016/j.abb.2014.07.011 (2014).
171 Ito, Y. & Miyazono, K. RUNX transcription factors as key targets of TGF-beta superfamily signaling. *Curr Opin Genet Dev* **13**, 43-47, doi:10.1016/s0959-437x(03)00007-8 (2003).
172 Miyazawa, K. & Miyazono, K. Regulation of TGF-beta Family Signaling by Inhibitory Smads. *Cold Spring Harb Perspect Biol* **9**, doi:10.1101/cshperspect.a022095 (2017).
173 Karst, M., Gorny, G., Galvin, R. J. & Oursler, M. J. Roles of stromal cell RANKL, OPG, and M-CSF expression in biphasic TGF-beta regulation of osteoclast differentiation. *J Cell Physiol* **200**, 99-106, doi:10.1002/jcp.20036 (2004).
174 Kim, S. I. *et al.* TGF-beta-activated kinase 1 and TAK1-binding protein 1 cooperate to mediate TGF-beta1-induced MKK3-p38 MAPK activation and stimulation of type I collagen. *Am J Physiol Renal Physiol* **292**, F1471-1478, doi:10.1152/ajprenal.00485.2006 (2007).
175 Zhou, S. TGF-beta regulates beta-catenin signaling and osteoblast differentiation in human mesenchymal stem cells. *J Cell Biochem* **112**, 1651-1660, doi:10.1002/jcb.23079 (2011).
176 Bonewald, L. F. The amazing osteocyte. *J Bone Miner Res* **26**, 229-238, doi:10.1002/jbmr.320 (2011).
177 Tanaka-Kamioka, K., Kamioka, H., Ris, H. & Lim, S. S. Osteocyte shape is dependent on actin filaments and osteocyte processes are unique actin-rich projections. *J Bone Miner Res* **13**, 1555-1568, doi:10.1359/jbmr.1998.13.10.1555 (1998).
178 Cowin, S. C., Moss-Salentijn, L. & Moss, M. L. Candidates for the mechanosensory system in bone. *J Biomech Eng* **113**, 191-197, doi:10.1115/1.2891234 (1991).
179 Tatsumi, S. *et al.* Targeted ablation of osteocytes induces osteoporosis with defective mechanotransduction. *Cell Metab* **5**, 464-475, doi:10.1016/j.cmet.2007.05.001 (2007).
180 Nakashima, T. *et al.* Evidence for osteocyte regulation of bone homeostasis through RANKL expression. *Nat Med* **17**, 1231-1234, doi:10.1038/nm.2452 (2011).

181 Seeman, E. & Delmas, P. D. Bone quality--the material and structural basis of bone strength and fragility. *N Engl J Med* **354**, 2250-2261, doi:10.1056/NEJMra053077 (2006).
182 Li, X. *et al.* Sclerostin binds to LRP5/6 and antagonizes canonical Wnt signaling. *J Biol Chem* **280**, 19883-19887, doi:10.1074/jbc.M413274200 (2005).
183 van Bezooijen, R. L. *et al.* Wnt but not BMP signaling is involved in the inhibitory action of sclerostin on BMP-stimulated bone formation. *J Bone Miner Res* **22**, 19-28, doi:10.1359/jbmr.061002 (2007).
184 Wijenayaka, A. R. *et al.* Sclerostin stimulates osteocyte support of osteoclast activity by a RANKL-dependent pathway. *PLoS One* **6**, e25900, doi:10.1371/journal.pone.0025900 (2011).
185 Tu, X. *et al.* Osteocytes mediate the anabolic actions of canonical Wnt/beta-catenin signaling in bone. *Proc Natl Acad Sci U S A* **112**, E478-486, doi:10.1073/pnas.1409857112 (2015).
186 Ota, K. *et al.* Sclerostin is expressed in osteoclasts from aged mice and reduces osteoclast-mediated stimulation of mineralization. *J Cell Biochem* **114**, 1901-1907, doi:10.1002/jcb.24537 (2013).
187 Lee, K., Seo, I., Choi, M. H. & Jeong, D. Roles of Mitogen-Activated Protein Kinases in Osteoclast Biology. *Int J Mol Sci* **19**, doi:10.3390/ijms19103004 (2018).
188 Lee, K. *et al.* Selective Regulation of MAPK Signaling Mediates RANKL-dependent Osteoclast Differentiation. *Int J Biol Sci* **12**, 235-245, doi:10.7150/ijbs.13814 (2016).
189 Teitelbaum, S. L. & Ross, F. P. Genetic regulation of osteoclast development and function. *Nat Rev Genet* **4**, 638-649, doi:10.1038/nrg1122 (2003).
190 Ikeda, F. *et al.* JNK/c-Jun signaling mediates an anti-apoptotic effect of RANKL in osteoclasts. *J Bone Miner Res* **23**, 907-914, doi:10.1359/jbmr.080211 (2008).
191 Bohm, C. *et al.* The alpha-isoform of p38 MAPK specifically regulates arthritic bone loss. *J Immunol* **183**, 5938-5947, doi:10.4049/jimmunol.0901026 (2009).
192 Kyriakis, J. M. & Avruch, J. Mammalian mitogen-activated protein kinase signal transduction pathways activated by stress and inflammation. *Physiol Rev* **81**, 807-869, doi:10.1152/physrev.2001.81.2.807 (2001).
193 Kondoh, K. & Nishida, E. Regulation of MAP kinases by MAP kinase phosphatases. *Biochim Biophys Acta* **1773**, 1227-1237, doi:10.1016/j.bbamcr.2006.12.002 (2007).
194 Boyle, D. L. *et al.* Differential roles of MAPK kinases MKK3 and MKK6 in osteoclastogenesis and bone loss. *PLoS One* **9**, e84818, doi:10.1371/journal.pone.0084818 (2014).
195 Huang, H. *et al.* Osteoclast differentiation requires TAK1 and MKK6 for NFATc1 induction and NF-kappaB transactivation by RANKL. *Cell Death Differ* **13**, 1879-1891, doi:10.1038/sj.cdd.4401882 (2006).
196 Matsumoto, M., Sudo, T., Saito, T., Osada, H. & Tsujimoto, M. Involvement of p38 mitogen-activated protein kinase signaling pathway in osteoclastogenesis mediated by receptor activator of NF-kappa B ligand (RANKL). *J Biol Chem* **275**, 31155-31161, doi:10.1074/jbc.M001229200 (2000).
197 Cong, Q. *et al.* p38alpha MAPK regulates proliferation and differentiation of osteoclast progenitors and bone remodeling in an aging-dependent manner. *Sci Rep* **7**, 45964, doi:10.1038/srep45964 (2017).

198 Zhu, N. *et al.* cAMP modulates macrophage development by suppressing M-CSF-induced MAPKs activation. *Cell Mol Immunol* **5**, 153-157, doi:10.1038/cmi.2008.19 (2008).
199 Li, X. *et al.* p38 MAPK-mediated signals are required for inducing osteoclast differentiation but not for osteoclast function. *Endocrinology* **143**, 3105-3113, doi:10.1210/endo.143.8.8954 (2002).
200 Theoleyre, S. *et al.* Cellular activity and signaling induced by osteoprotegerin in osteoclasts: involvement of receptor activator of nuclear factor kappaB ligand and MAPK. *Biochim Biophys Acta* **1644**, 1-7, doi:10.1016/j.bbamcr.2003.10.005 (2004).
201 Zhao, H. *et al.* Osteoprotegerin induces podosome disassembly in osteoclasts through calcium, ERK, and p38 MAPK signaling pathways. *Cytokine* **71**, 199-206, doi:10.1016/j.cyto.2014.10.007 (2015).
202 Matsumoto, M., Sudo, T., Maruyama, M., Osada, H. & Tsujimoto, M. Activation of p38 mitogen-activated protein kinase is crucial in osteoclastogenesis induced by tumor necrosis factor. *FEBS Lett* **486**, 23-28, doi:10.1016/s0014-5793(00)02231-6 (2000).
203 Matsuno, H. *et al.* The role of TNF-alpha in the pathogenesis of inflammation and joint destruction in rheumatoid arthritis (RA): a study using a human RA/SCID mouse chimera. *Rheumatology (Oxford)* **41**, 329-337, doi:10.1093/rheumatology/41.3.329 (2002).
204 Azuma, Y., Kaji, K., Katogi, R., Takeshita, S. & Kudo, A. Tumor necrosis factor-alpha induces differentiation of and bone resorption by osteoclasts. *J Biol Chem* **275**, 4858-4864, doi:10.1074/jbc.275.7.4858 (2000).
205 Kobayashi, K. *et al.* Tumor necrosis factor alpha stimulates osteoclast differentiation by a mechanism independent of the ODF/RANKL-RANK interaction. *J Exp Med* **191**, 275-286, doi:10.1084/jem.191.2.275 (2000).
206 Abu-Amer, Y., Ross, F. P., Edwards, J. & Teitelbaum, S. L. Lipopolysaccharide-stimulated osteoclastogenesis is mediated by tumor necrosis factor via its P55 receptor. *The Journal of Clinical Investigation* **100**, 1557-1565, doi:10.1172/JCI119679 (1997).
207 Assuma, R., Oates, T., Cochran, D., Amar, S. & Graves, D. T. IL-1 and TNF antagonists inhibit the inflammatory response and bone loss in experimental periodontitis. *J Immunol* **160**, 403-409 (1998).
208 Merkel, K. D. *et al.* Tumor necrosis factor-alpha mediates orthopedic implant osteolysis. *Am J Pathol* **154**, 203-210, doi:10.1016/s0002-9440(10)65266-2 (1999).
209 Pacifici, R. *et al.* Effect of surgical menopause and estrogen replacement on cytokine release from human blood mononuclear cells. *Proc Natl Acad Sci U S A* **88**, 5134-5138, doi:10.1073/pnas.88.12.5134 (1991).
210 Kim, J. H. *et al.* The mechanism of osteoclast differentiation induced by IL-1. *J Immunol* **183**, 1862-1870, doi:10.4049/jimmunol.0803007 (2009).
211 Mansky, K. C., Sankar, U., Han, J. & Ostrowski, M. C. Microphthalmia transcription factor is a target of the p38 MAPK pathway in response to receptor activator of NF-kappa B ligand signaling. *J Biol Chem* **277**, 11077-11083, doi:10.1074/jbc.M111696200 (2002).

212 Kwak, H. B. *et al.* Monokine induced by interferon-gamma is induced by receptor activator of nuclear factor kappa B ligand and is involved in osteoclast adhesion and migration. *Blood* **105**, 2963-2969, doi:10.1182/blood-2004-07-2534 (2005).
213 Cuadrado, A. & Nebreda, A. R. Mechanisms and functions of p38 MAPK signalling. *Biochem J* **429**, 403-417, doi:10.1042/BJ20100323 (2010).
214 Zarubin, T. & Han, J. Activation and signaling of the p38 MAP kinase pathway. *Cell Res* **15**, 11-18, doi:10.1038/sj.cr.7290257 (2005).
215 Braun, T. *et al.* Mitogen-activated protein kinase 2 regulates physiological and pathological bone turnover. *J Bone Miner Res* **28**, 936-947, doi:10.1002/jbmr.1816 (2013).
216 Lee, J. *et al.* STAT5 is a key transcription factor for IL-3-mediated inhibition of RANKL-induced osteoclastogenesis. *Sci Rep* **6**, 30977, doi:10.1038/srep30977 (2016).
217 Kalliolias, G. D., Zhao, B., Triantafyllopoulou, A., Park-Min, K. H. & Ivashkiv, L. B. Interleukin-27 inhibits human osteoclastogenesis by abrogating RANKL-mediated induction of nuclear factor of activated T cells c1 and suppressing proximal RANK signaling. *Arthritis Rheum* **62**, 402-413, doi:10.1002/art.27200 (2010).
218 Wei, S., Wang, M. W., Teitelbaum, S. L. & Ross, F. P. Interleukin-4 reversibly inhibits osteoclastogenesis via inhibition of NF-kappa B and mitogen-activated protein kinase signaling. *J Biol Chem* **277**, 6622-6630, doi:10.1074/jbc.M104957200 (2002).
219 Carlson, J. *et al.* Role of MKP-1 in osteoclasts and bone homeostasis. *Am J Pathol* **175**, 1564-1573, doi:10.2353/ajpath.2009.090035 (2009).
220 Sartori, R., Li, F. & Kirkwood, K. L. MAP kinase phosphatase-1 protects against inflammatory bone loss. *J Dent Res* **88**, 1125-1130, doi:10.1177/0022034509349306 (2009).
221 He, Y. *et al.* Erk1 positively regulates osteoclast differentiation and bone resorptive activity. *PLoS One* **6**, e24780, doi:10.1371/journal.pone.0024780 (2011).
222 Kinoshita, T. *et al.* Raf/MAPK and rapamycin-sensitive pathways mediate the anti-apoptotic function of p21Ras in IL-3-dependent hematopoietic cells. *Oncogene* **15**, 619-627, doi:10.1038/sj.onc.1201234 (1997).
223 Raman, M., Chen, W. & Cobb, M. H. Differential regulation and properties of MAPKs. *Oncogene* **26**, 3100-3112, doi:10.1038/sj.onc.1210392 (2007).
224 Nakamura, H., Hirata, A., Tsuji, T. & Yamamoto, T. Role of osteoclast extracellular signal-regulated kinase (ERK) in cell survival and maintenance of cell polarity. *J Bone Miner Res* **18**, 1198-1205, doi:10.1359/jbmr.2003.18.7.1198 (2003).
225 Chung, Y. H. *et al.* Interleukin-1beta promotes the LC3-mediated secretory function of osteoclast precursors by stimulating the Ca(2)(+)-dependent activation of ERK. *Int J Biochem Cell Biol* **54**, 198-207, doi:10.1016/j.biocel.2014.07.018 (2014).
226 Baud'huin, M. *et al.* Interleukin-34 is expressed by giant cell tumours of bone and plays a key role in RANKL-induced osteoclastogenesis. *J Pathol* **221**, 77-86, doi:10.1002/path.2684 (2010).
227 Lee, M. S. *et al.* GM-CSF regulates fusion of mononuclear osteoclasts into bone-resorbing osteoclasts by activating the Ras/ERK pathway. *J Immunol* **183**, 3390-3399, doi:10.4049/jimmunol.0804314 (2009).

228 Amcheslavsky, A. & Bar-Shavit, Z. Toll-like receptor 9 ligand blocks osteoclast differentiation through induction of phosphatase. *J Bone Miner Res* **22**, 1301-1310, doi:10.1359/jbmr.070501 (2007).
229 Hirose, J. *et al.* Bone resorption is regulated by cell-autonomous negative feedback loop of Stat5-Dusp axis in the osteoclast. *J Exp Med* **211**, 153-163, doi:10.1084/jem.20130538 (2014).
230 Otero, J. E. *et al.* Defective osteoclastogenesis by IKKbeta-null precursors is a result of receptor activator of NF-kappaB ligand (RANKL)-induced JNK-dependent apoptosis and impaired differentiation. *J Biol Chem* **283**, 24546-24553, doi:10.1074/jbc.M800434200 (2008).
231 Qi, B. *et al.* Ablation of Tak1 in osteoclast progenitor leads to defects in skeletal growth and bone remodeling in mice. *Sci Rep* **4**, 7158, doi:10.1038/srep07158 (2014).
232 David, J. P., Sabapathy, K., Hoffmann, O., Idarraga, M. H. & Wagner, E. F. JNK1 modulates osteoclastogenesis through both c-Jun phosphorylation-dependent and -independent mechanisms. *J Cell Sci* **115**, 4317-4325, doi:10.1242/jcs.00082 (2002).
233 Chang, E. J. *et al.* The JNK-dependent CaMK pathway restrains the reversion of committed cells during osteoclast differentiation. *J Cell Sci* **121**, 2555-2564, doi:10.1242/jcs.028217 (2008).
234 Jimi, E. *et al.* Osteoclast differentiation factor acts as a multifunctional regulator in murine osteoclast differentiation and function. *J Immunol* **163**, 434-442 (1999).
235 Ke, D. *et al.* IL-17A regulates the autophagic activity of osteoclast precursors through RANKL-JNK1 signaling during osteoclastogenesis in vitro. *Biochem Biophys Res Commun* **497**, 890-896, doi:10.1016/j.bbrc.2018.02.164 (2018).
236 Dikic, I. Proteasomal and Autophagic Degradation Systems. *Annu Rev Biochem* **86**, 193-224, doi:10.1146/annurev-biochem-061516-044908 (2017).
237 Lu, K., den Brave, F. & Jentsch, S. Pathway choice between proteasomal and autophagic degradation. *Autophagy* **13**, 1799-1800, doi:10.1080/15548627.2017.1358851 (2017).
238 Lippai, M. & Low, P. The role of the selective adaptor p62 and ubiquitin-like proteins in autophagy. *Biomed Res Int* **2014**, 832704, doi:10.1155/2014/832704 (2014).
239 Huang, L. *et al.* Structure of an E6AP-UbcH7 complex: insights into ubiquitination by the E2-E3 enzyme cascade. *Science* **286**, 1321-1326, doi:10.1126/science.286.5443.1321 (1999).
240 Petroski, M. D. & Deshaies, R. J. Function and regulation of cullin-RING ubiquitin ligases. *Nat Rev Mol Cell Biol* **6**, 9-20, doi:10.1038/nrm1547 (2005).
241 Pickart, C. M. Back to the future with ubiquitin. *Cell* **116**, 181-190, doi:10.1016/s0092-8674(03)01074-2 (2004).
242 Schulman, B. A. & Harper, J. W. Ubiquitin-like protein activation by E1 enzymes: the apex for downstream signalling pathways. *Nat Rev Mol Cell Biol* **10**, 319-331, doi:10.1038/nrm2673 (2009).
243 Finley, D. Recognition and processing of ubiquitin-protein conjugates by the proteasome. *Annu Rev Biochem* **78**, 477-513, doi:10.1146/annurev.biochem.78.081507.101607 (2009).

244 Verma, R., Oania, R., Graumann, J. & Deshaies, R. J. Multiubiquitin chain receptors define a layer of substrate selectivity in the ubiquitin-proteasome system. *Cell* **118**, 99-110, doi:10.1016/j.cell.2004.06.014 (2004).
245 Chau, V. *et al.* A multiubiquitin chain is confined to specific lysine in a targeted short-lived protein. *Science* **243**, 1576-1583, doi:10.1126/science.2538923 (1989).
246 Spence, J., Sadis, S., Haas, A. L. & Finley, D. A ubiquitin mutant with specific defects in DNA repair and multiubiquitination. *Mol Cell Biol* **15**, 1265-1273, doi:10.1128/mcb.15.3.1265 (1995).
247 Kocaturk, N. M. & Gozuacik, D. Crosstalk Between Mammalian Autophagy and the Ubiquitin-Proteasome System. *Front Cell Dev Biol* **6**, 128, doi:10.3389/fcell.2018.00128 (2018).
248 Heinemeyer, W., Ramos, P. C. & Dohmen, R. J. The ultimate nanoscale mincer: assembly, structure and active sites of the 20S proteasome core. *Cell Mol Life Sci* **61**, 1562-1578, doi:10.1007/s00018-004-4130-z (2004).
249 Tomkinson, B. & Lindas, A. C. Tripeptidyl-peptidase II: a multi-purpose peptidase. *Int J Biochem Cell Biol* **37**, 1933-1937, doi:10.1016/j.biocel.2005.02.009 (2005).
250 Groll, M. & Huber, R. Substrate access and processing by the 20S proteasome core particle. *Int J Biochem Cell Biol* **35**, 606-616, doi:10.1016/s1357-2725(02)00390-4 (2003).
251 Klionsky, D. J. Autophagy: from phenomenology to molecular understanding in less than a decade. *Nat Rev Mol Cell Biol* **8**, 931-937, doi:10.1038/nrm2245 (2007).
252 Lamb, C. A., Yoshimori, T. & Tooze, S. A. The autophagosome: origins unknown, biogenesis complex. *Nat Rev Mol Cell Biol* **14**, 759-774, doi:10.1038/nrm3696 (2013).
253 Daroszewska, A. *et al.* A point mutation in the ubiquitin-associated domain of SQSMT1 is sufficient to cause a Paget's disease-like disorder in mice. *Hum Mol Genet* **20**, 2734-2744, doi:10.1093/hmg/ddr172 (2011).
254 Hochstrasser, M. Lingering mysteries of ubiquitin-chain assembly. *Cell* **124**, 27-34, doi:10.1016/j.cell.2005.12.025 (2006).
255 Ye, Y. & Rape, M. Building ubiquitin chains: E2 enzymes at work. *Nat Rev Mol Cell Biol* **10**, 755-764, doi:10.1038/nrm2780 (2009).
256 Thrower, J. S., Hoffman, L., Rechsteiner, M. & Pickart, C. M. Recognition of the polyubiquitin proteolytic signal. *EMBO J* **19**, 94-102, doi:10.1093/emboj/19.1.94 (2000).
257 Baumeister, W., Walz, J., Zuhl, F. & Seemuller, E. The proteasome: paradigm of a self-compartmentalizing protease. *Cell* **92**, 367-380, doi:10.1016/s0092-8674(00)80929-0 (1998).
258 Coux, O., Tanaka, K. & Goldberg, A. L. Structure and functions of the 20S and 26S proteasomes. *Annu Rev Biochem* **65**, 801-847, doi:10.1146/annurev.bi.65.070196.004101 (1996).
259 Murata, S., Yashiroda, H. & Tanaka, K. Molecular mechanisms of proteasome assembly. *Nat Rev Mol Cell Biol* **10**, 104-115, doi:10.1038/nrm2630 (2009).
260 Demartino, G. N. & Gillette, T. G. Proteasomes: machines for all reasons. *Cell* **129**, 659-662, doi:10.1016/j.cell.2007.05.007 (2007).
261 Tanaka, K. The proteasome: overview of structure and functions. *Proc Jpn Acad Ser B Phys Biol Sci* **85**, 12-36, doi:10.2183/pjab.85.12 (2009).

262 Nalepa, G., Rolfe, M. & Harper, J. W. Drug discovery in the ubiquitin-proteasome system. *Nat Rev Drug Discov* **5**, 596-613, doi:10.1038/nrd2056 (2006).
263 Ravid, T. & Hochstrasser, M. Diversity of degradation signals in the ubiquitin-proteasome system. *Nat Rev Mol Cell Biol* **9**, 679-690, doi:10.1038/nrm2468 (2008).
264 Hanna, J., Guerra-Moreno, A., Ang, J. & Micoogullari, Y. Protein Degradation and the Pathologic Basis of Disease. *Am J Pathol* **189**, 94-103, doi:10.1016/j.ajpath.2018.09.004 (2019).
265 Keller, J. N., Huang, F. F. & Markesbery, W. R. Decreased levels of proteasome activity and proteasome expression in aging spinal cord. *Neuroscience* **98**, 149-156, doi:10.1016/s0306-4522(00)00067-1 (2000).
266 Jung, K. M. *et al.* A key role for diacylglycerol lipase-alpha in metabotropic glutamate receptor-dependent endocannabinoid mobilization. *Mol Pharmacol* **72**, 612-621, doi:10.1124/mol.107.037796 (2007).
267 Tydlacka, S., Wang, C. E., Wang, X., Li, S. & Li, X. J. Differential activities of the ubiquitin-proteasome system in neurons versus glia may account for the preferential accumulation of misfolded proteins in neurons. *J Neurosci* **28**, 13285-13295, doi:10.1523/JNEUROSCI.4393-08.2008 (2008).
268 Low, K. & Aebischer, P. Use of viral vectors to create animal models for Parkinson's disease. *Neurobiol Dis* **48**, 189-201, doi:10.1016/j.nbd.2011.12.038 (2012).
269 Andre, R. & Tabrizi, S. J. Misfolded PrP and a novel mechanism of proteasome inhibition. *Prion* **6**, 32-36, doi:10.4161/pri.6.1.18272 (2012).
270 Mathes, E., O'Dea, E. L., Hoffmann, A. & Ghosh, G. NF-kappaB dictates the degradation pathway of IkappaBalpha. *EMBO J* **27**, 1357-1367, doi:10.1038/emboj.2008.73 (2008).
271 Morozov, A. V. *et al.* Interplay between recombinant Hsp70 and proteasomes: proteasome activity modulation and ubiquitin-independent cleavage of Hsp70. *Cell Stress Chaperones* **22**, 687-697, doi:10.1007/s12192-017-0792-y (2017).
272 Alvarez-Castelao, B. & Castano, J. G. Mechanism of direct degradation of IkappaBalpha by 20S proteasome. *FEBS Lett* **579**, 4797-4802, doi:10.1016/j.febslet.2005.07.060 (2005).
273 Adler, J., Reuven, N., Kahana, C. & Shaul, Y. c-Fos proteasomal degradation is activated by a default mechanism, and its regulation by NAD(P)H:quinone oxidoreductase 1 determines c-Fos serum response kinetics. *Mol Cell Biol* **30**, 3767-3778, doi:10.1128/MCB.00899-09 (2010).
274 Pickering, A. M. & Davies, K. J. Degradation of damaged proteins: the main function of the 20S proteasome. *Prog Mol Biol Transl Sci* **109**, 227-248, doi:10.1016/B978-0-12-397863-9.00006-7 (2012).
275 Aiken, C. T., Kaake, R. M., Wang, X. & Huang, L. Oxidative stress-mediated regulation of proteasome complexes. *Mol Cell Proteomics* **10**, R110 006924, doi:10.1074/mcp.M110.006924 (2011).
276 van der Lee, R. *et al.* Classification of intrinsically disordered regions and proteins. *Chem Rev* **114**, 6589-6631, doi:10.1021/cr400525m (2014).
277 Xu, H. & Ren, D. Lysosomal physiology. *Annu Rev Physiol* **77**, 57-80, doi:10.1146/annurev-physiol-021014-071649 (2015).
278 Bitensky, L. Lysosomes and the connective tissue diseases. *J Clin Pathol Suppl (R Coll Pathol)* **12**, 105-116 (1978).

279 Chen, J. & Long, F. mTOR signaling in skeletal development and disease. *Bone Res* **6**, 1, doi:10.1038/s41413-017-0004-5 (2018).
280 Zhang, H. & Baehrecke, E. H. Eaten alive: novel insights into autophagy from multicellular model systems. *Trends Cell Biol* **25**, 376-387, doi:10.1016/j.tcb.2015.03.001 (2015).
281 Mizushima, N., Levine, B., Cuervo, A. M. & Klionsky, D. J. Autophagy fights disease through cellular self-digestion. *Nature* **451**, 1069-1075, doi:10.1038/nature06639 (2008).
282 Yang, Z. & Klionsky, D. J. Eaten alive: a history of macroautophagy. *Nat Cell Biol* **12**, 814-822, doi:10.1038/ncb0910-814 (2010).
283 Chen, Y. & Klionsky, D. J. The regulation of autophagy - unanswered questions. *J Cell Sci* **124**, 161-170, doi:10.1242/jcs.064576 (2011).
284 Weidberg, H., Shvets, E. & Elazar, Z. Biogenesis and cargo selectivity of autophagosomes. *Annu Rev Biochem* **80**, 125-156, doi:10.1146/annurev-biochem-052709-094552 (2011).
285 Axe, E. L. *et al.* Autophagosome formation from membrane compartments enriched in phosphatidylinositol 3-phosphate and dynamically connected to the endoplasmic reticulum. *J Cell Biol* **182**, 685-701, doi:10.1083/jcb.200803137 (2008).
286 Hailey, D. W. *et al.* Mitochondria supply membranes for autophagosome biogenesis during starvation. *Cell* **141**, 656-667, doi:10.1016/j.cell.2010.04.009 (2010).
287 Longatti, A. *et al.* TBC1D14 regulates autophagosome formation via Rab11- and ULK1-positive recycling endosomes. *J Cell Biol* **197**, 659-675, doi:10.1083/jcb.201111079 (2012).
288 Puri, C., Renna, M., Bento, C. F., Moreau, K. & Rubinsztein, D. C. Diverse autophagosome membrane sources coalesce in recycling endosomes. *Cell* **154**, 1285-1299, doi:10.1016/j.cell.2013.08.044 (2013).
289 Ravikumar, B., Moreau, K., Jahreiss, L., Puri, C. & Rubinsztein, D. C. Plasma membrane contributes to the formation of pre-autophagosomal structures. *Nat Cell Biol* **12**, 747-757, doi:10.1038/ncb2078 (2010).
290 Nakatogawa, H. Two ubiquitin-like conjugation systems that mediate membrane formation during autophagy. *Essays Biochem* **55**, 39-50, doi:10.1042/bse0550039 (2013).
291 Ciani, B., Layfield, R., Cavey, J. R., Sheppard, P. W. & Searle, M. S. Structure of the ubiquitin-associated domain of p62 (SQSTM1) and implications for mutations that cause Paget's disease of bone. *J Biol Chem* **278**, 37409-37412, doi:10.1074/jbc.M307416200 (2003).
292 Pankiv, S. *et al.* p62/SQSTM1 binds directly to Atg8/LC3 to facilitate degradation of ubiquitinated protein aggregates by autophagy. *J Biol Chem* **282**, 24131-24145, doi:10.1074/jbc.M702824200 (2007).
293 Hegedus, K., Takats, S., Kovacs, A. L. & Juhasz, G. Evolutionarily conserved role and physiological relevance of a STX17/Syx17 (syntaxin 17)-containing SNARE complex in autophagosome fusion with endosomes and lysosomes. *Autophagy* **9**, 1642-1646, doi:10.4161/auto.25684 (2013).

294 Itakura, E., Kishi-Itakura, C. & Mizushima, N. The hairpin-type tail-anchored SNARE syntaxin 17 targets to autophagosomes for fusion with endosomes/lysosomes. *Cell* **151**, 1256-1269, doi:10.1016/j.cell.2012.11.001 (2012).
295 Jiang, P. *et al.* The HOPS complex mediates autophagosome-lysosome fusion through interaction with syntaxin 17. *Mol Biol Cell* **25**, 1327-1337, doi:10.1091/mbc.E13-08-0447 (2014).
296 Zerial, M. & McBride, H. Rab proteins as membrane organizers. *Nat Rev Mol Cell Biol* **2**, 107-117, doi:10.1038/35052055 (2001).
297 Zucchi, P. C. & Zick, M. Membrane fusion catalyzed by a Rab, SNAREs, and SNARE chaperones is accompanied by enhanced permeability to small molecules and by lysis. *Mol Biol Cell* **22**, 4635-4646, doi:10.1091/mbc.E11-08-0680 (2011).
298 Chen, Y. & Yu, L. Recent progress in autophagic lysosome reformation. *Traffic* **18**, 358-361, doi:10.1111/tra.12484 (2017).
299 Mora, R. & Regnier-Vigouroux, A. Autophagy-driven cell fate decision maker: activated microglia induce specific death of glioma cells by a blockade of basal autophagic flux and secondary apoptosis/necrosis. *Autophagy* **5**, 419-421, doi:10.4161/auto.5.3.7881 (2009).
300 Bjorkoy, G. *et al.* p62/SQSTM1 forms protein aggregates degraded by autophagy and has a protective effect on huntingtin-induced cell death. *J Cell Biol* **171**, 603-614, doi:10.1083/jcb.200507002 (2005).
301 Nezis, I. P. *et al.* Ref(2)P, the Drosophila melanogaster homologue of mammalian p62, is required for the formation of protein aggregates in adult brain. *J Cell Biol* **180**, 1065-1071, doi:10.1083/jcb.200711108 (2008).
302 Tian, Y. *et al.* C. elegans screen identifies autophagy genes specific to multicellular organisms. *Cell* **141**, 1042-1055, doi:10.1016/j.cell.2010.04.034 (2010).
303 Komatsu, M. *et al.* Homeostatic levels of p62 control cytoplasmic inclusion body formation in autophagy-deficient mice. *Cell* **131**, 1149-1163, doi:10.1016/j.cell.2007.10.035 (2007).
304 Myeku, N. & Figueiredo-Pereira, M. E. Dynamics of the degradation of ubiquitinated proteins by proteasomes and autophagy: association with sequestosome 1/p62. *J Biol Chem* **286**, 22426-22440, doi:10.1074/jbc.M110.149252 (2011).
305 Pankiv, S. *et al.* Nucleocytoplasmic shuttling of p62/SQSTM1 and its role in recruitment of nuclear polyubiquitinated proteins to promyelocytic leukemia bodies. *J Biol Chem* **285**, 5941-5953, doi:10.1074/jbc.M109.039925 (2010).
306 Sahani, M. H., Itakura, E. & Mizushima, N. Expression of the autophagy substrate SQSTM1/p62 is restored during prolonged starvation depending on transcriptional upregulation and autophagy-derived amino acids. *Autophagy* **10**, 431-441, doi:10.4161/auto.27344 (2014).
307 Lin, X. *et al.* Interaction domains of p62: a bridge between p62 and selective autophagy. *DNA Cell Biol* **32**, 220-227, doi:10.1089/dna.2012.1915 (2013).
308 Wang, X. & Terpstra, E. J. Ubiquitin receptors and protein quality control. *J Mol Cell Cardiol* **55**, 73-84, doi:10.1016/j.yjmcc.2012.09.012 (2013).
309 Itakura, E. & Mizushima, N. p62 Targeting to the autophagosome formation site requires self-oligomerization but not LC3 binding. *J Cell Biol* **192**, 17-27, doi:10.1083/jcb.201009067 (2011).

310 Lamark, T. *et al.* Interaction codes within the family of mammalian Phox and Bem1p domain-containing proteins. *J Biol Chem* **278**, 34568-34581, doi:10.1074/jbc.M303221200 (2003).
311 Wilson, M. I., Gill, D. J., Perisic, O., Quinn, M. T. & Williams, R. L. PB1 domain-mediated heterodimerization in NADPH oxidase and signaling complexes of atypical protein kinase C with Par6 and p62. *Mol Cell* **12**, 39-50, doi:10.1016/s1097-2765(03)00246-6 (2003).
312 Moscat, J., Diaz-Meco, M. T., Albert, A. & Campuzano, S. Cell signaling and function organized by PB1 domain interactions. *Mol Cell* **23**, 631-640, doi:10.1016/j.molcel.2006.08.002 (2006).
313 Nakamura, K., Kimple, A. J., Siderovski, D. P. & Johnson, G. L. PB1 domain interaction of p62/sequestosome 1 and MEKK3 regulates NF-kappaB activation. *J Biol Chem* **285**, 2077-2089, doi:10.1074/jbc.M109.065102 (2010).
314 Sanz, L., Sanchez, P., Lallena, M. J., Diaz-Meco, M. T. & Moscat, J. The interaction of p62 with RIP links the atypical PKCs to NF-kappaB activation. *EMBO J* **18**, 3044-3053, doi:10.1093/emboj/18.11.3044 (1999).
315 Wooten, M. W. *et al.* The p62 scaffold regulates nerve growth factor-induced NF-kappaB activation by influencing TRAF6 polyubiquitination. *J Biol Chem* **280**, 35625-35629, doi:10.1074/jbc.C500237200 (2005).
316 Lee, S. J. *et al.* A functional role for the p62-ERK1 axis in the control of energy homeostasis and adipogenesis. *EMBO Rep* **11**, 226-232, doi:10.1038/embor.2010.7 (2010).
317 Rodriguez, A. *et al.* Mature-onset obesity and insulin resistance in mice deficient in the signaling adapter p62. *Cell Metab* **3**, 211-222, doi:10.1016/j.cmet.2006.01.011 (2006).
318 Duran, A. *et al.* p62 is a key regulator of nutrient sensing in the mTORC1 pathway. *Mol Cell* **44**, 134-146, doi:10.1016/j.molcel.2011.06.038 (2011).
319 Pikkarainen, M., Hartikainen, P., Soininen, H. & Alafuzoff, I. Distribution and pattern of pathology in subjects with familial or sporadic late-onset cerebellar ataxia as assessed by p62/sequestosome immunohistochemistry. *Cerebellum* **10**, 720-731, doi:10.1007/s12311-011-0281-2 (2011).
320 Sudo, T., Maruyama, M. & Osada, H. p62 functions as a p38 MAP kinase regulator. *Biochem Biophys Res Commun* **269**, 521-525, doi:10.1006/bbrc.2000.2333 (2000).
321 Kawai, K., Saito, A., Sudo, T. & Osada, H. Specific regulation of cytokine-dependent p38 MAP kinase activation by p62/SQSTM1. *J Biochem* **143**, 765-772, doi:10.1093/jb/mvn027 (2008).
322 Zhang, C., Gao, J., Li, M., Deng, Y. & Jiang, C. p38delta MAPK regulates aggresome biogenesis by phosphorylating SQSTM1 in response to proteasomal stress. *J Cell Sci* **131**, doi:10.1242/jcs.216671 (2018).
323 Linares, J. F. *et al.* K63 polyubiquitination and activation of mTOR by the p62-TRAF6 complex in nutrient-activated cells. *Mol Cell* **51**, 283-296, doi:10.1016/j.molcel.2013.06.020 (2013).
324 Linares, J. F. *et al.* Amino Acid Activation of mTORC1 by a PB1-Domain-Driven Kinase Complex Cascade. *Cell Rep* **12**, 1339-1352, doi:10.1016/j.celrep.2015.07.045 (2015).

325 Lim, J. *et al.* Proteotoxic stress induces phosphorylation of p62/SQSTM1 by ULK1 to regulate selective autophagic clearance of protein aggregates. *PLoS Genet* **11**, e1004987, doi:10.1371/journal.pgen.1004987 (2015).
326 Pilli, M. *et al.* TBK-1 promotes autophagy-mediated antimicrobial defense by controlling autophagosome maturation. *Immunity* **37**, 223-234, doi:10.1016/j.immuni.2012.04.015 (2012).
327 Matsumoto, G., Wada, K., Okuno, M., Kurosawa, M. & Nukina, N. Serine 403 phosphorylation of p62/SQSTM1 regulates selective autophagic clearance of ubiquitinated proteins. *Mol Cell* **44**, 279-289, doi:10.1016/j.molcel.2011.07.039 (2011).
328 Maharjan, S., Oku, M., Tsuda, M., Hoseki, J. & Sakai, Y. Mitochondrial impairment triggers cytosolic oxidative stress and cell death following proteasome inhibition. *Sci Rep* **4**, 5896, doi:10.1038/srep05896 (2014).
329 Puissant, A., Fenouille, N. & Auberger, P. When autophagy meets cancer through p62/SQSTM1. *Am J Cancer Res* **2**, 397-413 (2012).
330 Jain, A. *et al.* p62/SQSTM1 is a target gene for transcription factor NRF2 and creates a positive feedback loop by inducing antioxidant response element-driven gene transcription. *J Biol Chem* **285**, 22576-22591, doi:10.1074/jbc.M110.118976 (2010).
331 Ichimura, Y. *et al.* Phosphorylation of p62 activates the Keap1-Nrf2 pathway during selective autophagy. *Mol Cell* **51**, 618-631, doi:10.1016/j.molcel.2013.08.003 (2013).
332 Komatsu, M. *et al.* The selective autophagy substrate p62 activates the stress responsive transcription factor Nrf2 through inactivation of Keap1. *Nat Cell Biol* **12**, 213-223, doi:10.1038/ncb2021 (2010).
333 Tonelli, C., Chio, I. I. C. & Tuveson, D. A. Transcriptional Regulation by Nrf2. *Antioxid Redox Signal* **29**, 1727-1745, doi:10.1089/ars.2017.7342 (2018).
334 Fan, W. *et al.* Keap1 facilitates p62-mediated ubiquitin aggregate clearance via autophagy. *Autophagy* **6**, 614-621, doi:10.4161/auto.6.5.12189 (2010).
335 Kageyama, S. *et al.* Proteasome dysfunction activates autophagy and the Keap1-Nrf2 pathway. *J Biol Chem* **289**, 24944-24955, doi:10.1074/jbc.M114.580357 (2014).
336 Itoh, K. *et al.* Keap1 represses nuclear activation of antioxidant responsive elements by Nrf2 through binding to the amino-terminal Neh2 domain. *Genes Dev* **13**, 76-86, doi:10.1101/gad.13.1.76 (1999).
337 Korolchuk, V. I., Mansilla, A., Menzies, F. M. & Rubinsztein, D. C. Autophagy inhibition compromises degradation of ubiquitin-proteasome pathway substrates. *Mol Cell* **33**, 517-527, doi:10.1016/j.molcel.2009.01.021 (2009).
338 Sarkar, S., Davies, J. E., Huang, Z., Tunnacliffe, A. & Rubinsztein, D. C. Trehalose, a novel mTOR-independent autophagy enhancer, accelerates the clearance of mutant huntingtin and alpha-synuclein. *J Biol Chem* **282**, 5641-5652, doi:10.1074/jbc.M609532200 (2007).
339 Gal, J., Strom, A. L., Kilty, R., Zhang, F. & Zhu, H. p62 accumulates and enhances aggregate formation in model systems of familial amyotrophic lateral sclerosis. *J Biol Chem* **282**, 11068-11077, doi:10.1074/jbc.M608787200 (2007).
340 Paine, M. G., Babu, J. R., Seibenhener, M. L. & Wooten, M. W. Evidence for p62 aggregate formation: role in cell survival. *FEBS Lett* **579**, 5029-5034, doi:10.1016/j.febslet.2005.08.010 (2005).

341 Roodman, G. D. & Windle, J. J. Paget disease of bone. *J Clin Invest* **115**, 200-208, doi:10.1172/JCI24281 (2005).
342 Kurihara, N., Ishizuka, S., Demulder, A., Menaa, C. & Roodman, G. D. Paget's disease-a VDR coactivator disease? *J Steroid Biochem Mol Biol* **89-90**, 321-325, doi:10.1016/j.jsbmb.2004.03.023 (2004).
343 Kurihara, N. *et al.* Role of TAFII-17, a VDR binding protein, in the increased osteoclast formation in Paget's Disease. *J Bone Miner Res* **19**, 1154-1164, doi:10.1359/JBMR.040312 (2004).
344 Neale, S. D., Smith, R., Wass, J. A. & Athanasou, N. A. Osteoclast differentiation from circulating mononuclear precursors in Paget's disease is hypersensitive to 1,25-dihydroxyvitamin D(3) and RANKL. *Bone* **27**, 409-416, doi:10.1016/s8756-3282(00)00345-8 (2000).
345 Roodman, G. D. Insights into the pathogenesis of Paget's disease. *Ann N Y Acad Sci* **1192**, 176-180, doi:10.1111/j.1749-6632.2009.05214.x (2010).
346 Cui, Q., Tashiro, S., Onodera, S., Minami, M. & Ikejima, T. Oridonin induced autophagy in human cervical carcinoma HeLa cells through Ras, JNK, and P38 regulation. *J Pharmacol Sci* **105**, 317-325, doi:10.1254/jphs.fp0070336 (2007).
347 Yamamoto, M., Suzuki, S. O. & Himeno, M. Resveratrol-induced autophagy in human U373 glioma cells. *Oncol Lett* **1**, 489-493, doi:10.3892/ol_00000086 (2010).
348 Bhui, K., Tyagi, S., Prakash, B. & Shukla, Y. Pineapple bromelain induces autophagy, facilitating apoptotic response in mammary carcinoma cells. *Biofactors* **36**, 474-482, doi:10.1002/biof.121 (2010).
349 Liao, P. C. *et al.* Resveratrol arrests cell cycle and induces apoptosis in human hepatocellular carcinoma Huh-7 cells. *J Med Food* **13**, 1415-1423, doi:10.1089/jmf.2010.1126 (2010).
350 Gunn, J. M., Clark, M. G., Knowles, S. E., Hopgood, M. F. & Ballard, F. J. Reduced rates of proteolysis in transformed cells. *Nature* **266**, 58-60, doi:10.1038/266058a0 (1977).
351 Kisen, G. O. *et al.* Reduced autophagic activity in primary rat hepatocellular carcinoma and ascites hepatoma cells. *Carcinogenesis* **14**, 2501-2505, doi:10.1093/carcin/14.12.2501 (1993).
352 Liang, X. H. *et al.* Induction of autophagy and inhibition of tumorigenesis by beclin 1. *Nature* **402**, 672-676, doi:10.1038/45257 (1999).
353 Duan, W. J. *et al.* Silibinin activated p53 and induced autophagic death in human fibrosarcoma HT1080 cells via reactive oxygen species-p38 and c-Jun N-terminal kinase pathways. *Biol Pharm Bull* **34**, 47-53, doi:10.1248/bpb.34.47 (2011).
354 Webber, J. L. & Tooze, S. A. Coordinated regulation of autophagy by p38alpha MAPK through mAtg9 and p38IP. *EMBO J* **29**, 27-40, doi:10.1038/emboj.2009.321 (2010).
355 Helfrich, M. H. & Hocking, L. J. Genetics and aetiology of Pagetic disorders of bone. *Arch Biochem Biophys* **473**, 172-182, doi:10.1016/j.abb.2008.02.045 (2008).
356 Cavey, J. R. *et al.* Loss of ubiquitin-binding associated with Paget's disease of bone p62 (SQSTM1) mutations. *J Bone Miner Res* **20**, 619-624, doi:10.1359/JBMR.041205 (2005).
357 Zach, F., Polzer, F., Mueller, A. & Gessner, A. p62/sequestosome 1 deficiency accelerates osteoclastogenesis in vitro and leads to Paget's disease-like bone phenotypes in mice. *J Biol Chem* **293**, 9530-9541, doi:10.1074/jbc.RA118.002449 (2018).

358 Li, R. F. *et al.* The adaptor protein p62 is involved in RANKL-induced autophagy and osteoclastogenesis. *J Histochem Cytochem* **62**, 879-888, doi:10.1369/0022155414551367 (2014).
359 Chung, Y. H. *et al.* Microtubule-associated protein light chain 3 regulates Cdc42-dependent actin ring formation in osteoclast. *Int J Biochem Cell Biol* **44**, 989-997, doi:10.1016/j.biocel.2012.03.007 (2012).
360 Salminen, A. & Kaarniranta, K. Regulation of the aging process by autophagy. *Trends Mol Med* **15**, 217-224, doi:10.1016/j.molmed.2009.03.004 (2009).
361 Vellai, T., Takacs-Vellai, K., Sass, M. & Klionsky, D. J. The regulation of aging: does autophagy underlie longevity? *Trends Cell Biol* **19**, 487-494, doi:10.1016/j.tcb.2009.07.007 (2009).
362 Wu, J. J. *et al.* Mitochondrial dysfunction and oxidative stress mediate the physiological impairment induced by the disruption of autophagy. *Aging (Albany NY)* **1**, 425-437, doi:10.18632/aging.100038 (2009).
363 Yen, W. L. & Klionsky, D. J. How to live long and prosper: autophagy, mitochondria, and aging. *Physiology (Bethesda)* **23**, 248-262, doi:10.1152/physiol.00013.2008 (2008).
364 Ebato, C. *et al.* Autophagy is important in islet homeostasis and compensatory increase of beta cell mass in response to high-fat diet. *Cell Metab* **8**, 325-332, doi:10.1016/j.cmet.2008.08.009 (2008).
365 Jung, H. S. *et al.* Loss of autophagy diminishes pancreatic beta cell mass and function with resultant hyperglycemia. *Cell Metab* **8**, 318-324, doi:10.1016/j.cmet.2008.08.013 (2008).
366 Mortensen, M. *et al.* Loss of autophagy in erythroid cells leads to defective removal of mitochondria and severe anemia in vivo. *Proc Natl Acad Sci U S A* **107**, 832-837, doi:10.1073/pnas.0913170107 (2010).
367 Pua, H. H., Guo, J., Komatsu, M. & He, Y. W. Autophagy is essential for mitochondrial clearance in mature T lymphocytes. *J Immunol* **182**, 4046-4055, doi:10.4049/jimmunol.0801143 (2009).
368 Singh, R. *et al.* Autophagy regulates lipid metabolism. *Nature* **458**, 1131-1135, doi:10.1038/nature07976 (2009).
369 Droge, W. & Schipper, H. M. Oxidative stress and aberrant signaling in aging and cognitive decline. *Aging Cell* **6**, 361-370, doi:10.1111/j.1474-9726.2007.00294.x (2007).
370 Almeida, M. & O'Brien, C. A. Basic biology of skeletal aging: role of stress response pathways. *J Gerontol A Biol Sci Med Sci* **68**, 1197-1208, doi:10.1093/gerona/glt079 (2013).
371 Manolagas, S. C. & Parfitt, A. M. What old means to bone. *Trends Endocrinol Metab* **21**, 369-374, doi:10.1016/j.tem.2010.01.010 (2010).
372 Wu, Q. *et al.* Advanced Oxidation Protein Products as a Novel Marker of Oxidative Stress in Postmenopausal Osteoporosis. *Med Sci Monit* **21**, 2428-2432, doi:10.12659/MSM.894347 (2015).
373 Ma, Y. *et al.* Autophagy controls mesenchymal stem cell properties and senescence during bone aging. *Aging Cell* **17**, doi:10.1111/acel.12709 (2018).

374 Cejka, D. *et al.* Mammalian target of rapamycin signaling is crucial for joint destruction in experimental arthritis and is activated in osteoclasts from patients with rheumatoid arthritis. *Arthritis Rheum* **62**, 2294-2302, doi:10.1002/art.27504 (2010).
375 Sanchez, C. P. & He, Y. Z. Bone growth during rapamycin therapy in young rats. *BMC Pediatr* **9**, 3, doi:10.1186/1471-2431-9-3 (2009).
376 Westenfeld, R. *et al.* Impact of sirolimus, tacrolimus and mycophenolate mofetil on osteoclastogenesis--implications for post-transplantation bone disease. *Nephrol Dial Transplant* **26**, 4115-4123, doi:10.1093/ndt/gfr214 (2011).
377 Wise, G. E., Frazier-Bowers, S. & D'Souza, R. N. Cellular, molecular, and genetic determinants of tooth eruption. *Crit Rev Oral Biol Med* **13**, 323-334, doi:10.1177/154411130201300403 (2002).
378 Zhou, L. *et al.* Monocyte chemoattractant protein-1 induces a novel transcription factor that causes cardiac myocyte apoptosis and ventricular dysfunction. *Circ Res* **98**, 1177-1185, doi:10.1161/01.RES.0000220106.64661.71 (2006).
379 Wang, K., Niu, J., Kim, H. & Kolattukudy, P. E. Osteoclast precursor differentiation by MCPIP via oxidative stress, endoplasmic reticulum stress, and autophagy. *J Mol Cell Biol* **3**, 360-368, doi:10.1093/jmcb/mjr021 (2011).
380 Raisz, L. G. & Seeman, E. Causes of age-related bone loss and bone fragility: an alternative view. *J Bone Miner Res* **16**, 1948-1952, doi:10.1359/jbmr.2001.16.11.1948 (2001).
381 Jilka, R. L. & O'Brien, C. A. The Role of Osteocytes in Age-Related Bone Loss. *Curr Osteoporos Rep* **14**, 16-25, doi:10.1007/s11914-016-0297-0 (2016).
382 Almeida, M. *et al.* Skeletal involution by age-associated oxidative stress and its acceleration by loss of sex steroids. *J Biol Chem* **282**, 27285-27297, doi:10.1074/jbc.M702810200 (2007).
383 Almeida, M., Han, L., Martin-Millan, M., O'Brien, C. A. & Manolagas, S. C. Oxidative stress antagonizes Wnt signaling in osteoblast precursors by diverting beta-catenin from T cell factor- to forkhead box O-mediated transcription. *J Biol Chem* **282**, 27298-27305, doi:10.1074/jbc.M702811200 (2007).
384 Chen, C. Y. *et al.* Overexpression of Insulin-Like Growth Factor 1 Enhanced the Osteogenic Capability of Aging Bone Marrow Mesenchymal Stem Cells. *Theranostics* **7**, 1598-1611, doi:10.7150/thno.16637 (2017).
385 Pfeilschifter, J. *et al.* Mitogenic responsiveness of human bone cells in vitro to hormones and growth factors decreases with age. *J Bone Miner Res* **8**, 707-717, doi:10.1002/jbmr.5650080609 (1993).
386 Corrado, A., Cici, D., Rotondo, C., Maruotti, N. & Cantatore, F. P. Molecular Basis of Bone Aging. *Int J Mol Sci* **21**, doi:10.3390/ijms21103679 (2020).
387 Eguchi, K. *et al.* Insulin-like growth factor binding Protein-3 suppresses osteoblast differentiation via bone morphogenetic protein-2. *Biochem Biophys Res Commun* **507**, 465-470, doi:10.1016/j.bbrc.2018.11.065 (2018).
388 Mukherjee, A. & Rotwein, P. Insulin-like growth factor-binding protein-5 inhibits osteoblast differentiation and skeletal growth by blocking insulin-like growth factor actions. *Mol Endocrinol* **22**, 1238-1250, doi:10.1210/me.2008-0001 (2008).
389 Moerman, E. J., Teng, K., Lipschitz, D. A. & Lecka-Czernik, B. Aging activates adipogenic and suppresses osteogenic programs in mesenchymal marrow stroma/stem cells: the

role of PPAR-gamma2 transcription factor and TGF-beta/BMP signaling pathways. *Aging Cell* **3**, 379-389, doi:10.1111/j.1474-9728.2004.00127.x (2004).

390 Owen, M. Marrow stromal stem cells. *J Cell Sci Suppl* **10**, 63-76, doi:10.1242/jcs.1988.supplement_10.5 (1988).

391 Lecka-Czernik, B. *et al.* Inhibition of Osf2/Cbfa1 expression and terminal osteoblast differentiation by PPARgamma2. *J Cell Biochem* **74**, 357-371 (1999).

392 Nishii, N., Arai, M., Yanai, N., Togari, A. & Nakabayashi, T. Effect of bone morphogenetic protein-2 (BMP-2) or troglitazone, as an inducer of osteogenic cells or adipocytes, on differentiation of a bone marrow mesenchymal progenitor cell line established from temperature-sensitive (ts) simian virus (SV) 40 T-antigen gene transgenic mice. *Biol Pharm Bull* **32**, 10-17, doi:10.1248/bpb.32.10 (2009).

393 Bruunsgaard, H. & Pedersen, B. K. Age-related inflammatory cytokines and disease. *Immunol Allergy Clin North Am* **23**, 15-39, doi:10.1016/s0889-8561(02)00056-5 (2003).

394 McInnes, I. B. & Schett, G. The pathogenesis of rheumatoid arthritis. *N Engl J Med* **365**, 2205-2219, doi:10.1056/NEJMra1004965 (2011).

395 Lewis, M. *et al.* Cloning and expression of cDNAs for two distinct murine tumor necrosis factor receptors demonstrate one receptor is species specific. *Proc Natl Acad Sci U S A* **88**, 2830-2834, doi:10.1073/pnas.88.7.2830 (1991).

396 Abbas, S., Zhang, Y. H., Clohisy, J. C. & Abu-Amer, Y. Tumor necrosis factor-alpha inhibits pre-osteoblast differentiation through its type-1 receptor. *Cytokine* **22**, 33-41, doi:10.1016/s1043-4666(03)00106-6 (2003).

397 Gilbert, L. *et al.* Inhibition of osteoblast differentiation by tumor necrosis factor-alpha. *Endocrinology* **141**, 3956-3964, doi:10.1210/endo.141.11.7739 (2000).

398 Gilbert, L. *et al.* Expression of the osteoblast differentiation factor RUNX2 (Cbfa1/AML3/Pebp2alpha A) is inhibited by tumor necrosis factor-alpha. *J Biol Chem* **277**, 2695-2701, doi:10.1074/jbc.M106339200 (2002).

399 Boros, K. & Freemont, T. Physiology of ageing of the musculoskeletal system. *Best Pract Res Clin Rheumatol* **31**, 203-217, doi:10.1016/j.berh.2017.09.003 (2017).

400 Pouresmaeili, F., Kamalidehghan, B., Kamarehei, M. & Goh, Y. M. A comprehensive overview on osteoporosis and its risk factors. *Ther Clin Risk Manag* **14**, 2029-2049, doi:10.2147/TCRM.S138000 (2018).

401 Kleerekoper, M., Villanueva, A. R., Stanciu, J., Rao, D. S. & Parfitt, A. M. The role of three-dimensional trabecular microstructure in the pathogenesis of vertebral compression fractures. *Calcif Tissue Int* **37**, 594-597, doi:10.1007/BF02554913 (1985).

402 Szulc, P., Seeman, E., Duboeuf, F., Sornay-Rendu, E. & Delmas, P. D. Bone fragility: failure of periosteal apposition to compensate for increased endocortical resorption in postmenopausal women. *J Bone Miner Res* **21**, 1856-1863, doi:10.1359/jbmr.060904 (2006).

403 Cosman, F. *et al.* Clinician's Guide to Prevention and Treatment of Osteoporosis. *Osteoporos Int* **25**, 2359-2381, doi:10.1007/s00198-014-2794-2 (2014).

404 Eastell, R. *et al.* Postmenopausal osteoporosis. *Nat Rev Dis Primers* **2**, 16069, doi:10.1038/nrdp.2016.69 (2016).

405 Sweet, M. G., Sweet, J. M., Jeremiah, M. P. & Galazka, S. S. Diagnosis and treatment of osteoporosis. *Am Fam Physician* **79**, 193-200 (2009).

406 van Staa, T. P., Dennison, E. M., Leufkens, H. G. & Cooper, C. Epidemiology of fractures in England and Wales. *Bone* **29**, 517-522, doi:10.1016/s8756-3282(01)00614-7 (2001).
407 Cauley, J. A., Chalhoub, D., Kassem, A. M. & Fuleihan Gel, H. Geographic and ethnic disparities in osteoporotic fractures. *Nat Rev Endocrinol* **10**, 338-351, doi:10.1038/nrendo.2014.51 (2014).
408 Cheng, S. Y. *et al.* Geographic trends in incidence of hip fractures: a comprehensive literature review. *Osteoporos Int* **22**, 2575-2586, doi:10.1007/s00198-011-1596-z (2011).
409 Melton, L. J., 3rd, Chrischilles, E. A., Cooper, C., Lane, A. W. & Riggs, B. L. Perspective. How many women have osteoporosis? *J Bone Miner Res* **7**, 1005-1010, doi:10.1002/jbmr.5650070902 (1992).
410 Johnell, O., Gullberg, B., Allander, E., Kanis, J. A. & Group, M. S. The apparent incidence of hip fracture in Europe: a study of national register sources. *Osteoporos Int* **2**, 298-302, doi:10.1007/BF01623186 (1992).
411 Sozen, T., Ozisik, L. & Basaran, N. C. An overview and management of osteoporosis. *Eur J Rheumatol* **4**, 46-56, doi:10.5152/eurjrheum.2016.048 (2017).
412 Manolagas, S. C., O'Brien, C. A. & Almeida, M. The role of estrogen and androgen receptors in bone health and disease. *Nat Rev Endocrinol* **9**, 699-712, doi:10.1038/nrendo.2013.179 (2013).
413 Clowes, J. A., Riggs, B. L. & Khosla, S. The role of the immune system in the pathophysiology of osteoporosis. *Immunol Rev* **208**, 207-227, doi:10.1111/j.0105-2896.2005.00334.x (2005).
414 Dempster, D. W. & Lindsay, R. Pathogenesis of osteoporosis. *Lancet* **341**, 797-801, doi:10.1016/0140-6736(93)90570-7 (1993).
415 Khosla, S. New Insights Into Androgen and Estrogen Receptor Regulation of the Male Skeleton. *J Bone Miner Res* **30**, 1134-1137, doi:10.1002/jbmr.2529 (2015).
416 Gennari, L., Khosla, S. & Bilezikian, J. P. Estrogen and fracture risk in men. *J Bone Miner Res* **23**, 1548-1551, doi:10.1359/jbmr.0810c (2008).
417 Khosla, S. Update on estrogens and the skeleton. *J Clin Endocrinol Metab* **95**, 3569-3577, doi:10.1210/jc.2010-0856 (2010).
418 Santen, R. J., Brodie, H., Simpson, E. R., Siiteri, P. K. & Brodie, A. History of aromatase: saga of an important biological mediator and therapeutic target. *Endocr Rev* **30**, 343-375, doi:10.1210/er.2008-0016 (2009).
419 Komm, B. S. *et al.* Estrogen binding, receptor mRNA, and biologic response in osteoblast-like osteosarcoma cells. *Science* **241**, 81-84, doi:10.1126/science.3164526 (1988).
420 Oursler, M. J., Osdoby, P., Pyfferoen, J., Riggs, B. L. & Spelsberg, T. C. Avian osteoclasts as estrogen target cells. *Proc Natl Acad Sci U S A* **88**, 6613-6617, doi:10.1073/pnas.88.15.6613 (1991).
421 Tomkinson, A., Gevers, E. F., Wit, J. M., Reeve, J. & Noble, B. S. The role of estrogen in the control of rat osteocyte apoptosis. *J Bone Miner Res* **13**, 1243-1250, doi:10.1359/jbmr.1998.13.8.1243 (1998).
422 Smith, C. L. & O'Malley, B. W. Coregulator function: a key to understanding tissue specificity of selective receptor modulators. *Endocr Rev* **25**, 45-71, doi:10.1210/er.2003-0023 (2004).

423 Stein, B. & Yang, M. X. Repression of the interleukin-6 promoter by estrogen receptor is mediated by NF-kappa B and C/EBP beta. *Mol Cell Biol* **15**, 4971-4979, doi:10.1128/mcb.15.9.4971 (1995).
424 Kousteni, S. *et al.* Nongenotropic, sex-nonspecific signaling through the estrogen or androgen receptors: dissociation from transcriptional activity. *Cell* **104**, 719-730 (2001).
425 Kousteni, S. *et al.* Kinase-mediated regulation of common transcription factors accounts for the bone-protective effects of sex steroids. *J Clin Invest* **111**, 1651-1664, doi:10.1172/JCI17261 (2003).
426 Weitzmann, M. N. *et al.* T cell activation induces human osteoclast formation via receptor activator of nuclear factor kappaB ligand-dependent and -independent mechanisms. *J Bone Miner Res* **16**, 328-337, doi:10.1359/jbmr.2001.16.2.328 (2001).
427 Chow, J., Tobias, J. H., Colston, K. W. & Chambers, T. J. Estrogen maintains trabecular bone volume in rats not only by suppression of bone resorption but also by stimulation of bone formation. *J Clin Invest* **89**, 74-78, doi:10.1172/JCI115588 (1992).
428 Cenci, S. *et al.* Estrogen deficiency induces bone loss by enhancing T-cell production of TNF-alpha. *J Clin Invest* **106**, 1229-1237, doi:10.1172/JCI11066 (2000).
429 Kim, N. *et al.* Osteoclast differentiation independent of the TRANCE-RANK-TRAF6 axis. *J Exp Med* **202**, 589-595, doi:10.1084/jem.20050978 (2005).
430 Hofbauer, L. C. *et al.* Interleukin-1beta and tumor necrosis factor-alpha, but not interleukin-6, stimulate osteoprotegerin ligand gene expression in human osteoblastic cells. *Bone* **25**, 255-259, doi:10.1016/s8756-3282(99)00162-3 (1999).
431 Eghbali-Fatourechi, G. *et al.* Role of RANK ligand in mediating increased bone resorption in early postmenopausal women. *J Clin Invest* **111**, 1221-1230, doi:10.1172/JCI17215 (2003).
432 Weitzmann, M. N. & Pacifici, R. Estrogen deficiency and bone loss: an inflammatory tale. *J Clin Invest* **116**, 1186-1194, doi:10.1172/JCI28550 (2006).
433 Ammann, P. *et al.* Transgenic mice expressing soluble tumor necrosis factor-receptor are protected against bone loss caused by estrogen deficiency. *J Clin Invest* **99**, 1699-1703, doi:10.1172/JCI119333 (1997).
434 Kimble, R. B., Bain, S. & Pacifici, R. The functional block of TNF but not of IL-6 prevents bone loss in ovariectomized mice. *J Bone Miner Res* **12**, 935-941, doi:10.1359/jbmr.1997.12.6.935 (1997).
435 Roggia, C. *et al.* Up-regulation of TNF-producing T cells in the bone marrow: a key mechanism by which estrogen deficiency induces bone loss in vivo. *Proc Natl Acad Sci U S A* **98**, 13960-13965, doi:10.1073/pnas.251534698 (2001).
436 Hofbauer, L. C. & Schoppet, M. Clinical implications of the osteoprotegerin/RANKL/RANK system for bone and vascular diseases. *JAMA* **292**, 490-495, doi:10.1001/jama.292.4.490 (2004).
437 Khosla, S. Minireview: the OPG/RANKL/RANK system. *Endocrinology* **142**, 5050-5055, doi:10.1210/endo.142.12.8536 (2001).
438 Sharaf-Eldin, W. E., Abu-Shahba, N., Mahmoud, M. & El-Badri, N. The Modulatory Effects of Mesenchymal Stem Cells on Osteoclastogenesis. *Stem Cells Int* **2016**, 1908365, doi:10.1155/2016/1908365 (2016).

439 Cao, J., Venton, L., Sakata, T. & Halloran, B. P. Expression of RANKL and OPG correlates with age-related bone loss in male C57BL/6 mice. *J Bone Miner Res* **18**, 270-277, doi:10.1359/jbmr.2003.18.2.270 (2003).
440 Cao, J. J. *et al.* Aging increases stromal/osteoblastic cell-induced osteoclastogenesis and alters the osteoclast precursor pool in the mouse. *J Bone Miner Res* **20**, 1659-1668, doi:10.1359/JBMR.050503 (2005).
441 Eriksen, C. G. *et al.* The expression of IL-6 by osteoblasts is increased in healthy elderly individuals: stimulated proliferation and differentiation are unaffected by age. *Calcif Tissue Int* **87**, 414-423, doi:10.1007/s00223-010-9412-x (2010).
442 Makhluf, H. A., Mueller, S. M., Mizuno, S. & Glowacki, J. Age-related decline in osteoprotegerin expression by human bone marrow cells cultured in three-dimensional collagen sponges. *Biochem Biophys Res Commun* **268**, 669-672, doi:10.1006/bbrc.2000.2182 (2000).
443 Chung, P. L. *et al.* Effect of age on regulation of human osteoclast differentiation. *J Cell Biochem* **115**, 1412-1419, doi:10.1002/jcb.24792 (2014).
444 Heaney, R. P. *et al.* Calcium nutrition and bone health in the elderly. *Am J Clin Nutr* **36**, 986-1013, doi:10.1093/ajcn/36.5.986 (1982).
445 Cormick, G. & Belizan, J. M. Calcium Intake and Health. *Nutrients* **11**, doi:10.3390/nu11071606 (2019).
446 Turner, A. G., Anderson, P. H. & Morris, H. A. Vitamin D and bone health. *Scand J Clin Lab Invest Suppl* **243**, 65-72, doi:10.3109/00365513.2012.681963 (2012).
447 Zebaze, R. M. *et al.* Intracortical remodelling and porosity in the distal radius and post-mortem femurs of women: a cross-sectional study. *Lancet* **375**, 1729-1736, doi:10.1016/S0140-6736(10)60320-0 (2010).
448 Lips, P. Vitamin D deficiency and secondary hyperparathyroidism in the elderly: consequences for bone loss and fractures and therapeutic implications. *Endocr Rev* **22**, 477-501, doi:10.1210/edrv.22.4.0437 (2001).
449 Nemere, I. & Larsson, D. Does PTH have a direct effect on intestine? *J Cell Biochem* **86**, 29-34, doi:10.1002/jcb.10199 (2002).
450 Bikle, D. D. Vitamin D metabolism, mechanism of action, and clinical applications. *Chem Biol* **21**, 319-329, doi:10.1016/j.chembiol.2013.12.016 (2014).
451 Eastell, R. *et al.* Interrelationship among vitamin D metabolism, true calcium absorption, parathyroid function, and age in women: evidence of an age-related intestinal resistance to 1,25-dihydroxyvitamin D action. *J Bone Miner Res* **6**, 125-132, doi:10.1002/jbmr.5650060205 (1991).
452 Ledger, G. A. *et al.* Role of parathyroid hormone in mediating nocturnal and age-related increases in bone resorption. *J Clin Endocrinol Metab* **80**, 3304-3310, doi:10.1210/jcem.80.11.7593443 (1995).
453 Duque, G. & Troen, B. R. Understanding the mechanisms of senile osteoporosis: new facts for a major geriatric syndrome. *J Am Geriatr Soc* **56**, 935-941, doi:10.1111/j.1532-5415.2008.01764.x (2008).
454 Rizzoli, R., Slosman, D. & Bonjour, J. P. The role of dual energy X-ray absorptiometry of lumbar spine and proximal femur in the diagnosis and follow-up of osteoporosis. *Am J Med* **98**, 33S-36S, doi:10.1016/s0002-9343(05)80043-9 (1995).

455 Assessment of fracture risk and its application to screening for postmenopausal osteoporosis. Report of a WHO Study Group. *World Health Organ Tech Rep Ser* **843**, 1-129 (1994).
456 Bristow, S. M. *et al.* Acute and 3-month effects of microcrystalline hydroxyapatite, calcium citrate and calcium carbonate on serum calcium and markers of bone turnover: a randomised controlled trial in postmenopausal women. *Br J Nutr* **112**, 1611-1620, doi:10.1017/S0007114514002785 (2014).
457 Reid, I. R. & Bolland, M. J. Calcium and/or Vitamin D Supplementation for the Prevention of Fragility Fractures: Who Needs It? *Nutrients* **12**, doi:10.3390/nu12041011 (2020).
458 Chapuy, M. C., Arlot, M. E., Delmas, P. D. & Meunier, P. J. Effect of calcium and cholecalciferol treatment for three years on hip fractures in elderly women. *BMJ* **308**, 1081-1082, doi:10.1136/bmj.308.6936.1081 (1994).
459 Chapuy, M. C. *et al.* Vitamin D3 and calcium to prevent hip fractures in elderly women. *N Engl J Med* **327**, 1637-1642, doi:10.1056/NEJM199212033272305 (1992).
460 Coxon, F. P., Thompson, K. & Rogers, M. J. Recent advances in understanding the mechanism of action of bisphosphonates. *Curr Opin Pharmacol* **6**, 307-312, doi:10.1016/j.coph.2006.03.005 (2006).
461 Dunford, J. E., Rogers, M. J., Ebetino, F. H., Phipps, R. J. & Coxon, F. P. Inhibition of protein prenylation by bisphosphonates causes sustained activation of Rac, Cdc42, and Rho GTPases. *J Bone Miner Res* **21**, 684-694, doi:10.1359/jbmr.060118 (2006).
462 Drake, M. T., Clarke, B. L. & Khosla, S. Bisphosphonates: mechanism of action and role in clinical practice. *Mayo Clin Proc* **83**, 1032-1045, doi:10.4065/83.9.1032 (2008).
463 Ebetino, F. H. *et al.* The relationship between the chemistry and biological activity of the bisphosphonates. *Bone* **49**, 20-33, doi:10.1016/j.bone.2011.03.774 (2011).
464 Riggs, B. L. & Melton, L. J., 3rd. Involutional osteoporosis. *N Engl J Med* **314**, 1676-1686, doi:10.1056/NEJM198606263142605 (1986).
465 Russell, R. G. Bisphosphonates: from bench to bedside. *Ann N Y Acad Sci* **1068**, 367-401, doi:10.1196/annals.1346.041 (2006).
466 Lin, J. T. & Lane, J. M. Osteoporosis: a review. *Clin Orthop Relat Res*, 126-134 (2004).
467 Black, D. M. *et al.* Fracture risk reduction with alendronate in women with osteoporosis: the Fracture Intervention Trial. FIT Research Group. *J Clin Endocrinol Metab* **85**, 4118-4124, doi:10.1210/jcem.85.11.6953 (2000).
468 Fujita, T. *et al.* Clinical effect of bisphosphonate and vitamin D on osteoporosis: reappraisal of a multicenter double-blind clinical trial comparing etidronate and alfacalcidol. *J Bone Miner Metab* **25**, 130-137, doi:10.1007/s00774-006-0738-4 (2007).
469 Whitaker, M., Guo, J., Kehoe, T. & Benson, G. Bisphosphonates for osteoporosis--where do we go from here? *N Engl J Med* **366**, 2048-2051, doi:10.1056/NEJMp1202619 (2012).
470 Rodan, G., Reszka, A., Golub, E. & Rizzoli, R. Bone safety of long-term bisphosphonate treatment. *Curr Med Res Opin* **20**, 1291-1300, doi:10.1185/030079904125004475 (2004).
471 Miller, P. D. *et al.* Effect of denosumab on bone density and turnover in postmenopausal women with low bone mass after long-term continued, discontinued,

and restarting of therapy: a randomized blinded phase 2 clinical trial. *Bone* **43**, 222-229, doi:10.1016/j.bone.2008.04.007 (2008).

472 Aubry-Rozier, B., Gonzalez-Rodriguez, E., Stoll, D. & Lamy, O. Severe spontaneous vertebral fractures after denosumab discontinuation: three case reports. *Osteoporos Int* **27**, 1923-1925, doi:10.1007/s00198-015-3380-y (2016).

473 Chen, C. M. *et al.* Effects of teriparatide on lung function and pain relief in women with multiple osteoporotic vertebral compression fractures. *Surg Neurol Int* **5**, S339-342, doi:10.4103/2152-7806.139653 (2014).

474 McClung, M. R. *et al.* Opposite bone remodeling effects of teriparatide and alendronate in increasing bone mass. *Arch Intern Med* **165**, 1762-1768, doi:10.1001/archinte.165.15.1762 (2005).

475 Neer, R. M. *et al.* Effect of parathyroid hormone (1-34) on fractures and bone mineral density in postmenopausal women with osteoporosis. *N Engl J Med* **344**, 1434-1441, doi:10.1056/NEJM200105103441904 (2001).

476 Saag, K. G. *et al.* Teriparatide or alendronate in glucocorticoid-induced osteoporosis. *N Engl J Med* **357**, 2028-2039, doi:10.1056/NEJMoa071408 (2007).

477 Cosman, F. *et al.* Effects of intravenous zoledronic acid plus subcutaneous teriparatide [rhPTH(1-34)] in postmenopausal osteoporosis. *J Bone Miner Res* **26**, 503-511, doi:10.1002/jbmr.238 (2011).

478 Cosman, F. *et al.* Effects of teriparatide in postmenopausal women with osteoporosis on prior alendronate or raloxifene: differences between stopping and continuing the antiresorptive agent. *J Clin Endocrinol Metab* **94**, 3772-3780, doi:10.1210/jc.2008-2719 (2009).

479 Paget, J. On a Form of Chronic Inflammation of Bones (Osteitis Deformans). *Med Chir Trans* **60**, 37-64 39, doi:10.1177/095952877706000105 (1877).

480 Al Nofal, A. A. *et al.* Bone turnover markers in Paget's disease of the bone: A Systematic review and meta-analysis. *Osteoporos Int* **26**, 1875-1891, doi:10.1007/s00198-015-3095-0 (2015).

481 Ooi, C. G. & Fraser, W. D. Paget's disease of bone. *Postgrad Med J* **73**, 69-74, doi:10.1136/pgmj.73.856.69 (1997).

482 Roodman, G. D. Paget's disease and osteoclast biology. *Bone* **19**, 209-212, doi:10.1016/8756-3282(96)00211-6 (1996).

483 Shaker, J. L. Paget's Disease of Bone: A Review of Epidemiology, Pathophysiology and Management. *Ther Adv Musculoskelet Dis* **1**, 107-125, doi:10.1177/1759720X09351779 (2009).

484 Melton, L. J., 3rd, Tiegs, R. D., Atkinson, E. J. & O'Fallon, W. M. Fracture risk among patients with Paget's disease: a population-based cohort study. *J Bone Miner Res* **15**, 2123-2128, doi:10.1359/jbmr.2000.15.11.2123 (2000).

485 van Staa, T. P. *et al.* Incidence and natural history of Paget's disease of bone in England and Wales. *J Bone Miner Res* **17**, 465-471, doi:10.1359/jbmr.2002.17.3.465 (2002).

486 Ralston, S. H., Langston, A. L. & Reid, I. R. Pathogenesis and management of Paget's disease of bone. *Lancet* **372**, 155-163, doi:10.1016/S0140-6736(08)61035-1 (2008).

487 Smith, S. E. *et al.* From the archives of the AFIP. Radiologic spectrum of Paget disease of bone and its complications with pathologic correlation. *Radiographics* **22**, 1191-1216, doi:10.1148/radiographics.22.5.g02se281191 (2002).

488 Corral-Gudino, L., Borao-Cengotita-Bengoa, M., Del Pino-Montes, J. & Ralston, S. Epidemiology of Paget's disease of bone: a systematic review and meta-analysis of secular changes. *Bone* **55**, 347-352, doi:10.1016/j.bone.2013.04.024 (2013).
489 Cooper, C., Harvey, N. C., Dennison, E. M. & van Staa, T. P. Update on the epidemiology of Paget's disease of bone. *J Bone Miner Res* **21 Suppl 2**, P3-8, doi:10.1359/jbmr.06s201 (2006).
490 Selby, P. L. *et al.* Guidelines on the management of Paget's disease of bone. *Bone* **31**, 366-373, doi:10.1016/s8756-3282(02)00817-7 (2002).
491 Tan, A. & Ralston, S. H. Paget's disease of bone. *QJM* **107**, 865-869, doi:10.1093/qjmed/hcu075 (2014).
492 Altman, R. D., Bloch, D. A., Hochberg, M. C. & Murphy, W. A. Prevalence of pelvic Paget's disease of bone in the United States. *J Bone Miner Res* **15**, 461-465, doi:10.1359/jbmr.2000.15.3.461 (2000).
493 Lecuyer, N. *et al.* Prevalence of Paget's disease of bone and spinal hemangioma in French women older than 75 years: data from the EPIDOS study. *Joint Bone Spine* **67**, 315-318 (2000).
494 Maurer, K. Basic data on arthritis knee, hip, and sacroiliac joints in adults ages 25-74 years. *Vital Health Stat 11*, 1-31 (1979).
495 Paul Tuck, S., Layfield, R., Walker, J., Mekkayil, B. & Francis, R. Adult Paget's disease of bone: a review. *Rheumatology (Oxford)* **56**, 2050-2059, doi:10.1093/rheumatology/kew430 (2017).
496 Seitz, S. *et al.* Paget's disease of bone: histologic analysis of 754 patients. *J Bone Miner Res* **24**, 62-69, doi:10.1359/jbmr.080907 (2009).
497 Meunier, P. J., Coindre, J. M., Edouard, C. M. & Arlot, M. E. Bone histomorphometry in Paget's disease. Quantitative and dynamic analysis of pagetic and nonpagetic bone tissue. *Arthritis Rheum* **23**, 1095-1103, doi:10.1002/art.1780231005 (1980).
498 Pestka, J. M. *et al.* Paget disease of the spine: an evaluation of 101 patients with a histomorphometric analysis of 29 cases. *Eur Spine J* **21**, 999-1006, doi:10.1007/s00586-011-2133-7 (2012).
499 Chappard, D., Alexandre, C., Laborier, J. C., Robert, J. M. & Riffat, G. Paget's disease of bone. A scanning electron microscopic study. *J Submicrosc Cytol* **16**, 341-348 (1984).
500 Hoyland, J. A., Freemont, A. J. & Sharpe, P. T. Interleukin-6, IL-6 receptor, and IL-6 nuclear factor gene expression in Paget's disease. *J Bone Miner Res* **9**, 75-80, doi:10.1002/jbmr.5650090111 (1994).
501 Teramachi, J. *et al.* Increased IL-6 expression in osteoclasts is necessary but not sufficient for the development of Paget's disease of bone. *J Bone Miner Res* **29**, 1456-1465, doi:10.1002/jbmr.2158 (2014).
502 Hoyland, J. & Sharpe, P. T. Upregulation of c-fos protooncogene expression in pagetic osteoclasts. *J Bone Miner Res* **9**, 1191-1194, doi:10.1002/jbmr.5650090808 (1994).
503 Menaa, C. *et al.* Enhanced RANK ligand expression and responsivity of bone marrow cells in Paget's disease of bone. *J Clin Invest* **105**, 1833-1838, doi:10.1172/JCI9133 (2000).
504 Poor, G., Donath, J., Fornet, B. & Cooper, C. Epidemiology of Paget's disease in Europe: the prevalence is decreasing. *J Bone Miner Res* **21**, 1545-1549, doi:10.1359/jbmr.060704 (2006).

505 Rebel, A. *et al.* Ultrastructural characteristics of osteoclasts in Paget's disease. *Rev Rhum Mal Osteoartic* **41**, 767-771 (1974).
506 Gordon, M. T., Anderson, D. C. & Sharpe, P. T. Canine distemper virus localised in bone cells of patients with Paget's disease. *Bone* **12**, 195-201, doi:10.1016/8756-3282(91)90042-h (1991).
507 Gordon, M. T., Mee, A. P., Anderson, D. C. & Sharpe, P. T. Canine distemper virus transcripts sequenced from pagetic bone. *Bone Miner* **19**, 159-174, doi:10.1016/0169-6009(92)90923-2 (1992).
508 Mee, A. P. *et al.* Detection of canine distemper virus in 100% of Paget's disease samples by in situ-reverse transcriptase-polymerase chain reaction. *Bone* **23**, 171-175, doi:10.1016/s8756-3282(98)00079-9 (1998).
509 Birch, M. A. *et al.* Absence of paramyxovirus RNA in cultures of pagetic bone cells and in pagetic bone. *J Bone Miner Res* **9**, 11-16, doi:10.1002/jbmr.5650090103 (1994).
510 Helfrich, M. H. *et al.* A negative search for a paramyxoviral etiology of Paget's disease of bone: molecular, immunological, and ultrastructural studies in UK patients. *J Bone Miner Res* **15**, 2315-2329, doi:10.1359/jbmr.2000.15.12.2315 (2000).
511 Ooi, C. G., Walsh, C. A., Gallagher, J. A. & Fraser, W. D. Absence of measles virus and canine distemper virus transcripts in long-term bone marrow cultures from patients with Paget's disease of bone. *Bone* **27**, 417-421, doi:10.1016/s8756-3282(00)00343-4 (2000).
512 Ralston, S. H., Digiovine, F. S., Gallacher, S. J., Boyle, I. T. & Duff, G. W. Failure to detect paramyxovirus sequences in Paget's disease of bone using the polymerase chain reaction. *J Bone Miner Res* **6**, 1243-1248, doi:10.1002/jbmr.5650061115 (1991).
513 Ralston, S. H. *et al.* Multicenter blinded analysis of RT-PCR detection methods for paramyxoviruses in relation to Paget's disease of bone. *J Bone Miner Res* **22**, 569-577, doi:10.1359/jbmr.070103 (2007).
514 Lever, J. H. Paget's disease of bone in Lancashire and arsenic pesticide in cotton mill wastewater: a speculative hypothesis. *Bone* **31**, 434-436, doi:10.1016/s8756-3282(02)00833-5 (2002).
515 Siris, E. S. Epidemiological aspects of Paget's disease: family history and relationship to other medical conditions. *Semin Arthritis Rheum* **23**, 222-225, doi:10.1016/0049-0172(94)90037-x (1994).
516 Barker, D. J. & Gardner, M. J. Distribution of Paget's disease in England, Wales and Scotland and a possible relationship with vitamin D deficiency in childhood. *Br J Prev Soc Med* **28**, 226-232, doi:10.1136/jech.28.4.226 (1974).
517 Solomon, L. R. Billiard-player's fingers: an unusual case of Paget's disease of bone. *Br Med J* **1**, 931, doi:10.1136/bmj.1.6168.931 (1979).
518 Albagha, O. M. Genetics of Paget's disease of bone. *Bonekey Rep* **4**, 756, doi:10.1038/bonekey.2015.125 (2015).
519 Ralston, S. H. & Albagha, O. M. Genetic determinants of Paget's disease of bone. *Ann N Y Acad Sci* **1240**, 53-60, doi:10.1111/j.1749-6632.2011.06228.x (2011).
520 Osterberg, P. H. *et al.* Familial expansile osteolysis. A new dysplasia. *J Bone Joint Surg Br* **70**, 255-260, doi:10.1302/0301-620X.70B2.3346299 (1988).
521 Ralston, S. H. & Layfield, R. Pathogenesis of Paget disease of bone. *Calcif Tissue Int* **91**, 97-113, doi:10.1007/s00223-012-9599-0 (2012).

522 Hughes, A. E. *et al.* Mutations in TNFRSF11A, affecting the signal peptide of RANK, cause familial expansile osteolysis. *Nat Genet* **24**, 45-48, doi:10.1038/71667 (2000).
523 Nakatsuka, K., Nishizawa, Y. & Ralston, S. H. Phenotypic characterization of early onset Paget's disease of bone caused by a 27-bp duplication in the TNFRSF11A gene. *J Bone Miner Res* **18**, 1381-1385, doi:10.1359/jbmr.2003.18.8.1381 (2003).
524 Whyte, M. P. & Hughes, A. E. Expansile skeletal hyperphosphatasia is caused by a 15-base pair tandem duplication in TNFRSF11A encoding RANK and is allelic to familial expansile osteolysis. *J Bone Miner Res* **17**, 26-29, doi:10.1359/jbmr.2002.17.1.26 (2002).
525 Whyte, M. P. *et al.* Osteoprotegerin deficiency and juvenile Paget's disease. *N Engl J Med* **347**, 175-184, doi:10.1056/NEJMoa013096 (2002).
526 Cundy, T. *et al.* A mutation in the gene TNFRSF11B encoding osteoprotegerin causes an idiopathic hyperphosphatasia phenotype. *Hum Mol Genet* **11**, 2119-2127, doi:10.1093/hmg/11.18.2119 (2002).
527 Dai, R. M., Chen, E., Longo, D. L., Gorbea, C. M. & Li, C. C. Involvement of valosin-containing protein, an ATPase Co-purified with IkappaBalpha and 26 S proteasome, in ubiquitin-proteasome-mediated degradation of IkappaBalpha. *J Biol Chem* **273**, 3562-3573, doi:10.1074/jbc.273.6.3562 (1998).
528 Watts, G. D. *et al.* Inclusion body myopathy associated with Paget disease of bone and frontotemporal dementia is caused by mutant valosin-containing protein. *Nat Genet* **36**, 377-381, doi:10.1038/ng1332 (2004).
529 Langston, A. L. *et al.* Randomized trial of intensive bisphosphonate treatment versus symptomatic management in Paget's disease of bone. *J Bone Miner Res* **25**, 20-31, doi:10.1359/jbmr.090709 (2010).
530 Hocking, L. J. *et al.* Domain-specific mutations in sequestosome 1 (SQSTM1) cause familial and sporadic Paget's disease. *Hum Mol Genet* **11**, 2735-2739, doi:10.1093/hmg/11.22.2735 (2002).
531 Laurin, N., Brown, J. P., Morissette, J. & Raymond, V. Recurrent mutation of the gene encoding sequestosome 1 (SQSTM1/p62) in Paget disease of bone. *Am J Hum Genet* **70**, 1582-1588, doi:10.1086/340731 (2002).
532 Sofaer, J. A., Holloway, S. M. & Emery, A. E. A family study of Paget's disease of bone. *J Epidemiol Community Health* **37**, 226-231, doi:10.1136/jech.37.3.226 (1983).
533 Cody, J. D. *et al.* Genetic linkage of Paget disease of the bone to chromosome 18q. *Am J Hum Genet* **61**, 1117-1122, doi:10.1086/301601 (1997).
534 Morales-Piga, A. A., Rey-Rey, J. S., Corres-Gonzalez, J., Garcia-Sagredo, J. M. & Lopez-Abente, G. Frequency and characteristics of familial aggregation of Paget's disease of bone. *J Bone Miner Res* **10**, 663-670, doi:10.1002/jbmr.5650100421 (1995).
535 Haslam, S. I. *et al.* Paget's disease of bone: evidence for a susceptibility locus on chromosome 18q and for genetic heterogeneity. *J Bone Miner Res* **13**, 911-917, doi:10.1359/jbmr.1998.13.6.911 (1998).
536 Laurin, N. *et al.* Paget disease of bone: mapping of two loci at 5q35-qter and 5q31. *Am J Hum Genet* **69**, 528-543, doi:10.1086/322975 (2001).
537 Hocking, L. *et al.* Familial Paget's disease of bone: patterns of inheritance and frequency of linkage to chromosome 18q. *Bone* **26**, 577-580, doi:10.1016/s8756-3282(00)00278-7 (2000).

538 Hocking, L. J. *et al.* Novel UBA domain mutations of SQSTM1 in Paget's disease of bone: genotype phenotype correlation, functional analysis, and structural consequences. *J Bone Miner Res* **19**, 1122-1127, doi:10.1359/JBMR.0403015 (2004).
539 Gennari, L., Rendina, D., Falchetti, A. & Merlotti, D. Paget's Disease of Bone. *Calcif Tissue Int* **104**, 483-500, doi:10.1007/s00223-019-00522-3 (2019).
540 Eekhoff, E. W. *et al.* Familial Paget's disease in The Netherlands: occurrence, identification of new mutations in the sequestosome 1 gene, and their clinical associations. *Arthritis Rheum* **50**, 1650-1654, doi:10.1002/art.20224 (2004).
541 Falchetti, A. *et al.* Two novel mutations at exon 8 of the Sequestosome 1 (SQSTM1) gene in an Italian series of patients affected by Paget's disease of bone (PDB). *J Bone Miner Res* **19**, 1013-1017, doi:10.1359/JBMR.040203 (2004).
542 Yoshida, H. *et al.* The murine mutation osteopetrosis is in the coding region of the macrophage colony stimulating factor gene. *Nature* **345**, 442-444, doi:10.1038/345442a0 (1990).
543 Grandi, P. *et al.* Nup93, a vertebrate homologue of yeast Nic96p, forms a complex with a novel 205-kDa protein and is required for correct nuclear pore assembly. *Mol Biol Cell* **8**, 2017-2038, doi:10.1091/mbc.8.10.2017 (1997).
544 Yagi, M. *et al.* DC-STAMP is essential for cell-cell fusion in osteoclasts and foreign body giant cells. *J Exp Med* **202**, 345-351, doi:10.1084/jem.20050645 (2005).
545 Shen, X. *et al.* Processing of optineurin in neuronal cells. *J Biol Chem* **286**, 3618-3629, doi:10.1074/jbc.M110.175810 (2011).
546 Zhu, G., Wu, C. J., Zhao, Y. & Ashwell, J. D. Optineurin negatively regulates TNFalpha-induced NF-kappaB activation by competing with NEMO for ubiquitinated RIP. *Curr Biol* **17**, 1438-1443, doi:10.1016/j.cub.2007.07.041 (2007).
547 Kajiho, H. *et al.* RIN3: a novel Rab5 GEF interacting with amphiphysin II involved in the early endocytic pathway. *J Cell Sci* **116**, 4159-4168, doi:10.1242/jcs.00718 (2003).
548 Vallet, M. *et al.* Targeted sequencing of the Paget's disease associated 14q32 locus identifies several missense coding variants in RIN3 that predispose to Paget's disease of bone. *Hum Mol Genet* **24**, 3286-3295, doi:10.1093/hmg/ddv068 (2015).
549 Lin, H. K., Bergmann, S. & Pandolfi, P. P. Cytoplasmic PML function in TGF-beta signalling. *Nature* **431**, 205-211, doi:10.1038/nature02783 (2004).
550 Salomoni, P. & Pandolfi, P. P. The role of PML in tumor suppression. *Cell* **108**, 165-170, doi:10.1016/s0092-8674(02)00626-8 (2002).
551 Li, J. *et al.* RANK is the intrinsic hematopoietic cell surface receptor that controls osteoclastogenesis and regulation of bone mass and calcium metabolism. *Proc Natl Acad Sci U S A* **97**, 1566-1571, doi:10.1073/pnas.97.4.1566 (2000).
552 Ralston, S. H. *et al.* Diagnosis and Management of Paget's Disease of Bone in Adults: A Clinical Guideline. *J Bone Miner Res* **34**, 579-604, doi:10.1002/jbmr.3657 (2019).
553 Reid, I. R. *et al.* Biochemical and radiologic improvement in Paget's disease of bone treated with alendronate: a randomized, placebo-controlled trial. *Am J Med* **101**, 341-348, doi:10.1016/s0002-9343(96)00227-6 (1996).
554 Reid, I. R. *et al.* A single infusion of zoledronic acid produces sustained remissions in Paget disease: data to 6.5 years. *J Bone Miner Res* **26**, 2261-2270, doi:10.1002/jbmr.438 (2011).

555 Hosking, D. J., Eusebio, R. A. & Chines, A. A. Paget's disease of bone: reduction of disease activity with oral risedronate. *Bone* **22**, 51-55, doi:10.1016/s8756-3282(97)00222-6 (1998).
556 Miller, P. D. *et al.* A randomized, double-blind comparison of risedronate and etidronate in the treatment of Paget's disease of bone. Paget's Risedronate/Etidronate Study Group. *Am J Med* **106**, 513-520, doi:10.1016/s0002-9343(99)00062-5 (1999).
557 Siris, E. S. *et al.* Risedronate in the treatment of Paget's disease of bone: an open label, multicenter study. *J Bone Miner Res* **13**, 1032-1038, doi:10.1359/jbmr.1998.13.6.1032 (1998).
558 Reid, I. R. *et al.* Comparison of a single infusion of zoledronic acid with risedronate for Paget's disease. *N Engl J Med* **353**, 898-908, doi:10.1056/NEJMoa044241 (2005).
559 Kurihara, N. *et al.* Expression of measles virus nucleocapsid protein in osteoclasts induces Paget's disease-like bone lesions in mice. *J Bone Miner Res* **21**, 446-455, doi:10.1359/JBMR.051108 (2006).
560 Kurihara, N. *et al.* Mutation of the sequestosome 1 (p62) gene increases osteoclastogenesis but does not induce Paget disease. *J Clin Invest* **117**, 133-142, doi:10.1172/JCI28267 (2007).
561 Daroszewska, A. *et al.* Zoledronic acid prevents pagetic-like lesions and accelerated bone loss in the p62(P394L) mouse model of Paget's disease. *Dis Model Mech* **11**, doi:10.1242/dmm.035576 (2018).
562 Hiruma, Y. *et al.* A SQSTM1/p62 mutation linked to Paget's disease increases the osteoclastogenic potential of the bone microenvironment. *Hum Mol Genet* **17**, 3708-3719, doi:10.1093/hmg/ddn266 (2008).
563 Duran, A. *et al.* The atypical PKC-interacting protein p62 is an important mediator of RANK-activated osteoclastogenesis. *Dev Cell* **6**, 303-309, doi:10.1016/s1534-5807(03)00403-9 (2004).
564 ten Harkel, B. *et al.* The Foreign Body Giant Cell Cannot Resorb Bone, But Dissolves Hydroxyapatite Like Osteoclasts. *PLoS One* **10**, e0139564, doi:10.1371/journal.pone.0139564 (2015).
565 Stephens, A. S., Stephens, S. R. & Morrison, N. A. Internal control genes for quantitative RT-PCR expression analysis in mouse osteoblasts, osteoclasts and macrophages. *BMC Res Notes* **4**, 410, doi:10.1186/1756-0500-4-410 (2011).
566 van 't Hof, R. J., Rose, L., Bassonga, E. & Daroszewska, A. Open source software for semi-automated histomorphometry of bone resorption and formation parameters. *Bone* **99**, 69-79, doi:10.1016/j.bone.2017.03.051 (2017).
567 Chappard, D., Alexandre, C. & Riffat, G. Histochemical identification of osteoclasts. Review of current methods and reappraisal of a simple procedure for routine diagnosis on undecalcified human iliac bone biopsies. *Basic Appl Histochem* **27**, 75-85 (1983).
568 Chen, H., Zhou, X., Fujita, H., Onozuka, M. & Kubo, K. Y. Age-related changes in trabecular and cortical bone microstructure. *Int J Endocrinol* **2013**, 213234, doi:10.1155/2013/213234 (2013).

569 Saito, A., Kawai, K., Takayama, H., Sudo, T. & Osada, H. Improvement of photoaffinity SPR imaging platform and determination of the binding site of p62/SQSTM1 to p38 MAP kinase. *Chem Asian J* **3**, 1607-1612, doi:10.1002/asia.200800099 (2008).
570 Kwon, J. *et al.* Assurance of mitochondrial integrity and mammalian longevity by the p62-Keap1-Nrf2-Nqo1 cascade. *EMBO Rep* **13**, 150-156, doi:10.1038/embor.2011.246 (2012).
571 Chamoux, E. *et al.* The p62 P392L mutation linked to Paget's disease induces activation of human osteoclasts. *Mol Endocrinol* **23**, 1668-1680, doi:10.1210/me.2009-0066 (2009).
572 Koshihara, Y. *et al.* Osteoclastogenic potential of bone marrow cells increases with age in elderly women with fracture. *Mech Ageing Dev* **123**, 1321-1331, doi:10.1016/s0047-6374(02)00071-4 (2002).
573 Perkins, S. L., Gibbons, R., Kling, S. & Kahn, A. J. Age-related bone loss in mice is associated with an increased osteoclast progenitor pool. *Bone* **15**, 65-72, doi:10.1016/8756-3282(94)90893-1 (1994).
574 Islam, S. *et al.* Bacterial lipopolysaccharide induces osteoclast formation in RAW 264.7 macrophage cells. *Biochem Biophys Res Commun* **360**, 346-351, doi:10.1016/j.bbrc.2007.06.023 (2007).
575 Itoh, K. *et al.* Lipopolysaccharide promotes the survival of osteoclasts via Toll-like receptor 4, but cytokine production of osteoclasts in response to lipopolysaccharide is different from that of macrophages. *J Immunol* **170**, 3688-3695, doi:10.4049/jimmunol.170.7.3688 (2003).
576 Mormann, M. *et al.* Lipopolysaccharides (LPS) induce the differentiation of human monocytes to osteoclasts in a tumour necrosis factor (TNF) alpha-dependent manner: a link between infection and pathological bone resorption. *Mol Immunol* **45**, 3330-3337, doi:10.1016/j.molimm.2008.04.022 (2008).
577 Bruunsgaard, H. *et al.* A high plasma concentration of TNF-alpha is associated with dementia in centenarians. *J Gerontol A Biol Sci Med Sci* **54**, M357-364, doi:10.1093/gerona/54.7.m357 (1999).
578 Paolisso, G. *et al.* Advancing age and insulin resistance: role of plasma tumor necrosis factor-alpha. *Am J Physiol* **275**, E294-299, doi:10.1152/ajpendo.1998.275.2.E294 (1998).
579 Abu-Amer, Y. NF-kappaB signaling and bone resorption. *Osteoporos Int* **24**, 2377-2386, doi:10.1007/s00198-013-2313-x (2013).
580 Ferreiro, D. U. & Komives, E. A. Molecular mechanisms of system control of NF-kappaB signaling by IkappaBalpha. *Biochemistry* **49**, 1560-1567, doi:10.1021/bi901948j (2010).
581 Karin, M. & Greten, F. R. NF-kappaB: linking inflammation and immunity to cancer development and progression. *Nat Rev Immunol* **5**, 749-759, doi:10.1038/nri1703 (2005).
582 Witwicka, H. *et al.* TRAFD1 (FLN29) Interacts with Plekhm1 and Regulates Osteoclast Acidification and Resorption. *PLoS One* **10**, e0127537, doi:10.1371/journal.pone.0127537 (2015).
583 McEwan, D. G. *et al.* PLEKHM1 regulates autophagosome-lysosome fusion through HOPS complex and LC3/GABARAP proteins. *Mol Cell* **57**, 39-54, doi:10.1016/j.molcel.2014.11.006 (2015).

584 Reponen, P., Sahlberg, C., Munaut, C., Thesleff, I. & Tryggvason, K. High expression of 92-kDa type IV collagenase (gelatinase) in the osteoclast lineage during mouse development. *Ann N Y Acad Sci* **732**, 472-475, doi:10.1111/j.1749-6632.1994.tb24789.x (1994).
585 Kusano, K. *et al.* Regulation of matrix metalloproteinases (MMP-2, -3, -9, and -13) by interleukin-1 and interleukin-6 in mouse calvaria: association of MMP induction with bone resorption. *Endocrinology* **139**, 1338-1345, doi:10.1210/endo.139.3.5818 (1998).
586 Huang, C. Y. & Tan, T. H. DUSPs, to MAP kinases and beyond. *Cell Biosci* **2**, 24, doi:10.1186/2045-3701-2-24 (2012).
587 Dickinson, R. J. & Keyse, S. M. Diverse physiological functions for dual-specificity MAP kinase phosphatases. *J Cell Sci* **119**, 4607-4615, doi:10.1242/jcs.03266 (2006).
588 Dorfman, K. *et al.* Disruption of the erp/mkp-1 gene does not affect mouse development: normal MAP kinase activity in ERP/MKP-1-deficient fibroblasts. *Oncogene* **13**, 925-931 (1996).
589 Lawan, A. *et al.* Hepatic mitogen-activated protein kinase phosphatase 1 selectively regulates glucose metabolism and energy homeostasis. *Mol Cell Biol* **35**, 26-40, doi:10.1128/MCB.00503-14 (2015).
590 Alonso, A., Saxena, M., Williams, S. & Mustelin, T. Inhibitory role for dual specificity phosphatase VHR in T cell antigen receptor and CD28-induced Erk and Jnk activation. *J Biol Chem* **276**, 4766-4771, doi:10.1074/jbc.M006497200 (2001).
591 Ishibashi, T., Bottaro, D. P., Chan, A., Miki, T. & Aaronson, S. A. Expression cloning of a human dual-specificity phosphatase. *Proc Natl Acad Sci U S A* **89**, 12170-12174, doi:10.1073/pnas.89.24.12170 (1992).
592 Yuvaniyama, J., Denu, J. M., Dixon, J. E. & Saper, M. A. Crystal structure of the dual specificity protein phosphatase VHR. *Science* **272**, 1328-1331, doi:10.1126/science.272.5266.1328 (1996).
593 Al-Mutairi, M. S. *et al.* MAP kinase phosphatase-2 plays a critical role in response to infection by Leishmania mexicana. *PLoS Pathog* **6**, e1001192, doi:10.1371/journal.ppat.1001192 (2010).
594 Muda, M. *et al.* Molecular cloning and functional characterization of a novel mitogen-activated protein kinase phosphatase, MKP-4. *J Biol Chem* **272**, 5141-5151, doi:10.1074/jbc.272.8.5141 (1997).
595 Fukuda, H. *et al.* A single nucleotide polymorphism within DUSP9 is associated with susceptibility to type 2 diabetes in a Japanese population. *PLoS One* **7**, e46263, doi:10.1371/journal.pone.0046263 (2012).
596 Wu, C. C., Hsu, S. C., Shih, H. M. & Lai, M. Z. Nuclear factor of activated T cells c is a target of p38 mitogen-activated protein kinase in T cells. *Mol Cell Biol* **23**, 6442-6454, doi:10.1128/mcb.23.18.6442-6454.2003 (2003).
597 Feng, X. & McDonald, J. M. Disorders of bone remodeling. *Annu Rev Pathol* **6**, 121-145, doi:10.1146/annurev-pathol-011110-130203 (2011).
598 Sambandam, Y., Sundaram, K., Saigusa, T., Balasubramanian, S. & Reddy, S. V. NFAM1 signaling enhances osteoclast formation and bone resorption activity in Paget's disease of bone. *Bone* **101**, 236-244, doi:10.1016/j.bone.2017.05.013 (2017).

599 Wada, T., Nakashima, T., Hiroshi, N. & Penninger, J. M. RANKL-RANK signaling in osteoclastogenesis and bone disease. *Trends Mol Med* **12**, 17-25, doi:10.1016/j.molmed.2005.11.007 (2006).

600 Gingery, A., Bradley, E., Shaw, A. & Oursler, M. J. Phosphatidylinositol 3-kinase coordinately activates the MEK/ERK and AKT/NFkappaB pathways to maintain osteoclast survival. *J Cell Biochem* **89**, 165-179, doi:10.1002/jcb.10503 (2003).

601 Webber, J. L. & Tooze, S. A. New insights into the function of Atg9. *FEBS Lett* **584**, 1319-1326, doi:10.1016/j.febslet.2010.01.020 (2010).

602 Caunt, C. J. & Keyse, S. M. Dual-specificity MAP kinase phosphatases (MKPs): shaping the outcome of MAP kinase signalling. *FEBS J* **280**, 489-504, doi:10.1111/j.1742-4658.2012.08716.x (2013).

603 Slack, D. N., Seternes, O. M., Gabrielsen, M. & Keyse, S. M. Distinct binding determinants for ERK2/p38alpha and JNK map kinases mediate catalytic activation and substrate selectivity of map kinase phosphatase-1. *J Biol Chem* **276**, 16491-16500, doi:10.1074/jbc.M010966200 (2001).

604 Theodosiou, A. & Ashworth, A. MAP kinase phosphatases. *Genome Biol* **3**, REVIEWS3009, doi:10.1186/gb-2002-3-7-reviews3009 (2002).

605 Rohan, P. J. *et al.* PAC-1: a mitogen-induced nuclear protein tyrosine phosphatase. *Science* **259**, 1763-1766, doi:10.1126/science.7681221 (1993).

606 Camps, M., Nichols, A. & Arkinstall, S. Dual specificity phosphatases: a gene family for control of MAP kinase function. *FASEB J* **14**, 6-16 (2000).

607 Theodosiou, A., Smith, A., Gillieron, C., Arkinstall, S. & Ashworth, A. MKP5, a new member of the MAP kinase phosphatase family, which selectively dephosphorylates stress-activated kinases. *Oncogene* **18**, 6981-6988, doi:10.1038/sj.onc.1203185 (1999).

608 Tanoue, T., Yamamoto, T., Maeda, R. & Nishida, E. A Novel MAPK phosphatase MKP-7 acts preferentially on JNK/SAPK and p38 alpha and beta MAPKs. *J Biol Chem* **276**, 26629-26639, doi:10.1074/jbc.M101981200 (2001).

609 Masuda, K., Shima, H., Watanabe, M. & Kikuchi, K. MKP-7, a novel mitogen-activated protein kinase phosphatase, functions as a shuttle protein. *J Biol Chem* **276**, 39002-39011, doi:10.1074/jbc.M104600200 (2001).

610 Muda, M. *et al.* The dual specificity phosphatases M3/6 and MKP-3 are highly selective for inactivation of distinct mitogen-activated protein kinases. *J Biol Chem* **271**, 27205-27208, doi:10.1074/jbc.271.44.27205 (1996).

611 Tanoue, T., Moriguchi, T. & Nishida, E. Molecular cloning and characterization of a novel dual specificity phosphatase, MKP-5. *J Biol Chem* **274**, 19949-19956, doi:10.1074/jbc.274.28.19949 (1999).

612 Suda, K., Woo, J. T., Takami, M., Sexton, P. M. & Nagai, K. Lipopolysaccharide supports survival and fusion of preosteoclasts independent of TNF-alpha, IL-1, and RANKL. *J Cell Physiol* **190**, 101-108, doi:10.1002/jcp.10041 (2002).

613 Park, J. H., Lee, N. K. & Lee, S. Y. Current Understanding of RANK Signaling in Osteoclast Differentiation and Maturation. *Mol Cells* **40**, 706-713, doi:10.14348/molcells.2017.0225 (2017).

614 Ghosh, S. & Karin, M. Missing pieces in the NF-kappaB puzzle. *Cell* **109 Suppl**, S81-96, doi:10.1016/s0092-8674(02)00703-1 (2002).

615 Li, Q. & Verma, I. M. NF-kappaB regulation in the immune system. *Nat Rev Immunol* **2**, 725-734, doi:10.1038/nri910 (2002).
616 Ginaldi, L., Di Benedetto, M. C. & De Martinis, M. Osteoporosis, inflammation and ageing. *Immun Ageing* **2**, 14, doi:10.1186/1742-4933-2-14 (2005).
617 Sharma, S. M. *et al.* MITF and PU.1 recruit p38 MAPK and NFATc1 to target genes during osteoclast differentiation. *J Biol Chem* **282**, 15921-15929, doi:10.1074/jbc.M609723200 (2007).
618 Sundaram, K. *et al.* RANK ligand signaling modulates the matrix metalloproteinase-9 gene expression during osteoclast differentiation. *Exp Cell Res* **313**, 168-178, doi:10.1016/j.yexcr.2006.10.001 (2007).
619 Michaud, M. *et al.* Proinflammatory cytokines, aging, and age-related diseases. *J Am Med Dir Assoc* **14**, 877-882, doi:10.1016/j.jamda.2013.05.009 (2013).
620 Barbosa, M. C., Grosso, R. A. & Fader, C. M. Hallmarks of Aging: An Autophagic Perspective. *Front Endocrinol (Lausanne)* **9**, 790, doi:10.3389/fendo.2018.00790 (2018).
621 Ward, W. F. Protein degradation in the aging organism. *Prog Mol Subcell Biol* **29**, 35-42, doi:10.1007/978-3-642-56373-7_3 (2002).
622 Cuervo, A. M. *et al.* Autophagy and aging: the importance of maintaining "clean" cells. *Autophagy* **1**, 131-140, doi:10.4161/auto.1.3.2017 (2005).
623 Hubbard, V. M., Valdor, R., Macian, F. & Cuervo, A. M. Selective autophagy in the maintenance of cellular homeostasis in aging organisms. *Biogerontology* **13**, 21-35, doi:10.1007/s10522-011-9331-x (2012).
624 Takahashi, Y. *et al.* Bif-1 regulates Atg9 trafficking by mediating the fission of Golgi membranes during autophagy. *Autophagy* **7**, 61-73, doi:10.4161/auto.7.1.14015 (2011).
625 Young, A. R. *et al.* Starvation and ULK1-dependent cycling of mammalian Atg9 between the TGN and endosomes. *J Cell Sci* **119**, 3888-3900, doi:10.1242/jcs.03172 (2006).
626 Shacka, J. J., Klocke, B. J. & Roth, K. A. Autophagy, bafilomycin and cell death: the "a-B-cs" of plecomacrolide-induced neuroprotection. *Autophagy* **2**, 228-230, doi:10.4161/auto.2703 (2006).
627 Yamamoto, A. *et al.* Bafilomycin A1 prevents maturation of autophagic vacuoles by inhibiting fusion between autophagosomes and lysosomes in rat hepatoma cell line, H-4-II-E cells. *Cell Struct Funct* **23**, 33-42, doi:10.1247/csf.23.33 (1998).
628 Huang, R. *et al.* Deacetylation of nuclear LC3 drives autophagy initiation under starvation. *Mol Cell* **57**, 456-466, doi:10.1016/j.molcel.2014.12.013 (2015).
629 Huang, R. & Liu, W. Identifying an essential role of nuclear LC3 for autophagy. *Autophagy* **11**, 852-853, doi:10.1080/15548627.2015.1038016 (2015).
630 Mehrpour, M., Esclatine, A., Beau, I. & Codogno, P. Autophagy in health and disease. 1. Regulation and significance of autophagy: an overview. *Am J Physiol Cell Physiol* **298**, C776-785, doi:10.1152/ajpcell.00507.2009 (2010).
631 White, E. The role for autophagy in cancer. *J Clin Invest* **125**, 42-46, doi:10.1172/JCI73941 (2015).
632 Yang, Z., Goronzy, J. J. & Weyand, C. M. Autophagy in autoimmune disease. *J Mol Med (Berl)* **93**, 707-717, doi:10.1007/s00109-015-1297-8 (2015).

633 Del Roso, A. *et al.* Ageing-related changes in the in vivo function of rat liver macroautophagy and proteolysis. *Exp Gerontol* **38**, 519-527, doi:10.1016/s0531-5565(03)00002-0 (2003).
634 Cui, J. *et al.* Age-related changes in the function of autophagy in rat kidneys. *Age (Dordr)* **34**, 329-339, doi:10.1007/s11357-011-9237-1 (2012).
635 Liu, Y. *et al.* Impaired autophagic function in rat islets with aging. *Age (Dordr)* **35**, 1531-1544, doi:10.1007/s11357-012-9456-0 (2013).
636 Wohlgemuth, S. E., Seo, A. Y., Marzetti, E., Lees, H. A. & Leeuwenburgh, C. Skeletal muscle autophagy and apoptosis during aging: effects of calorie restriction and life-long exercise. *Exp Gerontol* **45**, 138-148, doi:10.1016/j.exger.2009.11.002 (2010).
637 Chen, K., Yang, Y. H., Jiang, S. D. & Jiang, L. S. Decreased activity of osteocyte autophagy with aging may contribute to the bone loss in senile population. *Histochem Cell Biol* **142**, 285-295, doi:10.1007/s00418-014-1194-1 (2014).
638 Matsumoto, N. *et al.* Essential Role of the a3 Isoform of V-ATPase in Secretory Lysosome Trafficking via Rab7 Recruitment. *Sci Rep* **8**, 6701, doi:10.1038/s41598-018-24918-7 (2018).
639 Zhao, H., Laitala-Leinonen, T., Parikka, V. & Vaananen, H. K. Downregulation of small GTPase Rab7 impairs osteoclast polarization and bone resorption. *J Biol Chem* **276**, 39295-39302, doi:10.1074/jbc.M010999200 (2001).
640 Sobota, J. A., Back, N., Eipper, B. A. & Mains, R. E. Inhibitors of the V0 subunit of the vacuolar H+-ATPase prevent segregation of lysosomal- and secretory-pathway proteins. *J Cell Sci* **122**, 3542-3553, doi:10.1242/jcs.034298 (2009).
641 Zhu, S. *et al.* Bafilomycin A1 Attenuates Osteoclast Acidification and Formation, Accompanied by Increased Levels of SQSTM1/p62 Protein. *J Cell Biochem* **117**, 1464-1470, doi:10.1002/jcb.25442 (2016).
642 Gelman, A. & Elazar, Z. Autophagic factors cut to the bone. *Dev Cell* **21**, 808-810, doi:10.1016/j.devcel.2011.10.021 (2011).
643 Wu, Y. C. *et al.* Inhibition of macroautophagy by bafilomycin A1 lowers proliferation and induces apoptosis in colon cancer cells. *Biochem Biophys Res Commun* **382**, 451-456, doi:10.1016/j.bbrc.2009.03.051 (2009).
644 Silva, G., Cunha, A., Gregoire, I. P., Seldon, M. P. & Soares, M. P. The antiapoptotic effect of heme oxygenase-1 in endothelial cells involves the degradation of p38 alpha MAPK isoform. *J Immunol* **177**, 1894-1903, doi:10.4049/jimmunol.177.3.1894 (2006).
645 Moser, B., Hochreiter, B., Herbst, R. & Schmid, J. A. Fluorescence colocalization microscopy analysis can be improved by combining object-recognition with pixel-intensity-correlation. *Biotechnol J* **12**, doi:10.1002/biot.201600332 (2017).
646 Cha-Molstad, H. *et al.* p62/SQSTM1/Sequestosome-1 is an N-recognin of the N-end rule pathway which modulates autophagosome biogenesis. *Nat Commun* **8**, 102, doi:10.1038/s41467-017-00085-7 (2017).
647 Garner, T. P., Long, J., Layfield, R. & Searle, M. S. Impact of p62/SQSTM1 UBA domain mutations linked to Paget's disease of bone on ubiquitin recognition. *Biochemistry* **50**, 4665-4674, doi:10.1021/bi200079n (2011).
648 Sundaram, K., Shanmugarajan, S., Rao, D. S. & Reddy, S. V. Mutant p62P392L stimulation of osteoclast differentiation in Paget's disease of bone. *Endocrinology* **152**, 4180-4189, doi:10.1210/en.2011-1225 (2011).

649 Cao, J. J., Gregoire, B. R. & Gao, H. High-fat diet decreases cancellous bone mass but has no effect on cortical bone mass in the tibia in mice. *Bone* **44**, 1097-1104, doi:10.1016/j.bone.2009.02.017 (2009).
650 Jevon, M. *et al.* Gender- and age-related differences in osteoclast formation from circulating precursors. *J Endocrinol* **172**, 673-681, doi:10.1677/joe.0.1720673 (2002).
651 Shinohara, M. & Takayanagi, H. Novel osteoclast signaling mechanisms. *Curr Osteoporos Rep* **5**, 67-72, doi:10.1007/s11914-007-0005-1 (2007).
652 Agas, D., Amaroli, A., Lacava, G., Yanagawa, T. & Sabbieti, M. G. Loss of p62 impairs bone turnover and inhibits PTH-induced osteogenesis. *J Cell Physiol*, doi:10.1002/jcp.29654 (2020).
653 Sabharwal, R. *et al.* An Insight in to Paget's Disease of Bone. *Niger J Surg* **20**, 9-15, doi:10.4103/1117-6806.127098 (2014).
654 Selbach, M. *et al.* Widespread changes in protein synthesis induced by microRNAs. *Nature* **455**, 58-63, doi:10.1038/nature07228 (2008).
655 Green, D., Mohorianu, I., McNamara, I., Dalmay, T. & Fraser, W. D. miR-16 is highly expressed in Paget's associated osteosarcoma. *Endocr Relat Cancer* **24**, L27-L31, doi:10.1530/ERC-16-0487 (2017).
656 Khosla, S. *et al.* Relationship of serum sex steroid levels and bone turnover markers with bone mineral density in men and women: a key role for bioavailable estrogen. *J Clin Endocrinol Metab* **83**, 2266-2274, doi:10.1210/jcem.83.7.4924 (1998).
657 Abidi, P., Leers-Sucheta, S., Cortez, Y., Han, J. & Azhar, S. Evidence that age-related changes in p38 MAP kinase contribute to the decreased steroid production by the adrenocortical cells from old rats. *Aging Cell* **7**, 168-178, doi:10.1111/j.1474-9726.2007.00364.x (2008).
658 Chlan-Fourney, J., Zhao, T., Walz, W. & Mousseau, D. D. The increased density of p38 mitogen-activated protein kinase-immunoreactive microglia in the sensorimotor cortex of aged TgCRND8 mice is associated predominantly with smaller dense-core amyloid plaques. *Eur J Neurosci* **33**, 1433-1444, doi:10.1111/j.1460-9568.2010.07597.x (2011).
659 Cheung, P. C., Campbell, D. G., Nebreda, A. R. & Cohen, P. Feedback control of the protein kinase TAK1 by SAPK2a/p38alpha. *EMBO J* **22**, 5793-5805, doi:10.1093/emboj/cdg552 (2003).
660 Lamothe, B., Lai, Y., Xie, M., Schneider, M. D. & Darnay, B. G. TAK1 is essential for osteoclast differentiation and is an important modulator of cell death by apoptosis and necroptosis. *Mol Cell Biol* **33**, 582-595, doi:10.1128/MCB.01225-12 (2013).
661 Chen, H. F., Chuang, H. C. & Tan, T. H. Regulation of Dual-Specificity Phosphatase (DUSP) Ubiquitination and Protein Stability. *Int J Mol Sci* **20**, doi:10.3390/ijms20112668 (2019).
662 Zhang, C., Dou, C. E., Xu, J. & Dong, S. DC-STAMP, the key fusion-mediating molecule in osteoclastogenesis. *J Cell Physiol* **229**, 1330-1335, doi:10.1002/jcp.24553 (2014).
663 Lee, S. H. *et al.* v-ATPase V0 subunit d2-deficient mice exhibit impaired osteoclast fusion and increased bone formation. *Nat Med* **12**, 1403-1409, doi:10.1038/nm1514 (2006).

664 Wu, H., Xu, G. & Li, Y. P. Atp6v0d2 is an essential component of the osteoclast-specific proton pump that mediates extracellular acidification in bone resorption. *J Bone Miner Res* **24**, 871-885, doi:10.1359/jbmr.081239 (2009).

665 Lin, N. Y. *et al.* Inactivation of autophagy ameliorates glucocorticoid-induced and ovariectomy-induced bone loss. *Ann Rheum Dis* **75**, 1203-1210, doi:10.1136/annrheumdis-2015-207240 (2016).

666 Onal, M. *et al.* Suppression of autophagy in osteocytes mimics skeletal aging. *J Biol Chem* **288**, 17432-17440, doi:10.1074/jbc.M112.444190 (2013).

667 Slobodnyuk, K. *et al.* Autophagy-induced senescence is regulated by p38alpha signaling. *Cell Death Dis* **10**, 376, doi:10.1038/s41419-019-1607-0 (2019).

668 Henson, S. M. *et al.* p38 signaling inhibits mTORC1-independent autophagy in senescent human CD8(+) T cells. *J Clin Invest* **124**, 4004-4016, doi:10.1172/JCI75051 (2014).

669 He, Y. *et al.* p38 MAPK inhibits autophagy and promotes microglial inflammatory responses by phosphorylating ULK1. *J Cell Biol* **217**, 315-328, doi:10.1083/jcb.201701049 (2018).

670 Webber, J. L. Regulation of autophagy by p38alpha MAPK. *Autophagy* **6**, 292-293, doi:10.4161/auto.6.2.11128 (2010).

671 Choi, W. S. *et al.* Phosphorylation of p38 MAPK induced by oxidative stress is linked to activation of both caspase-8- and -9-mediated apoptotic pathways in dopaminergic neurons. *J Biol Chem* **279**, 20451-20460, doi:10.1074/jbc.M311164200 (2004).

672 Gutierrez-Uzquiza, A., Arechederra, M., Bragado, P., Aguirre-Ghiso, J. A. & Porras, A. p38alpha mediates cell survival in response to oxidative stress via induction of antioxidant genes: effect on the p70S6K pathway. *J Biol Chem* **287**, 2632-2642, doi:10.1074/jbc.M111.323709 (2012).

673 Son, Y. *et al.* Mitogen-Activated Protein Kinases and Reactive Oxygen Species: How Can ROS Activate MAPK Pathways? *J Signal Transduct* **2011**, 792639, doi:10.1155/2011/792639 (2011).

674 de Bont, N. *et al.* LPS-induced release of IL-1 beta, IL-1Ra, IL-6, and TNF-alpha in whole blood from patients with familial hypercholesterolemia: no effect of cholesterol-lowering treatment. *J Interferon Cytokine Res* **26**, 101-107, doi:10.1089/jir.2006.26.101 (2006).

675 Gabellec, M. M., Griffais, R., Fillion, G. & Haour, F. Expression of interleukin 1 alpha, interleukin 1 beta and interleukin 1 receptor antagonist mRNA in mouse brain: regulation by bacterial lipopolysaccharide (LPS) treatment. *Brain Res Mol Brain Res* **31**, 122-130, doi:10.1016/0169-328x(95)00042-q (1995).

676 Lawson, M. A., McCusker, R. H. & Kelley, K. W. Interleukin-1 beta converting enzyme is necessary for development of depression-like behavior following intracerebroventricular administration of lipopolysaccharide to mice. *J Neuroinflammation* **10**, 54, doi:10.1186/1742-2094-10-54 (2013).